UNIVERSITÉ
LAVAL

From boron containing heterocycles to oxygen rich ligands for lanthanide coordination and extraction

Thèse

Ambreen Mushtaq

Doctorat en Chimie

Philosophiae Doctor (Ph.D.)

Québec, Canada

Résumé

Jusqu'à l'aube du 21e siècle, les lanthanides étaient considérés comme les métaux les plus difficiles à travailler et à manipuler. En effet, en raison de leur chimie de coordination imprévisible, la caractérisation des complexes de lanthanides représente un défi de taille pour les chimistes expérimentaux. Cependant, les dernières décennies ont vu une évolution considérable de la chimie organométallique de ces éléments du groupe *f*. Les orbitales-*f* non-perturbées contenant plusieurs éléctrons non-appariés dans certains lanthanides les ont rendu indispensables dans des applications modernes tels la catalyse, les diodes électroluminescents organiques, les luminophores, les agents de contraste en IRM et les matériaux magnétiques.

La coordination de composés déficients en électrons aux lanthanides est considérée difficile en raison de l'électrophilcité de ces éléments. Malgré tout, les uniques propriétés magnétiques et optiques des lanthanides rendent importante l'étude de leurs complexes avec divers ligands, en particulier avec ceux qui possèdent un caractère acide de Lewis.

Nous avons décidé de nous intéresser à ce défi en concevant des ligands hétéroaromatiques de bore capables de satisfaire les exigences électroniques et stériques des lanthanides. En plus de réaliser la coordination de ces ligands déficients en électrons à des lanthanides, nous avions pour but d'étudier leur effet sur les propriétés magnétiques de ces métaux. Premièrement, nous avons préparé un complexe monoanionique de boratabenzène et avons étudié sa coordination avec plusieurs ions de lanthanides. Un complexe inédit de tris(boratabenzène)lanthane a été isolé et caractérisé. Les composés diboratabenzènes de lanthanides, cependant, se sont révélés être difficiles à isoler. C'est pourquoi, nous avons synthétisé le 1-mesityl-4-*i*Pr-boratabenzene comme ligand encombré stériquement. Ce dernier a révélé une réactivité riche avec l'eau et différentes bases.

Nous avons aussi synthétisé une famille de diboraanthracènes dianioniques, dans le but de former des complexes « sandwich » et « triple-decker » de lanthanides. Une chimie intéressante a été observée pour ces ligands, alors que nous les avons coordonnés à

plusieurs lanthanides. Un complexe « triple-decker » inverse de lanthane a été obtenu et étudié.

Finalement, nous avons investigué la conception de ligands pour l'extraction sélective des lanthanides à partir de leurs minerais. Ce procédé coûteux et difficile nécessite une connaissance approfondie de la chimie de coordination des lanthanides. À cause de leur charge et de leur taille similaire, la séparation des différents lanthanides est un défi de taille. Pour cette raison, nous avons préparé des ligands polydentates qui agissent comme des donneurs « durs » d'électrons afin de lier les lanthanides. En variant l'angle de chélation, une certaine sélectivité peut être obtenue. De plus, en immobilisant ces ligands sur des supports solides, leur sélectivité et durabilité peut être améliorée pour donner une solution simple et « verte » au problème de l'extraction des lanthanides.

Abstract

Until the beginning of 21st century, lanthanides were considered to be the most difficult metals of the periodic table to work with. Due to the unpredictable coordination behavior of the lanthanide complexes, it was challenging for the chemists to know the exact nature of the complexes formed. However, the last decade has witnessed tremendous growth in the organometallic chemistry of these *f*-elements. Their unperturbed *f*-orbitals with large number of unpaired electrons have made them indispensable components in many modern day applications like catalysis, OLEDs, luminophores, MRI agents, magnetic materials, amongst others.

The coordination of electron deficient compounds to lanthanides is considered to be challenging due to the electrophilicity of these elements. Nevertheless, the interesting magnetic and optical properties shown by lanthanides makes it of interest to investigate the effect various ligands containing Lewis acidic moieties in order to expand the scope of their properties.

We decided to address this challenge by designing boron heterocyclic aromatic ligands for lanthanides that are able to satisfy both the electronic and steric requirements of these metals. Apart from achieving the coordination of these electron deficient boron compounds to lanthanides, we wanted to study their effect on the magnetic properties of the lanthanides. Initially, we synthesized a monoanionic boratabenzene ligand and studied its coordination to various lanthanide ions. A unique trisboratabenzene lanthanum complex was isolated and characterized. However, diboratabenzene lanthanide complexes were challenging to isolate and hence a sterically bulky 1-mesityl-4-*i*Pr-boratabenzene ligand was synthesized for this purpose. This bulky ligand showed some interesting reactivity towards bases and water.

We also synthesized several dianionic diboraanthracene ligands to isolate sandwich and triple-decker complexes of lanthanides. The interesting reactivity of these ligands to lanthanides was observed and the successful coordination of this electron deficient ligand

to lanthanides was achieved. An inverse sandwich and triple-decker complexes of lanthanum were studied.

We also investigated the design of ligands for the selective extraction of lanthanides from their ores. This is a challenging and expensive process where the knowledge of lanthanide coordination chemistry can highly profit. Due to their similar charge and size, it is difficult to separate individual lanthanides from their mixtures. We synthesized polydentate ethereal amides that act as hard donors and coordinate lanthanides. The selective extraction of smaller lanthanide ions was achieved by variation of *bite angle* of these ligands. The immobilization of the ligands on the solid support provided rigidity to the ligands and enhanced their selectivity and durability, thus providing an environmental friendly system for extraction.

Table of Contents

viii

List of Tables

List of Schemes

List of Figures

List of Abbreviations

$\{^{11}B\}$ = boron decoupled

$\{^{1}H\}$ = proton decoupled

Å = angstrom

APPI = Atmospheric pressure photoionization

BC = boracyclohexadiene

BB = borabenzene

COSY = NMR experiment correlating ^{1}H and ^{1}H nucleus

COT = cyclooctatetraene

Cp = cyclopentadienyl

cy = cyclohexyl

d = doublet

DCM = dichloromethane

dd = doublet of doublets

DFT = Density functional theory

DBA = diboraanthracene

DMF = dimethylformamide

DME = dimethoxyethane

DGA = diglycolamide

ESI = Electron spray ionization

FDGA = Furan-diglycolamide

FTIR = Fourier transform infrared spectroscopy

H = magnetic field

HOMO = highest occupied molecular orbital

iPr = isopropyl

LFSE = ligand field stabilization energy

J = spin-orbit coupling constant

KIT-6 = Korean Institute of Technology - 6

L = orbital angular momentum

LUMO = lowest unoccupied molecular orbital

m = multiplet

M = magnetization

MA = malonyl amide

Me = Methyl

Mes = 2,4,6,-trimethylphenyl

NMR = nuclear magnetic resonance

pc = pthalocyanin

Ph = phenyl

ppm = parts per million

r.t. = room temperature

REE = rare earth elements

s = singlet

SMM = single molecule magnet

SIM = single ion magnet

t = triplet

THF = tetrahydrofuran

TMS = trimethylsilane

*t*Bu = tertiary butyl

δ = chemical shift

Π = pi orbitals

σ = sigma orbitals

μ_B = Bohr magneton

Acknowledgements

I would like to take advantage of this occasion to thank some people who have greatly contributed to my journey at University Laval.

I would first of all like to thank my supervisor, Prof. Frédéric-Georges Fontaine, without whom this work could never have been done. Thank you very much for all the support provided over my years at Laval. I am extremely grateful to you for making me a part of your team. There are innumerable things that I have learnt from you in these years. Your guidance taught me the real meaning of research. Your multidimensional thinking and your way of solving problems have greatly influenced my thinking and personality. I really appreciate the freedom and support you give to your students, which helps them in developing independent thinking and research skills. I was very lucky to be one of your students.

I would like to thank my committee members – Profs. Kathryn Preuss, Dominic Larivière and Jesse Greener for serving on my candidacy and defense committee. Thank you for your helpful discussions.

I would like to thank all the members of chemistry department especially Pierre Audet for his help in NMR and MS spectroscopy. I would also like to thank Wenhua Bi for his help in collecting and interpreting X-ray crystallographic data. Thank you also to Professor Laurent Maron for work with DFT calculations.

I am grateful to Profs Freddy Kleitz and Dominic Larivière for their cooperative work during our collaborative project. I would like to thank Justyna Florek and Gabrielle Cantin for their teamwork.

I have worked with a number of excellent chemists in Fontaine group. I would like to thank all of them for providing a healthy and joyful environment for working. All of you have always been helpful and cooperative. I would like to specially thank MAL and MAC for their helpful discussions and beautiful company. I am glad to have been able to work with

Chapter 1 - Introduction

Ligand design is an important aspect of organometallic chemistry. Although it is one of the most explored areas of chemistry, enormous amounts of efforts are still being directed towards this field and remain one of the preferable topics for many research groups. It not only involves the modification of the pre-existing ligand molecules but also includes the synthesis of new molecules and the study of their properties. The importance of ligand design lies in the changes that a ligand brings in the properties of a metal ion upon coordination. The geometry of the metal complex, the splitting of the orbitals of the metal ions, their reactivity and physical properties are all dictated by the type of ligand coordinated to them.

The creation of new ligands is always directed towards a particular aim. Most of the work in this field has been focused in increasing catalytic efficiency of the complexes for many purposes, such as increasing the strength and durability of different polymers or increase the yield and activity of pharmaceutical products. In addition, many environmental problems like CO_2 capture, industrial waste management and generation of green sources of energy are being addressed by ligand design approaches to catalysis. There are various parameters of a ligand molecule that need to be taken care of while designing them for a particular application. They include the steric and electronic properties, their binding mode, the coordinating atoms and their oxidation state.

Another field that might take advantage of ligand design is molecular magnetism. With the advancements of informatics and electronics, there has been an increasing demand for scaling up the capacity of memory storage devices while keeping a limit on their size. Until the beginning of the 21st century, the miniaturization of these storage devices was achieved by decreasing the size of the bulk magnets into thin sheets and small grains so as to reduce any loss of magnetism by reorientation of neighboring domains. But below a certain limit, the size of the magnetic grains cannot be reduced as each grain behaves as an independent domain and hence further reduction in the size will cause the domain to shatter and loose its magnetism. This has led scientists to look for alternative ways of producing efficient

magnets. The advancements in the field of molecular magnetism in the last two decades have provided a new route for addressing this issue. The study of molecular magnetic properties of different metal complexes have shown that each single metal center can act as independent magnet provided it has unpaired electrons and an appropriate coordination geometry. Recent advancements in the field have given a great deal of information about the choice of ligands and metal ions that can be used for making better molecular magnets.

The best molecular magnets obtained so far come from lanthanide complexes. The high-unpaired spin of lanthanides along with their unquenched orbital angular momentum has been shown to provide interesting magnetic properties when having the right symmetric geometry. Ligand design plays a very important role in optimizing the magnetic properties of these metal centers. For transition metals, a low coordination geometry was found to be better than aromatic π coordinate sandwich complexes as it helps to preserve the orbital angular momentum of the metal centers, thereby increasing the potential barrier for thermal relaxation. However, for lanthanides the aromatic π coordinate sandwich and triple-decker complexes have provided the best molecular magnets. These types of coordination geometries have been able to increase the anisotropies of lanthanide ions and the superexchange between them, thus decreasing both the thermal and non-thermal relaxation processes.

In our approach, we aim to design aromatic ligands that can better the molecular magnetic properties of lanthanides upon coordination. We want to use boron as a heteroatom in different aromatic molecules and study their coordination behavior to different transition metals and lanthanides. We also want to study the effect the boron atom will have on the magnetic properties of these complexes as compared to their carbocyclic analogues. It has been very well established that the introduction of a boron atom in aromatic molecules lowers the energy of its lowest unoccupied molecular orbital (LUMO), so we expect these ligands to show stronger binding to the metal centers as compared to their normal arene analogues. This stronger binding can effect the communication between the metal centers when used in the bridging position and hence modify their magnetic properties. However, the electron deficient nature of boron atom makes it very prone to be attacked by various nucleophiles and as a result makes it challenging to synthesize stable boron lanthanide

complexes. So proper synthetic approaches need to be developed to synthesize boron heterocycles of interest. But in order to synthesize these boron heterocycles and study their coordination behavior, background knowledge of different boron heterocycles needs to be gathered. A study of the coordination behavior of lanthanides with different aromatic ligands will be necessary for successful coordination of these ligands to lanthanides.

1.1 Outline of Thesis:

This thesis will discuss about the synthesis of various boron heterocyclic ligands and study their coordination behavior to transition metals and lanthanides. The aim of designing these ligands is to study the effect of introducing a boron atom into the aromatic coordination sphere of lanthanides on their magnetic properties. This thesis is divided into eight chapters. The motivation behind the work discussed in the thesis is presented in Chapter 1.

In Chapter 2, I will present the background needed to understand the novel results presented. It will include a discussion on the physical properties and coordination properties of lanthanides and a literature background of boron heterocycles.

In Chapter 3, a brief summary of the various experimental techniques used in the research will be presented.

A study of the synthesis of boratabenzene ligands and their coordination mode to transition metals and lanthanides is presented in chapter 4.

The synthesis of a bulky boratabenzene ligand is presented in chapter 5. The interesting reactivity of the ligand, its precursors and their coordination chemistry to transition metals is discussed. The results of this chapter have been published as Mushtaq, A; Wenhua, B; Légaré, M.-A.; Fontaine, F-G. "Synthesis and reactivity of novel mesityl boratabenzene ligands and their coordination to transition metals." *Organometallics*, **2014**, *33*, 3173-3181. All the experimental work, including the design of experiments, the synthesis, the isolation and the characterization of all the molecules described in the manuscript was done by myself. I wrote the manuscript, with Frédéric-Georges Fontaine helping in the editing.

Wenhua Bi contributed by collecting the X-ray data and solving the X-ray structures of the metal complexes. The DFT calculations were done by Marc-André Légaré.

In Chapter 6, the synthesis of various dianionic 9,10-diboraanthracene ligands is discussed. A study of the coordination behavior of these ligands with lanthanides to make the sandwich and triple-decker complexes are presented.

Chapter 7 describes the results of a collaborative project between our research group and that of professor Freddy Kleitz and Dominic Larivière at University Laval. A discussion on the importance of ligand design for the selective extraction of lanthanides is presented. Some new ligands and their extraction properties have been discussed. Our group developed the concept of alteration of the *bite angle* of ligands for selective trapping of lanthanides by exploiting the differences in ionic radii of the lanthanide ions. The synthesis of ligands was carried in our lab.

Section 7.3, explaining the outcome of the ligand design aspect, has been published as an article in RSC advances, where I am one of the co-authors. I would like to acknowledge Justyna Florek, first author of the manuscript, and Gabrielle Cantin for their important contribution to the latter work. Indeed, I synthesized the ligands and contributed to the design of the experiments, but the synthesis of the solid supports, the grafting of the ligands on the support and the solid-liquid extraction studies have been carried out by Justyna Florek, a postdoctoral fellow working with Larivière and Kleitz groups. Gabrielle Cantin also contributed in performing the liquid-liquid extraction studies.

In Chapter 8, the work discussed in the thesis will be summarized up with a conclusion and future perspective of the work will be presented.

Chapter 2 - Literature Review

2.1 Introduction of Lanthanides

The history of lanthanides dates back to 1787 when a black mineral was obtained from ytterby Sweden. This mineral was named as gadolinite after Johan Gadolin, who isolated an impure form of yttrium oxide from this ore in 1794.[1,2] In 1803, J. J. Berzelius, M. H. Klaproth and W. Hisenger independently isolated a new oxide (ceria) containing lanthanum, cerium, presodymium, neodymium and europium. However it was Henry Moseley who demonstrated using X-ray spectroscopy that there were 14 elements between lanthanum and hafnium. They were initially known as rare earth elements (REE) but this terminology does not refer to their abundance in the earth's crust.[3]

Lanthanides are also known as f-block elements because of the gradual filling of the electrons in the 4*f*-orbitals. They have a general electronic configuration given by [Xe] $4f^n6s^2$. The electronic configuration of lanthanides shows some irregularities and is given in Table 2-1 below. Lanthanides have a universal tendency to exhibit a +3 oxidation state, although the +2 (Sm, Eu, Tm, Yb) and +4 (Ce, Pr, Tb) oxidation states are seen for some of the lanthanide atoms since these configurations will lead to have the 4*f* orbitals either empty, half-filled or completely filled. For example Ce^{4+} has $4f^0$, Eu^{2+} has $4f^7$, and Yb^{2+} has $4f^{14}$ configuration. The preference for the +3 oxidation state and their similarity in size makes it challenging to separate individual lanthanides from their ores. Another important feature of lanthanides is the decrease in their ionic radius with the increase in atomic number, also known as the lanthanide contraction. This phenomenon occurs because of the insufficient shielding of the outer electrons (6*s*, 6*p*) by 4*f* electrons. The 4*f* orbitals are highly diffused and as a result the electrons in these orbitals do not stay well inside the electronic core and do not shield the outer electrons, as can do the electrons in the 6*s* and 6*p* orbitals. Thus when the atomic number increase the effective nuclear charge and hence the

attraction between the nucleus and the outer electrons increases causing a shrinking in the atomic and ionic radius.[4]

Table 2-1: Selected properties of Lanthanides and their ions.

Atomic Number	Element	Symbol	Neutral Valence Electrons	M^{3+} Valance Electrons	Ionic Radius $(M^{3+}, Å)$	Oxidation State of Ln ions
57	Lanthanum	La	$5d^1 6s^2$	-	1.06	+3
58	Cerium	Ce	$4f^1 5d^1 6s^2$	$4f^1$	1.03	+3
59	Praseodymium	Pr	$4f^3 6s^2$	$4f^2$	1.01	+3
60	Neodymium	Nd	$4f^4 6s^2$	$4f^3$	0.99	+2, +3, +4
61	Promethium	Pm	$4f^5 6s^2$	$4f^4$	0.98	+3
62	Samarium	Sm	$4f^6 6s^2$	$4f^5$	0.96	+2, +3
63	Europium	Eu	$4f^7 6s^2$	$4f^6$	0.95	+2, +3
64	Gadolinium	Gd	$4f^7 5d^1 6s^2$	$4f^7$	0.94	+3
65	Terbium	Tb	$4f^9 6s^2$	$4f^8$	0.92	+3, +4
66	Dysprosium	Dy	$4f^{10} 6s^2$	$4f^9$	0.91	+2, +3, +4
67	Holmium	Ho	$4f^{11} 6s^2$	$4f^{10}$	0.89	+2, +3
68	Erbium	Er	$4f^{12} 6s^2$	$4f^{11}$	0.88	+3
69	Thulium	Tm	$4f^{13} 6s^2$	$4f^{12}$	0.87	+2, +3
70	Ytterbium	Yb	$4f^{14} 6s^2$	$4f^{13}$	0.86	+2, +3
71	Lutetium	Lu	$4f^{14} 5d^1 6s^2$	$4f^{14}$	0.85	+3

Despite of their tendency to form +3 ions, the lanthanides do not resemble the transition metals. The free metals are more reactive and in this respect resemble more to alkali and alkaline earth metals. They all evolve hydrogen upon reaction with water. The trivalent lanthanide ions are hard Lewis acids and as a result they prefer to bind hard Lewis bases.[4] The hard donors like fluoride, oxygen, and nitrogen form stable complexes with lanthanides; however, in aqueous solutions the complexes with halogen, nitrogen and sulphur donors are not stable. It has been established that the nature of the bonding in these complexes is electrostatic. The interaction of ligands with the $4f$ orbitals is absent as they are deeply embedded, thus minimizing the ligand field stabilization energy (LFSE) and reducing the overall stability of the complex. Another consequence of the low LFSE in lanthanides is their flexible coordination environment. These tripositive ions are larger in size as compared to transition metal ions, and as a result their coordination number is high and can range from 6 to 9 and even get to a 12 coordination number in some of the complexes. However, the coordination number may decrease as we move towards the end of the series. This effect is attributed to the decrease in the size of the lanthanide ions along the series.

The trivalent lanthanide ions exhibit excellent spectroscopic properties. They show luminescence in the visible and near infrared regions when irradiated with ultraviolet light. Their emission spectra have fine lines, which result in high color purity. The fascinating emission properties of these lanthanides can be attributed to the f-f forbidden transitions. Since $4f$ orbitals are embedded in the core, they do not participate in bonding between the ligand and the metal ion. As a result, the emission spectra of the lanthanide complexes are sharp lines like that of free atoms or ions. The fascinating luminescent properties of lanthanides make them useful for several applications like OLEDS, optical fibers for telecommunication, biological imaging, and contrast agents, amongst others.[5]

2.1.1 Extraction of Lanthanides

The process of obtaining pure lanthanide metals is very challenging, unlike the extraction processes for transition metals. The similarities in the physical and chemical properties of lanthanides make it very difficult to separate individual lanthanides from their mixtures.

The industrial procedure for the extraction and purification of REEs involves multiple steps. The primary metallurgical process involves extraction and pre-concentration of lanthanides from their ores in the form of leachate. The secondary processes are then used to separate individual lanthanides from the leachate.

The most commonly used methods for purifying lanthanides are the solvent extraction and ion exchange chromatography.[6–8] Both these methods exploit the slight difference in the size of Ln^{3+} for purification. Ion exchange chromatography has been used to produce high purity single rare-earth solutions for electronics and analytical applications. It involves the impregnation of lanthanides on an ion exchange resin, which are then eluted by using complexing agents such as citrate or α-hydroxy-butyrate ions.[9] But this technology cannot be used for large-scale production of pure lanthanides. In solvent extraction, different neutral, cationic and anionic molecules have been used to coordinate the lanthanide ions in aqueous acidic solutions (HNO_3 and HCl solutions), these complexes are then extracted with organic solvents (hexane and kerosene).[10–13] The smaller lanthanide ions have larger hydration energies and are therefore extracted first in the organic phase as compared to the larger ions with lower hydration energies.[14–16] However, these liquid-liquid extractions use large volumes of solvents for repeated cycles of extraction. Also the ligands used (napthalic acid, 2-ethylhexyl phosphonic acid, 2-ethylhexyl esters) are not very selective for extracting a particular lanthanide. Thus in-order to isolate individual lanthanide ions further purification processes are needed.

The biggest producer of lanthanides is China. They have 51% of the total reserves of REEs. But due to the efficient optoelectronic and magnetic properties of lanthanides, their global consumption rate and hence, the demand for pure REEs has dramatically increased in the last two decades. As a result the export of REEs from China has decreased which had for effect to increase its cost. This has forced many countries to find alternative sources of REEs. The recovery of REEs from nuclear fuel wastes and their recycling from industrial wastes is a viable alternative many countries are looking into. But this will require the development of efficient techniques for isolating individual lanthanides from their mixtures and decreasing the production of large quantities of solvent wastes. One of the focuses of

our research group is to address these problems, which will be discussed in more details in Chapter 7.

2.1.2 Magnetic properties of lanthanides

An important characteristic feature of lanthanides is their interesting magnetic properties. The two strongest permanent magnets are $SmCo_5$ and $Nd_2Fe_{14}B$ and both are clusters including lanthanide ions and transition metals.[17] They have been used commercially for producing strong static magnetic fields. Lanthanide based magnets have also been used for heavy weight lifting, in storage devices, speakers and microphones. The large magnetic moments of these lanthanide tripositive ions arise from the large number of unpaired electrons (S) and high value of orbital angular momentum (L) of f orbitals. The embedded nature of the $4f$ orbitals prevents them from being affected by the coordination sphere of the lanthanides ions. Thus when coordinated with different ligands, the $4f$ orbitals remain degenerate and do not undergo crystal-field splitting. This helps them in preserving their unpaired spins and their orbital angular momentum.[4,18] As a result, the total spin (S) and the total orbital magnetic moment (L) couples with each other giving rise to a higher resultant magnetic moment (Figure 2-1). This coupling is known as spin-orbit coupling or Russel Saunders coupling and is denoted by a constant (J) called as total angular momentum.
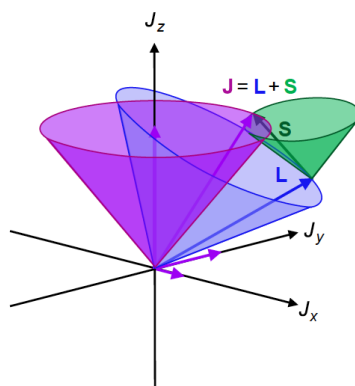
Figure 2-1: Representation of spin (S), orbital (L) and spin-orbit coupled (J) angular momentum.[19]

The value of J is calculated from the equation $J = L + S$, where $L = \Sigma_i l_i$ and is the value of sum of orbital angular momentum and varies from +3 to -3 for f orbitals and $S = \Sigma_i s_i$ is the total spin angular momentum and is the sum of spin of all the unpaired electrons. For

example, Dy^{3+} ion has an electronic configuration of $4f^9$, thus it has 5 unpaired electrons corresponding to S = 5(1/2). The orbital angular momentum for 9 electrons in seven $4f$ orbitals will be L = 3 + 2. (For the first seven electrons in f orbitals the value of orbital angular momentum will be calculated by the sum of angular momentum of all the seven f orbitals as each of them has one electron. Thus, L = 3 + 2 + 1 + 0 + (-1) + (-2) + (-3), which equals to zero. When eighth and ninth electron is added they will contribute an angular momentum of 3 + 2, giving a total value of L = 5). Therefore after spin orbit coupling it will have a total angular momentum of J = (5/2) + 5 = 15/2. In case of transition metal ions, the d-orbitals lose their degeneracy due to the crystal field splitting causing loss of the orbital angular momentum and hence, only unpaired spins are able to contribute to their magnetic moments.[17]

With the recent development of molecular magnets, the importance of the spin-orbit coupling for enhancing the molecular magnetic behavior of lanthanides has become more preeminent. The higher values of spin–orbit coupling not only increases the magnetic moments (M) of lanthanide ions but also gives them high intrinsic magnetic anisotropy which is an important parameter for efficient molecular magnets. Thus, even in absence of the applied magnetic field, the energy levels of the Ln^{3+} ions are not degenerate but are split into positive and negative energy levels ($\pm m_J$) that are separated by an energy barrier (U_{eff}) as shown in Figure 2-2 A. This splitting cause the Ln^{3+} ions to have their magnetic moments aligned in a particular direction, which is referred as uniaxial magnetic anisotropy. Thus when an external magnetic field is applied in the same direction, the molecule becomes magnetized and all its unpaired spins are aligned in the direction of the applied field. In other words, all the spins are transferred to the lowest energy ground state (m_J). The higher the value of ground state (m_J) the higher is the magnetic moment.[19] The time required to lose this magnetization is given by the Arrhenius equation:

$$\tau (T) = \tau_0 \exp (U_{eff}/k_B T)$$

Where τ_0 = characteristic of a material, U_{eff} = potential barrier, k_B = Boltzmann's constant, T = temperature.
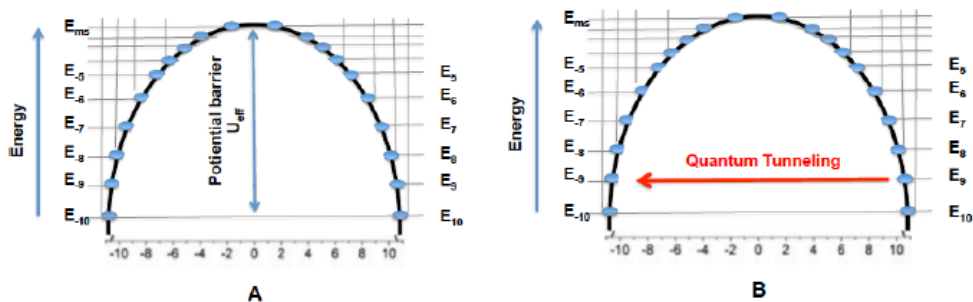
Figure 2-2: A) Zero field splitting of spin states of metal ions B) Quantum tunneling of spins through the potential barrier.

Since the magnetic anisotropy of the Ln^{3+} ions is governed by the occupancy of $4f$ orbitals, the shape of the f-electron charge cloud of these ions can be used to predict the type of geometry that can enhance their anisotropic ground states. An interesting study of this concept has been carried out by Rinehart and Long in 2011. According to their studies, the shape of the f-electron charge cloud for Ce^{3+}, Pr^{3+}, Nd^{3+}, Tb^{3+}, Dy^{3+} and Ho^{3+} is oblate (equatorially expanded) and hence, their anisotropy can be maximized in a sandwich geometry where the ligand electron density is concentrated above and below the xy plane (Figure 2-3). This will help to minimize the repulsion between the ligand and the f-electron clouds. While as for Pm^{3+}, Sm^{3+}, Er^{3+}, Tm^{3+} and Yb^{3+}, the f-electron charge cloud is prolate (axially expanded) and hence an equatorially coordinating geometry will be preferable for them so as to minimize the repulsion with the axially located f-electron density (Figure 2-3).[20] This concept has indeed proved to be a success with the report of molecular magnetic behaviors of sandwich complexes of Dy^{3+} and Ho^{3+} with cyclooctatetraenyl ligands.
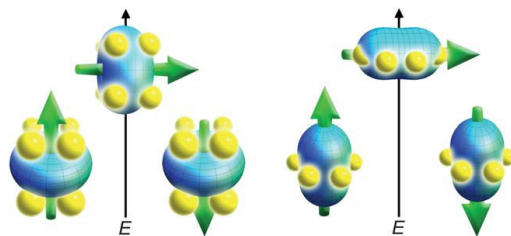
Figure 2-3: Representation of electron density and anisotropy axis of $4f$ ions. Depictions of low- and high-energy configurations of the f-orbital electron density with respect to the crystal field environment for a 4f ion of oblate (left) and prolate (right) electron density. The green arrow represents the orientation of the spin angular momentum coupled to the orbital moment.

These sandwich complexes have not only high blocking temperatures (the temperature below which the magnetic relaxation is slower than 100 seconds) of 5 - 12 K but have also been useful for studying the different magnetic relaxation pathways. The sandwich complexes with substituted cyclooctatetraenyl (COT) and pthalocyanin (Pc) ligands have highlighted the importance of symmetry for achieving high blocking temperatures.[21,22] Although the sandwich complexes Li[(COT*)$_2$Dy] (COT* = 1,4-bis(trimethylsilyl)cyclooctatetraenyl) and K[(COT)$_2$Dy] exhibit higher anisotropies as expected for oblate ions, the high symmetry of the prolate ion with Er^{3+} is much more important and accounts for the observation of higher blocking temperature of 12 K for K[(COT)$_2$Er]. The D_8 symmetry of K[(COT)$_2$Er] as compared to the D_4 symmetry of K[(COT*)$_2$Er] introduces a higher energy difference between the ground state and the first excited state and thus slows down its magnetic relaxation (Figure 2-4 A, B).[23,24] Although increasing the potential barrier decreases the thermal relaxation of these lanthanide molecular magnets, there is another important relaxation pathway known as quantum tunneling that causes these molecular magnets to lose their magnetization even at low temperatures. In quantum tunneling, the electrons move through the potential barrier (Figure 2-2 B). This occurs by the mixing of the positive and negative spin states caused by the presence of transverse magnetic fields. However, an increase in the symmetry of the molecule decreases the transverse components of magnetic fields and hence decreases quantum tunneling, as has been seen for the K[(COT)$_2$Er] complex. Another important factor that has been found to decrease the quantum tunneling is the increase in the exchange interaction between two Ln^{3+} ions. An interesting example is {(Me$_3$Si)$_2$Tb(THF)$_2$}$_2$(μ-η^2:η^2-N$_2$)$^-$ complex which has a blocking temperature of 14 K (Figure 2-4 C). The quantum tunneling in this complex is highly reduced due to the coupling of magnetic moments of two terbium centers by the nitride radical.[25,26]

12
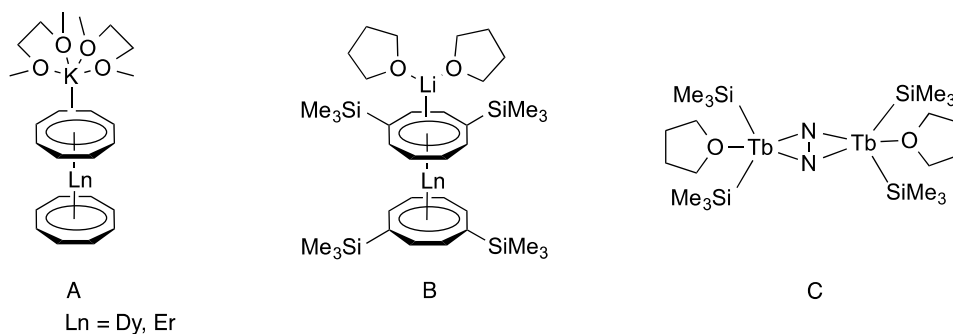
Figure 2-4: A, B) Cyclooctatetraenyl dysprosium and erbium sandwich complexes. C) Terbium nitride dimer.

2.1.3 Organometallic Chemistry of Lanthanides

Initially the bonding in lanthanides was considered to be predominantly electrostatic. However, in 1954 Wilkinson and Birmingham reported the first π-bonded tris(cyclopentadienyl)Ln complex which exhibited significant covalent ligand-lanthanide bond character and thus inspired the development of lanthanide organometallic chemistry.[27] The predominant electrostatic nature of bonding in organolanthanide complexes is due to the insignificant overlap of valence $4f$ orbitals with ligand orbitals. As a result, these complexes are highly reactive and are attractive candidates for catalysis. Their weak coordination behavior is also reflected by their paucity to bind CO, olefins and arenes, their irregular coordination geometries and facile ligand scrambling.[17]

Initially the cyclopentadienyl chemistry of lanthanides dominated the literature but for the last two decades all types of organic ligands have been coordinated to lanthanides. These include alkyls, aryls, heteroaryls and carbenes.[28,29] These σ-bonded carbon complexes of lanthanides are relatively unstable compared to π-complexes. Nevertheless, the chemistry of these complexes is very interesting but we are more focused on the organometallic chemistry of lanthanides with various π-anionic ligands. The coordination chemistry of lanthanides with π-ligands mostly includes their cyclopentadienyl (Cp) and cyclooctatetraenyl (COT) complexes.[29–34]

2.1.4 Cyclopentadienyl lanthanide chemistry

The coordination of cyclopentadienyl ligands to lanthanides was initially attempted to isolate ferrocene analogues, but Wilkinson observed instead the formation of triscyclopentadienyl lanthanide (LnCp$_3$) complexes.[27,35] This was attributed to the tripositive nature and the large coordination sphere of lanthanide ions. The selective coordination of one or two cyclopentadienyl ligands to lanthanides was later achieved by comproportionation reaction between LnX$_3$ and LnCp$_3$ or by selectively reacting two equivalents of the cyclopentadienyl ligand with lanthanide halides (Scheme 2-1).[36–38]

$$A\ LnCl_3\ +\ 5\ NaC_5H_5\ \xrightarrow{\text{THF}}\ (C_5H_5)_3Ln\ +\ 3\ NaCl$$

$$B\ LnCl_3\ +\ 2\ NaC_5H_5\ \xrightarrow{\text{THF}}\ (C_5H_5)_2LnCl\ +\ 2\ NaCl$$

$$C\ 2\ (C_5H_5)_3Ln\ +\ LnCl_3\ \xrightarrow{\text{THF}}\ 3\ (C_5H_5)_2LnCl$$

Ln = Sm, Gd, Tb, Dy, Ho, Er, Tm, Yb, Lu
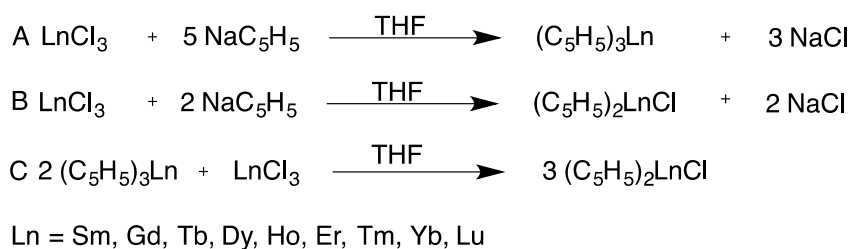
Scheme 2-1: Reactions for the synthesis of tricyclopentadienyl (A) and dicyclopentadienyl (B, C) lanthanide complexes.

Due to the trivalent nature of lanthanides, straight metallocenes are not isolated and instead the dicyclopentadienyl lanthanide complexes always have a halide ion bonded to it. In coordinating solvents they exist as solvates while in non-coordinating solvents they form dimers.[39–46] A study of magnetic properties of the dimers of dysprosium revealed that they behave as single molecule magnets (Figure 2-5 A). They show thermal relaxation above 6 K but below this temperature they lose their magnetism by quantum tunneling.[47] Although this dimer is symmetric in nature, the geometry is not appropriate for quenching any transverse fields. Also, the chloride bridges are not able to enhance the superexchange between the dysprosium centers. However, with a bipyrimidal radical as bridging ligand significant communication is observed between the two lanthanide centers (Figure 2-5 C), thus giving hysteresis loops between 2 and 7 K. Introduction of a benzotriazolate radical (Figure 2-5 B) was not able to enhance superexchange and showed predominant quantum tunneling after 4K.[48] These studies suggest that if the bridging ligand between two dysprosium atoms is able to increase the superexchange, then some interesting trends might be observed in their magnetic properties. Indeed, such an effect has been observed with

14

$\{(Me_3Si)_2Ln(THF)_2\}_2(\mu\text{-}\eta^2:\eta^2\text{-}N_2)^-$ complexes of dysprosium and terbium where the bridging radical is more localized than the bipyramidal ligand and increases the superexchange between the metal centers which reduces the quantum tunneling in them and gives a blocking temperature of 8 K and 14 K, respectively (Figure 2-5 C). [26,49] Thus not only the presence of radical, but also the geometry of the ligand containing the radical plays an important role in optimizing anisotropies.
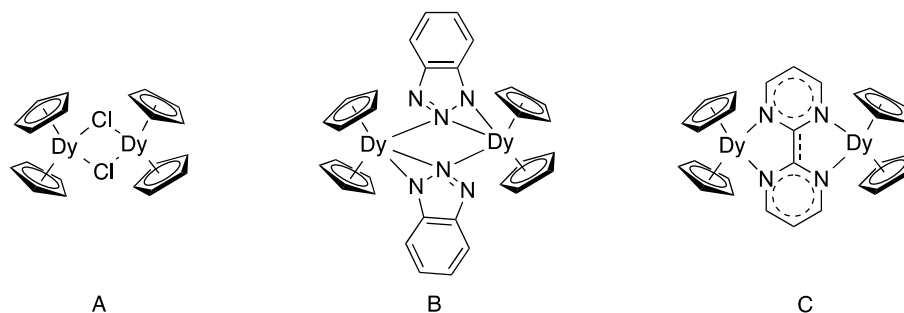
Figure 2-5: Dicyclopentadienyl lanthanide dimers with chlorides (A), benzotriazolates (B) and bipyrimidil C) bridges.

The tricyclopentadienyl lanthanide complexes have more or less spherical geometry and hence do not enhance the intrinsic anisotropy of lanthanide ions. As such there are no significant reports of study of molecular magnetic properties of these complexes. However, recently Long and Evans were able to successfully reduce the lanthanide center in $Ln(C_5Me_5)_3$ complexes to the +2 oxidation state. The dysprosium and holmium complexes after reduction exhibit magnetic moments of the order of 11.3 μ_B and 11.4 μ_B respectively. These high values of magnetic moment of a single metal center are attributed to the addition of the electron into the $5d$ orbital, which gives them higher values of spin-orbit coupling (J = 21/2) that are in accordance with the observed values of magnetic moment.[50] Thus, it provides important information about the method of increasing the magnetic moment of individual metal centers which when coupled with appropriate geometry can furnish interesting molecular magnets and give some new insights into the electronic structure of such complexes.

2.1.5 Cyclooctatetraenyl lanthanide chemistry

The cyclooctatetraenyl (COT^{2-}) has played a preeminent role in organolanthanide chemistry for the last four decades. This 10π dianionic ligand has been able to satisfy both the steric as well as the electronic needs of large metal ions. The coordination of COT^{2-} to rare earths was first observed by Streitwieser after isolating the $U(COT)_2$ sandwich.[51] Later, in 1969 Hays, Thomas, Mores, Hodgson joined him to report the COT^{2-} sandwich complexes for all lanthanides.[52–54] Synthesized by simple salt metathesis of $LnCl_3$ with alkali metal salt of cyclooctatetraenyl, these sandwich complexes are extremely pyrophoric and decompose on heating above 160 °C. Their insolubility in organic solvents made it difficult to characterize these complexes initially, but coordinating solvents help obtaining crystals of these complexes, which were studied by X-ray crystallography. The lanthanide ions in these complexes were found to bind both the COT^{2-} rings in a η^8 conformation. However, since these sandwich complexes were anionic, there was always a solvated alkali metal ion associated with the complex (Figure 2-6 A).[55–58] The anionic nature of these sandwiches promoted the formation of multidecker complexes, as observed with erbium and ytterbium (Figure 2-6 B).[56]
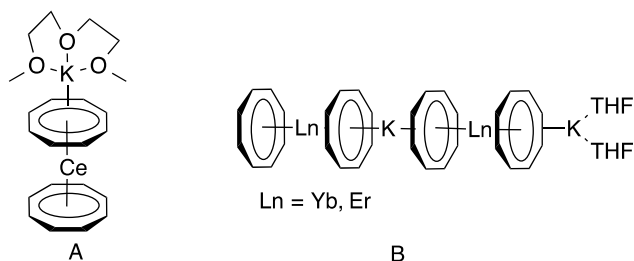
Figure 2-6: Sandwich (A) and multidecker (B) lanthanide cyclooctatetraenyl complexes.

J.D. Jamerson (1974) reported the first mixed sandwich of erbium with cyclooctatetraenyl and cyclopentadienyl ligand.[43,59–61] Unlike biscyclooctatetraenyl complexes, these heteroleptic complexes form bent sandwich structures (Figure 2-7 A). Thus variously substituted cyclopentadienyl ligands were used to form straight sandwich complexes (Figure 2-7 B, C).[62–70]

16
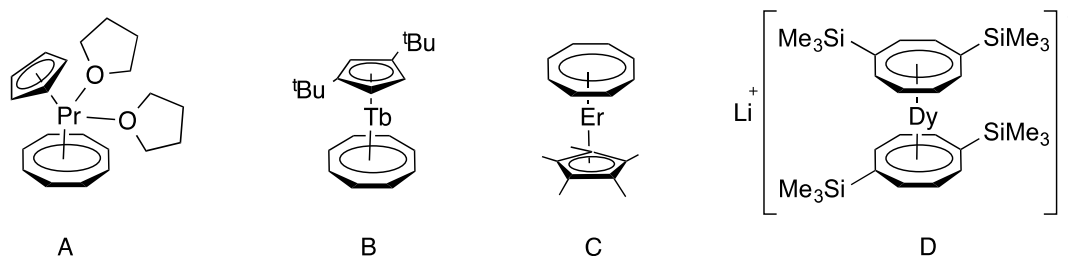
Figure 2-7: A, B) Effect of ligand size on planarity of COTLnCp complexes. C, D) First sandwich single ion magnets of lanthanides.

Although Cesca (1976) and Cloke (1997) had observed the formation of triple-decker complexes of lanthanides with different derivatives of cyclooctatetraenyl ligands, they were not able to characterize them structurally.[71,72] Only in 2010 was the first triple-decker $(COT^*)_3Nd_2$ (COT^* = 1,4-bis(trimethylsilyl)cyclooctatetraenyl) complex was characterized by X-ray crystallography. This complex was obtained from the reaction of $Li(COT^*)_2Nd$ sandwich with $CoCl_2$ (Scheme 2-2)[73]. This complex consists of three parallel (COT^*) rings. The terminal COT^* rings are η^8 coordinated to each neodymium ion while as the central COT^* ring bridges the two metal centers and exhibits η^8 binding to both of them.
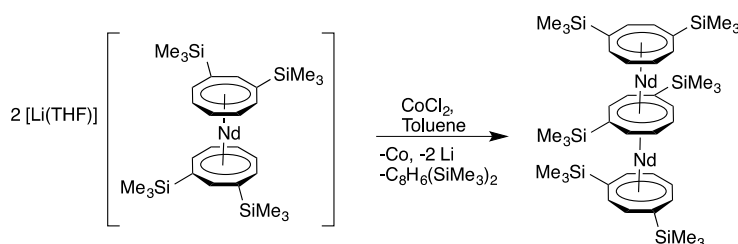
Scheme 2-2: Synthesis of triple-decker of cyclooctatetraenyl lanthanide complexes.

However, it was only after the remarkable discovery of dysprosium and erbium single ion magnets in 2011 that renewed the interest in the sandwich and triple-decker COT-lanthanide chemistry. The (COT)Er(Cp*) complex was identified as single ion magnet by Sang Gao.[62] Consisting of a butterfly shaped hysteresis loop at 1.8 K up to 5 K this molecule surpassed the magnetic behavior of all the reported transition metal and lanthanide single molecule magnets (Figure 2-7 C). Later in the same year Muralee Murugesu reported the single molecule magnetic behavior of the heterobimetallic Dy(COT*)₂Li(THF)(DME) sandwich (Figure 2-7 D).[74] These results and the study of lanthanide pthalocyanin sandwich and triple-decker complexes suggested that the

molecular magnetic properties of lanthanide complexes can be improved firstly by increasing the anisotropy of the molecule which can be achieved by making more symmetrical complexes. Secondly, the two lanthanide ions in the same molecule must be bridged together in such a way that the superexchange between them increases so as to reduce the low temperature relaxation by quantum tunneling.[75–78] Thus in the last four years the sandwich and triple-decker complexes of dysprosium, terbium and erbium with both COT^{2-} and COT^{*2-} ligands have been synthesized and studied for their magnetic properties.[24,74,79–82]

The straight sandwich complexes of lanthanides are very symmetrical and hence ideal for optimizing the anisotropy of the oblate ions (Tb, Dy, Ho). The triple-decker complexes with cyclooctatetraenyl ligands not only provide a symmetrical geometry but also bridges together two lanthanide ions, which can show superexchange through the bridging COT^{2-} ligand. This effect has been observed in the sandwich complex of $Li(COT^*)_2Dy$ that behaves as single ion magnet with blocking temperature of 3.7 K and in the triple decker complex $(COT^*)_3Dy_2$ where the quantum tunneling was found to be reduced to a greater extent. The magnetic measurements, as well as the *ab-initio* calculations, proved that the covalent bonding character between the dysprosium ions and the bridging COT^{*2-} ligand promoted the superexchange between the metal centers.[74,80] The effect of superexchange on the quantum tunneling and the blocking temperature was more evident in sandwich and triple-decker complex of Er^{3+} ion, demonstrated by Murugesu. An increase of 4 K in the blocking temperature was observed when the two erbium ions where coupled on $(COT^*)_3Er_2$, which shows hysteresis up to 12 K. [24] However, the $K(COT)_2Er$ sandwich was found to possess a higher blocking temperature of 10 K (Figure 2-8).[79,83] It was suggested that the $K(COT)_2Er$ complex has a high D_{8d} symmetry as compared to the D_{4h} symmetry of $Li(COT^*)_2Ln$. Due to trimethylsilyl groups the anisotropic axis changes from being axial to lateral and hence reduces their symmetry (Figure 2-8). These studies prove the importance of symmetric sandwich and triple-decker geometry for improving the magnetic properties of lanthanides.
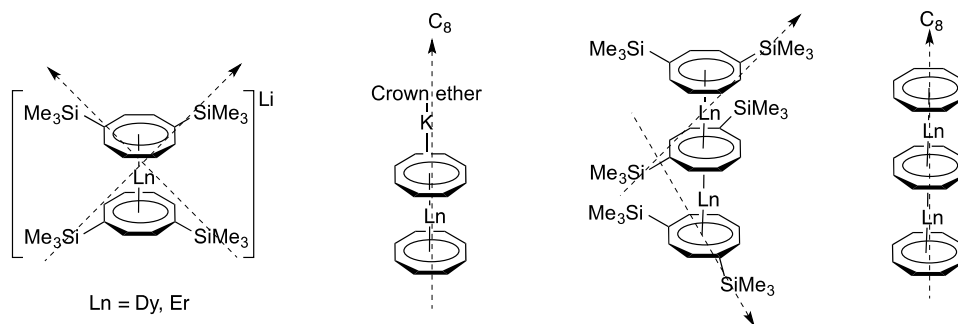
Figure 2-8: Anisotropic axis of multidecker lanthanides complexes with substituted and non-substituted COT ligands.

2.2 Boron heterocycles

As the name indicates boron heterocycles are aromatic and non-aromatic rings in which one or more boron atoms are present. The history of boron heterocycles dates back to 1965 when the iron metallocarborane complex $(NMe_2)[Fe(C_2H_9B_{11})_2]$ was synthesized, in an attempt to isolate metal-boron σ-bonded complexes.[84] The tendency of these carborane ligands to coordinate transition metals in a 6π aromatic pattern make them analogues of carbocyclic π ligands (like the benzene and cyclopentadienyl ligands).[85–87] R. N Grimes also demonstrated that such ligands could produce multidecker transition metal-carborane complexes (Figure 2-9 A).[88]

Nevertheless, G. Herberich renewed the interest in boron-metal chemistry in 1970 by reporting a cobalt sandwich featuring two planar C_5H_5B rings (Figure 2-9 B).[89] The efficient coordination of this molecule, known as boratabenzene, to transition metals gave a new face to coordination chemistry.[90–93] Several other mono and polycyclic boron heterocycles containing one or two boron atoms have been reported (Figure 2-9 C, D).[94–100] However, the study of their coordination behavior remains very limited.
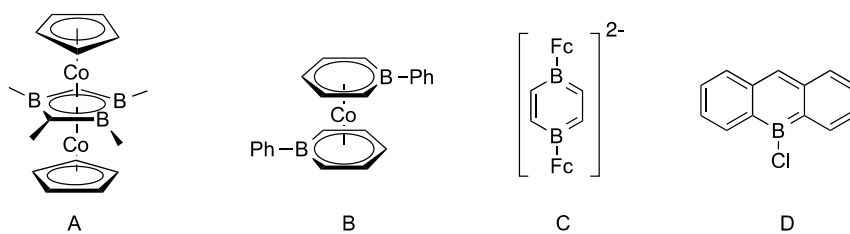
Figure 2-9: A) Cobalt carborane and B) boratabenzene complex C) 1,4-diboratabenzene D) 9-boraanthracene

However, our interest is more focused on boratabenzene and 9,10-diboraanthracene as they can be used as monoanionic and dianionic aromatic ligands in place of cyclopentadienyl ion and COT^{2-}, respectively, for coordinating them to lanthanides. These ligands will be able to saturate the lanthanide ions both electronically and coordinatively to form straight sandwich and triple-decker complexes. In addition to that, the low energy LUMO of these boron heterocycles will help to increase their bonding with lanthanides that can in turn enhance the superexchange at bridging positions. Background knowledge of these two boron heterocycles is discussed below.

2.3 Borabenzene

2.3.1 Structure of Borabenzene

The term borabenzene is used for a molecule that consists of a cyclic benzene ring in which one C-H fragment has been replaced by a boron atom (Figure 2-10). The early theoretical studies on this molecule suggest that this heterocyclic ring is planar and aromatic.[101,102] In this 6π electron system, the boron atom is sp^2 hybridized with one empty sp^2 orbital. This empty σ* orbital is very low in energy and hence imparts a very strong Lewis acidic character to the molecule. The high reactivity of this orbital makes it impossible to isolate free borabenzene. Even the attempts to isolate free borabenzene by flash thermolysis in an argon and nitrogen matrix were met with failure. Thus, at 10 K a very unstable adduct of borabenzene with dinitrogen was observed.[103]
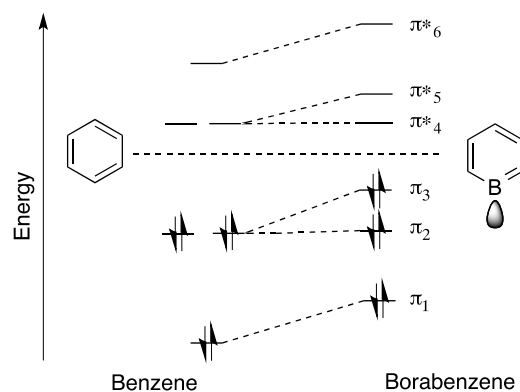
Figure 2-10: Electronic structure of benzene and boratabenzene.

As a result, the chemistry of borabenzene mainly consists of its different nucleophilic adducts. If the nucleophile stabilizing the empty *p*-orbital of borabenzene is a neutral Lewis base then this adduct is termed as borabenzene. It is a stable isoelectronic analogue of benzene and pyridine (Figure 2-11 A). It readily undergoes ligand exchange reactions with anionic and stronger nucleophiles to form a more stable adduct.[90] G. C. Fu initially investigated the exchange mechanism of neutral ligands by anionic ones and proposed that an associative mechanism was taking place (Scheme 2-3).[104] Our research group accomplished further investigations on the mechanism and rate of exchange with neutral nucleophiles. These studies showed that the initial step of the ligand exchange is the generation of borenium species which is followed by ligand exchange (Scheme 2-3).[105]
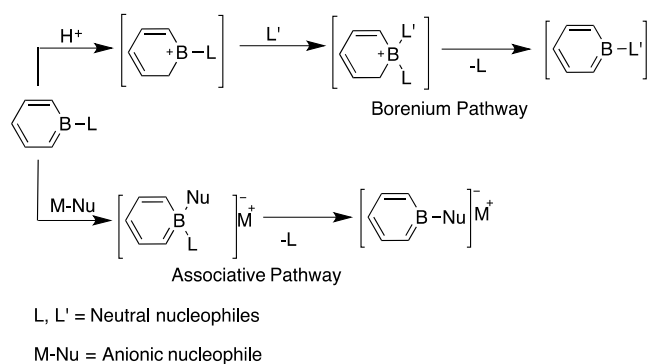
Scheme 2-3: Associative and borenium pathways of borabenzene ligand exchange.

If the nucleophile coordinated to boron atom is anionic then the molecule is termed as boratabenzene. This molecule is regarded as an analogue of the cyclopentadienyl (Cp) anion and acts as an anionic ligand for transition metals (Figure 2-11 B). The distribution of the negative charge in the boratabenzene ring is asymmetric and has been found to be concentrated on the carbon atoms at the α position of boron (Figure 2-11 A).[90]
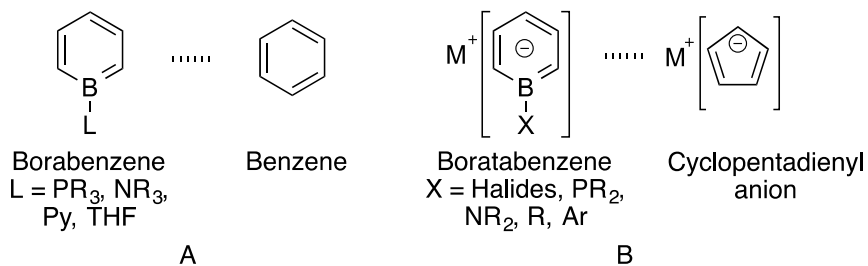
Figure 2-11: Nomenclature and analogy of A) neutral and B) anionic adducts of borabenzene, with pyridine and cyclopentadienyl.

In boratabenzene molecules the nature of exocyclic bond between boron and the nucleophile is covalent (Figure 2-12 B). However, with nitrogen nucleophiles which have an additional lone pair of electrons, these exocyclic bonds have a partial double-bond character due to the π-interaction (Figure 2-12 C).[106,107] Such lone pair donation is not observed for larger nucleophiles like phosphorous as the orbital overlap in them is not efficient enough for a successful π-interaction.[108]
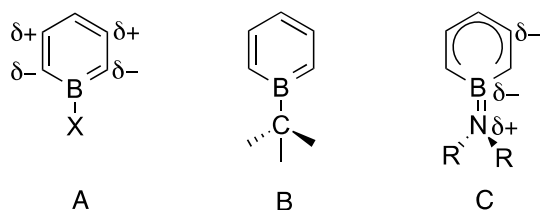
Figure 2-12: Representation of A) charge distribution and B, C) bond character of borabenzene-nucleophile adduct.

2.3.2 Synthesis of Borabenzene and Boratabenzene species

G. E. Herberich developed the initial route to the synthesis of boratabenzene in 1970. It involved the expansion of cyclopentadienyl ring in a cobaltocene complex by insertion of organoboron dihalides (RBX$_2$) (Scheme 2-4). The reducing power of cobaltocene and its ability to add radical account for the successful generation of boratabenzene in the coordination sphere of the metal. Both mono and bisboratabenzene cobalt complexes were produced in the reaction which led to the theory that boratabenzene was isoelectric with the cyclopentadienyl anion.[109]
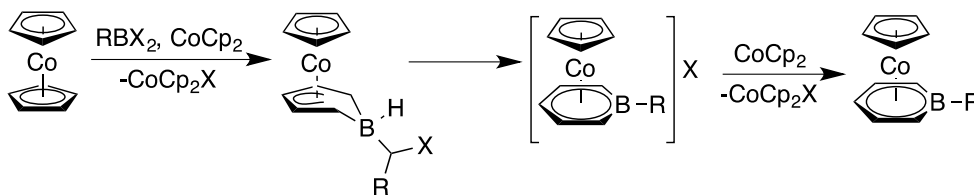
Scheme 2-4: Initial synthesis of boratabenzene by insertion.

Later, Ashe reported the synthesis of an isolated phenylboratabenzene adduct,[110] but it was Fu and coworkers who generated an efficient protocol for the synthesis of neutral

borabenzene adducts. Until now this is the most widely used synthetic route to access borabenzene adducts. It involves a three step transformation from the commercially available 1-trimethylsilyl-1,4-pentadiyne to neutral borabenzene adduct as shown in Scheme 2-5.[104] The first step of the transformation is the hydrostannation of the 1-trimethylsilyl-1,4-pentadiyne with Bu_2SnH_2 to form 1,1-di(n-butyl)-2-(trimethylsilyl)stanna-2,5-cyclohexadiene followed by transmetallation of tin with BCl_3 to form 1-chloro-2-(trimethylsilyl)bora-2,5-cyclohexadiene. The neutral borabenzene adduct is then obtained by the aromatization of the boracyclohexadiene with the Lewis base. It has been found to be dependent on the capacity of the Lewis base to isomerize the 2,5-boracyclohexadiene to 2,4-boracyclohexadiene and its tendency to stabilize the aromatic product. Herberich had demonstrated that weak bases like $CpFe(3,4-Me_2C_4H_2P)$ failed to perform this step.[111]
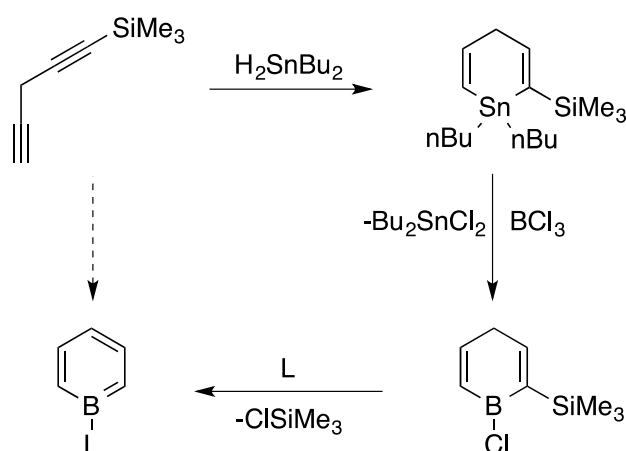
Scheme 2-5: General synthetic approach for the synthesis of borabenzene adducts developed by Fu.

These neutral borabenzene adducts readily undergo ligand exchange reactions with stronger nucleophiles as shown by Fu and coworkers.[104] Ligand exchange with anionic bases results in the formation of anionic boratabenzene salts, thus providing an efficient route for their synthesis. This protocol has opened up the access to a wide range of neutral and anionic borabenzene molecules.[90,112–115] Mechanistic investigations have established that this aromatic substitution occurs via an addition elimination pathway (Scheme 2-6).
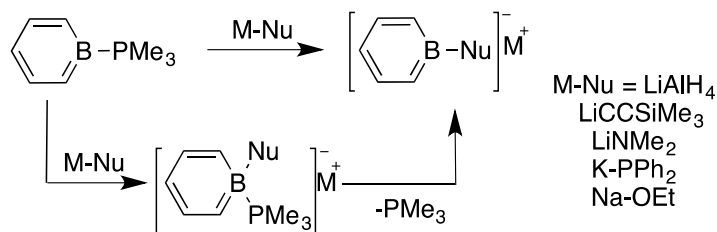
Scheme 2-6: Mechanism of ligand substitution on a borabenzene molecule.

Although the nucleophilicity of the *ortho* position on borabenzene has been established, it has been found to be very challenging to modify the backbone of borabenzene after its synthesis. Usually, substitutions at *ortho, meta* and *para* positions have to be carried out during the early stages of the synthetic protocol. The *para* position can be substituted with alkyl groups by deprotonating the 1,1-dibutyl-2,5-stannacyclohexadiene followed by its reaction with alkyl halide. This method was initially developed by Ashe and latter optimized by Piers and coworkers (Scheme 2-7).[99,116]
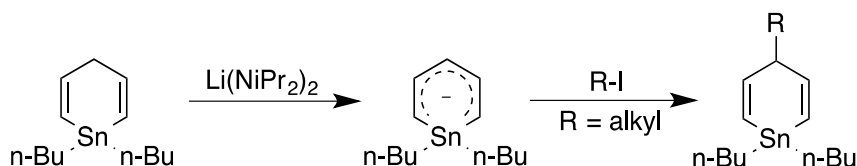
Scheme 2-7: Reaction for substituting the para position of borabenzene.

Herberich accomplished the *meta* functionalization by using a 1,4-pentadiene substituted at 2 and 4 positions. In this case, ring closing has been carried out by reacting the double alkylated diene with $(NMe_2)BCl_2$ as shown in the Scheme 2-8.[107,117,118]
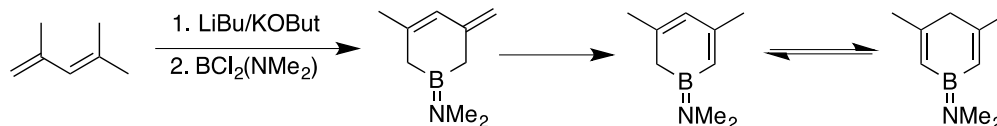
Scheme 2-8: Schematic representation for the synthesis of meta substituted borabenzene.

2.3.3 Coordination chemistry of Borabenzene

The initial approach of coordinating boratabenzene to transition metals involved its generation in the coordination sphere of the metal by insertion of boron halides into the coordinated cyclopentadienyl anion (Scheme 2-4).[89,119] However, transmetallation of boratabenzene from alkali metal salts to transition metal halides is the most efficient and widely used pathway.[120,121] This method opened up a library of transition metal boratabenzene complexes (Figure 2-13).
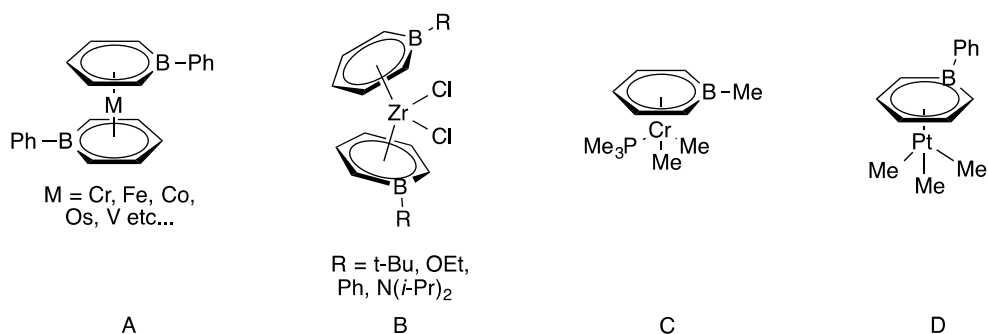
Figure 2-13: Examples of various boratabenzene transition metal complexes.

Nevertheless, the transmetallation results in the synthesis of bisboratabenzene metal complexes. Monoboratabenzene complexes have been synthesized by transmetallating it from cobalt complexes on a metal carbonyl precursor (Scheme 2-9 B).[122] Another strategy has been used by Bazan and coworkers which involves the coordination and intramolecular nucleophilic substitution of borabenzene on early transition metals (Scheme 2-9 A).[123]
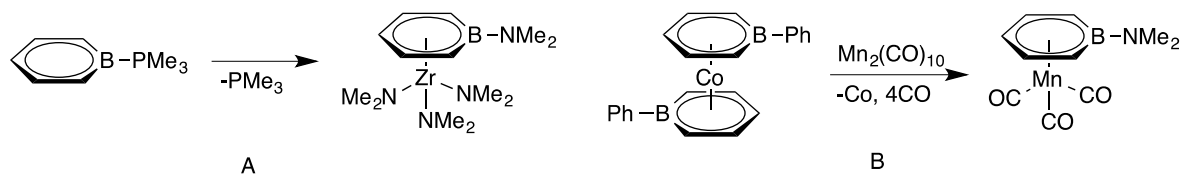
Scheme 2-9: A) Substitution and B) transmetallation approach for synthesis of monoboratabenzene metal complex.

The neutral η^6 borabenzene metal complexes have been obtained by ligand exchange with other weakly coordinated ligands and such complexes exist only with chromium (Scheme 2-10).[124–126]
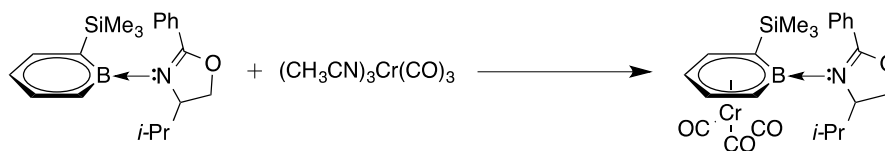
Scheme 2-10: Synthesis of neutral borabenzene transition metal complex.

Anionic boratabenzene complexes exist with all transition metals except copper, gold and silver. The coordination mode of the boratabenzene in these complexes is greatly dependent on the substituent on boron atom. The hapticity of the boratabenzene can vary from η^6, η^5, η^3 to η^1 depending on the metal and on the substituents on boron (Figure 2-15).[114,127,128] The π coordination of the aromatic ring is usually slipped away from the electropositive boron atom. However, the bonding situation is similar to that of metallocenes with quite noticeable interactions of the σ-orbitals of the ligand with the metal d-orbitals with efficient π-donation from the ligand π_2 and π_3 orbitals to the metal d-orbitals, as shown in Figure 2-16.[129,130]

Fe   (BB)$_2$Fe   BB
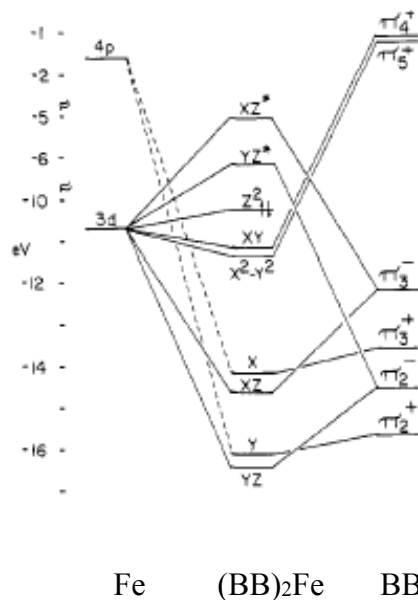
Figure 2-14: Molecular orbital representation of bonding between cyclopentadienyl and boratabenzene with transition metals.[129]

All sandwich complexes of boratabenzene with transition metals have η^6 coordination, except with nickel, which prefers to have a η^5, or η^3 coordination with one of the

26

boratabenzene rings to avoid the formation of a 20e complex (Figure 2-15 D).[121,130] With early transition metals they usually form *ansa* complexes analogues to cyclopentadienyl chemistry (Figure 2-13 B, C). These zirconium and chromium complexes have been found to show better catalytic activities for ethylene polymerization than their cyclopentadienyl analogues with a significant effect of substituent on the boron atom (Figure 2-17 A).[90,131–133]

A   B   C   D
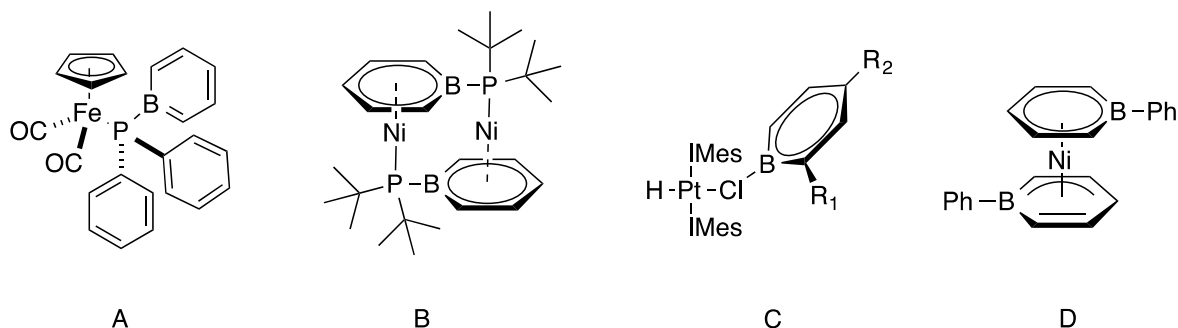
Figure 2-15: Different coordination modes of boratabenzene ligand to transition metals

Apart from these diverse coordination modes, several triple-decker complexes of boratabenzene have been synthesized either by ligand exchange or by insertion into cyclopentadienyl anion. The bridging capacity of boratabenzene is quiet prominent in these systems. These complexes find applications in optoelectronic materials as they can combine the donor cyclopentadienyl metal center to the acceptor boratabenzene metal fragment. Many of such complexes have been used in metallopolymers for optical applications (Figure 2-16).[93,134–137]

M = Co, Rh,
Ru, Ir
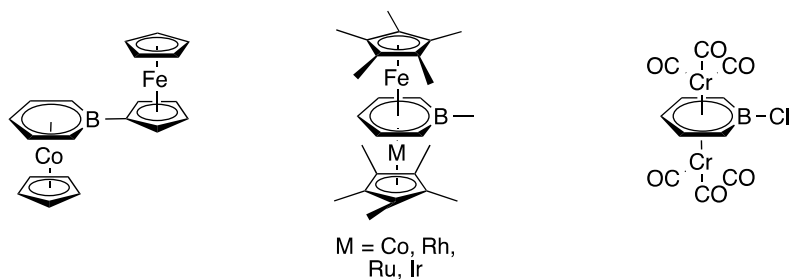
Figure 2-16: Examples of different triple-decker complexes of boratabenzene.

2.3.4 Lanthanide boratabenzene chemistry

In comparison to transition metal chemistry, the lanthanide boratabenzene chemistry is still in its infancy. There are only a few boratabenzene lanthanide complexes that have been reported so far (Figure 2-17). The first report was by Herberich in 1999 of boratabenzene complexes of yttrium and scandium (Figure 2-17 B).[138] In 2002, a similar lutetium complex was reported by the same group.[113] No other report was made until 2007 when Chen reported the first samarium boratabenzene complex and studied its reactivity towards ethylene polymerization (Figure 2-17 A).[139] Other lanthanide complexes mostly include the *ansa* analogues of samarium, dysprosium, lutetium and yttrium. Their reactivity with different nucleophiles has been explored (Figure 2-17 A).[140–143]
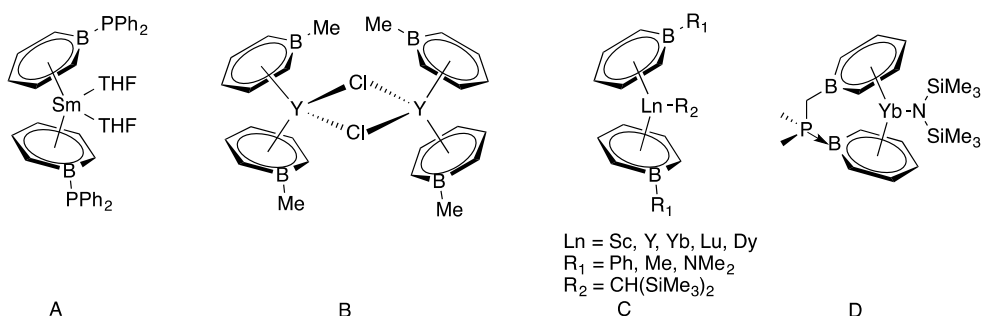
Figure 2-17: Examples of rare earth boratabenzene complexes.

The $(C_5H_5BR)_2LnCl$ are synthesized by reacting two equivalents of alkali metal salt of boratabenzene with one equivalent of LnX_3 in THF or toluene. When synthesized from non-coordinating solvents they exist as dimers (Figure 2-17 B), in which the lanthanide ion has an intermediate coordination of η^6- η^3 with each boratabenzene ring. They form bent sandwich structures like the metallocene analogues and the two boratabenzene rings are arranged in an anti-periplaner manner.

Interesting reactions for the borabenzene has been observed with $Yb[N(SiMe_3)_2]_2$. When reacted with borabenzene trimethylphosphine, it cleaves the C-H bond of the phosphine on coordination to give the only example of a metal complex containing both borabenzene and boratabenzene coordinated to the same metal center. Reaction of KCp* and NaO^{i}Pr results in the formation of a bimetallic polymeric structure (Figure 2-18).[143–145]
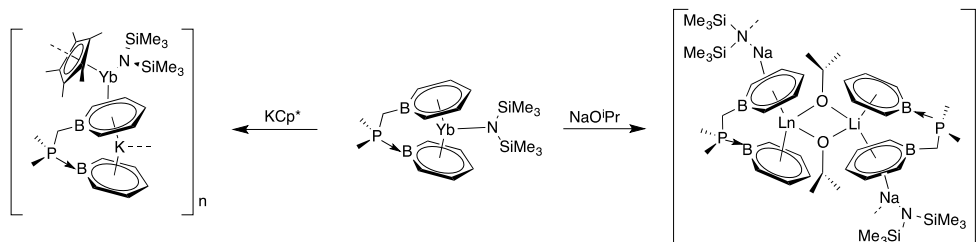
Figure 2-18: Ytterbium complex containing both neutral and anionic borabenzene.

Monoboratabenzene complexes have also been reported with lutetium. These complexes show promising activities for styrene polymerization and the hydroboration of alkenes, alkynes, carbodimides and imines.[139,141,146–148] However, this chemistry has not been extended to study the effect of boratabenzene analogues on the magnetic and optical behavior of lanthanide ions as compared to their cyclopentadienyl analogues.

2.4 9, 10-Diboraanthracene

The discovery of borabenzene and its aromatic character analogous to that of benzene drove the interest of researchers in creating a family of aromatic boron heterocycles analogous to that of acenes. The acene family of boron now known as boracenes contains analogues of naphthalene, anthracene, pentacene and other polyacenes. The presence of a boron atom in these cycles creates electron deficient centers, which make them useful as p-type semiconductors. Moreover, the HOMO and LUMO gap of the polycene is lowered due to the introduction of the boron center, thus making the excitation easier. They find many applications in OLEDS and optoelectronic materials. However, the application of these boracenes as ligands for metals has not been well explored.

The 9,10-diboraanthracene has two boron atoms in its framework at the 9 and 10 positions. They are presently very popular for making luminophores. Due to their high electron affinities and intense luminescence, they find applications in semiconducting materials. This is because of their low-lying LUMO and small band gap.[100,149–151] Most of the 9, 10 dihydrodiboraanthracene (DBA) used presently have bulky substituents on the boron atoms which protect them from hydrolysis and oxidation at ambient conditions to make them

viable for practical applications. The synthesis of these 9,10-dihydrodiboraanthracene species dates back to 1987 when Kaufmann and Wolfgang observed them while carrying out the thermolysis of [O-(dichloroboryl)phenyl]trimethylsilane in presence of a tetramethyltin reagent. When heated between 45 and 130 °C, the 1,2-disubstituted phenyl dimerizes in presence of alkyl-tin molecules to form the 9,10-dihydrodiboraanthracene (Scheme 2-11). It was later observed that this product can be obtained by thermolysis of 1,2-bis(dihalo)phenylboranes and does not require the presence of any other alkylating reagent.[152,153]
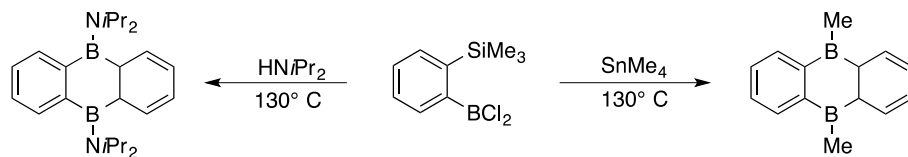
Scheme 2-11: Initial synthesis of 9, 10-dihydrodiboraanthracene.

In 1995, Müller and coworkers developed an elegant synthetic protocol to synthesize and characterize a family of 9,10-dihydrodiboranthracene with different substituents at the boron atoms (Scheme 2-12).[154] They used Kaufmann's thermolysis procedure to obtain the dihalo derivatives of 9,10-dihydrodiboraanthracene. Then by transmetallating the halide with alkyl and aryl lithium salts, different 9,10-disubstituted boraanthracenes were obtained. By using N,N-(di*iso*propyl)trimethylsilane and ammonia they were also able to make the amine derivatives. Their successful crystallization of the methyl and amine derivatives of diboraanthracene gave an insight into the structural properties of this molecule. In the case of the 9,10-dimethyldihydrodiboraanthracene and of the 9,10-diaminodihydrodiboraanthracene, all three rings were found to be planar with bond distances and angles in accordance with other boracene derivatives. However, the di*iso*propyl derivative shows deviation from the planarity suggesting that the type of substituent on the boron atoms governs the geometry of the molecule (Figure 2-19 A). A significant double bond character was observed for the B-N bond of amino derivatives.

30
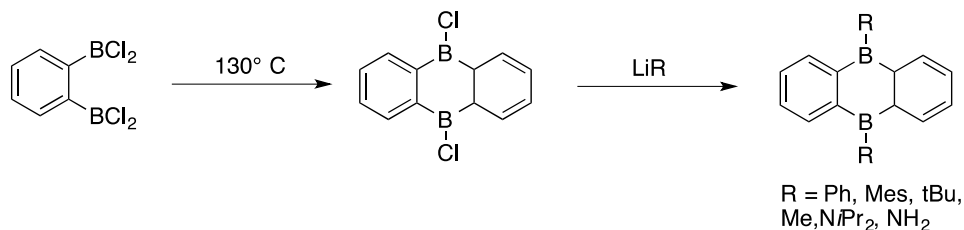
Scheme 2-12: Muller's approach for the synthesis of 9,10-dihydrodiboraanthracene molecules.

The dihydrodiboraanthracene molecules are anti-aromatic with 12π electrons. They can be reduced to form the aromatic 14π systems. Two aromatic derivatives of diboraanthracenes have been reported so far which includes the alkali metal salts of 9,10-dimethyl and 9,10-dimesityldiboraanthracene. The bulky dimesityl derivative exists as an isolated ion with two lithium ions coordinated to the central boron ring (Figure 2-19 C).[150] The dimethyl derivative forms zigzag chains in which one anthracene molecule has two potassium ions η^6 coordinated to central boron ring and two more potassium ions coordinated η^2 to the phenyl rings (Figure 2-19 B).[154] In addition, the single reduction product of 9,10-dimethyldiboraanthracene has also been isolated. In all these reduced derivatives the three rings of the anthracene fragments are planar supporting their aromatic character. Recently, two more synthetic routes have been developed which involves the transmetallation of 9,10-distannaanthracene with BCl_3 and the stepwise substitution of iodobromobenzene with $B(OMe)_3$. However, the thermolysis approach is the most widely used.[155]
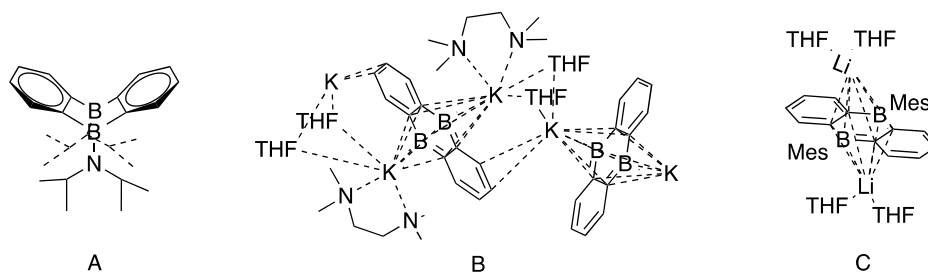
Figure 2-19: Representation of (A) diisopropylamino (B) dimethyl and C) dimesityl diboraanthracene molecules.

The coordination chemistry of diboraanthracene has been studied with many electron rich transition metals. The diboraanthracene molecule shows great diversity in its coordination

behavior. The non-reduced 9,10-dimethyldihydrodiboraanthracene acts as a neutral arene ligand and coordinates transition metals in a η^6 mode. It has been easily coordinated to different transition metals by ligand exchange with other neutral ligands like toluene, ethylene, carbonyl, acetonitrile, COD, resulting in the formation of sandwich and piano-stool complexes (Figure 2-20).[156,157] It is interesting to observe that in most of these complexes the three rings are planar with the exception of (Tol)Fe(DMDBA) and (Cp)Co(DMDBA) sandwich complexes where the phenyl rings are slightly bent away from the metal center (Figure 2-20 A). The diboraanthracene molecule has a tendency to act as a bridging ligand and form triple-decker complexes. It is clear from the triple decker complex $(Cp)_2M(\mu^6\text{-}\mu^6\text{-}DMDBA)$ of cobalt and iron that this ligand binds both the metal centers in a η^6 mode on the two faces of the boron heterocycle (Figure 2-20 B). However, the chromium carbonyl prefers to bind the arene ring instead of the boron heterocycles in some sandwich and triple-decker complexes, as shown in the Figure 2-20 D.

A	B	C	D
M = Fe, Co, Rh, Ru	M = Ni, Pt, Pd	M = Fe, Co	
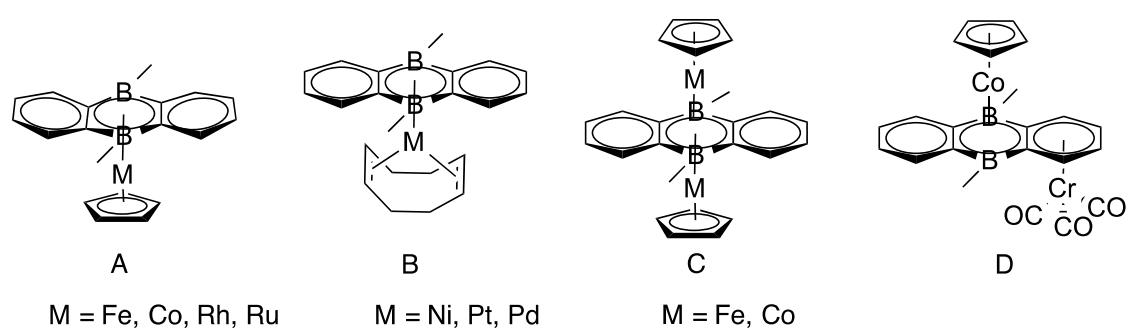
Figure 2-20: Examples of various transition metal 9,10-dimethyldiboraanthracene complexes.

The mono and dianionic 9,10-dimethyldiboraanthracene (DMDBA) molecules have also been coordinated to transition metals to form different sandwich and triple-decker complexes. The binding mode to the metal centers is again η^6. There is only one example of coordinating the monoanion to a transition metal (Ni) and it forms the sandwich complex (Figure 2-21 A). The dianion has been coordinated to nickel and cobalt and has produced both sandwich and triple-decker complexes. In $(Cp)Co(\mu^6\text{-}\mu^4\text{-}\mu^4\text{-}DMDBA)(CoCp)_2$ complex the dianionic 9,10-dimethyldiboraanthracene ligand is coordinated η^6 to one Co atom through its boron heterocycles and exhibits a η^4 coordination with the other two cobalt atoms through its phenyl fragments (Figure 2-21 C). However, in the nickel allyl complex, it coordinates both the nickel centers to the central boron ring in a η^6 mode (Figure 2-21 B).

The coordination of this dianionic ligand to other transition metals has not been explored. When compared to boratabenzene, boratanapthalene, and 9-boraanthracene, the 9,10-diboraanthracene has two boron atoms and is therefore considered as an electron deficient cycle. Thus, its coordination to early transition metals is considered to be challenging.
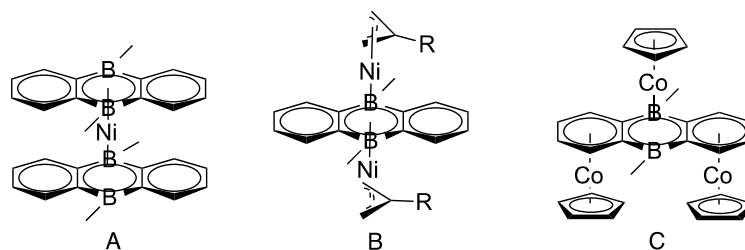
Figure 2-21: (A, C) Mono and (B) dianionic 9,10-dimethyldiboraanthracene metal complexes.

Chapter 3 - Experimental methods

This section is devoted to the description of the various techniques that have been used to accomplish the goals of the project. A description of various methods and assemblies is provided with a brief explanation of their manipulation. The need for utilizing these techniques is also discussed

3.1 Inert atmosphere chemistry

Most of the reagents, target compounds and synthetic procedures described in the thesis are highly sensitive towards traces of moisture and oxygen. As a result, these manipulations need to be carried out under inert atmosphere of dinitrogen in order to exclude traces of water and oxygen and hence prevent the decomposition of the reagents and products. Accordingly, we use equipment's that provide us these inert conditions. The two main apparatus used for this project are Schlenk lines and gloveboxes.

3.1.1 Schlenk line

A Schlenk line is a glass mounting consisting of two parallel tubes that are interconnected by a series of bidirectional valves. These valves connect each output to the two tubes alternately. One of the tubes is connected to a vacuum pump at its inlet while the other to a source of inert gas (ultra high purity nitrogen in our case). The other end of each tube is connected to mercury bubblers. This assembly makes it possible to control the atmosphere in closed vessels and alternate between positive and negative pressures without exposing the system to ambient atmosphere. A positive pressure of nitrogen keeps the moisture and oxygen away from the system. The solvent traps connected between the Schlenk line and the vacuum pump are cooled down in liquid nitrogen and are used to condense solvents and other volatile chemicals that are evaporated on the line. Special glassware commonly known as Schlenk tubes and Schlenk flasks is used to carry out sensitive manipulations. These tubes and flasks have a side arm fitted with a stopcock, through which they can be connected to the Schlenk line, hence, enables effective purging of the and maintaining of an inert atmosphere in the reaction vessels. Specially designed NMR tubes called J-Young are

used for carrying out NMR scale reactions under inert atmosphere. These tubes are fitted with a Teflon cap, which isolates them from outside atmosphere and serves as an attachment site to Schlenk line.
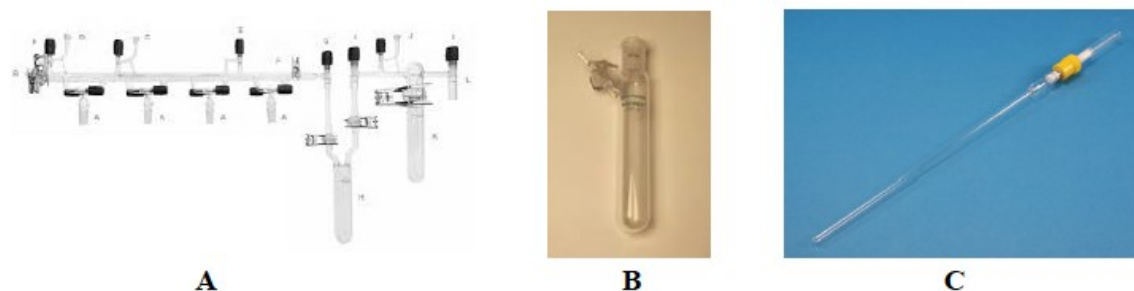
Figure 3-1: A) Schlenk line, B) Schlenk tube, C) J-Young.

3.1.2 Glovebox

As the name implies, a glovebox is an air and watertight box fitted with a transparent plastic casing and one or more pairs of neoprene gloves. The inside of the box is always filled with an inert atmosphere of argon or nitrogen. It is very useful for carrying out reactions on smaller scale and for storing air sensitive reagents. It is continuously fed by a controlled flow of inert gas, which maintains positive pressure inside the box and thus prevents the infiltration of air. The atmosphere inside the box is continuously purified by a copper catalyst and molecular sieves, this helps in keeping the levels of oxygen and water to less than 0.1 ppm. This box is fitted with two chambers through which materials are taken in and out of the box after purging them through a series of alternating cycles of vacuum and inert atmosphere.

Figure 3-2: Glovebox.

36

3.2 Nuclear Magnetic Resonance Spectroscopy (NMR)

NMR spectroscopy is a technique that is used to analyze and characterize chemical compounds. It provides valuable information about the chemical environment of a nucleus and the atoms bonded to it, by studying its behavior in a strong magnetic field. All the nuclei with a non-zero spin can be studied using multinuclear NMR spectroscopy. As a result it helps solving structures of both organic and organometallic compounds. The various nuclei that were studied during this project are compiled in the Table 3-1.

Table 3-1: NMR active nuclei of relevance in this project.

Nuclei	Spin	Abundance (%)	Frequency (MHZ) at 9.3947 T)
^{1}H	1/2	99.98	400
^{11}B	3/2	80.42	128.3347
^{13}C	1/2	1.108	100.576
^{31}P	1/2	100	161.9227

In our project, many of the molecules were oils and their structure was confirmed solely using NMR spectroscopy. The study of their ^{1}H, ^{11}B and ^{13}C spectra and their comparison with the precursors provided valuable details for the assignment of the structures. In addition to the specific study of each nucleus, multidimensional NMR spectroscopy helped us in solving the structures of different isomers of our products. For example in our project we obtained two different isomers of 1-mesityl-2-trimethylsilyl-4-isopropylboracyclohexadiene. They could be easily distinguished by their proton NMR spectra and COSY experiments were helpful in assigning the position of the protons at the 2 and 4 positions (Chapter 5). Similarly, it is also possible to correlate the chemical shift of a nucleus to an adjacent core, either chemically or spatially. This correlation is very useful

as it solves complex structures highlighting the various relationships between the atoms present.

Another important feature of this technique is that it can be used to follow the course of a reaction. By conducting the NMR spectra at different time intervals, the rate of a chemical reaction can be determined. More importantly, different intermediates formed during the course of a reaction can be observed which are helpful in determining the mechanism of the reaction.

Figure 3-3: NMR Spectrometer.

3.3 X-ray Diffraction Crystallography (XRD)

X-ray crystallography is another powerful technique used for the characterization of organometallic compounds. This method makes use of single crystals to determine the various bond lengths, bond angles and the overall structure of a molecule. In a crystal, the distance between the molecules is extremely regular. As a result, when a X-ray beam is bombarded at the crystal, it diffracts the X-rays using a relation that is dependent upon the angle of incidence and wavelength of the beam. A constructive interference is observed if the diffraction satisfies Bragg's law ($n\lambda = 2d\sin\vartheta$) where n = positive integer, λ = wave length, ϑ = diffraction angle, d = diameter of the aperture. By turning the crystal in all directions, it is possible to obtain the interference pattern in three dimensions. The resolution of this interference pattern then provides the structure in the solid state of the compound. The initial acquisition of 30 minutes gives information about the unit cell of the

38

molecule and in order to get the complete structural details a longer acquisition time of 24 – 48 hours is required.

Although X-ray crystallography is an efficient technique for structure determination, it has some limitations. The obligation of using a single crystal for the analysis makes it difficult to obtain a good structure of the molecule. Growing a single crystal of appropriate size and of good quality is indeed challenging, especially with air and water sensitive compounds. Many attempts and numerous solvent systems have to be tried to obtain a good quality crystal. Even there, many compounds do not tend to form large enough crystals for X-ray diffraction studies.

It is also important to note that a crystal structure is the delineation of the molecule at the solid state. In solution, the molecules are more dynamic and can have different structures. This phenomenon is observed with our iron boratabenzene sandwich discussed in Chapter 5. Thus NMR spectroscopy is also used along with X-ray data to provide a more accurate structure. However, with paramagnetic compounds it is an indispensable tool for characterization, since paramagnetic compounds give broad signal in NMR and their extreme sensitivity to air and moisture makes it difficult to fully characterize them by infrared (IR) and ultraviolet (UV) spectroscopy.

A Bruker Apex II Diffractometer is used in our department. Our former crystallographer Dr. Wenhua Bi has solved all the crystal structures discussed in this thesis.

Figure 3-4: X-ray Diffractometer.

3.4 Mass Spectroscopy

Mass spectroscopy is another important analytical technique that has been used for the analysis of sensitive molecules in this project. A typical mass spectrum consists of a plot of an ion as a function of mass to charge ratio. This technique measures the mass of the ions that are present in the sample or are generated by the spectrometer. As a result, that mass and fragmentation pattern of the ion in the spectrometer is compared with the mass of the expected compound, hence giving information about the type of molecules in the sample. This technique is used to identify both ionic and neutral molecules by making use of two types of sources Electrospray Ionization (ESI) and Atmospheric Pressure Photoionization (APPI).

In ESI, ionic samples are analyzed. The sample is introduced in the form of a solution into the nebulizer, which is a needle held at high voltage. It sprays the solution in the form of a mist of droplets that are attracted towards the analyzer by a strong magnetic field. The analyzer then determines the mass of these ions and the result is plotted in the form of a graph of charge by mass.

However, if the molecule is neutral with no ions, the APPI technique is preferred. In APPI, the neutral molecule is introduced in the form of a solution into the nebulizer, which sprays it in the form of vapors that are ionized by high-energy photons from a Krypton (Kr) lamp causing photoionization. These ions are then carried to analyzer by magnetic field. This technique was very useful for characterizing neutral ligands and metal complexes that did not survive elemental analysis due to air and moisture sensitivity. In our department we used the Agilent Technologies 6210 LC Time of Flight Mass Spectrometer.
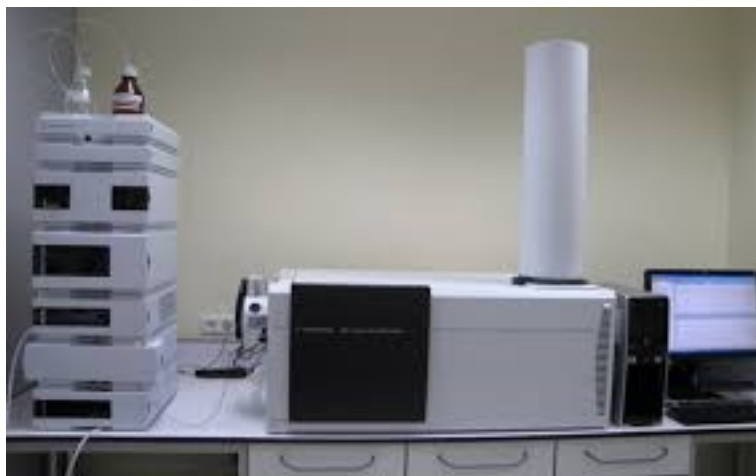
Figure 3-5: LC-MS-TOF Spectrometer.

3.5 Computational Chemistry (DFT)

Density functional theory (DFT) is a modern computational technique that has gained a lot of importance during the last decade. It is a relatively fast and accurate computational method that calculates the electronic structure of molecules of interest through an iterative optimization process. This technique has been used to predict the chemical properties, thermodynamics and structural parameters of a molecular system. The results obtained from DFT methods are in close agreement with the experimental details and are widely accepted by the scientific community. It is a powerful tool in the hand of researchers that helps to understand the nature of complex structures and transformations.

During the course of this project, few DFT calculations were performed to understand some finer details of our systems. I did not do any of the computational work that is described in the thesis, but I have a general understanding of the technique. Professor Lauren Maron from university of Toulouse performed the calculations on our neutral, mono-anionic and dianionic 9,10-diboraanthracene molecules. These calculations were very helpful in understanding the effect of aromatization on the structural parameters of these molecules. Important information was obtained about the distribution of HOMO and LUMO orbitals of the molecules and is discussed in Chapter 6 of this thesis.

My colleague Marc-Andre Légaré also performed DFT calculations on one of our iron boratabenzene sandwich complexes discussed in chapter 5 of the thesis.

3.6 Magnetism

Although we did not carried out many magnetic studies because several synthesis proved to be quite challenging, the work done during the course of my PhD was focused on creating molecules that behave as single molecule magnets. As a result, many properties of magnetic materials have been discussed in the thesis. In order, to make it easy for the reader to understand these details, some basic magnetic properties of molecules will be discussed in this section.

In simple words, magnetism is a force of attraction or repulsion that acts at a distance. This force can also be defined as a magnetic field, which originates from electric charges that are in motion (like electrons). This force is directional and is defined by two extremities called dipoles. Depending upon the behavior of a material or molecule in presence of a magnetic field, magnetism is classified into five major types: Diamagnetism, Paramagnetism, Ferromagnetism, Ferrimagnetism and Antiferromagnetism. Thus, when placed in magnetic field, diamagnets are repelled as they get magnetized in a direction opposite to the applied field, while paramagnets, ferromagnets and ferrimagnets are attracted as they get magnetized in the direction of the applied field. Antiferromagnets have adjacent magnetic moments that are equal in magnitude, aligned in opposite directions in absence of magnetic fields and hence they have no net magnetic moment. While as in ferrimagnets the adjacent magnetic moments are aligned antiparallel but are not equal in magnitude. Thus an overall magnetization is produced.

However, the paramagnets lose their magnetization after the removal of the applied field while as the ferromagnets stay magnetized. This is due to the presence of domains in ferromagnets, each of which has a particular alignment of spins and when placed in a magnetic field, they orient in the same direction, which is known as long range ordering (Figure 3-6).

42
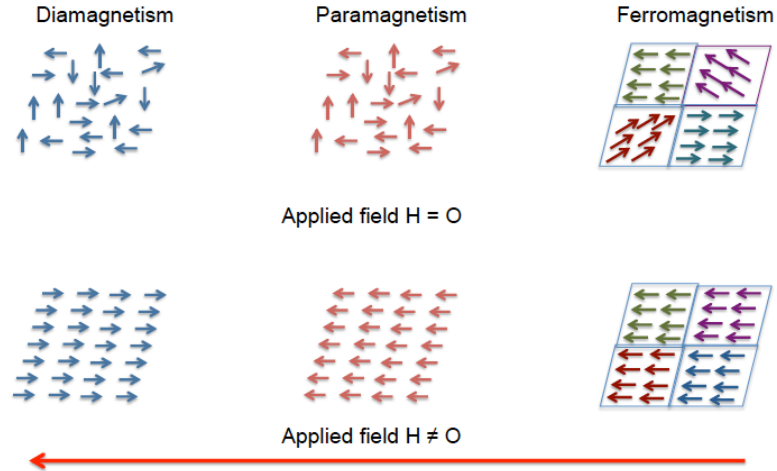
Figure 3-6: Magnetic properties of materials.

However, when the magnetic field is removed it takes a long time for the domains to revert back to the original alignment and hence stay magnetized. This retention of magnetization by ferromagnets is given by the hysteresis curve (Figure 3-7). Thus, when a magnetic field is applied to ferromagnets they get magnetized in the direction of magnetic field and reach saturation. In order to demagnetize a ferromagnet, a magnetic field is applied in the opposite direction. This behavior of ferromagnets makes them useful for memory storage applications.
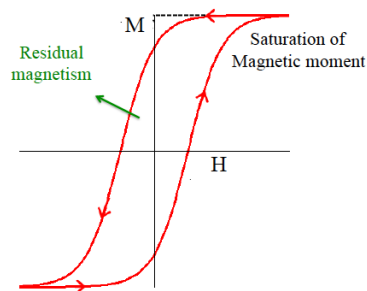
H = applied magnetic field, M = magnetization induced.

Figure 3-7: Magnetic hysteresis curve of a ferromagnetic material.[19]

In case of an atom or a molecule there are two parameters that contribute to its magnetism. One is the spin magnetic moment (M_s) and the second is the orbital magnetic moment (M_L). An electron is considered as a magnetic dipole and has therefore a magnetic field associated with it, which is given by $m_s = -g_s \mu_B s / \hbar$ where "s" is the spin angular

momentum of the electron (s = ½) g_s is called as g-factor and has a value of 2, μ_B is Bohr magneton. Thus when we have unpaired electrons in the system, they will have spin magnetic moments associated to them. The pairing of electrons in these orbitals causes the compensation of this magnetic moment, as the dipoles are aligned antiparallel to each other. Since the electron is a charged particle, its motion will produce a magnetic field. This magnetic field produced by the revolution of an electron in an orbital is called the orbital magnetic moment (m_L) and is given by $m_L = -g_L\mu_B l/\hbar$ where l is the orbital angular momentum of the electron. The values of l are obtained from the azimuthal quantum number (l). For example, for *d* orbitals l = 2, 1, 0, -1, -2. Thus when there are n electrons in *d* orbitals, the n lowest *l* values are used to give the overall value of L, which in this case of n = 2 would be l = (2 + 1) = 3. A total of five electrons in *d* orbitals would give an angular moment of L = (2 + 1 + 0 -1 -2) = 0. Although more than one value of L is possible, the ground state is determined by the multiplicity first and the by L.

The resultant magnetic moment of a molecule that has contribution from both spin and orbital magnetic moments is given by $M = g_J\mu_B\sqrt{J(J+1)}$. Where J is known as spin-orbit coupling constant and is the total angular momentum of the molecule (J = L + S).

The magnetic properties molecules are measured by using a SQUID magnetometer (superconducting quantum interference device). It is a very sensitive device that measures extremely subtle magnetic fields. The magnetic measurement discussed in the thesis has been done on a SQUID by professor Muralee Murugesu at University of Ottawa. I have not done any magnetic measurements myself

Chapter 4 - Synthesis and reactivity of the phenylboratabenzene ligand

4.1 Introduction

As mentioned previously, the boratabenzene ligands are analogues of the cyclopentadienyl ion (Cp). The similarity of the coordination behavior between the cyclopentadienyl ion and boratabenzene with transition metals has already been discussed in Chapter 2. It is clear that various derivatives of boratabenzene will show diverse coordination behavior to transition metals.[112,158,159] But the boratabenzene derivatives with carbon nucleophiles on boron show similar π coordination to metals as the cyclopentadienyl ion.[121] Although, Chen and co-workers have reported several interesting reactivities of the boratabenzene derivatives with lanthanides, the coordination chemistry of the boratabenzene ligands with lanthanides has not been explored as much as that of transition metals and remains limited to a few species like La, Dy, Yb and Lu. The boratabenzene derivatives that have been coordinated to these lanthanides have electron rich substituents on boron atom like amido and phosphido ligands.[140,144–146,160] There was no report of coordinating boratabenzene derivatives with carbon nucleophiles on lanthanides until recently when Chen reported in 2015, while we were working on the results presented in this chapter, the synthesis of a trisboratabenzene lanthanum complex containing boratabenzene ligands having carbon nucleophiles on boron (Figure 4-1). These ligands were generated by carrying out the hydroboration of the coordinated hydrido boratabenzene species with alkenes and alkynes.[161] It has been suggested that the boratabenzene coordination to lanthanides is not as favored compared to the more nucleophilic cyclopentadienyl ligands and hence these reactions need to be heated between 80 °C - 110 °C for several days in order to establish the coordination.
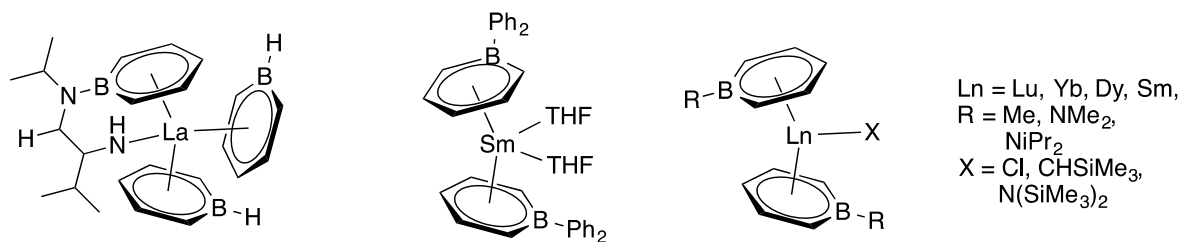
Figure 4-1: Representation of various boratabenzene lanthanide complexes.[140,160,162]

Considering the amelioration of the catalytic and optoelectronic properties of transition metal complexes with boratabenzene over cyclopentadienyl analogues, it becomes important to investigate if a similar trend is observed for lanthanides also. A few reports in this regard have already been published using samarium and lanthanum complexes of boratabenzene.[141,147,160] However, most of these complexes are homoleptic and there are no more than two reports of heteroleptic chemistry of lanthanides with boratabenzene ligands. With the recent report of heteroleptic COTLnCp complexes as single ion magnets, we became interested in investigating the effect the boratabenzene ligand will have on the magnetic properties of such complexes.[62,163] As it has been already discussed in Chapter 2, the HOMO and LUMO orbitals of boratabenzene transition metal complexes are lower in energy than their cyclopentadienyl analogues, a similar behavior with lanthanide complexes is expected to augment their magnetic properties as it can enhance the super-exchange between two lanthanide ions, thus coupling their magnetic moment. In addition, ^{11}B, the most abundant isotope for boron, has a nuclear spin (I) of 3/2 and it would be interesting to see if the spin of the boron atom in these complexes can couple with the large spins of lanthanide ions. This coupling can boost the magnetic behavior of the lanthanide complexes and provide new insights in this chemistry.

In this chapter we will discuss the synthesis of the boratabenzene ligands and the attempts we made to synthesize the heteroleptic complexes of lanthanides with boratabenzene and COT^{2-} ligands. We will also discuss the observed reactivity of lanthanides in these reactions and the synthesis and characterization of new boratabenzene lanthanide complexes.

4.2 Synthesis and characterization of the lithium salt of phenylboratabenzene (LiBBPh)

In the beginning of this project, we wanted to investigate the effect of boratabenzene ligands on the magnetic properties of transition metal sandwich and triple-decker complexes. Our initial target was to synthesize the bisboratabenzene complexes of cobalt, chromium and nickel that are 19e and 20e species and analyze them for their molecular magnetic behavior. Since, some initial measurements on the magnetic moment of cobalt and chromium bis(boratabenzene) complexes had been reported by Herberich and coworkers, we decided to explore these two complexes for their single molecule magnetic properties.[130,164] In order to synthesize these sandwich complexes, Herberich carried out an insertion reaction on cobaltocene with phenyldichloroborane (PhBCl$_2$). The yield of this reaction was as low as 10% and utilized large amounts of the expensive reagent PhBCl$_2$. Ash and coworkers reported another route for the synthesis of phenylboratabenzene ligand from a 1,1-dibutylstannacyclohexa-2,5-diene precursor (**stannacycle**); however, they also used PhBCl$_2$ to transmetallate with the **stannacycle** to form the 1-phenylboracyclohexa-2,5-diene (**Ph-boracycle**) which was then deprotonated by n-butyllithium to form the lithium salt of phenylboratabenzene (**LiBBPh**) (Scheme 4-1).[110]
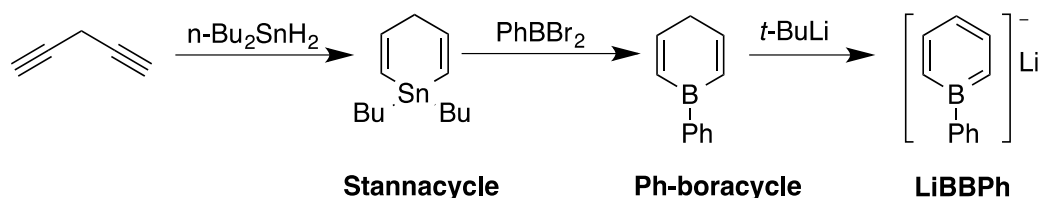
Scheme 4-1: Synthesis of phenylboratabenzene by Ashe.

But since, borabenzene chemistry has made a lot of advancements. Fu and coworkers developed an elegant procedure for synthesizing neutral borabenzene adducts. They have used these adducts for synthesizing various anionic boratabenzene derivatives by carrying out a nucleophilic substitution on the boron atom. We opted for the same route for the synthesis of our phenylboratabenzene ligand.

The fundamental precursor used for the synthesis of various anionic boratabenzene ligands is the trimethylphosphine adduct of borabenzene (**BBPMe$_3$**) (Scheme 4-2).[126] In their study

of the nucleophilic substitution of neutral borabenzene adducts, Fu and coworkers observed a better reactivity with **BBPMe₃** adduct. Moreover, it was very easy to purify the product as the trimethylphosphine (PMe₃) that was produced in the reaction as a by-product could be easily removed under reduced pressure.
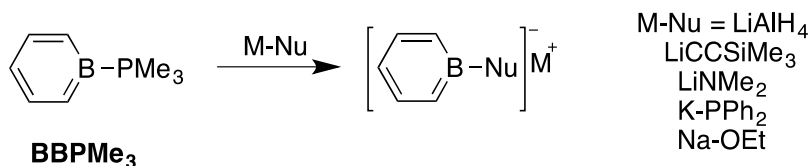
Scheme 4-2: Nucleophilic substitution on BBPMe₃.

The **BBPMe₃** was synthesized by reacting trimethylphosphine (PMe₃) with 1-chloro-2-trimethylsilylboracyclohexa-2,5-diene (**boracycle-TMS**) in hexane over 12 h. The **boracycle-TMS** was synthesized by the procedure reported by Fu and is given in Chapter 2 (Scheme 2-5). Trimethylphoshine acts as a Lewis base and attacks the electrophilic boron atom, inducing the release of a SiMe₃Cl molecule from the **boracycle-TMS**, resulting in the aromatization of the cycle (Scheme 4-3). Washing with hexane easily purifies the product. The **BBPMe₃** formed was easily characterized by NMR spectroscopy. The $^{31}P\{^{1}H\}$ NMR shows a quartet at -22.6 ppm due to its coupling with boron and the $^{11}B\{^{1}H\}$ NMR shows a doublet at 20.8 ppm. The ^{1}H and $^{13}C\{^{1}H\}$ values are also in accordance with the reported values.
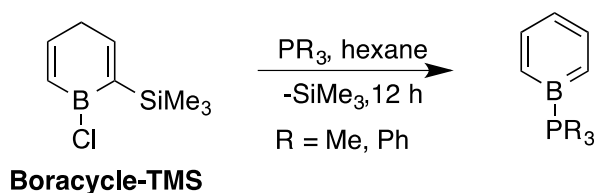
Scheme 4-3: Lewis base induced aromatization of boracyclohexadiene.

Initially the commercially available solution of phenyllithium (**PhLi**) in dibutylether was used as nucleophile to synthesize the lithium salt of phenylboratabenzene **(LiPhBB).** But due to the high boiling point of dibutylether, it was difficult to remove this solvent from the reaction mixture and remained coordinated to the lithium ion. Instead, we synthesized ourselves the phenyllithium using a modified protocol starting from bromobenzene and n-butyllithium.[165] Pure **PhLi** was isolated in the form of a white solid and was reacted with 1

equivalent of **BBPMe₃** in benzene-*d₆* at room temperature. Within 10 minutes, complete conversion of **BBPMe₃** to the lithium salt of phenyl boratabenzene (**LiPhBB**) was observed. The reaction was monitored by $^{31}P\{^1H\}$ and ^1H NMR and it showed the complete disappearance of the quartet at -22.6 and the appearance of a new peak at -62.2 ppm, which corresponds to free PMe₃. The reaction was scaled up in toluene where the two reactants were reacted for 2 h at room temperature (Scheme 4-4). The reaction was evacuated after 2 h to remove the PMe₃ released during the reaction and the solid obtained was washed with hexane to isolate pure **LiPhBB** as a white solid in 75% isolated yield. It was characterized by NMR and MS spectroscopy and corresponded to the values reported in literature.[104]
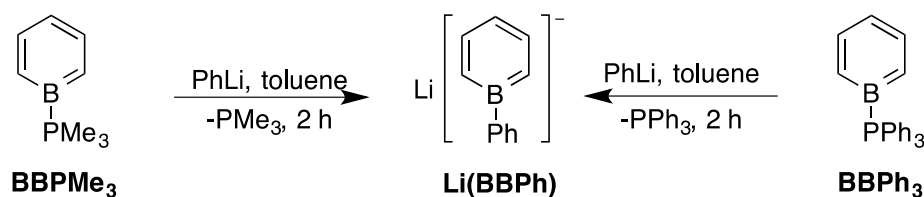
Scheme 4-4: Nucleophilic substitution on borabenzene-phosphine adducts to form Li(PhBB).

Since PMe₃ is an expensive reagent, using it as a leaving group is not economical. So we decided to use cheaper triphenylphosphine (**PPh₃**) as a leaving group. In order to synthesize the triphenylphosphine adduct of borabenzene (**BBPPh₃**), we used the same strategy as used for the synthesis of **BBPMe₃**. Reaction of PPh₃ with **boracycle-TMS** at room temperature for 12 h results in the formation of the **BBPh₃** in 75% isolated yields (Scheme 4-3). The product was purified by a 1:1 solution of toluene : hexane to remove the unreacted PPh₃ and the boracycle left unreacted. The ^1H NMR spectrum consists of broad peaks at 8.04, 7.42, and 7.03 ppm for the *ortho, meta*, and *para* protons of the boratabenzene ring, respectively. All the phenyl groups of PPh₃ are equivalent and appear as resonances at 7.53, 7.00 and 6.90 ppm for the *ortho, para* and *meta* protons, respectively. The $^{11}B\{^1H\}$ NMR consists of a doublet at 20.0 ppm that is consistent with the value observed for **BBPMe₃** (20.8 ppm) and for the borabenzene-P*t*Bu₂Cl (19.7 ppm).[158,159] The $^{31}P\{^1H\}$ NMR shift is observed as a broad quartet at 6.6 ppm, which is shifted downfield compared to free PPh₃ due to the transfer of the electron pair of phosphorous to the empty orbital of boron. The reactivity of **BBPPh₃** with phenyl lithium was very similar to that observed with **BBPMe₃** and gave (**LiPhBB**) in 78% yield. The

reaction was carried out under similar conditions as with **BBPMe₃** and purification of the product was achieved by washing the reaction residue with toluene to remove the released PPh₃.

4.3 Reactivity with transition metals

The lithium salt of the phenylboratabenzene ligand was coordinated to cobalt and chromium to confirm the structural parameters of the ligand and investigate the magnetic properties of the complexes. These complexes were synthesized by a simple salt metathesis reaction between **Li(BBPh)** and the transition metal dichloride in THF at room temperature over 12 h (Scheme 4-5). The red colored solutions obtained were evaporated and dried to give red solids. The chromium complex was crystallized in ether while the cobalt complex was crystallized in toluene at -80 °C. The X-ray analysis and mass spectroscopy confirmed the synthesis of sandwich complexes of cobalt and chromium.[121,166,167] Since the X-ray structure of these complexes has already been reported in the literature, it will not be discussed here.
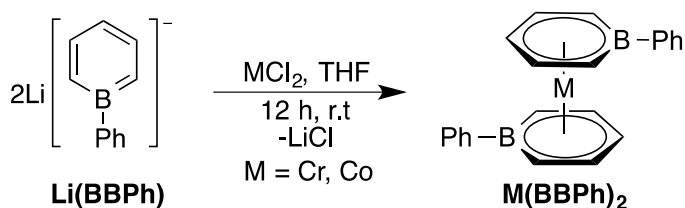
Scheme 4-5: Synthesis of chromium and cobalt boratabenzene complexes.

The study of the magnetic properties of cobalt(bisboratabenzene) sandwich **[Co(BBPh)₂]** was done using a SQUID magnetometer. The DC susceptibility data for **Co(BBPh)₂** were collected under an applied field of 1 T and 0.1 T over the temperature range of 1.8 - 300 K (Figure 4-2). At room temperature, the value of susceptibility product ($\chi_m T$) at 1 T is 0.6 cm³.K.mol⁻¹. This value corresponds to a magnetic moment of 2.19 μ_B, calculated by using the formula [$\mu = 2.84\ (\chi_m T)^{1/2}$]. The observed magnetic moment is almost equal to the magnetic moment of 2 μ_B calculated for one unpaired electron This indicates that there is only one unpaired electron in the **Co(BBPh)₂** complex that contributes to its observed magnetic moment, suggesting that **Co(BBPh)₂** is a low-spin coordination complex with negligible contribution from orbital magnetic moment (Figure 4-4 A). As the temperature is

50

lowered, $\chi_m T$ product remains constant down to 50 K, below which the values decreases sharply and reach's a minimum value of 0.2 cm³K.mol⁻¹ at 2 K. This sharp decrease below 50 K can be attributed to the presence of magnetic anisotropy in the molecule, which can originate from the crystal field splitting.
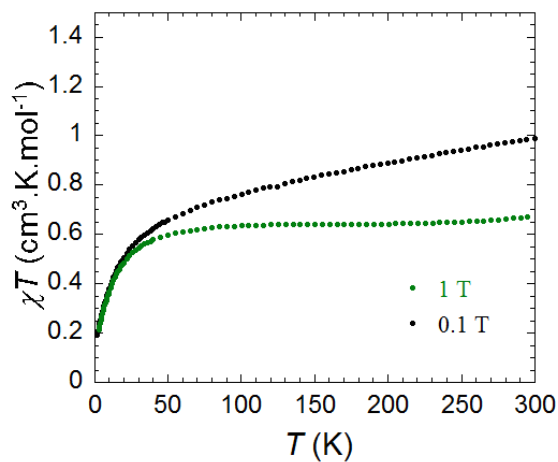
Figure 4-2: Temperature dependence of static magnetic susceptibility times temperature (χmT) of Co(BBPh)₂.
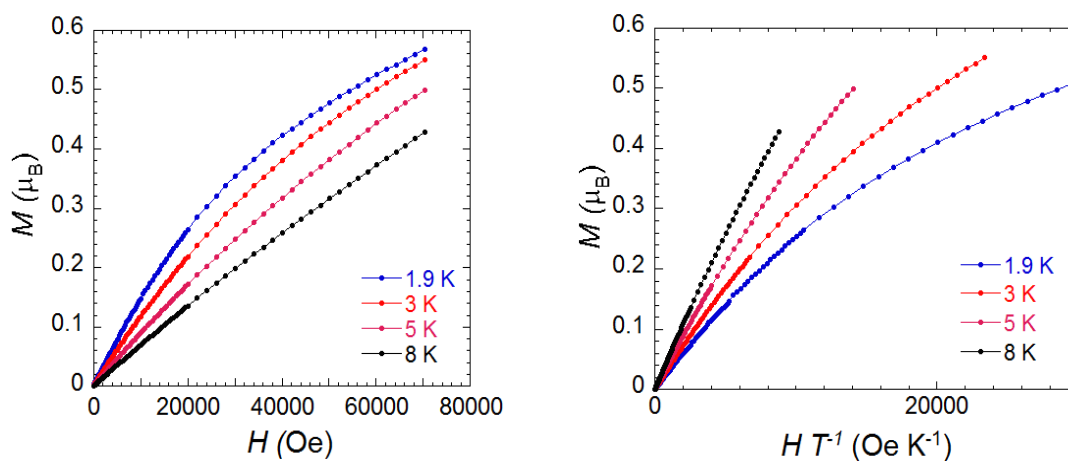
Figure 4-3: Field dependence of magnetization (left), variable temperature, variable field magnetization (right) of Co(BBPh)₂.
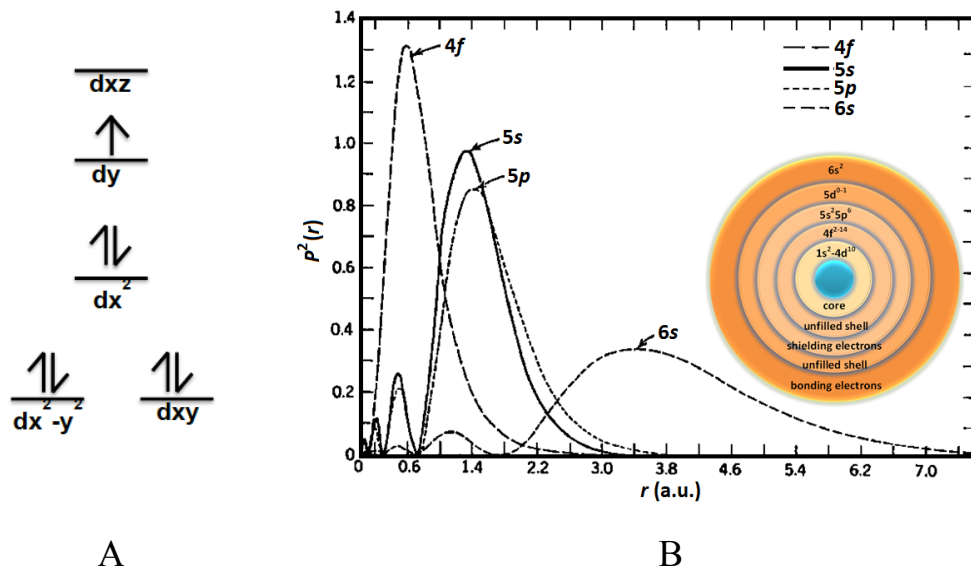
Figure 4-4: (A) Low-spin configuration of cobalt d^7 complex. (B) Radial wave function of lanthanide atoms.

The presence of magnetic anisotropy in the molecule is further supported by the presence of non-superimposing isofield lines on a single master curve of M vs H/T (Figure 4-3 right).[80,168,169] This plot also displays a linear increase in the magnetization at low fields that increases in magnitude with the increase in temperature. The magnetization does not reach saturation even at 20×10^3 Oe. The M vs H curve also shows a linear increase in magnetization (M) with increase in applied field (H) with no magnetic saturation, which is indicative of a pure paramagnetic behavior (Figure 4-3 left). The hysteresis is also not observed for this cobalt complex with the sweep rates and temperature range attainable by the SQUID magnetometer. This suggests that **Co(BBPh)** does not behave as a single molecule magnet even at 2 K.

With the above results, it is clear that the sandwich complex of boratabenzene and transition metals have similar orbital splitting and occupancy as the cyclopentadienyl analogues. Thus their magnetic properties are very analogous to those of metallocenes and are hence not interesting for molecular magnetism. Therefore, we decided to use lanthanides in place of transition metals for our study. Since, lanthanides have deeply buried 4f orbitals (Figure 4-4 B), they are not affected by the crystal field and hence retain

their orbital magnetic moment. Thus, they contribute to magnetic moment of the metal center and give higher potential barriers for spin reversal.

4.4 Reactivity of LiBBPh with lanthanides

Although Ishawaka and coworkers reported the molecular magnetic properties of lanthanides in 2003, it was actually in 2011 that the real potential of lanthanides as molecular magnets was recognized. Various organometallic complexes of lanthanides with cyclopentadienyl and cyclooctatetraenyl ligands were found to act as single molecule magnets.[62,74,170] Studies on the magnetic properties of these complexes suggested that their proficiency as molecular magnets could be improved by providing a symmetric coordination sphere to the metal ion and by increasing the electronic communication between the lanthanide ions. The shape of the electron cloud of lanthanide ion plays a very important role in determining the type of geometry that would enhance its anisotropy. Thus, it was seen that for the Tb, Dy and Ho ions, COTLnCp complexes with more axial symmetry are better molecular magnets then $[Cp_2Ln(\mu\text{-}Cl)]_2$ that have an equatorial symmetry (Figure 4-5).[47,163,171] Thus we wanted to synthesize analogous complexes with boratabenzene ligands to study its effect on their molecular magnetic behavior. Our initial goal was to synthesize a bisboratabenzene complex of terbium and dysprosium and compare their behavior with the analogous cyclopentadienyl complexes.
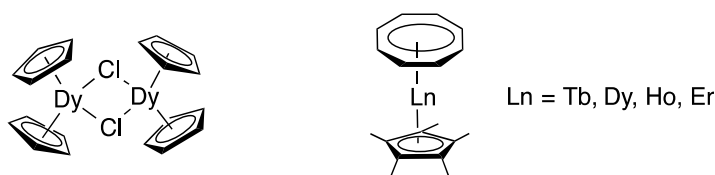
Figure 4-5: Lanthanide cyclopentadienyl complexes as single molecule magnets.

In order to synthesize the desired complexes we followed the procedure reported by Herberich and Chen.[138,140] Two equivalents **LiBBPh** were refluxed in toluene with one equivalent of $LnCl_3$ (Ln = Dy, Tb) for three days (Scheme 4-6), during which the solution becomes bright yellow in color. The hot solution was filtered and gave a yellow solid after evaporation. Several attempts were made to obtain the crystals of these solids to get their structural information, but were met with failure. The NMR spectra of these powders gave

very broad signals and hence, it was not possible to confirm the type of complex formed. The low solubility and the unsuccessful crystallization of these complexes suggested that probably these complexes form polymeric chains by bridging through the chloride ions. This has been observed with analogous cyclopentadienyl complexes also, since they form polymeric chains, dimers and tetramers, because of the large size of the lanthanide ions, which compels them to have higher coordination numbers.[31]
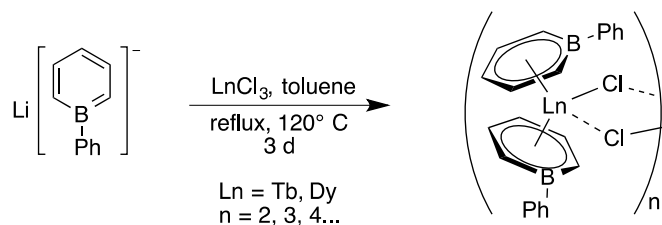
Scheme 4-6: Proposed scheme for the reaction of Li(BBPh) with terbium and dysprosium chlorides.

In order to overcome the difficulties of analyzing the proposed complexes we decided to use bulky boratabenzene ligands having substituents at the *para* position and bulky nucleophile on boron so as to prevent the formation of these bridged complexes. The work done on the synthesis and reactivity of the bulky ligand 1-mesityl-4-*i*Prboratabenzene **MesBB*** is discussed in Chapter 5.

Another type of complex that we wanted to synthesize was an analogue of COTLnCp. We wanted to coordinate the boratabenzene ligand in place of the cyclopentadienyl ligand and investigate its effect on the bonding and molecular magnetic properties of these complexes. Our initial target was to obtain the dysprosium and terbium sandwich complexes because these two lanthanide ions have the highest value of spin-orbit coupling (L = 15/2 for Dy and L = 6 for Tb) and have an oblate shape which is favorable for sandwich type complexes.[20] In order to synthesize these species, we followed the protocol used by Strietwieser and Gao for the synthesis of COTLnCp complexes.[163,172] Thus, precursors COTLnCl(THF) of Tb, Dy and Er were synthesized by reacting a freshly prepared solution of the cyclooctatetraenyl potassium salt (K$_2$COT) with a suspension of LnCl$_3$ in THF. After stirring the reaction mixture for 24 h, the solid was filtered and washed with THF to remove the K[(COT)$_2$Ln] sandwich, which is formed as a by-product in the reaction. The product of interest COTLnCl(THF) was obtained by soxhlet extraction of the solid with

THF. The removal of the solvent from the extract gave yellow solids for Dy and Tb and a pink solid for Er. These solids were reacted with one equivalent of **LiBBPh** in toluene over 24 hours to form the product (Scheme 4-7). Repeated attempts to crystallize these products failed and ended up giving brown oils similar to borabenzene decomposition products.
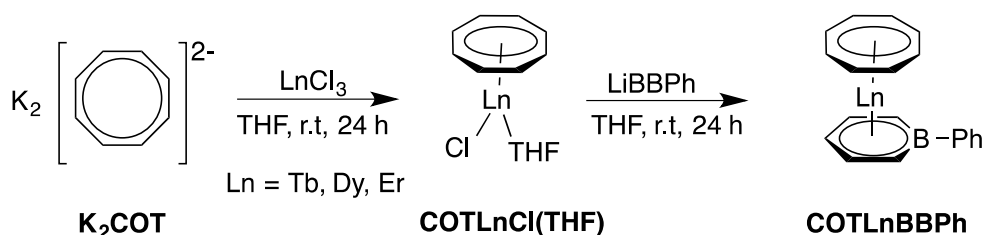
Scheme 4-7: Proposed scheme for the synthesis of heteroleptic COTLnBBPh complex.

Since it was hard to monitor these reactions by available spectroscopic techniques due to their paramagnetic nature and extreme sensitivity of the compounds to ambient conditions, the exact nature of the products formed can only be determined from crystal structures. With the failure to get crystals of the reaction products, we decided to study the reactivity of lanthanum and ytterbium triiodides for the synthesis of **COTLnBBPh** type complexes. These salts are not paramagnetic and hence their reactions and products can be very well analyzed using NMR spectroscopy. If the **COTLnBBPh** complexes of La and Yb were obtained, it would be possible to follow the same protocol to isolate analogous complexes with other lanthanides. Also, 1,4-bis(trimethylsilyl)cyclooctatetraenyl ion (**COT***) gives more soluble complexes with lanthanides than the unsubstituted cyclooctatetraenyl anion, therefore we decided to use **COT*** in these complexes. The lithium salt of 1,4-bis(trimethylsilyl)cyclooctatetraenyl (**Li₂COT***) was synthesized from cyclooctadiene (COD) using a reported protocol.[173]

4.4.1 Lanthanum complexes of phenylboratabenzene (**BBPh**)

In order to study the reactivity of lanthanum (La), a suspension of LaI₃ in THF/ benzene-d_6 was reacted with one equivalent of **Li(BBPh)** for 4 h and then one equivalent of the lithium salt of 1,4-bis(trimethylsilyl)cyclooctatetraenyl (**Li₂COT***) was added to it and the solution was sonicated for 24 h at room temperature. ¹H NMR spectra of the reaction mixture were recorded after each addition in order to follow the course of the reaction and are given in

Figure 4-6. The signals for the pure **Li(BBPh)** are given in the bottom spectrum (Figure 4-6). After the addition of LaI$_3$ to the solution, three signals were observed for the *ortho* protons (d) of the phenyl group of boratabenzene at 8.36, 8.29 and 8.25 ppm, which indicated the presence of three different types of phenylboratabenzene (**BBPh**) molecules (Figure 4-6, B). The disappearance of the signal at 6.60 ppm for the *para* proton (c) of borabenzene ring suggests that there is no unreacted ligand left. After one hour of the addition of **Li$_2$COT*** to the reaction mixture, a significant change is observed in the ^{1}H NMR spectrum. The doublets at 8.36 and 8.29 ppm disappeared while a new doublet appeared at 8.32 ppm. Another new triplet was present at 6.58 ppm that corresponds to the *para* proton (c) of the borabenzene ring. This suggests that a reaction is occurring with **Li$_2$COT***. There were no further changes in the spectrum after 24 hours. The ^{1}H NMR spectrum indicates the presence of two types of products (Figure 4-6 C). The integration values rule out the possibility of forming the COT*LaBBPh complex. After 2 days, colorless square crystals were obtained from the reaction mixture. An X-ray analysis of the crystal revealed the formation of trisboratabenzene lanthanum complex **[La(BBPh)$_3$(I)]Li,** suggesting that the reaction between lanthanum and **Li(BBPh)** is fast and the product formed from the reaction is the homoleptic complex **[La(BBPh)$_3$(I)]Li** (Scheme 4-8). The second set of signals is very similar in shift, pattern and integration to the signals of **[La(BBPh)$_3$(I)]Li** suggesting that it might be the **La(BBPh)$_3$** species without LiI associated with it. Therefore, the presence of the three sets of signals for the *ortho* proton of the phenyl groups mentioned above and seen in the spectrum of Figure 4-6 B suggests the presence of three types of boratabenzene molecules. They can be attributed to the formation of the two trisboratabenzene lanthanum complexes and a mono or bisboratabenzene lanthanum complex. This type of reactivity of lanthanides has been observed with NaCp also. After the addition of **Li$_2$COT*** the other signals disappeared. This can happen due to the coordination of COT* to lanthanum which causes the redistribution of ligands on lanthanum ions. This ligand redistribution is very common with lanthanides and has been used as one of the methods for synthesizing Cp$_2$LnCl complexes from LnCp$_3$.[66]
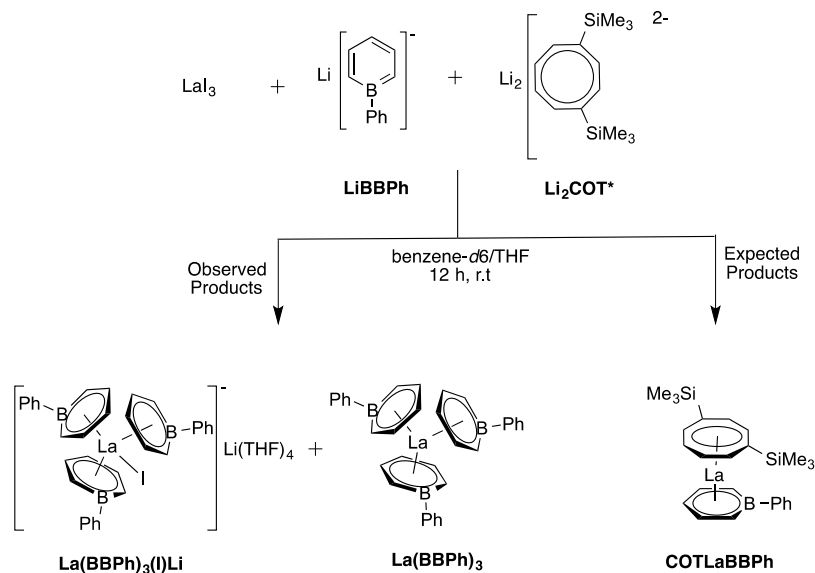
Scheme 4-8: Proposed scheme for the reaction of LaI₃ with LiBBPh and Li₂COT*.
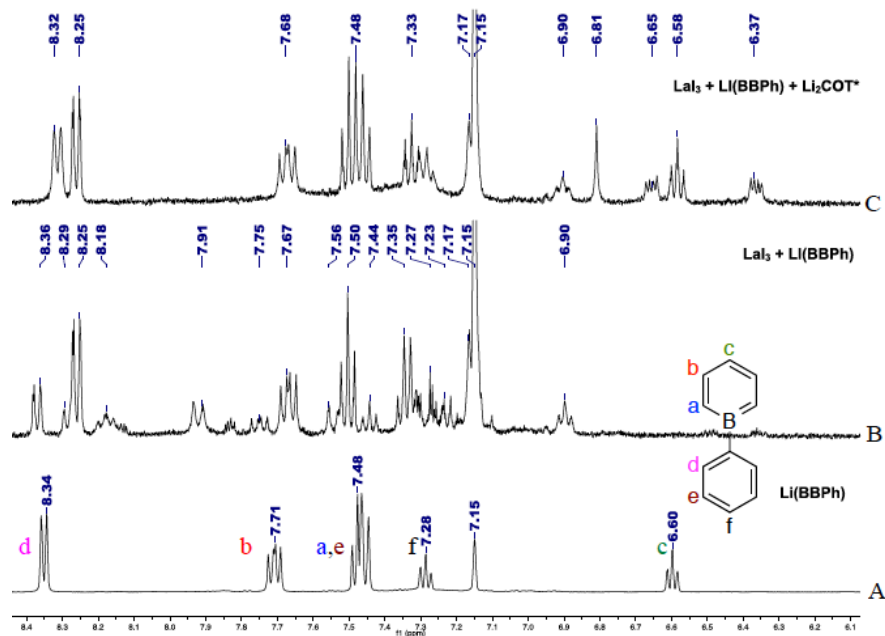
Figure 4-6: Stacked ^{1}H NMR spectra for the reaction between LaI₃, LiBBPh and Li₂COT*.

This **[La(BBPh)₃(I)]Li** complex was then independently synthesized by reacting three equivalents of **LiBBPh** with one equivalent of LaI₃ in THF at room temperature. Although the suspension of LaI₃ in THF dissolved within 30 minutes of the addition of the **LiBBPh** solution, the reaction mixture was stirred overnight to ensure complete conversion to the desired product. The ^{1}H NMR spectrum of the product was in accordance with the previous reaction. The *ortho* proton of the phenyl substituents appeared at 8.22 ppm while the *meta* protons of the phenyl of the borabenzene ring overlaps at 7.50 ppm. The *para* proton of the boratabenzene ring was observed at 6.57 ppm. Removal of THF from the reaction mixture under vacuum and extraction of the residue with toluene provided the trisboratabenzene lanthanum complex **La(BBPh)₃** without lithium iodide. It was characterized by ^{1}H, ^{13}C{^{1}H} and ^{11}B{^{1}H} NMR spectroscopy.

The **La(BBPh)₃** species is analogous to the triscyclopentadienyl lanthanide complexes (LnCp₃) and has not been observed with other lanthanides until now. The LnCp₃ are well known to form –ate complexes with halides and isocyanides due to the Lewis acidic character of the lanthanum atom.[174] This tendency to form quasi-tetrahedral –ate complexes exists with **La(BBPh)₃** also and results in the formation of **[La(BBPh)₃(I)]Li** complex. Analogous trisboratabenzene lanthanum complexes were reported by Chen very recently.[162] But they have been synthesized by refluxing the reaction mixture at 80 °C for several days.
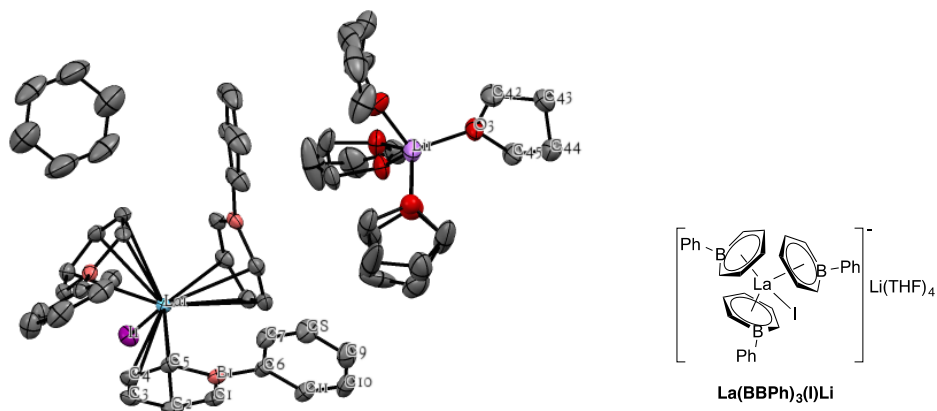
Figure 4-7: ORTEP view of molecular structure of [La(BBPh)₃(I)]Li complex. Anisotropic atomic displacement ellipsoids shown at 50% probability level. *Hydrogen atoms have been omitted for clarity (R1 = 2.71%). Anisotropic atomic displacement ellipsoids for the non-hydrogen atoms are shown at 50% probability level. Selected bond distances [Å] and angles [°]: La1-B1 3.166(4) La1-C1 3.067 La1-C2 2.966(2) La1-C3 2.887(2)La1-C4 2.931(3)La1-C5 2.979(2) B1-C1 1.524(3) B1-C5 1.518(4) B1-C6 1.581(3) C1-C2 = 1.383(3) C2-C3 1.407(4) C3-C4 1.396(4) C4-C5 1.396(3) La-I 3.2025(4) B1-La1-B2 97.51(7) B2-La1-B3 98.55(7) B3-La1-B1 96.79(7) C1-B1-C5 113.2(2) C1-C2-C3 122.0(2) C3-C4-C5 121.6(2) C7-C6-B1 122.3(3).

The ORTEP plot of the complex **[La(BBPh)₃(I)]Li** is given in Figure 4-7. The complex crystalizes in a P-1 space group. Each lanthanum atom is coordinated to three phenylboratabenzene rings and to one iodide. The association of a lithium ion coordinated to four molecules of THF stabilizes this anionic complex. Each unit cell contains two molecules of the complex and two molecules of benzene-d_6 that co-crystalizes with the complex (Figure 4-9 B). Unlike the tris(hydridoboratabenzene)lanthanum complex [(C₅H₅BH)₃La(μ-Cl)]₂ recently reported by Chen and coworkers that exists as a dimer bridged by a chloride ion, this complex exists as a monomer which can be attributed to the steric hindrance caused by the larger phenyl substituent on boron as compared to smaller hydrogen atom and the decreased bridging tendency of iodide over the chloride ion (Figure 4-8 A). The lanthanum ion shows slippage away from the boron atom resulting in longer La-B distances (3.167(2) – 3.197(3) Å) and the lanthanum ion is closer to the *para* carbon (2.886(13) Å) atoms as compared to the *ortho* carbon atoms (2.979(13) Å). This type of slipping has been observed in boratabenzene transition metal complexes, but the difference in the distance is much less than the lanthanum complex. The La-I bond distance is

3.2025(4) Å is much longer than the La-Cl (2.821(3) Å) distance observed in the bridged complex [(C$_5$H$_5$BH)$_3$La(μ-Cl)]$_2$ (Figure 4-8). An interesting thing to note in the structure is the distance between the ring centroids and the lanthanum atoms, which varies from 2.625 Å for one ring to 2.637 and 2.645 Å for the other two boratabenzene rings. The phenyl ring of the ligand is not co-planar with the boratabenzene ring and has a dihedral angle of 21.3°. The three boratabenzene rings are placed at an angle of 62.5° with respect to each other around the lanthanum ion making an equilateral triangle (Figure 4-9 A). There is no significant change in the bond lengths and bond angles of the coordinated boratabenzene ligands as compared to the free ligand.
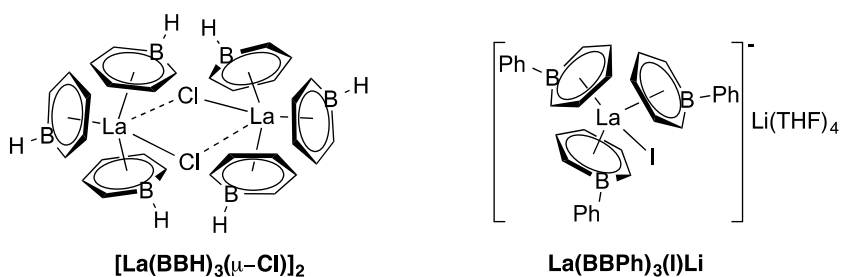
Figure 4-8: Representation of chloro bridged [La(BBH)$_3$(μ-Cl)]$_2$ and [La(BBPh)$_3$(I)]Li complexes.
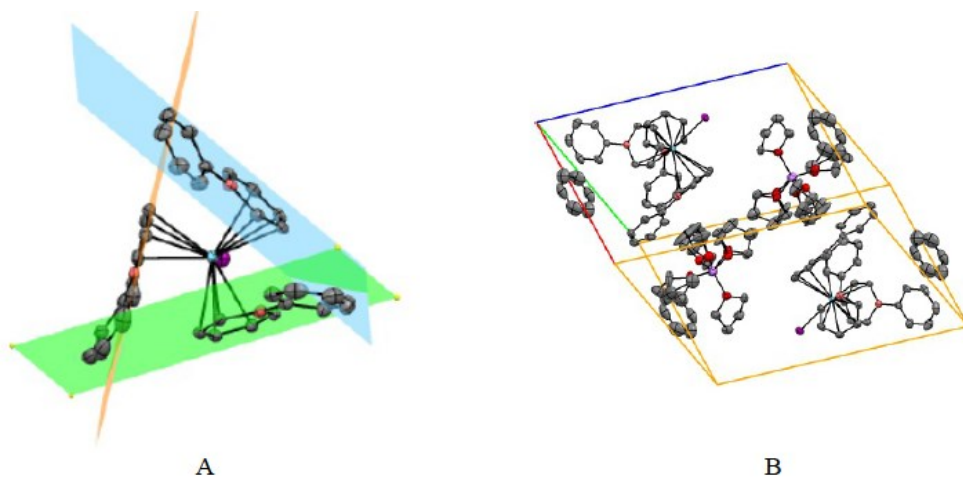
Figure 4-9: Representation of A) boratabenzene planes and B) unit cell of [La(BBPh)$_3$(I)]Li complex.

60

4.4.2 Ytterbium complexes of phenylboratabenzene

With the isolation of the trisboratabenzene lanthanum complex **[La(BBPh)$_3$(I)]Li(THF)$_4$** and its analogy with triscyclopentadienyl lanthanides (LnCp$_3$), we became interested in investigating if similar complexes can be obtained with other lanthanides. The LnCp$_3$ type complexes exist for all lanthanides from La to Yb, which is the smallest tripositive ion of the family. So we decided to synthesize the similar complex with YbI$_3$. Although Chen has observed very interesting chemistry of boratabenzene with ytterbium and the complexes are analyzable by NMR spectroscopy, it would be interesting to investigate if a **Ln(BBPh)$_3$** series exists that would be similar to the analogous LnCp$_3$ series. Furthermore, Long and coworkers recently reported the reduction of tris(pentamethylcyclopentadienyl)lanthanide complexes and they obtained a value of magnetic moment of 11.3 BM for the reduced dysprosium and holmium complex, which is the highest value for a single metal ion reported till now.[50] Considering the magnetic implications of these complexes it would be interesting to obtain a series of Ln(BBPh)$_3$ complexes and study their redox-reactions and magnetic properties.

In order to synthesize tris(phenylboratabenzene) ytterbium complex **[Yb(BBPh)$_3$]**, three equivalents of **Li(BBPh)** were reacted with one equivalent of a suspension of YbI$_3$ in THF/ benzene-d_6. The reaction mixture was sonicated for 12 h during which all the suspension disappeared and a yellow solution was formed. Monitoring of the reaction by ^{1}H NMR spectroscopy suggested the formation of **Yb(BBPh)$_3$** complex (Scheme 4-9). The proton signals at 8.24, 7.40, 7.22 ppm are consistent with the *ortho, meta* and *para* protons of phenyl substituent of boratabenzene ligand and have similar values as that for **La(BBPh)$_3$**. The protons of the boratabenzene ring are observed at 7.64, 7.33 and 6.54 ppm for *meta, ortho* and *para* positions and are also consistent with the values observed for analogous lanthanum complex. However, the crystals of this complex have not yet been obtained
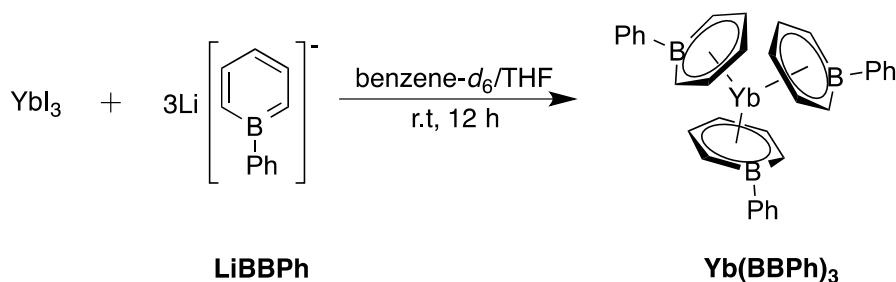
Scheme 4-9: Synthesis of trisboratabenzene complex of ytterbium.

Analogous reactions were attempted with terbium and dysprosium iodides also. The conversion of the suspension of LnI_3 in THF to clear yellow solutions upon reaction with **LiBBPh** has been observed for these salts also. However, NMR could not analyze these species and no crystal was obtained for these species.

4.5 Conclusion:

This chapter presented study of coordination behavior of **LiBBPh** ligand with lanthanide salts. Various attempts were made to form the sandwich and *ansa* complexes of lanthanides with **LiBBPh** that are of interest for molecular magnetism. Although the synthesis of **COTLnBBPh** sandwich complexes was not successful, we were able to isolate a unique homoleptic **[La(BBPh)₃(I)]Li** complex that was characterized by NMR and X-ray spectroscopy. Attempts to isolate similar homoleptic **Ln(BBPh)₃** complexes with other lanthanide ions were presented. An economical synthesis of **LiBBPh** from **BBPPh₃** was also presented.

62

4.6 Experimental procedure

4.6.1 General Procedures

All manipulations were carried out under an atmosphere of nitrogen using standard Schlenk techniques or in nitrogen filled gloveboxes, unless specified otherwise. All solvents were distilled from sodium and benzophenone. Benzene-d_6 was distilled under reduce pressure from a Na/K alloy. 1-Chloro-2-(trimethylsilyl)boracyclohexa-2,5-diene[104] and 1,4-bistrimethylsilyl cyclooctatettraene[173] were prepared according to the literature procedures. Anhydrous cobalt(II) chloride and chromium(II) chloride was purchased from Sigma Aldrich and used without further purification. Anhydrous lanthanum(III) iodide, dysprosium(III) chloride, terbium(III) chloride and ytterbium(III) iodide were purchased from Alfa Aeser and used without further purification. NMR spectra were recorded on an Agilent Technologies NMR spectrometer at 500 MHz (^{1}H), 125.758 MHz (^{13}C), 160.46 MHz (^{11}B), and on a Varian Inova NMR AS400 spectrometer, at 400.0 MHz (^{1}H), 100.580 MHz (^{13}C), 202.456 MHz (^{31}P). ^{1}H NMR and ^{13}C{^{1}H} NMR chemical shifts are referenced to residual solvent signals in deuterated solvent. Multiplicities are reported as singlet (s), doublet (d), triplet (t), quartet (q), multiplet (m) or broad (br). Chemical shifts are reported in ppm. Coupling constants are reported in Hz. HRMS characterization was possible using an Agilent Technologies 6210 LC time of flight mass spectrometer. Products in toluene and THF solutions were introduced to the nebulizer by direct injection. Neutral borabenzene adducts were characterized using APPI ionization in positive and negative mode. Ionic species were ionised by electrospray (ESI-MS) in both positive and negative modes.

Synthesis of borabenzene-triphenylphosphine (BBPPh₃). Triphenylphosphine (2.82 g, 10.7 mmol) dissolved in 30 ml of hexane was added to a solution of 1-chloro-2-(trimethylsilyl)boracyclohexa-2,5-diene (2.00 g, 10.7 mmol) in 10 ml of hexane. The reaction mixture was stirred overnight at room temperature during which a white precipitate was formed. The precipitate was filtered and washed with 3 X 10 ml of toluene-hexane

solution. The pale solid was dried under vacuum to give 2.70 g (7.98 mmol, 75%) of borabenzene-triphenylphosphine.

^{1}H NMR [500 MHz] (*benzene-d$_6$*) δ: 8.04 (br, 2H, H^2), 7.53 (m, 6H, Ph^{ortho}), 7.42 (m, 2H, H^3), 7.03 (m, 1H, H^4), 7.00 (m, 3H, Ph^{para}), 6.90 (m, 6H, Ph^{meta}). ^{13}C{^{1}H} NMR (*benzene-d$_6$*) δ: 134.5 (d, J_{C-P} = 10.8 Hz, PPh$_3$), 134.2 (s), 134.0(s), 131.6 (d, J_{C-P} = 2.51 Hz, PPh$_3$), 128.9 (d, J_{C-P} = 11.6, PPh$_3$), 121.0 (s). ^{11}B{^{1}H} NMR (*benzene-d$_6$*) δ: 20.0 (d, J_{B-P} = 100.6 Hz). ^{31}P{^{1}H} NMR [121 MHz] (*benzene-d$_6$*; referenced to H$_3$PO$_4$) δ: 6.6 (br).

Synthesis of borabenzene-trimethylphosphine (BBPMe$_3$). Trimethylphosphine (0.4 mL, 0.294 g, 3.86 mmol) was syringed in dropwise into a small reaction Schlenk containing (1.175 g, 3.17 mmol) of 1-chloro-2-(trimethylsilyl)boracyclohexa-2,5-diene solvated in hexane. After 11 h, a white solid precipitated out of the yellow solution, which was filtered and dried under vacuum to remove SiMe$_3$Cl and unreacted boracycle. This white product was washed with cold pentane twice and the solids were collected inside of the glovebox. Yield: 69% (0.341 g, 2.25 mmol) of a white powder.

^{1}H NMR [400 MHz] (*benzene-d$_6$*) δ: 8.04 (br s, 2H, H^2), 7.41 (br t, J_{H-H} = 7.3 Hz, 1H, H^4), 7.23 (br t, J_{H-H} = 8.9 Hz, 2H, H^3), 0.64 (d, J_{P-H} = 11.3 Hz, 9H, P(CH$_3$)$_3$). ^{13}C{^{1}H} NMR (*benzene-d$_6$*) δ: 133.6 (d, J_{C-P} = 17.5 Hz), 128 (br s), 120.7 (s), 10.6(d, J_{C-P} = 42.0 Hz) ^{11}B{^{1}H} NMR (*benzene-d$_6$*) δ: 20.8 (d, J_{B-P} = 110 Hz) [13]. ^{31}P{^{1}H} NMR [121 MHz] (*benzene-d$_6$*; referenced to H$_3$PO$_4$) δ: -22.6 (q, J_{P-B} = 108 Hz). These values are in accordance with the reported values.[104]

Synthesis of Lithium salt of Phenyl boratabenzene (LiBBPh). A suspension of phenyl lithium (249.7 mg, 2.9 mmol) in 5 ml toluene was cooled down to 0 °C. To it was added a solution of **BBPPh$_3$** (1.00 g, 2.9 mmol) in 10 ml toluene. The reaction mixture was stirred at room temperature for 2 h. Toluene was filtered off and the solid was washed with 2 X 10 ml of toluene. The white solid left behind was dried under vacuum. Yield 363 mg (78%).

^{1}H NMR [400 MHz] (*benzene-d$_6$*) δ: 8.34 (d, J_{H-H} = 8.0 Hz, 2H, Ph^{ortho}), 7.71 (dd, J_{H-H} = 10.0, 7.0 Hz, 2H, H^3), 7.47 (m, 4H, H^2, Ph^{meta}), 7.28 (t, J_{H-H} = 7.3 Hz, 1H, Ph^{para}), 6.60 (t, J_{H-H} = 7.0 Hz, 1H, H^4). ^{13}C{^{1}H} NMR (*benzene-d$_6$*) δ: 133.6 (s), 132.9 (s), 126.0 (s), 124.4

(br), 110.3 (s). $^{11}B\{^1H\}$ NMR (*benzene-d6*) δ: 33.5 (br). DI-MSTOF (ESI, m/e): Calcd. for $C_{11}H_{10}B^-$ 153.0876; found 153.0876.

Synthesis of bis(phenylboratabenzene)cobalt complex [Co(BBPh)$_2$]. 0.169 g (1.06 mmol) of **LiBBPh** was mixed with 0.069 m (0.53 mmol) of CoCl$_2$ in a Schlenk tube. The solids were cooled down to -20 °C and 20 ml of THF was added to it. The solution was vigorously stirred and allowed to warm to room temperature overnight. The dark red solution obtained was evaporated and dried under vacuum. The dark red residue was extracted with toluene. The toluene solution was evaporated to minimum and layered with ether. Dark red crystals were obtained after cooling the solution to -80 °C overnight. Yield 146 mg (69.7%).

DI-MSTOF (APPI, m/e): Calcd. for $C_{22}H_{20}B_2Co$ 365.1083 found 365.1108.

Synthesis of bis(phenylboratabenzene)chromium complex [Cr(BBPh)$_2$]. 100 mg (0.625 mmol) of **LiBBPh** was mixed with 38.4 mg (0.313 mmol) of CrCl$_2$ in a Schlenk tube. 10 ml of THF was added to the solids at room temperature. The solution became bright red in 10 min and was allowed to react for 12 h. THF was removed under vacuum and the red residue was extracted with ether. The ether filtrate was evaporated to minimum and cooled to -80 °C overnight during which red block crystals grew in the solution. Yield 78.0 mg (64.2%).

DI-MSTOF (APPI, m/e): Calcd. for $C_{22}H_{20}B_2Co$ 358.1156 found 358.1148.

Synthesis of bis(phenylboratabenzene)lanthanide chloride [Ln(BBPh)$_2$Cl]. One equivalent of lanthanide chloride (LnCl$_3$) was mixed with two equivalents of **LiBBPh** in a Schlenk tube. 10 ml of toluene was added to the solids and the solution was refluxed at 120 °C for 3 days. The white suspension became yellow over 3 days and is then filtrated to give yellow solution. Removal of toluene from the filtrate gave pale yellow solids.

Tb(BBPh)$_2$Cl: TbCl$_3$ = 132 mg (0.497 mmol), LiBBPh = 160 mg (1.00 mmol), Tb(BBPh)$_2$Cl = 150 mg

Dy(BBPh)₂Cl: $DyCl_3$ = 124 mg (0.387 mmol), LiBBPh = 124 mg (0.775 mmol) $Dy(BBPh)_2Cl$ = 120 mg

Synthesis of COTLnCl complexes. 2.3 equivalent of potassium (K_{metal}) was reacted with 1 equivalent of cyclooctatettraene in 20 ml of THF at 0 °C for two hours during which the solution became dark brown in color. This brown solution was filtered and added to a suspension of 1 equivalent of $LnCl_3$ in 10 ml THF at 0 °C. The reaction mixture was stirred at room temperature for 24 h during which it became yellow for Dy and Tb, and pink for Er. The reaction mixture was filtered and the residue left behind was dried under vacuum. This residue was subjected to soxhlet extraction with THF for 24 h and the product was obtained after evaporation of filtrate.

COTDyCl(THF)₂: COT = 424 mg (4.07 mmol), K_{metal} = 366 mg (9.36 mmol), $DyCl_3$ = 1.09 g (4.07 mmol), COTDyCl 780 mg (51.2%).

COTTbCl(THF)₂: : COT = 275 mg (2.60 mmol), K_{metal} = 233 mg (5.98 mmol), $TbCl_3$ = 700 mg (2.60 mmol), COTbCl 270 mg (30%).

COTErCl(THF)₂: COT = 300 mg (2.88 mmol), K_{metal} = 258 mg (6.62 mmol), $ErCl_3$ = 788. mg (2.88 mmol), COTErCl = 100 mg (10%).

Reaction of COTLnCl(THF)₂ with LiBBPh. A suspension of 1 equivalent of COTLnCl was reacted with 1 equivalent of LiBBPh in 20 ml of THF at room temperature for 24 h. There was no change in the color or appearance of reaction mixture. The solution was evaporated and extracted with toluene. Evaporation of the toluene filtrate gave dark yellow solids, which could not be characterized.

COTDyCl(THF)₂: 339 mg (0.729 mmol) LiBBPh = 116 mg (0.729 mmol).

COTTbCl(THF)₂: 55 mg (0.120 mmol) LiBBPh = 19.2 mg (0.120 mmol).

Reaction of LaI₃ with LiBBPh and Li₂COT*. A suspension of 4 mg (0.0076 mmol) of LaI_3 was made in benzene-d_6 and THF. To it was added a solution of 1.22 mg (0.076 mmol) of LiBBPh. The reaction was sonicated for 4 h during which the suspension disappeared, a

clear liquid and a solid was formed. Li_2COT^* (1 mg, 0.0038 mmol) was added as a solid. It dissolved and the solution became yellow and was allowed to react for 1 hour. Two products were observed in the reaction.

La(BBPh)₃(I)Li : [1H] NMR [400 MHz] (*benzene-d₆*) δ: 8.25 (d, J_{H-H} = 8.0 Hz, 2H, Ph^{ortho}), 7.45 (m, H^3, Ph^{meta}), 7.33 (t, J_{H-H} = 7.1 Hz, 1H, Ph^{meta}), 7.26 (m, Ph^{para}), 7.16 (overlapped with solvent, H^2), 6.60 (t, J_{H-H} = 6.8 Hz, 1H, H^4).

La(BBPh)₃: [1H] NMR [400 MHz] (*benzene-d₆*) δ: 8.32 (d, J_{H-H} = 7.8 Hz, 2H, Ph^{ortho}), 7.67 (dd, J_{H-H} = 10.2, 6.9 Hz, 2H, H^3), 7.51 (m, Ph^{meta}), 7.28 (m Hz, 1H, Ph^{para}), 6.91 (br, 1H, H^4). H^2 is not seen and probably overlap with other signals in the spectrum.

Synthesis of tris(phenylboratabenzene) lanthanum iodide [La(BBPh)₃(I)]Li(THF). 46.2 mg (0.288 mmol) of **LiBBPh** was dissolved in 7 ml of THF. It was added slowly to a suspension of 50.0 mg (0.096 mmol) of LaI_3 in 3 ml of THF. Within 30 min of addition the suspension dissolved and a light yellow solution was formed. The reaction mixture was stirred overnight to ensure the completion of the reaction. Solvent was removed under vacuum and the solid was dried to furnish the product as a grey white solid. Yield 49 mg (65.7%).

[1H] NMR [400 MHz] (*benzene-d₆*) δ: 8.22 (d, J_{H-H} = 7.8 Hz, 2H, Ph^{ortho}), 7.44 (m, 2H, H^3), 7.26 (m, 3H, H^2, Ph^{para}), 7.37 (m, Ph^{meta}), 6.66 (br, 1H, H^4), 3.59 (m, THF), 1.25 (m, THF). [13C]{[1H]} NMR (*benzene-d₆*) δ: 140.1 (s), 133.1 (s), 128.5 (s), 127.2 (s), 115.7 (s), 58.6 (s), 25.9 (s). [11B]{[1H]} NMR (*benzene-d₆*) δ: 33.0 (br).

Synthesis of tris(phenylboratabenzene) lanthanum [La(BBPh)₃]. **La(BBPh)₃(I)Li(THF)** was dried under vacuum and washed with hexane to remove coordinated THF molecules. The pale solid was then extracted with toluene. Removal of toluene from the filtrate gives the product as a pale yellow solid.

[1H] NMR [400 MHz] (*benzene-d₆*) δ: 8.41 (d, J_{H-H} = 7.8 Hz, 2H, Ph^{ortho}), 7.72 (m, 2H, H^3), 7.53 (d, 2H, Ph^{meta}), 7.30 (m, H^2, Ph^{para}), 6.60 (br, 1H, H^4). [13C]{[1H]} NMR (*benzene-d₆*) δ: 140.1 (s), 133.6 (s), 133.1 (s), 127.2 (s), 114.3 (s). [11B]{[1H]} NMR (*benzene-d₆*) δ: 33.0 (br).

Synthesis of tris(phenylboratabenzene) ytterbium [La(BBPh)₃]. 7 mg (0.043 mg) of **LiBBPh** was dissolved in benzene-d_6 and a few drops of THF. It was added to a suspension of YbI₃ (8.07 mg, 0.0146 mmol) in benzene-d_6 /THF. The reaction mixture was sonicated overnight to give a clear yellow solution.

^{1}H NMR [400 MHz] (*benzene-d₆*) δ: 8.24 (d, J_{H-H} = 7.8 Hz, 2H, Ph^{ortho}), 7.64 (m, 2H, H^3), 7.40 (t, J_{H-H} = 7.1 Hz, Ph^{meta}), 7.31 (br, 2H, H^2), 7.22 (m, Ph^{para}), 6.54 (br, 1H, H^4). ^{13}C{^{1}H} NMR (*benzene-d₆*) δ: 133.6 (s), 132.7 (s), 127.6 (s), 124.5 (br), 110.5 (s), 58.6 (s), 25.9 (s). ^{11}B{^{1}H} NMR (*benzene-d₆*) δ: 33.2 (br).

Synthesis of tris(phenylboratabenzene) complexes of Dy and Tb. A suspension of one equivalent of LnI₃ in 3 ml of THF was reacted with a solution of three equivalents of **LiBBPh** in 7 ml of THF. The reaction mixture was stirred at room temperature for 12 h. The solvent was removed under vacuum and the residue was extracted with toluene. Evaporation of toluene from filtrate provides yellow solids.

Dy(BBPh)₃: DyCl₃ = 44.7 mg (0.16 mmol), LiBBPh = 80.0 mg (0.49 mmol). Yield 41mg (38.3%).

Tb(BBPh)₃: DyCl₃ = 44.0 mg (0.16 mmol), LiBBPh = 80.0 mg (0.49 mmol). Yield = 38 mg (35.8%).

4.6.2 Crystallographic Studies:

Nice single crystals with suitable size of all compounds were mounted on CryoLoops with Paratone-N and optically aligned on a Bruker SMART APEX-II X-ray diffractometer with 1K CCD detector using a digital camera. Initial intensity measurements were performed using a fine-focused sealed tube, graphite-monochromated, X-ray source (Mo *Kα*, *λ* = 0.71073 Å) at 50 kV and 30 mA. Standard APEX-II software package was used for determining the unit cells, generating the data collection strategy, and controlling data collection. SAINT was used for data integration including Lorentz and polarization corrections. Semi-empirical absorption corrections were applied using SCALE (SADABS). The structures of all compounds were solved by direct methods and refined by full-matrix

least-squares methods with SHELX-97 in the SHELXTL6.14 package. All of the H atoms were generated geometrically and refined in riding mode.

Chapter 5 - Synthesis and reactivity of novel mesityl boratabenzene ligands and their coordination to transition metals

In chapter 4 we have discussed about our attempts to synthesize **Ln(BBPh)₂Cl** type of complexes. However, the insolubility of the complexes due to their tendency to form dimeric and polymeric molecules made it difficult to characterize them. Hence, we decided to synthesize a bulky boratabenzene ligand that has bulky groups at the *para* carbon atom and at the boron atom. The introduction of this steric bulk was expected to prevent the formation of *ate* complexes and hence dimerization. Thus a boratabenzene with a bulky mesityl group on boron atom and an *iso*-propyl group at the *para* position of the borabenzene, Li(1-mesityl-4-*i*Prboratabenzene) (**LiMesBB***) was synthesized. The coordination of this ligand to lanthanides was found to be challenging. While reacting the **LiMesBB*** with lanthanide halides they would decompose to give hydrolyzed boracycles. However, during the synthesis of the **LiMesBB*** ligand we observed some interesting reactivity of this ligand and its precursors, which were published in *Organometallics* in 2014 and are presented here.

5.1 Absract

La synthèse et la caractérisation de nouveaux ligands mésitylboratabenzène encombrés ont été effectuées. Les boracyclohexadiènes (**2,5-MesBC*, 3,5-MesBC***) isolés dans ces reactions se sont révélés être extrêmement stables et peuvent être désilylées sélectivement par hydrolyse. Ces ligands ont été coordonnés au Fe(II) et au Cr(II). La désilylation sélective des boratabenzènes a aussi été observée dans le cas des complexes de fer et a permis d'isoler trois complexes « sandwich » boratabenzène de fer contenant zéro, un ou deux groupes TMS ((**Fe(MesBB)₂**, (**Fe(MesBB)₂SiMe₃**), et (**Fe(MesBBSiMe₃)₂**) respectivement). **Fe(MesBB)₂** représente le premier complexe bisboratabenzène de métal n'adoptant pas une conformation *trans* dans sa structure cristalline.

5.2 Abstract:

The synthesis and characterization of novel bulky mesitylboratabenzene ligands have been achieved. The isolated boracyclohexadienes (**2,5-MesBC*, 3,5-MesBC***) were found to be extremely stable and could be selectively desilylated by hydrolysis. These ligands have been successfully coordinated to Fe(II) and Cr(II). The selective desilylation of the boratabenzene ring was also observed in the iron complexes, thus furnishing three ironboratabenzene sandwich complexes without a TMS group (**Fe(MesBB)$_2$**), with one (**Fe(MesBB)$_2$SiMe$_3$**), and two (**Fe(MesBBSiMe$_3$)$_2$**) TMS groups, respectively. Interestingly, species **Fe(MesBB)$_2$** represents the first structurally characterized bis(boratabenzene) metallic species not exhibiting the expected *trans* geometry.

5.3 Introduction

A variety of heterocyclic boron containing molecules have been synthesized in recent years and these species have shown unique properties and rich coordination chemistry.[175,176] One of such systems, the borabenzene ring, has been the object of considerable interest because of the flexibility of its coordination modes and its potential as ancillary ligand for transition metals.[91,121,177] Although the base-free borabenzene molecule is a highly reactive species that is yet to be isolated (Figure 5-1, I), a variety of neutral or anionic Lewis bases have been used to stabilize neutral borabenzene (Figure 5-1, II) and anionic boratabenzene adducts (Figure 5-1, III), respectively.

$$L = PMe_3, PPh_3, NEt_3, Py...$$
$$X = Me, Et, Ph, NEt_2, H, Cl...$$
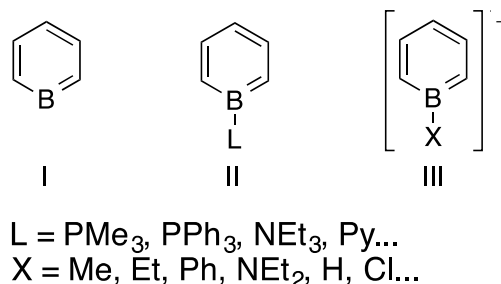
Figure 5-1: Neutral borabenzene and anionic boratabenzene adducts.

Since their discovery, base-stabilized borabenzene and boratabenzene derivatives and metal complexes have created a niche for themselves in a large array of applications,[108,160,178–184] notably in the field of catalysis[90,91,93,131,132,160,177–179,185–188] and in the generation of optoelectronic materials.[89,97–99,106,189–191] The first boratabenzene derivative was synthesized by the ring expansion of a cyclopentadienyl ligand on 19-electron cobaltocene by Herberich in 1970.[89] However, Fu developed an elegant synthetic route in 1996, where the transmetallation of trimethylsilyl substituted dibutylstannacyclohexa-2,5-diene with BCl$_3$ furnishes the 2-trimethylsilyl-2,5-boracyclohexadiene (**2,5-BC**), (Scheme 5-1).[104] The attack of a neutral Lewis base (PMe$_3$, PPh$_3$, NEt$_3$ etc.) on the boracyclohexadiene (Scheme 5-1) leads to the formation of borabenzene adduct with the elimination of SiMe$_3$Cl. It has been suggested that the first step in this reaction is the isomerization of **2,5-BC** to **3,5-BC** (Scheme 5-1), followed by base coordination-induced aromatization.[104,192] A variety of boratabenzene salts can be subsequently synthesized by carrying out a nucleophilic attack

of an anionic base on neutral borabenzene adducts (Scheme 5-1). The reaction is believed to proceed through an associative mechanism.[127,159]
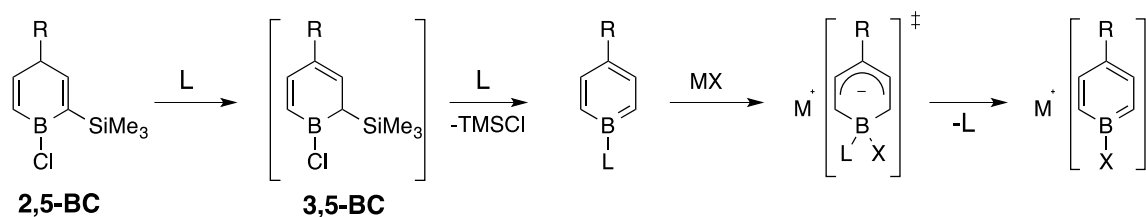
Scheme 5-1: General synthesis of borabenzene and boratabenzene adducts.

As part of a research program focused on unusual coordination modes for borabenzene and boratabenzene ligands[112,158,193,194] we have been interested in the coordination chemistry of boratabenzene analogues featuring bulky substituents on the boron atom. More specifically, our study of 1-mesitylboratabenzene salts, led us to synthesize 1-mesityl-4-isopropyl-2,5-boracyclohexadiene (**2,5-MesBC***) and 1-mesityl-4-isopropyl-3,5-boracyclohexadiene (**3,5-MesBC***) as two non-aromatic isomeric precursors for the generation of mesitylboratabenzene complexes. In contrast to other boracyclohexadiene species reported, the 3,5-boracyclohexadiene (**3,5-MesBC***) isomer was found to be highly stable and was thus isolated and characterized. While exploring the reactivity of the two isomers of boracyclohexadiene (**2,5-MesBC*** and **3,5-MesBC***), we were able to demonstrate that several of these species are water tolerant. The corresponding boratabenzene salts and their coordination chemistry to Fe(II) and Cr(II) have been studied and are herein presented.

5.4 Results and Discussion

5.4.1 Synthesis of the lithium salts of mesitylboratabenzene

The general method for the synthesis of anionic boratabenzene ligands, as reported by Fu, involves the attack of a nucleophile on a neutral borabenzene adduct such as borabenzene-PMe₃ (**BBPMe₃**) and borabenzene-NEt₃ (**BBNEt₃**) to form the anionic boratabenzene species (Scheme 5-1).[159] However, when mesityl lithium was used as a nucleophile in presence of **BBPMe₃**, a mixture of products, containing the expected lithium mesitylboratabenzene in addition to the starting material and several side-products, was obtained. The lack of selectivity for this reaction can be attributed to the steric hindrance

provided by the methyl groups in *ortho* position of the mesityl ring, shielding the nucleophilic carbon of the lithium salt. A new route for the synthesis of the lithium salt of 1-mesityl-2-trimethylsilyl-boratabenzene (**LiMesBBSiMe₃**) was adopted where 2 equivalents of mesityl lithium were reacted with 1 equivalent of 1-chloro-2-trimethylsilyl-2,5-boracyclohexadiene (**2,5-BC**) to give **LiMesBBSiMe₃** in 75% yield. This reaction proceeded with an initial nucleophilic attack of mesityl lithium on boron followed by the deprotonation of the corresponding 1-mesityl-2-trimethylsilyl-boracyclohexa-2,5-diene (**2,5-MesBC**), as depicted in Scheme 5-2.

The reaction was monitored using ^{1}H NMR spectroscopy at 300K. After 4 h, the complete conversion of **2,5-BC** to **LiMesBBSiMe₃** was observed. The trimethylsilyl group remained on the aromatic ring ($\delta = 0.28$) and four new aromatic protons attributed to **LiMesBBSiMe₃** were found at $\delta = 7.89$ (H^3), 7.58 (H^5), 6.78 (H^6) and 6.61 (H^4) with all expected coupling constants for such species (for the typical numbering scheme used for the boron heterocycles see **3,5-MesBC** in Scheme 5-2). The ^{11}B{^{1}H} NMR resonance shifted from 53.5 to 39.4 ppm, which is within the expected range for boratabenzene salts.[118,158,194] Intermediate **3,5-MesBC** was short lived when 2 equivalents of mesityl lithium was used. However, in presence of 1 equivalent of mesityl lithium, it was possible to observe the formation of intermediate **3,5-MesBC**, which was notably confirmed by the appearance of a doublet of doublets at $\delta = 7.43$ (H^5), a doublet at $\delta = 7.00$ (H^6), a triplet at $\delta = 6.91$ (H^4), and a doublet of doublets at $\delta = 6.50$ (H^3). In addition to the resonances associated with the mesityl ring, another doublet at $\delta = 4.09$ corresponding to the H^2 proton next to SiMe₃ group ($\delta = -0.12$) was observed. The ^{11}B{^{1}H} NMR appears at $\delta = 63.0$ which is consistent with a BR₃ (R = alkyl, aryl) type species.
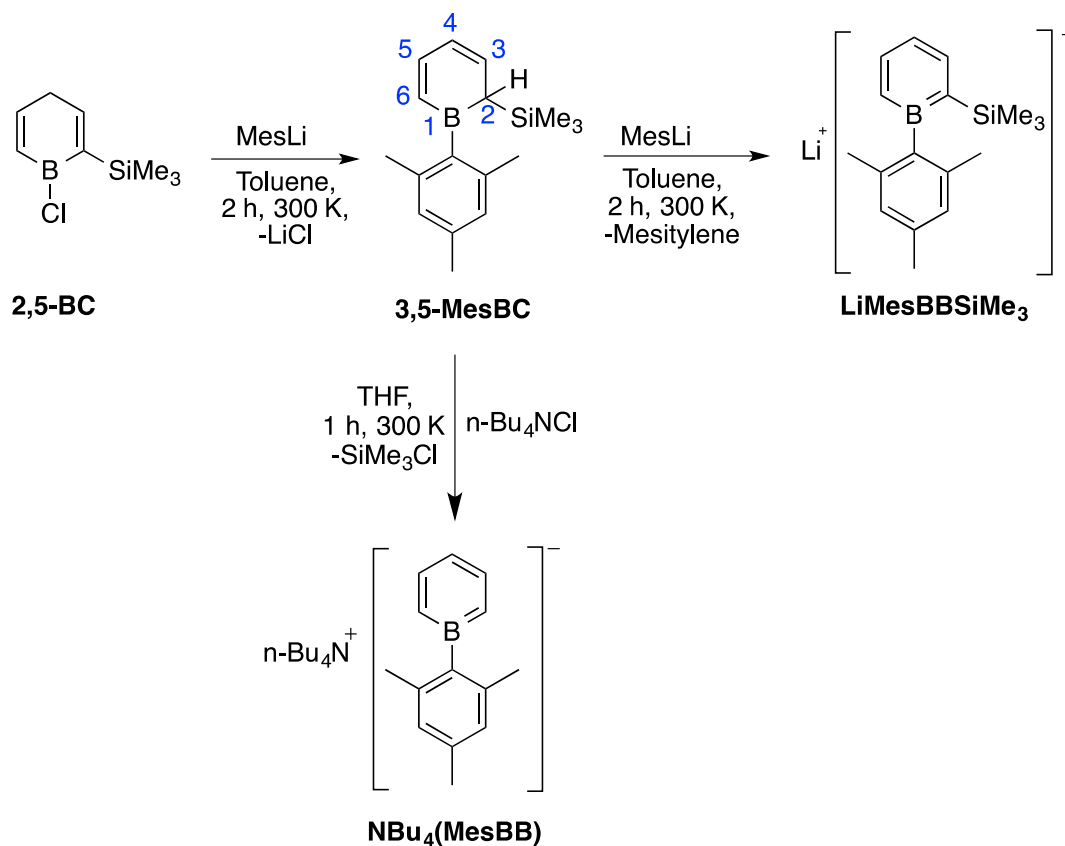
Scheme 5-2: Synthesis of the lithium salt of 1-mesityl-2-(trimethylsilyl)boratabenzene and 1-mesitylboratabenzene.

The analogue of **LiMesBBSiMe₃** without the trimethylsilyl group, compound **NBu₄(MesBB)**, was synthesized by reacting first **2,5-BC** with one equivalent of mesityl lithium. The lithium chloride that formed was removed by filtration and the desilylation of **3,5-MesBC** was carried out with tetrabutylammonium chloride (n-Bu₄NCl) to give **NBu₄(MesBB)**, in 75% yield (Scheme 5-2). Boratabenzene **NBu₄(MesBB)**, was also characterized using ^{1}H NMR spectroscopy. The boratabenzene moiety displays a set of three aromatic resonances confirming the presence of a plane of symmetry. The proton resonances appeared at δ = 6.61 (H^4), 6.99 (H$^{2/6}$) and 7.72 (H$^{3/5}$) in a 1:2:2 ratio. The ^{11}B{^{1}H} NMR resonance was observed at δ = 33.1, shielded in comparison to that of **LiMesBBSiMe₃** (δ = 39.4).

The reaction of 1-chloro-2-trimethylsilyl-4-isopropyl-2,5-boracyclohexadiene (**2,5-BC***)[99] with two equivalents of mesityl lithium did not furnish 1-mesityl-2-trimethylsilyl-4-isopropyl-boratabenzene (**LiMesBB*SiMe₃**) as expected, even after 12 hours at 300 K. Instead, species 1-mesityl-2-trimethylsilyl-4-isopropyl-3,5-boracyclohexadiene (**3,5-MesBC***) was formed, indicating that the initial nucleophilic substitution on boron took place but that the following deprotonation did not occur. This suggests that the presence of the *iso*-propyl group at the *para* position and of the trimethylsilyl group at the *ortho* position of **3,5-MesBC***makes it too sterically demanding for mesityl lithium to abstract the proton and aromatize the corresponding boracyclohexadiene. The isolation of **3,5-MesBC*** as a yellow oil was possible by extracting the reaction mixture with hexane (Scheme 5-3). The latter compound was characterized using ^{1}H and COSY NMR experiments. The H^5, H^3 and H^6 protons appeared as doublets at δ = 7.46, 6.74 and 7.07, respectively. The trimethylsilyl group was observed at δ = -0.09 while the H^2 was observed as a doublet at δ = 4.06. The presence of this methyne proton at the 2-position was confirmed using COSY experiments, which indicated that the proton couples only with H^3 and did not show any coupling with the CH proton of the isopropyl fragment. A shift of the resonance was also witnessed by ^{11}B{^{1}H} NMR spectroscopy where the peak was displaced from δ = 53.5 to δ = 62.0, which is in close agreement with the assignation of **3,5-MesBC**.
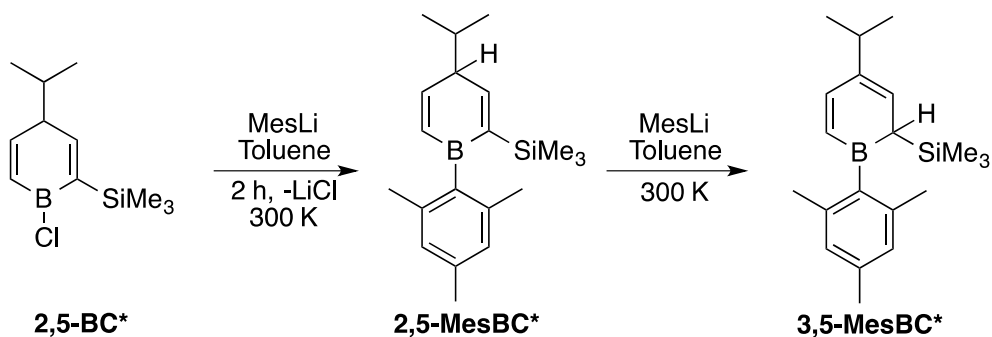
Scheme 5-3: Synthesis of the 3,5-diene and 2,5-diene isomers of 1-mesityl-4-isopropyl-boracyclohexadiene.

Another isomer of 1-mesityl-4-isopropylboracyclohexadiene was isolated from the latter reaction (Scheme 5-3). The isomer **2,5-MesBC*** (1-mesityl-2-trimethylsilyl-4-isopropyl-2,5-boracyclohexadiene) was obtained as a light yellow oil and was characterized by ^{1}H

NMR and COSY spectroscopy experiments. One notable feature when compared to isomer **3,5-MesBC*** is the presence of an aliphatic proton as a multiplet at $\delta = 2.74$. COSY experiments confirmed the coupling of this aliphatic proton with the H^3 and H^5 protons and with the CH proton of *iso*-propyl group, supporting that it can be attributed to a proton on C^4. Studying the reactivity of the isomers **2,5-MesBC*** and **3,5-MesBC***, it was observed that **2,5-MesBC*** could be converted into **3,5-MesBC*** by adding 1 equivalent of mesityllithium or a catalytic amount of lithium mesitylboratabenzene (**LiMesBBSiMe₃**). This phenomenon is in accordance with the proposition of Fu,[159] suggesting that the initial step of the reaction of 2-(trimethylsilyl)-2,5-boracyclohexadiene (**2,5-BC**) with Lewis bases (PMe₃, PPh₃, NEt₃), consists in the isomerization to 2-trimethylsilyl-3,5-boracyclohexadiene (**3,5-BC**). However, the 3,5-diene isomer of most borabenzene derivatives are very reactive and cannot be isolated. The 3,5-diene isomer **3,5-MesBC*** is very stable and can be stored at room temperature for months. However, the 2,5-diene isomer **2,5-MesBC*** is stable in its pure form, but remains sensitive to thermal or base-catalyzed isomerization to **3,5-MesBC***. Treatment of THF solutions of **2,5-MesBC*** with LiNMe₂, LiNiPr₂ or metallic potassium (under completely anhydrous conditions) selectively yielded 1-mesityl-2-trimethylsilyl-4-isopropyl-boratabenzene (**LiMesBB*SiMe₃**) (Scheme 5-4). It was characterized on the basis of its ¹H NMR spectrum, which consists of three aromatic peaks at $\delta = 7.86$ (H^3), 7.56 (H^5) and 6.86 (H^6) corresponding to the *meta* and *ortho* ring protons respectively and a peak for SiMe₃ appears at $\delta = 0.29$. The ¹¹B{¹H} NMR spectrum gives a peak at $\delta = 38.1$ which is upfield from **2,5-MesBC*** and **3,5-MesBC***.
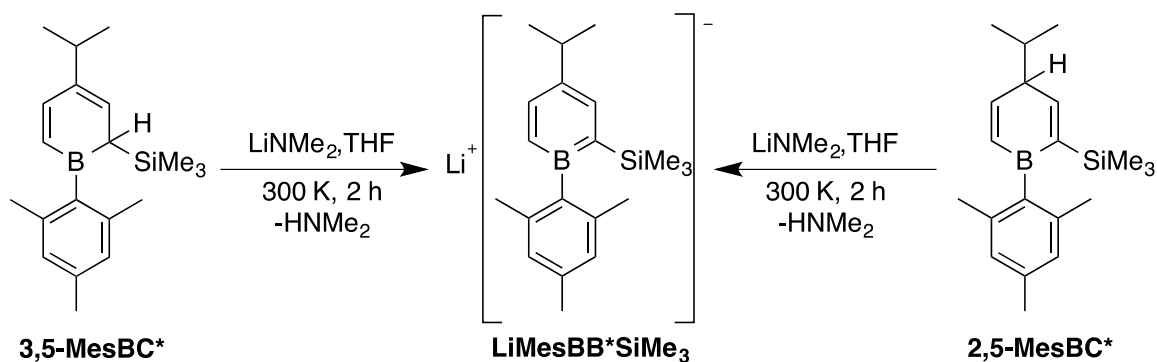
Scheme 5-4: Synthesis of the lithium salt of 1-mesityl-2-trimethylsilyl-4-isopropyl-boratabenzene.

An important reactivity observed for **3,5-MesBC*** was the selective desilylation to form **3,5-MesBC*H**. Addition of 1 equivalent or more of water to a solution of **3,5-MesBC*** in THF results in the formation of **3,5-MesBC*H** (Scheme 5-5). The trimethylsilyl group is selectively hydrolysed to form a trimethylsilylether leaving behind the 1-mesityl-4-isopropyl-3,5-boracyclohexadiene **(3,5-MesBC*H)**, which was characterized by the disappearance of the trimethylsilyl peak at δ = -0.09 and of the doublet at δ = 4.06 and the appearance of a doublet at δ = 2.41 which integrates for two protons in the ^{1}H NMR spectrum. **3,5-MesBC*H** was reacted with NaOH or LiNMe$_2$ to form the 1-mesityl-4-isopropyl-boratabenzene salt (**LiMesBB*, NaMesBB***), as observed in Scheme 5-5. The former reagent is of particular interest since it implies that the conjugated acid, H$_2$O, does not react with the boratabenzene alkali-metal salt generated. Characterization of **LiMesBB*** using ^{1}H NMR spectroscopy indicated a downfield shift for the H$^{3/5}$ and H$^{2/6}$ protons of the ring to δ = 7.50 and 6.94, respectively, as compared to **3,5-MesBC*H**. The *iso*-propyl group shifted to δ = 1.35 for CH$_3$ and δ = 2.87 for CH. The hydrolysis reaction of mesitylboracycle **3,5-MesBC*** is particularly interesting because it does not involve the isolation of a boron hydroxyl species, a reaction that is usually observed with all other boron heterocycles.[107,195–197] Thus, the steric bulk of the mesityl group protects the electrophilic boron atom from being attacked by nucleophiles and thus favors desilylation.
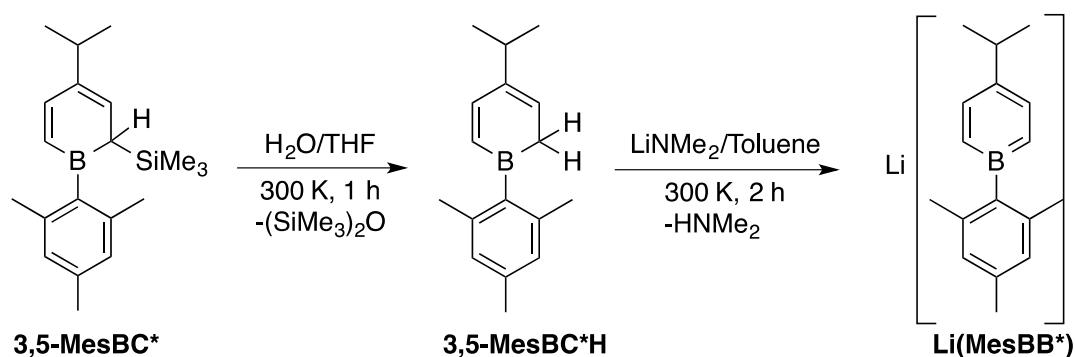
Scheme 5-5: Synthesis of 1-mesityl-4-isopropyl-3,5-boracyclohexadiene and its lithium salt

5.4.2 Synthesis of Metal Complexes:

It is well known that the boratabenzene ligands coordinate transition metals through their π electron cloud to form sandwich-type complexes. It was thus with little surprise that we observed that **LiMesBBSiMe$_3$** readily reacted when mixed with 1/2 equivalent of CrCl$_2$ in

THF. Within 10 minutes of the addition, the reaction mixture became dark red and complete conversion of **LiMesBBSiMe₃** was achieved in 1 day (Scheme 5-6). The product was isolated from the ether extracts of the reaction mixture as reddish yellow crystals. An NMR study of **Cr(MesBBSiMe₃)₂** was not conclusive, since this complex is paramagnetic, but X-ray quality crystals were obtained from the saturated ether solution at 243 K. Compound **Cr(MesBBSiMe₃)₂** crystallizes in the triclinic space group P-1. Like all other chromium boratabenzene sandwich complexes[132], compound **Cr(MesBBSiMe₃)₂** adopts an ideal eclipsed conformation in which the two boron centers assume a *trans* orientation (B1-Cr-B1A = 180°). The angle between the ring centroids is 180°, and the distance is 3.422 Å. An ORTEP representation is shown in Figure 5-2. The B1-C9 bond length is of 1.5880(18) Å, which is in the same range as the 1.568(8) Å observed by Bazan for the bis(phenylboratabenzene)chromium sandwich.[132] The distances between the carbon atoms of the ring and chromium are in the 2.1571(13) - 2.2290(13) Å range and are also in good agreement with the previously reported complexes. However, it can be observed that the B1-Cr bond distance is significantly longer in **Cr(MesBBSiMe₃)₂** (2.4771(13) Å) than in the bis(phenylboratabenzene)chromium sandwich complex (2.375(6) Å) which can be attributed to the sheer steric bulk of the mesityl ring on boron.
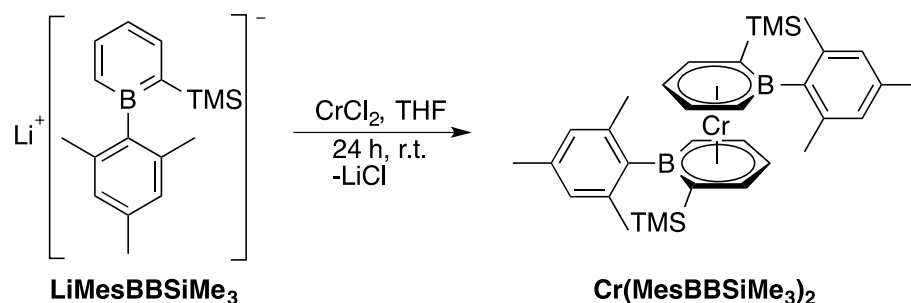
Scheme 5-6: Synthesis of bis(1-mesityl-2-trimethylsilyl-boratabenzene)chromium.

Like all other boratabenzene sandwich complexes, the carbon and the boron atom of the ring are slightly bent away from the metal center.[115,198,199] The C4-Cr1 and C8-Cr1 distances (2.2149(12) and 2.2289(12) Å) and B1-Cr1 distance (2.4771(13) Å) of the ring from the chromium center are longer than the distance of *meta* ($C^{5,7}$) (2.1571(13), 2.1721(13)Å) and *para* carbon atoms (2.1872(13) Å). The trimethylsilyl groups on the two rings also adopt an *anti*-conformation to minimize the steric hindrance. However, unlike the case

for phenylboratabenzene complexes[132,178,200,201] the boratabenzene ring is not coplanar with the mesityl ring, having a dihedral angle of 83.0° between the plane of mesityl ring and the plane of boratabenzene ring. This perpendicular arrangement is favored because of the steric demand of the *o*-methyl groups of the mesityl rings. The tilt angle between the plane defined by the carbon atoms of the boratabenzene ring (C4 to C8 in Figure 5-2) and the plane defined by the C4-B1-C8 (Figure 5-2) is 20.75°.
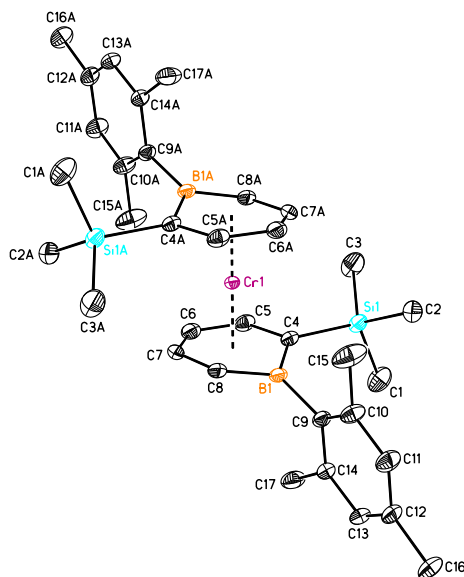
Figure 5-2: Thermal atomic displacement parameter plot of $Cr(MesBBSiMe_3)_2$. Hydrogen atoms have been omitted for clarity (R1 = 3.55%). Anisotropic atomic displacement ellipsoids for the non-hydrogen atoms are shown at 50% probability level. Selected bond distances [Å] and angles [°]: Cr_1-B_1 2.4771(16), Cr_1-C_4 2.2149(12), Cr_1-C_5 2.1571(13), Cr_1-C_6 2.1872(13), C_4-Si 1.8814(13), B_1-C_9 1.5880(18), B_1-C_4 1.5425(18), C_4-C_5 1.4344(17), C_5-C_6 1.408(2), B_1-Cr_1-B_{1A} 180.0, C_9-B_1-C_4 126.10(11), C_8-B_1-C_9 120.51(11), B_1-C_4-Si 124.82(9), C_4-B_1-C_8 113.29(11), C_4-C_5-C_6 122.68(12), C_5-C_6-C_7 120.94(12), C_6-C_7-C_8 120.71(12).

When $FeCl_2$ was reacted with 2 equivalents of **LiMesBBSiMe₃** and the workup was done without any precaution to avoid all protic sources, complex **Fe(MesBB)₂SiMe₃** was formed as the main product. In addition to the major product **Fe(MesBB)₂SiMe₃**, complex **Fe(MesBB)₂** was also formed in small quantities, as illustrated in Scheme 5-7.
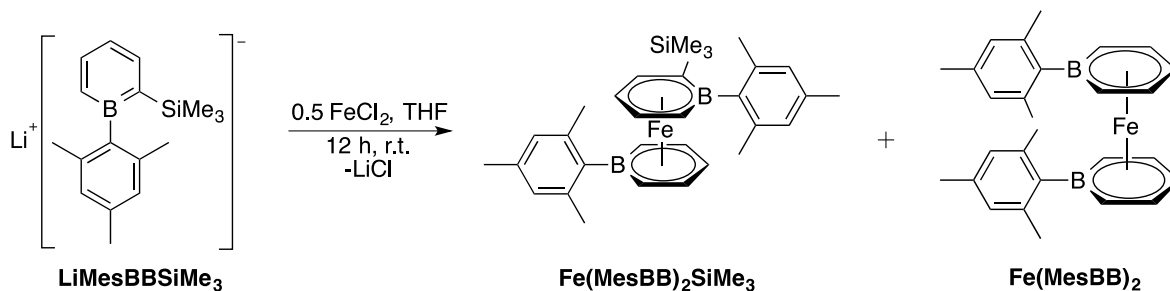
Scheme 5-7: Synthesis of Fe(MesBB)₂SiMe₃ and Fe(MesBB)₂ complexes.

The loss of trimethylsilyl from boratabenzene in **Fe(MesBB)₂** and **Fe(MesBB)₂SiMe₃** can be attributed to the exposure of reaction mixture to traces of water or silanol groups from the glass during the reaction manipulations and/or the crystallization process. This phenomenon of hydrolysis of trimethylsilyl was also observed during the synthesis of ligand **3,5-MesBC*H**. Complex **Fe(MesBB)₂** was independently synthesized by reacting two equivalents of **Bu₄N(MesBB)** with FeCl₂.

In complex **Fe(MesBB)₂SiMe₃** the two boratabenzene rings are not equivalent, because one of them has lost the trimethylsilyl fragment. Thus, in the ^{1}HNMR spectrum we observe single resonances for each proton of the boratabenzene moieties. In an assignment using COSY experiments, for the boratabenzene ring with the SiMe₃ group, H^6 appears at $\delta =$ 3.93 while the H^4 proton is shifted to $\delta = 5.59$. H^5 is observed at $\delta = 5.33$ with the second *meta* proton (H^3) seen at $\delta = 5.28$. The protons of the boratabenzene ring without the SiMe₃ group are seen at $\delta = 4.36$ and 4.52 ($H^{2/6}$), $\delta = 5.29$ and 5.16 ($H^{3/5}$) and $\delta = 5.67$ (H^4). The absence of symmetry for the latter ring suggests that the rotation of the boratabenzene ring is hindered by the steric bulk of the substituents on the rings. Whereas the mesityl ring on the 1-mesityl-boratabenzene ring does show equivalent resonances for the methyl groups in *ortho* positions and hydrogen atoms in *meta* positions, the presence of unique resonances for all positions on the mesityl ring of the 1-mesityl-2-(trimethylsilyl)-borabenzene ring demonstrate that the rotation of the aromatic ring is hindered by the steric bulk of the system. In **Fe(MesBB)₂** the two boratabenzene rings are equivalent and give only one set of peaks for each of the $H^{2/6}$, $H^{3/5}$ and H^4 at $\delta = 4.43$, 5.05 and 5.14, respectively. The ^{11}B{^{1}H}

NMR shifts are of δ = 22.5, 29.2 for **Fe(MesBB)₂SiMe₃** and δ = 22.6 for **Fe(MesBB)₂**, respectively, which is in the expected range for iron boratabenzene sandwiches.[93,118,194] In order to confirm that the loss of trimethylsilyl group occurs due to hydrolysis, the reaction of the ligand **LiMesBBSiMe₃** and FeCl₂ was carried out under complete anhydrous conditions in a silylated J-young NMR tube (Scheme 5-7). The product formed was confirmed to be **Fe(MesBBSiMe₃)₂** using NMR spectroscopy. The two boratabenzene rings were inequivalent and gave two sets of signals in the ¹H NMR spectrum containing notably the SiMe₃ groups**.**
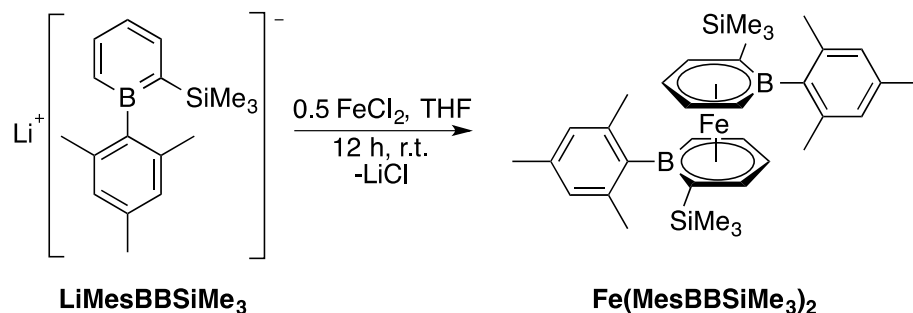
Scheme 5-8: Synthesis of bis(1-mesityl-2-trimethylsilylboratabenzene) Iron (II) sandwich.

Single crystals suitable for X-ray studies were obtained from saturated hexane solutions by slow diffusion at 243 K. Compound **Fe(MesBB)₂SiMe₃** crystallized in the triclinic space group P-1with one molecule in the unit cell. The two boratabenzene rings adopt an eclipsed conformation, where the two boron centers are *trans* to each other (bond-angle B1-Fe-B2 = 171.07°). However, the two boratabenzene rings are not completely parallel to each other and have a dihedral angle of 5.4°. The ORTEP diagram is given in Figure 5-3. The plane of the mesityl ring is perpendicular to the plane of the boratabenzene rings. For the boratabenzene with a SiMe₃ group, the dihedral angle between the plane of boratabenzene ring and the plane of mesityl ring is 79.9°, whereas the boratabenzene ring without the SiMe₃ group has a dihedral angle of 40.8° with the mesityl ring. This clearly indicates that the steric bulk of the trimethylsilyl group has an effect on the orientation of the mesityl ring. The two mesityl rings are also inequivalent and have a dihedral angle of 43.2°. All other bond distances and bond angles are in good agreement with those for the previously reported iron boratabenzene sandwiches.[93,202] The distances between the ring centroids and

the iron center are of 1.601Å and 1.607Å for the boratabenzene without $SiMe_3$ and with $SiMe_3$ respectively, which are shorter in comparison to those for the chromium complex.
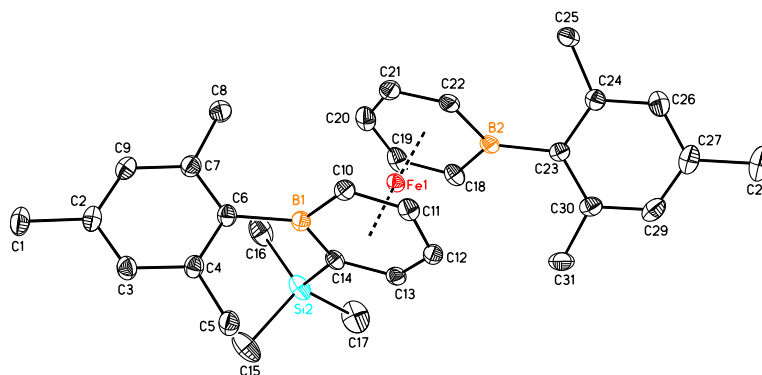
Figure 5-3: Thermal atomic displacement parameter plot of Fe(MesBB)$_2$SiMe$_3$. Hydrogen atoms have been omitted for clarity (R1 = 3.55%). Anisotropic atomic displacement ellipsoids for the non-hydrogen atoms are shown at 50% probability level. Selected bond distances [Å] and angles [°]: Fe1-B1 2.3954(16), Fe1-B2 2.3540(16), Fe1-C10 2.1609(14), Fe1-C11 2.0838(14), Fe1-C12 2.0683(14), Fe1-C13 2.0745(14), Fe1-C14 2.1949(14), Fe1-C18 2.1786(15), Fe1-C19 2.1101(15), Fe1-C20 2.0850(15), Fe1-C21 2.0802(15), Fe1-C22 2.1345(15), C14-Si 1.8840(15), B1-C6 1.598(2), B1-C14 1.543(2), C14-C13 1.422(2), C13-C12 1.419(2), B1-Fe1-B2 171.07(6), C6-B1-C10 122.13(13), C23-B2-C22 122.33(14), C14-B1-C6 124.63(13), C23-B2-C18 126.40(14), B1-C14-Si 123.71(11), C22-B2-C18 111.24(13), C14-B1-C10 113.03(13), C4-C5-C6 122.68(12), C5-C6-C7 120.94(12), C6-C7-C8 120.71(12).

Compound **Fe(MesBB)$_2$** crystalized in the monoclinic space group P2$_1$ (Figure 5-4). The two boratabenzene rings adopt the eclipsed conformation as in **Fe(MesBB)$_2$SiMe$_3$**, but surprisingly the two boron centers are not *trans* to each other. Indeed, the *trans* conformation of the boratabenzene rings is always observed in sandwich bis(boratabenzene) complexes.[132,167,203] A dihedral angle (B-centroid-centroid-B) of 65.29° is observed for **Fe(MesBB)$_2$** as compared to 167.94° in **Fe(MesBB)$_2$SiMe$_3$** and 180° in bis(1-ethynylborinato)iron and bis(1-phospholeboratabenzene)iron.[93,194]
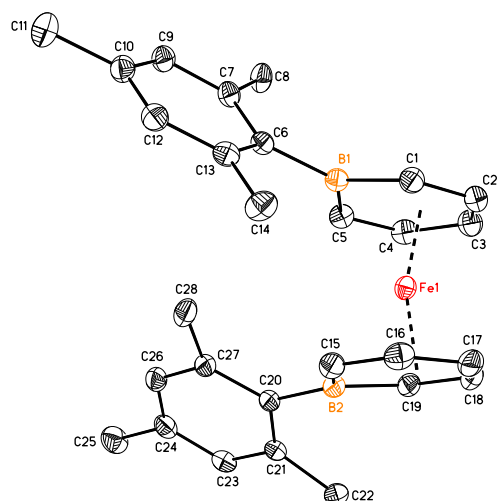
Figure 5-4: Thermal atomic displacement parameter plot of Fe(MesBB)$_2$. Hydrogen atoms have been omitted for clarity (R1= 2.95%). Anisotropic atomic displacement ellipsoids for the non-hydrogen atoms are shown at the 50% probability level. Selected bond distances [Å] and angles [°]: Fe1-B1 2.369(15), Fe1-C1 2.163(15), Fe1-C2 2.088 (15), Fe1-C3 2.074(13), B1-C6 1.596(3), B1-C1 1.526(2), C1-C2 1.411(2), C2-C3 1.412(3), B1-Fe1-B2 112.66(5), C6-B1-C1 125.89(13), (14), C5-B1-C6 122.83(12), C22-B2-C18 111.24(13), C1-B1-C5 111.26(12), C1-C2-C3 121.69(13), C2-C3-C4 120.04(14), C3-C4-C5 121.44(16).

In order to better understand the reason for this unusual conformation, an optimized structure of **Fe(MesBB)$_2$** was obtained using a computational model using the density functional theory (DFT) level using the B3LYP method. Being in good agreement with the crystal structure, it did not exhibit any atomic distances hinting at agostic interactions. In order to quantify the stability of the *syn* conformation in the gas phase, we modelized an *anti* structure for **Fe(MesBB)$_2$**. Interestingly, the latter conformation was found to be slightly more stable (ΔH = -1.2 kcal.mol^{-1} at 298K). These calculations suggest that the *syn* conformation adopted by **Fe(MesBB)$_2$** in the crystalline form should be attributed to intermolecular factors, most likely because of crystal packing.

Once again the boratabenzene rings are not in the same plane as the mesityl rings, and thus had a dihedral angle of 52.6° for boratabenzene (B$_1$) and mesityl ring and 38.0° for the boratabenzene (B$_2$) and the second mesityl ring. These values indicate the non-equivalent

orientations for the two ligand rings in the complex. The dihedral angle between the two mesityl ring planes is 69.31°. The bond angles between C1-B1-C5 = 111.26(12)°, C1-C2-C3 = 121.69(13)°, C2-C3-C4 = 120.04(14)°, C3-C4-C5 = 121.44(16)°, for the boratabenzene ring are in close agreement with those for **Fe(MesBB)₂SiMe₃** and for previously reported iron boratabenzene sandwiches.[93,194] The $C^{2/6}$ carbon atoms and the boron atom are again bent away from the iron center as is evident by the bond distances in Figure 5-4. The distances between the iron center and the ring centroids is 1.596 and 1.586Å.

An iron sandwich of the 1-mesityl-4-isopropylboratabenzene **Fe(MesBB*)₂** was also synthesized as illustrated in Scheme 5-9. This sandwich also consists of two equivalent mesitylboratabenzene rings coordinated to iron. The coordination of the boratabenzene ring is indicated by the upfield shift of ring $H^{3/5}$ protons from δ = 7.50 to 5.27 and $C^{2/6}$ protons from δ = 6.94 to 4.76. The $^{11}B\{^1H\}$ NMR is also shifted from δ = 34.2 to 21.8. However, no crystals could be obtained for this species.
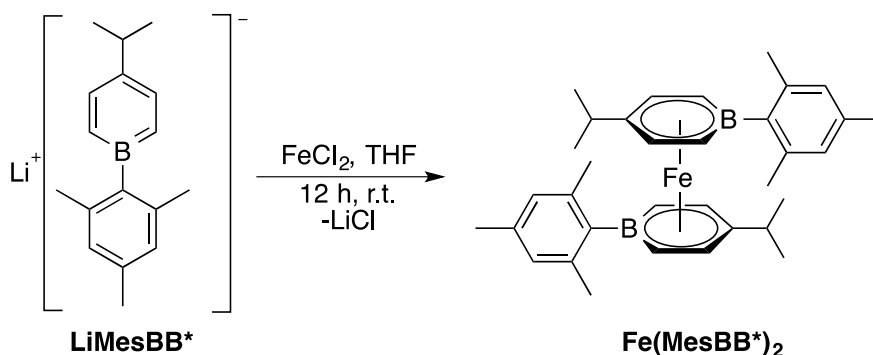
Scheme 5-9: Synthesis of bis(1-mesityl-4-isopropyl-boratabenzene)iron(II) sandwich.

5.5 Conclusions

Two new isomers of mesitylboracyclohexadiene (3,5-diene and 2,5-diene) have been synthesized, isolated and characterized spectroscopically. The first water-stable boracyclohexadiene **3,5-MesBC*H** was reported. The reactivity of the mesityl boracyclohexadienes (**2,5-MesBC*** and **3,5-MesBC***) was studied, and selective desilylation of these heterocycles was achieved by hydrolysis. The corresponding mesitylboratabenzene salts were coordinated to iron, which furnished a series of three

different ironboratabenzene sandwiches characterized using X-ray diffraction. The desilylation of the boratabenzene rings with water was also observed in these complexes. Unlike the normal conformation for sandwich complexes, a sterically demanding geometry, with the two mesityl rings in proximity, has been structurally characterized for sandwich **Fe(MesBB)₂**. The water stability of these ligands when no SiMe$_3$ group is present and of their metal complexes makes them suitable candidates for different air and water stable chemistries where boron heterocycles play an important role. They could be of use in the generation of optoelectronic materials, in catalysis and in polymers when the integrity of the sp^2-hybridized boron center is needed.

5.6 Experimental Section

5.6.1 General Procedures.

All manipulations were carried out under an atmosphere of nitrogen using standard Schlenk techniques or in nitrogen filled gloveboxes, unless specified otherwise. The glassware was silylated by rinsing it with a solution of $SiMe_3Cl/CHCl_3$ and dried overnight prior to use. All solvents were distilled from sodium and benzophenone. Benzene-d_6 was distilled under reduce pressure from a Na/K alloy. 1-chloro-2-(trimethylsilyl)-4-isopropylboracyclohexa-2,5-diene[204],1-chloro-2-(trimethylsilyl)boracyclohexa-2,5-diene[99] and mesityllithium[165] were prepared according to the literature procedures. Anhydrous iron(II) chloride and chromium(II) chloride was purchased from Sigma Aldrich and used without further purification. NMR spectra were recorded on an Agilent Technologies NMR spectrometer at 500 MHz (^{1}H), 125.758 MHz (^{13}C), 160.46 MHz (^{11}B), and on a Varian Inova NMR AS400 spectrometer, at 400.0 MHz (^{1}H), 100.580 MHz (^{13}C). ^{1}H NMR and ^{13}C NMR chemical shifts are referenced to residual solvent signals in deuterated solvent. Multiplicities are reported as singlet (s), doublet (d), triplet (t), quartet (q), multiplet (m) or broad (br). Chemical shifts are reported in ppm. Coupling constants are reported in Hz. HRMS characterization was possible using an Agilent Technologies 6210 LC time of flight mass spectrometer. Products in toluene and THF solutions were introduced to the nebulizer by direct injection. Neutral borabenzene adducts were characterized using APPI ionization in positive and negative mode. Ionic species were ionised by electrospray (ESI-MS) in both positive and negative modes.

Lithium (1-mesityl-2-trimethylsilyl-boratabenzene) (LiMesBBSiMe₃). A solution of 1-chloro-2-trimethylsilyl-2,5-boracyclohexadiene (1.30 g, 7.0 mmol) in toluene (10 mL) was added dropwise to a suspension of mesityllithium (1.70 g, 14.0 mmol) in toluene (15 mL). The white suspension turned yellow and was left stirring at room temperature for 4 h. The solvent was removed under vacuum, and the residue was washed with hexanes and diethyl ether to yield 1.40 g (yield = 75%) of a white powder.

^{1}H NMR (500 MHz) (benzene-d_6/drops of THF) δ: 7.89 (d, $^3J_{H-H}$ = 6.7 Hz, 1H, H^3), 7.58 (dd, $^3J_{H-H}$ = 7.5, 9.6 Hz, 1H, H^5), 7.06 (s, 2H, H^{meta} Mes), 6.78 (d, $^3J_{H-H}$ = 10.1 Hz, 1H, H^6), 6.61 (t, $^3J_{H-H}$ = 6.7 Hz, 1H, H^4), 2.41 (s, 6H, Me^{ortho} Mes), 2.36 (s, 3H, Me^{para} Mes), 0.28 (s, 9H, TMS). ^{13}C{^{1}H} NMR (125.76 MHz) (benzene-d_6) δ: 139.2 (C^3), 138.8 (C^{ortho} Mes), 134.7 (C^5), 133.9 (C^{para} Mes), 127.1 (C^{meta} Mes), 109.1 (C^4), 25.5 (Me^{ortho} Mes), 21.5 (Me^{para} Mes), 1.3 (TMS). C^2, C^6 and the *ipso* carbon of mesitylene were not located. ^{11}B{^{1}H} NMR (160.46 MHz) (benzene-d_6) δ: 39.4. DI-MSTOF (ESI, m/e) calcd for C$_{17}$H$_{24}$BSi$^-$ = 267.1746; found 267.1758.

Tetrabutylammonium salt of 1-mesityl-boratabenzene (LiMesBB). A solution of 1-chloro-2-trimethylsilyl-2,5-boracyclohexadiene (0.100 g, 0.53 mmol) in toluene (5 mL) was added dropwise to a suspension of mesityllithium (0.067 g, 0.53 mmol) in toluene (5 mL). The white suspension turned yellow and was left stirring at room temperature for 2 h. The solvent was removed under vacuum and the residue was washed with hexanes. The hexanes filtrate was evaporated to give yellow oil (**3,5-MesBC**). This yellow oil was dissolved in THF (5 mL) and was added slowly to a solution of n-Bu$_4$NCl (0.125 g, 0.45 mmol) in 10 mL of THF. The reaction was stirred at 300 K for 1 h during which the color of the solution became bright yellow. The solvent was removed and the grey solid was extracted with 2 x 7 mL of hexanes to yield 0.173 g (yield = 75%) of a grey solid. ^{1}H NMR (500 MHz) (benzene-d_6) δ: 7.72 (dd, $^3J_{H-H}$ = 7.0, 9.7 Hz, 2H, H$^{3/5}$), 7.07 (s, 2H, H^{meta} Mes), 6.99 (d, $^3J_{H-H}$ = 9.7 Hz, 2H, H$^{2/6}$), 6.61 (t, $^3J_{H-H}$ = 6.8 Hz, 1H, H^4), 2.98 (CH$_2$ of nBu$_4$N), 2.83 (s, 6H, Me^{ortho} Mes), 2.41 (s, 3H, Me^{para} Mes) 1.32 (CH$_2$ of nBu$_4$N), 1.26 (CH$_2$ of nBu$_4$N), 0.92 (Me of nBu$_4$N). ^{13}C{^{1}H} NMR (125.76 MHz) (benzene-d_6) δ: 139.9 (C^{ortho} Mes), 132.8 (C$^{3/5}$), 132.1 (C^{para} Mes), 129.3 (C$^{2/6}$), 128.6 (C^{ipso} Mes), 127.5 (C^{meta} Mes), 110.1 (C^4), 58.5 (CH$_2$N of nBu$_4$N), 26.0 (Me^{ortho} Mes), 24.3 (CH$_2$ of nBu$_4$N), 21.4 (Me^{para} Mes), 20.0 (CH$_2$ of nBu$_4$N), 14.0 (Me-nBu$_4$N). ^{11}B{^{1}H} NMR (160.46 MHz) (benzene-d_6) δ: 33.1. DI-MSTOF (ESI, m/e): calcd for C$_{14}$H$_{16}$B$^-$ 195.1351; found 195.1354.

1-mesityl-2-trimethylsilyl-4-isopropyl-2,5-boracyclohexadiene (2,5-MesBC*). A solution of 1-chloro-2-trimethylsilyl-4-isopropyl-2,5-boracyclohexadiene (0.050 g, 0.22 mmol) in toluene (0.8 mL) was added dropwise to a suspension of mesityllithium (0.033 g, 0.26 mmol) in toluene (0.8 mL), while stirring continuously. The white suspension turned

into a fine, slightly yellow suspension. The reaction was stirred at room temperature for 2 h. The solvent was removed under vacuum and the residue was extracted with 2×5 mL of hexanes. Hexanes filtrate was evaporated to give a yellow oil. ^{1}H NMR (500 MHz) (benzene-d_6) δ: 7.57 (dd, $^3J_{H-H}$ = 2.8, 2.0 Hz, 1H, H^3), 7.03 (ddd, $^3J_{H-H}$ = 11.8, 2.8, 2.0 Hz, 1H, H^5), 6.82 (dd, $^3J_{H-H}$ = 11.8, 1.7 Hz, 1H, H^6), 6.81 (dm, 2H, H^{meta} Mes), 2.74 (m, 1H, H^4), 2.22 (s, 3H, Me^{ortho} Mes), 2.19 (s, 3H, Me^{ortho} Mes), 2.15 (s, 3H, Me^{para} Mes), 1.93 (m, CH^{iPr}), 0.80 (d, $^3J_{H-H}$ = 7.3, 3H, Me^{iPr}), 0.77 (d, $^3J_{H-H}$ = 7.3, 3H, Me^{iPr}), 0.07 (s, 9H, TMS); traces of **3,5-MesBC*** were always present in solution. ^{13}C{^{1}H} NMR (125.76 MHz) (benzene-d_6) δ: 167.3 (C^3), 156.5 (C^5), 136.3 (C^{ortho} Mes), 136.2 (C^{para} Mes), 127.4 (C^{meta} Mes), 127.3 (C^{meta} Mes), 52.9 (C^4), 32.1 (iPr), 22.7 (Me^{ortho} Mes), 21.3 (Me^{para} Mes), 19.8 (iPr), 19.2 (iPr), -0.2 (TMS). C^2, C^6 and the ipso carbon of mesitylene were not located. ^{11}B{^{1}H} NMR (160.46 MHz) (benzene-d_6) δ: 59.2. DI-MSTOF (APPI, m/e): Calcd for C$_{20}$H$_{31}$BSi [-H$^+$] 309.2215; found 309.2439.

1-mesityl-2-trimethylsilyl-4-isopropyl-3,5-boracyclohexadiene **(3,5-MesBC*).** A solution of 1-chloro-2-trimethylsilyl-4-isopropyl-3,5-boracyclohexadiene (0.200 g, 0.88 mmol) in toluene (4 mL) was added dropwise to a suspension of mesityllithium (0.221 g, 1.76 mmol) in toluene (7 mL) over a 10 min period. The white suspension turned into a slightly yellow suspension. The reaction was stirred at room temperature for 2 h. The solvent was removed under vacuum and the residue was extracted with 3×8 mL of hexanes. The hexanes filtrate was evaporated to give 0.207 g (yield = 76%) of a light yellow oil. ^{1}H NMR (500 MHz) (benzene-d_6) δ: 7.46 (dd, $^3J_{H-H}$ = 11.8 Hz, 1.8 Hz, 1H, H^5), 7.07 (d, $^3J_{H-H}$ =11.5 Hz, 1H, H^6), 6.86 (s, 2H, H^{meta} Mes), 6.74 (d, $^3J_{H-H}$ = 5.2 Hz, 1H, H^3), 4.06 (d, $^3J_{H-H}$ = 5.2 Hz, 1H, H^2), 2.52 (m, 1H, CH^{iPr}), 2.37 (br, 6H, Me^{ortho} Mes), 2.21 (s, 3H, Me^{para} Mes), 1.13 (d, $^3J_{H-H}$ = 6.0 Hz, 3H, Me^{iPr}), 1.11 (d, $^3J_{H-H}$ = 6.0 Hz, 3H, Me^{iPr}), -0.09 (s, 9H, TMS). ^{13}C{^{1}H} NMR (125.76 MHz) (benzene-d_6) δ: 149.5 (C^5), 141.9 (C^{ortho} Mes), 137.3 (C^3), 137.2 (C^{para} Mes), 129.3 (C^4), 128.4 (C^{meta} Mes), 34.8 (Me^{iPr}), 23.8 (Me^{ortho} Mes), 23.0 (Me^{para} Mes), 21.3 (CH^{iPr}), -0.1 (TMS). C^2, C^6 and the ipso carbon of mesitylene were not located. ^{11}B{^{1}H} NMR (160.46 MHz) (benzene-d_6) δ: 62.0. DI-MSTOF (APPI, m/e): Calcd for C$_{20}$H$_{31}$BSi [-H$^+$] 309.2215; found 309.2428.

1-mesityl-4-isopropyl-3,5-boracyclohexadiene (3,5-MesBC*H). To a solution of **3,5-MesBC*** (0.200 g, 0.64 mmol) in THF (10 mL) was added 0.2 mL of THF solution of water (1.02 mmol), while stirring continuously. The yellow solution became dark orange in color. The reaction was stirred at room temperature for 1 h. The solvent was removed under vacuum and 0.105 g of a dark orange-red oil was obtained (Yield = 68%). ^{1}H NMR (500 MHz) (benzene-d_6) δ: 7.36 (d, $^3J_{H-H}$ = 11.7 Hz, 1H, H^5), 6.88 (d, $^3J_{H-H}$ = 11.7 Hz, 1H, H^6), 6.81 (s, 2H, H^{meta} Mes), 6.36 (t, $^3J_{H-H}$ = 4.2 Hz, 1H, H^3), 2.41 (d, $^3J_{H-H}$ = 4.3 Hz, 2H, H^2), 2.37 (m, 1H, CH ^{iPr}), 2.22 (s, 3H, Me^{para} Mes), 2.10 (s, 6H, Me^{ortho} Mes), 1.05 (d, $^3J_{H-H}$ = 6.7 Hz, 6H, Me^{iPr}). ^{13}C{^{1}H} NMR (125.76 MHz) (benzene-d_6) δ: 153.2 (C^5), 136.8 (C^{ortho} Mes), 136.7 (C^{para} Mes), 133.8 (C^3), 127.6 (C^{meta} Mes), 34.6 (Me^{iPr}), 22.9 (Me^{para} Mes), 22.5 (Me^{ortho} Mes), 21.3 (CH^{iPr}), C^2, C^4, C^6 and the ipso carbon of mesitylene were not located. ^{11}B{^{1}H} NMR (160.46 MHz) (benzene-d_6) δ: 69.3. DI-MSTOF (APPI, m/e): Calcd for C$_{17}$H$_{23}$B 238.1893; found 238.1872.

Lithium 1-mesityl-2-trimethylsilyl-4-isopropyl-boratabenzene (LiMesBB*SiMe$_3$). A solution of **3,5-MesBC*** (0.150 g, 0.48 mmol) in 8 mL of THF was added slowly at room temperature to a solution of LiNMe$_2$ (0.0245 g, 0.48 mmol) in 5 mL of THF. The reaction was stirred at room temperature for 2 h. The solvent was removed under reduced pressure and the residue was washed with 2 x 5 mL of hexane to give a white solid in 60% yield (0.091 g). ^{1}H NMR (500MHz) (benzene-d_6/ drops of THF) δ: 7.86 (s, 1H, H^3), 7.56 (d, $^3J_{H-H}$ = 10.4 Hz, 1H, H^5), 7.07 (s, 2H, H^{meta} Mes), 6.86 (d, $^3J_{H-H}$ = 10.4 Hz, 1H, H^6), 2.85 (m, 1H, CH ^{iPr}), 2.37 (s, 6H, Me^{ortho} Mes), 2.35 (br, 3H, Me^{para} Mes), 1.25 (d, $^3J_{H-H}$ = 6.9 Hz, 6H, Me^{iPr}), 0.29 (s, 9H, TMS). ^{13}C{^{1}H} NMR (125.76 MHz) (benzene-d_6) δ: 137.2 (C^{ortho} Mes), 134.0 (C^3), 132.9 (C^5), 131.3 (C^{para} Mes), 127.2 (C^{meta} Mes), 35.2 (Me^{iPr}), 35.2 (Me^{iPr}), 25.6 (Me^{ortho} Mes), 25.4 (Me^{para} Mes), 21.5 (CH^{iPr}), 1.4 (TMS). C^2, C^4, C^6 and the ipso carbon of mesitylene were not located. ^{11}B{^{1}H} NMR (160.46 MHz) (benzene-d_6) δ: 38.1. DI-MSTOF (ESI, m/e): Calcd for C$_{20}$H$_{30}$BSi 309.2210; found 309.2227.

Lithium 1-mesityl-4-isopropyl-boratabenzene (LiMesBB*). At room temperature, a solution of **3,5-MesBC*H** (0.300 g, 1.25 mmol) in 15 mL of toluene was added slowly to a solution of LiNMe$_2$ (0.0638 g, 1.25 mmol) in 10 mL of toluene. The reaction was stirred at room temperature for 2 h. The solvent was removed under reduced pressure and the residue

was washed with 3 x 10 mL of pentane to give a white solid in 76% yield (0.231 g). ^{1}H NMR (500 MHz) (benzene-d_6/ drops of THF) δ: 7.50 (d, $^3J_{H-H}$ = 10.4 Hz, 2H, H$^{3/5}$), 7.07 (s, 2H, H^{meta} Mes), 6.94 (d, $^3J_{H-H}$ = 10.5 Hz, 2H, H$^{2/6}$), 2.87 (m, 1H, CH^{iPr}), 2.54 (s, 6H, Me^{ortho} Mes), 2.36 (s, 3H, Me^{para} Mes), 1.33 (d, $^3J_{H-H}$ = 6.9 Hz, 6H, Me^{iPr}). ^{13}C{^{1}H} NMR (125.76 MHz) (benzene-d_6/ drops of THF) δ: 139.6 (C^{ortho} Mes), 133.7 (C^{para} Mes), 131.3 (C$^{3/5}$), 127.5 (C^{meta} Mes), 35.0 (Me^{iPr}), 25.8 (Me^{ortho} Mes), 25.4 (Me^{para} Mes), 21.5 (CH^{iPr}), C^2, C^4, C^6 and the ipso carbon of mesitylene were not located. ^{11}B{^{1}H} NMR (160.46 MHz) (benzene-d_6) δ: 34.2. DI-MSTOF (ESI, m/e): Calcd for C$_{17}$H$_{22}$B$^-$ 237.1815; found 237.1825.

Bis[1-mesityl-2-trimethylsilyl-boratabenzene]chromium(II) [Cr(MesBBSiMe$_3$)$_2$]. CrCl$_2$ (0.440 g, 0.36 mmol) and **LiMesBBSiMe$_3$** (0.200 g, 0.72 mmol) were mixed in a schlenk inside the glovebox. THF (10 mL) was added to the solids at room temperature and within 10 min the solution became dark red. The reaction was kept stirring at room temperature for 24 h. THF was evaporated and the dark red residue was extracted with 2 × 5 mL of ether. The filtrate was evaporated to minimum and stored at 243 K for 2 days. Yellow-brown crystals were obtained. Yield = 0.147 g (70%). DI-MSTOF (APPI, m/e): Calcd for C$_{34}$H$_{48}$B$_2$CrSi$_2$ 586.2897; found 586.2995.

(1-mesityl-boratabenzene)(1-mesityl-2-trimethylsilyl-boratabenzene)iron(II)
Fe(MesBB)$_2$SiMe$_3$. FeCl$_2$ (0.017 g, 0.13 mmol) and **LiMesBBSiMe$_3$** (0.072 g, 0.26 mmol) were mixed in a Schlenk inside the glovebox. The solids were cooled down to 258 K and THF (5 mL) was added to it. An orange solution formed and was stirred at 258 K for 2 h, then allowed to warm up to room temperature overnight. THF was removed under reduce pressure. The residue was dried and extracted with 2 × 5 mL of diethyl ether. The diethyl ether was evaporated and the orange red sticky residue was extracted with 2 × 5 mL of hexanes. The red-pink hexanes filtrate was evaporated to minimum and kept at 243 K overnight to give reddish-brown crystals. Yield = 0.040 g (60%). ^{1}H NMR (500 MHz) (benzene-d_6) δ: 7.03 (s, 2H, H^{meta} Mes), 7.00 (s, 1H, H^{meta} Mes^{TMS}), 6.76 (s, 1H, H^{meta} Mes^{TMS}), 5.67 (t, $^3J_{H-H}$ = 5.6 Hz, 1H, H^4), 5.59 (t, $^3J_{H-H}$ = 5.6 Hz, 1H, H^{4TMS}), 5.33 (dd, $^3J_{H-H}$ = 8.8 Hz, 5.9 Hz, 1H, H^{5TMS}), 5.29 (m, 1H, H$^{3/5}$), 5.28 (d, $^3J_{H-H}$ = 5.8 Hz, 1H, H^{3TMS}), 5.16 (dd, $^3J_{H-H}$ = 8.9 Hz, 6.0 Hz, 1H, H$^{3/5}$), 4.52 (d, $^3J_{H-H}$ = 9.1 Hz, 1H, H$^{2/6}$), 4.36 (d, $^3J_{H-H}$ = 9.2

Hz, 1H, H$^{2/6}$), 3.93 (d, $^3J_\text{H-H}$ = 9.0 Hz, 1H, H^{6TMS}), 2.96 (s, 3H, Me^{ortho} Mes^{TMS}), 2.65 (s, 6H, Me^{ortho} Mes), 2.30 (s, 3H, Me^{para} Mes), 2.23 (s, 3H, Me^{para} Mes^{TMS}), 1.62 (s, 3H, Me^{ortho} Mes^{TMS}), 0.03 (s, 9H, TMS). ^{13}C{^{1}H} NMR (125.76 MHz) (benzene-d_6) δ: 142.4, 140.6, 136.8, 135.7, 129.3, 127.7, 95.5, 93.2, 92.5, 91.6, 78.6, 78.4, 25.7, 24.6, 24.1, 21.2, 0.1. C^2, C^6 and the ipso carbon of mesitylene were not located. ^{11}B{^{1}H} NMR (160.46 MHz) (benzene-d_6) δ: 29.2, 22.5. DI-MSTOF (APPI, m/e): Calcd for C$_{31}$H$_{40}$B$_2$FeSi 518.2446; found 518.2460.

Bis-(1-mesityl-boratabenzene)iron(II) Fe(MesBB)$_2$. FeCl$_2$ (0.023 g, 0.18 mmol) and **Bu$_4$N(MesBB)** (0.157 g, 0.36 mmol) were mixed in a Schlenk flask inside a glovebox. The solids were cooled down to 258 K and THF (8 mL) was added to it. The orange solution was stirred at 258 K for 2 h and allowed to warm up to room temperature overnight. THF was removed under reduced pressure. The residue was dried and extracted with 2 × 5 mL of hexanes. The orange hexane filtrate was evaporated to a minimum and kept at 243 K overnight to give orange-red crystals. Yield = 0.059 g (74%).

^{1}H NMR (500 MHz) (benzene-d_6) δ: 7.00 (s, 4H, H^{meta} Mes), 5.14 (t, $^3J_\text{H-H}$ = 5.5 Hz, 2H, H^4), 5.05 (dd, $^3J_\text{H-H}$ = 5.7, 8.8 Hz, 4H, H$^{3/5}$), 4.43 (d, $^3J_\text{H-H}$ = 8.7 Hz, 4H, H$^{2/6}$), 2.60 (s, 12H, Me^{ortho} Mes), 2.28 (s, 6H, Me^{para} Mes). ^{13}C{^{1}H} NMR (125.76 MHz) (benzene-d_6) δ: 142.4 (C^{ortho} Mes), 136.6 (C^{para} Mes), 129.1 (C^{meta} Mes), 92.1 (C$^{3/5}$), 77.6 (C^4), 24.4 (Me^{ortho} Mes), 21.3 (Me^{para} Mes). C$^{2/6}$ and the ipso carbon of mesitylene were not located. ^{11}B{^{1}H} NMR (160.46 MHz) (benzene-d_6) δ: 22.6. DI-MSTOF (APPI, m/e): Calcd for C$_{28}$H$_{32}$B$_2$Fe 446.2040; found 446.2073.

Bis[1-mesityl-2-trimethylsilyl-boratabenzene]iron(II) Fe(MesBBSiMe$_3$)$_2$. A solution of **LiMesBBSiMe$_3$** (5.00 mg, 0.018 mmol) in THF (0.5 mL) was added to FeCl$_2$ (1.15 mg, 0.009 mmol) in THF (0.5 mL) in J-young. The solution turned orange and was allowed to react for 12 h. The solvent was removed and the residue was dissolved in benzene-d_6 and filtered. The filtrate was analyzed by NMR spectroscopy. The product was identified as bis[1-mesityl-2-trimethylsilylboratabenzene]iron(II). ^{1}H NMR (500 MHz) (benzene-d_6) δ: 7.07 (s, 1H, H^{meta}Mes), 6.98 (s, 1H, H^{meta}Mes), 6.79 (s, 1H, H^{meta}Mes), 6.77 (d, 1H, H^{meta}Mes), 6.25 (t, $^3J_\text{H-H}$ = 5.6 Hz, 1H, H^{4A}), 5.97 (dd, $^3J_\text{H-H}$ = 5.6Hz, 8.9 Hz, 1H, H^{5B}), 5.48

(d, $^3J_{H-H}$ = 5.6 Hz, 1H, H^{3A}), 5.43 (dd, $^3J_{H-H}$ = 5.6, 9.0 Hz, 1H, H^{5A}), 5.37 (d, $^3J_{H-H}$ = 5.6 Hz, 1H, H^{3B}), 5.27 (t, $^3J_{H-H}$ = 5.6 Hz, 1H, H^{4B}), 4.42 (d, $^3J_{H-H}$ = 8.9 Hz, 1H, H^{6B}), 3.77 (d, $^3J_{H-H}$ = 9.0 Hz, 1H, H^{6A}), 3.13 (s, 3H, Me^{ortho}Mes), 2.87 (s, 3H, Me^{ortho}Mes), 2.25 (s, 3H, Me^{para}Mes), 2.24 (s, 3H, Me^{para}Mes), 1.60 (s, 3H, Me^{ortho}Mes), 1.58 (s, 3H, Me^{ortho}Mes), 0.11 (s, 9H, TMS), 0.03 (s, 9H, TMS). ^{13}C{^{1}H} NMR (101 MHz) (benzene-d_6) δ: 140.7, 140.4, 137.3, 137.0, 135.7, 135.6, 127.7, 96.5, 94.8, 93.1, 92.2, 79.1, 76.8, 25.8, 25.6, 24.1, 24.1, 21.3, 21.2, 0.2, 0.1; C^2, C^6 and the ipso and meta carbons of mesitylene were not located. ^{11}B{^{1}H} NMR (160.46 MHz) (benzene-d_6) δ: 29.3. Calcd for $C_{34}H_{48}B_2FeSi_2$ 590.2830; found 590.2829.

Bis-(1-mesityl-4-isopropyl-boratabenzene)iron(II) Fe(MesBB*)₂. FeCl₂ (0.010 g, 0.08 mmol) and **LiMesBB*** (0.049 g, 0.16 mmol) were mixed in Schlenk flask inside the glovebox. The solids were cooled down to 258 K and THF (5 mL) was added to it. The orange solution was stirred at 258 K for 1 h and allowed to warm up to the room temperature overnight. THF was removed under reduced pressure. The residue was dried and extracted with 2 × 5 mL of hexanes. Hexanes filtrate was evaporated to minimum and kept at 243 K. Needle shaped crystals were obtained. Yield = 0.0315 g, (74%).

^{1}HNMR (500MHz) (benzene-d_6) δ: 6.99 (s, 4H, H^{meta} Mes), 5.27 (d, $^3J_{H-H}$ = 8.9 Hz, 4H, H$^{3/5}$), 4.76 (d, $^3J_{H-H}$ = 8.6 Hz, 4H, H$^{2/6}$), 2.68 (s, 12H, Me^{ortho} Mes), 2.43 (m, $^3J_{H-H}$ = 6.8 Hz, 2H, CH^{iPr}), 2.26 (s, 6H, Me^{para} Mes), 0.96 (d, $^3J_{H-H}$ = 6.8 Hz, 12H, Me^{iPr}). ^{13}C{^{1}H} NMR (125.76 MHz) (benzene-d_6) δ: 142.6 (C^{ortho} Mes), 136.5 (C^{para} Mes), 129.2 (C^{meta} Mes), 99.9 (C$^{2/6}$), 90.0 (C$^{3/5}$), 83.0 (C^4), 33.1 (Me^{iPr}), 24.5 (Me^{ortho} Mes), 22.8 (Me^{para} Mes), 21.3 (CH ^{iPr}). The ipso carbon of mesitylene was not located. ^{11}B{^{1}H} NMR (160.46 MHz) (benzene-d_6) δ: 21.8. DI-MSTOF (APPI, m/e): Calcd. for $C_{34}H_{44}B_2Fe$ 530.2979; found 530.3092.

5.6.2 Crystallographic Studies:

Nice single crystals with suitable size of all compounds were mounted on CryoLoops with Paratone-N and optically aligned on a Bruker SMART APEX-II X-ray diffractometer with 1K CCD detector using a digital camera. Initial intensity measurements were performed using a fine-focused sealed tube, graphite-monochromated, X-ray source (Mo $K\alpha$, λ =

0.71073 Å) at 50 kV and 30 mA. Standard APEX-II software package was used for determining the unit cells, generating the data collection strategy, and controlling data collection. SAINT was used for data integration including Lorentz and polarization corrections. Semi-empirical absorption corrections were applied using SCALE (SADABS). The structures of all compounds were solved by direct methods and refined by full-matrix least-squares methods with SHELX-97 in the SHELXTL6.14 package. All of the H atoms were generated geometrically and refined in riding mode. Crystallographic information for all obtained phases, atomic coordinates and additional structural information are provided in the CIF files. They can be accessed at http://www.pubs.acs.org/.

Chapter 6 - A boron heterocycles as a dianionic ligand for lanthanide coordination

As already discussed in Chapter 2, the most common oxidation state exhibited by lanthanide ions is +3. In order to coordinate a ligand to lanthanides, we have to make sure to satisfy all three positive charges on the metal center. This is usually achieved by coordinating three monoanionic ligands, or one monoanionic and one dianionic ligand. Another important factor in lanthanide coordination chemistry is the large coordination sphere of the metal ions. Irrespective of the charge, the ligand should be bulky enough to provide steric shielding of the metal ion. As a result, the unwanted coordination of solvent molecules and formation of –ate complexes will be inhibited. This type of coordination behavior has been very well observed with pthalocyanin (Pc)[21] (Figure 6-1 A) and cyclooctatetraenyl (COT^{2-}) ligands (Figure 6-1 B)[205]. Both these ligands are dianionic and form anionic sandwich complexes with lanthanide ions. Secondly, they satisfy the coordination sphere of these Ln^{3+} ions thus preventing the formation of bent sandwich complexes. The Pc ligands have four coordinating nitrogen atoms but the COT^{2-} ligand being a 10π aromatic system exhibits an η^8 coordination to the lanthanides thus making them coordinatively more satisfied.[206]
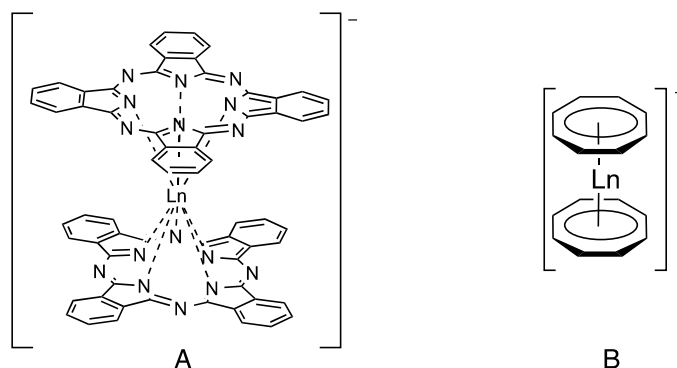
Figure 6-1: A) Pthalocyanin and B) cyclooctatetraenyl lanthanide sandwiches.

In our quest to coordinate aromatic boron heterocyclic ligands to lanthanides and explore the influence of these ligands on the properties of lanthanide complexes, we wanted to design a dianionic boron heterocycle, which would act as a boron analogue of the ubiquitous COT^{2-} ligand. The various dianionic boron ligands reported in the literature mostly include the five-membered carborane rings with two or three boron atoms (Figure 6-2);[88] however, we have seen from the literature and our previous results that each lanthanide ion prefers to coordinate three five-membered cyclopentadienyl rings or three six-membered boratabenzene rings. These aromatic cycles are too small to saturate the coordination sphere of the lanthanides and form sandwich complexes like the ones observed with COT^{2-} ligands.
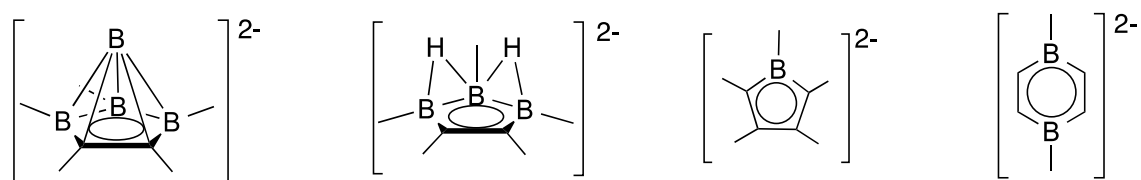
Figure 6-2: Examples of some dianionic boron heterocycles.[175]

Thus, we turned our attention towards larger boron heterocycles. Although there are examples in the literature of seven-membered borepin ligands[207], they are neutral and hence do not satisfy the +3 oxidation state of lanthanide ions in sandwich complexes like COT^{2-}.[208] The trianionic eight-membered boron analogue of COT, which was reported only once is very unstable and is generated in the coordination sphere of titanium by insertion of acetylene into boratabenzene. There are no reports of successful transmetallation of this molecule from titanium to other metals. Also the reaction is very sensitive to the concentration of acetylene and the titanium complex undergoes double insertion to form bicyclic molecules (Figure 6-3).[209]
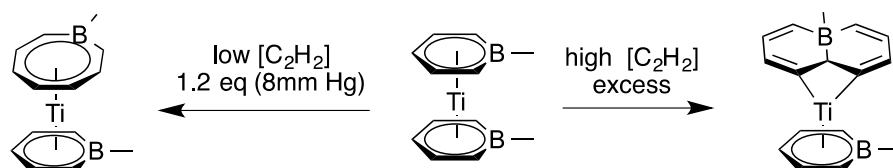
Figure 6-3: Synthesis of boratacyclooctatetraenyl complexes from boratabenzene titanium species.

So we decided to use the reduced form of 9,10-dihydrodiboraanthracene ligand (DBA).[150] This ligand has a large anthracene framework and two boron atoms at the 9 and 10 positions. After reduction, this antiaromatic molecule becomes a 14π aromatic system with two negative charges, thus respecting Hückel's rule. When coordinated to lanthanides, this ligand is expected to furnish monoanionic straight sandwiches like those observed with COT^{2-}.[210] This chapter will discuss the synthesis of various 9,10-diboraanthracene ligands and their coordination to different lanthanide ions.

6.1 Synthesis and characterization of 9,10-diboraanthracene ligands (DBA)

From the results of Chapter 4, it is clear that the bulky mesityl group provides an excellent steric protection around the oxophilic boron atom, thus making the ligand stable against the attack of nucleophiles in the reaction mixture. With that in mind, we decided to use 9,10-dimesityldiboraanthracene (**DMesDBA**) molecule as our dianionic ligand.

In order to synthesize the 9,10-dimesityldihydrodiboraanthracene framework, we started with the two-step route proposed by Agou and co-workers.[155] The first step of the reaction involves the synthesis of the Grignard reagent of 1-iodo-2-bromobenzene (PhIBr) followed by its coupling with half an equivalent of trimethoxyborane ($B(OMe)_3$) to form bis(2-bromophenyl)methoxyborane ($(PhBr)_2BOMe$) (Scheme 6-1). The magnesium salt of PhIBr has a tendency to decompose at higher temperatures by eliminating $MgBr_2$ to produce benzyne, which is extremely unstable and decomposes into diverse products. Thus it is important to maintain the reaction at -78 °C until the magnesium salt is reacted with $B(OMe)_3$. The air stable product bis(2-bromophenyl)mesitylborane ($(PhBr)_2BMes$) was produced by refluxing the reaction of mesitylmagnesiumbromide and $(PhBr)_2BOMe$. The product was obtained in high purity in 53% yield after performing a silica column using hexane as eluent.
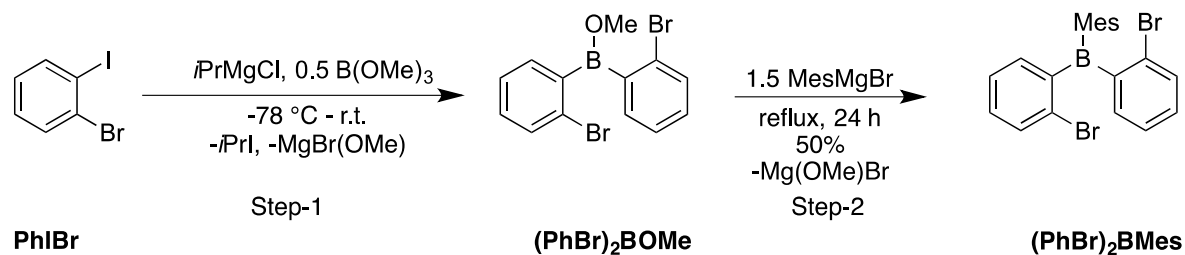
Scheme 6-1: Scheme for the synthesis of (PhBr)₂BOMe (Step-1) and (PhBr)₂BMes (Step-2) from iodobromobenzene.

(PhBr)₂BOMe was characterized by NMR spectroscopy. The aromatic signals corresponding to the phenyl rings appeared as three sets of multiplets at 7.56, 7.30 and 7.25 ppm. The ^{11}B NMR shift appears at 74 ppm, which is in accordance with the reported values. The second step of this reaction involves the dilithiation of **(PhBr)₂BMes** followed by ring closure in presence of B(OMe)₃ to form the anthracene framework. The *in-situ* mesitylation of **Mes(OMe)DBA** is expected to yield the 9,10-dimesityldihydrodiboraanthracene (**DMesDBA**) (Scheme 6-2). However, repeated attempts to isolate the product from this reaction failed. NMR spectra of the reaction mixture showed the formation of the desired product but only in minor quantities.
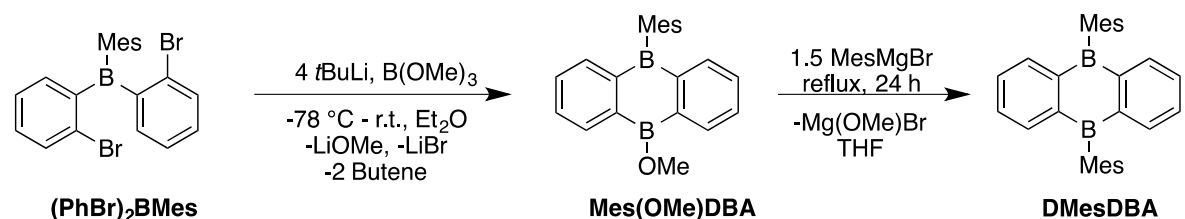
Scheme 6-2: Proposed reaction for the synthesis of 9,10-dimesitydiboraanthracene.

The major products formed in the reaction were dimesitylboronic acid (Mes₂BOH) and bis(2-phenol)mesitylborane (PhOH)₂BMes suggesting that the ring closing step of the dilithiated salt of (PhBr)₂BMes did not occur. That is why we observed the products formed by the substitution of methoxy groups of B(OMe)₃ by mesityl groups from MesMgBr (Scheme 6-3). This can occur because the steric hindrance of the mesityl group on **(PhBr)₂BMes** prevents the rotation of the phenyl fragment of the dilithiated salt that is needed in order to close the central ring of the anthracene molecule.
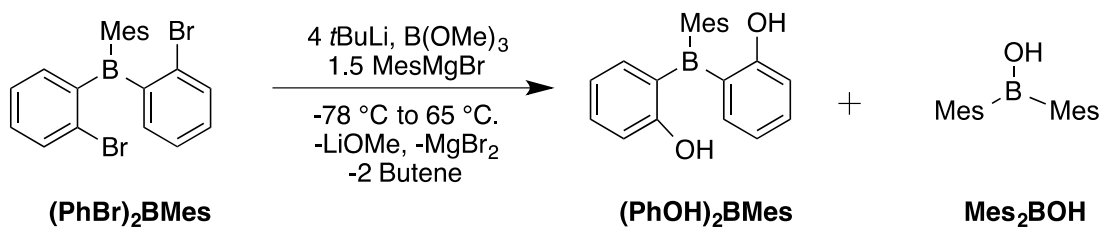
Scheme 6-3: Observed products from the reaction of (PhBr)₂BMes with B(OMe)₃ and MesMgBr.

In order to achieve a successful high yielding synthesis of **DMesDBA**, we decided to follow the thermolysis approach reported by Müller and Siebert. It involves the thermolysis of 1,2-bis(dihalo)phenylborane to obtain the 9,10-dihalodihydrodiboraanthracene (**DXDBA**) as the dimerization product. Due to the sensitivity of these phenylboranes their synthesis and purification is often difficult.[154]
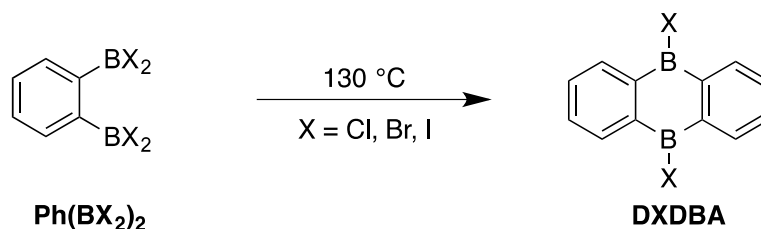
Scheme 6-4: Thermolysis approach for the synthesis of DBA molecules.

However, Wagner reported recently similar thermolysis of the stable 1,2-bis(trimethylsilyl)benzene **Ph(SiMe₃)₂** in presence of BBr₃ to obtain the 9,10-dibromodihydrodiboraanthracene (**DBrDBA**) in good yields.[151] The three step procedure furnishes the dihalo derivative of 9,10-diboraanthracene, which can be modified with different functional groups on boron by transmetallating the halide ions.

6.1.1 Synthesis of 1,2-bis(trimethylsilyl)benzene [Ph(SiMe₃)₂]

The first step of the reaction is the synthesis of 1,2-bis(trimethylsilyl)benzene **Ph(SiMe₃)₂** from 1,2-dibromobenzene (PhBr₂). In this reaction PhBr₂ is reacted with magnesium turnings to form its dimagnesium salt. 1,2-dibromoethane is used in catalytic amounts to activate the magnesium turnings. The dimagnesium salt is then quenched with trimethylsilylchloride (SiMe₃Cl) to form **Ph(SiMe₃)₂** (Scheme 6-5). The reaction generates a lot of heat, so the temperature is maintained between 5 – 15 °C in order to prevent the

formation of coupling products. The product is extracted from the magnesium salts with hexane. Further purification is achieved by vacuum distillation of the extract to remove the coupling product biphenylene and 1-(trimethylsilyl)-2-bromobenzene. The pure product is obtained in the form of clear oil in 55% yield.
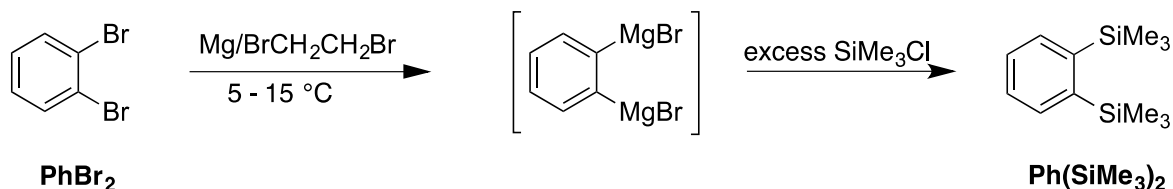
Scheme 6-5: Synthesis of 1, 2-bis(trimethylsilyl)benzene as reported by Wagner.

It was characterized by NMR spectroscopy. Both the ^{1}H and ^{13}C{^{1}H} NMR spectra consist of two signals in the aromatic region at 7.68 and 7.34 ppm, and 146.2 and 135.0 ppm, respectively. The SiMe$_3$ group appears at 0.36 ppm in the ^{1}H NMR spectrum.[211]

6.1.2 Synthesis of 9,10-dimesityldiboraanthracene derivatives

A toluene solution of the precursor **Ph(SiMe$_3$)$_2$** was heated with 1.8 equivalents of BBr$_3$ in a Schlenk bomb at 120 °C for 6 days during which the color of the solution became bright orange. This orange solution while hot was cannulated in a Schlenk and crystallized at -30 °C. The product 9,10-dibromodihydrodiboraanthracene (**DBrDBA**) crystallized as bright orange needles that are extremely sensitive to air and moisture (Scheme 6-6). The yield of the reaction was very sensitive to the purity of the starting materials. On exposure to ambient conditions **DBrDBA** is hydrolyzed to form white powdered hydroxy-borane analogue with the release of HBr. **DBrDBA** was characterized by NMR spectroscopy and is in accordance with the reported values.[212]
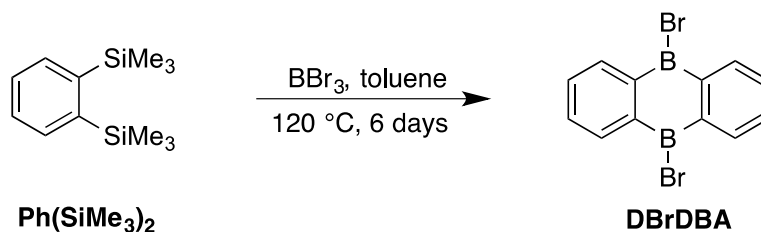
Scheme 6-6: Thermolytic coupling to form 9,10-dibromodihydrodiboraanthracene.

The molecule **DBrDBA** serves as a precursor for synthesizing different derivatives of 9,10-diboraanthracene. On reaction with 2.2 equivalents of mesityllithium at room temperature, both the bromides were transmetallated with a mesityl group in two hours to provide 9,10-dimesityldihydrodiboraanthracene (**DMesDBA**) in 80% yield (Scheme 6-7). The LiBr precipitated out and was removed by simple filtration. The product crystalized from the filtrate by slow evaporation. Mesitylmagnesiumbromide can also be used as a mesityl source but the purification from the magnesium salts was more time consuming. Agou reported the crystal structure of this molecule. It consists of three planer anthracene rings with two mesityl fragments perpendicular to the anthracene plane.[213] The replacement of the bromide ions by the mesityl groups stabilizes the anthracene framework against the attack of nucleophiles. As a result, **DMesDBA** is stable to ambient conditions and is not attacked by water or oxygen. The symmetrical structure of the molecule is evident from its ^{1}H NMR spectrum, which consists of two sets of multiplets at 7.77 and 7.12 ppm corresponding to the protons of the anthracene backbone, while the peaks for the mesityl group appear at 6.91, 2.33 and 2.11 ppm. The ^{11}B NMR signal is observed at 66 ppm, which is in accordance with the shift observed for mesitylboracyclohexadiene (62 ppm).

Stirring a THF solution of **DMesDBA** with excess of lithium metal at room temperature over 2 days reduces this 12π anti-aromatic system to the 14π aromatic 9,10-dimesityldiboraanthracene (**Li₂DMesDBA**). While **DMesDBA** forms a yellow solution in THF, when reduced it becomes dark red. The reduction was followed by ^{1}H and ^{11}B NMR spectroscopy and the completion of the reaction was indicated by complete disappearance of the peak in the ^{11}B spectrum at 66 ppm for **DMesDBA** and the appearance of a new peak at 26.4 ppm for **Li₂(DMesDBA)** indicating the formation of a tri-coordinate anionic boron center.[214,215] The boron shift is also in the same range as the one observed for mesitylboratabenzene derivatives. In ^{1}H NMR, the aromatic signals of the anthracene framework are shifted from 7.77 and 7.12 ppm in **DMesDBA** to 8.25 and 7.03 ppm in **Li₂DMesDBA**, which indicates the increase in the charge density at the *ortho* protons of the phenyl rings and a decrease in charge density at the *meta* protons.
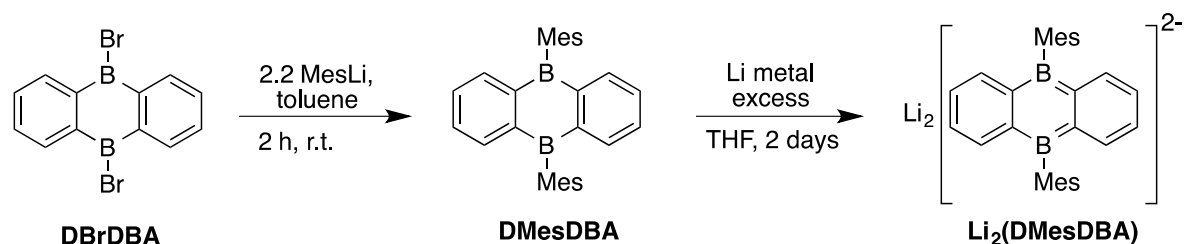
Scheme 6-7: Scheme for the synthesis of lithium salt of 9,10-dimesityldiboraanthracene.

The lithium salt **Li₂DMesDBA** was dried under vacuum and then dissolved in dimethoxyethane (DME) which crystalized after cooling the saturated solution at -30 °C. Since, the reduction of **DMesDBA** at room temperature with lithium metal is slow, we were able to observe the single reduction product, the lithium salt of 9,10-dimesityldiboraanthracene **LiDMesDBA.** This 13π radical is very unstable and decomposes to **DMesDBA**. Kawashima and coworkers had also observed two reversible one-electron reduction waves at $E_{1/2}$ = -1.82 and -2.78 V (vs Cp_2Fe/Cp_2Fe^+) for the **DMesDBA** molecule, suggesting the existence of both a monoradical and a diradical.[155] Although it was not observed by NMR spectroscopy, we were able to get a green block crystal from the reaction mixture. The molecular structures of **DMesDBA**, **LiDMesDBA** and **Li₂DMesDBA** are depicted in Figures 6-4 to 6-6, respectively. All three molecules crystallize in P2₁/c group. The monoanionic **LiDMesDBA** has a lithium ion associated with it, which is coordinated to four THF molecules. While as the dianionic **Li₂DMesDBA** has two lithium atoms coordinated to the central diboron ring on each face. Each lithium atom is further coordinated to one molecule of dimethoxyethane (DME).
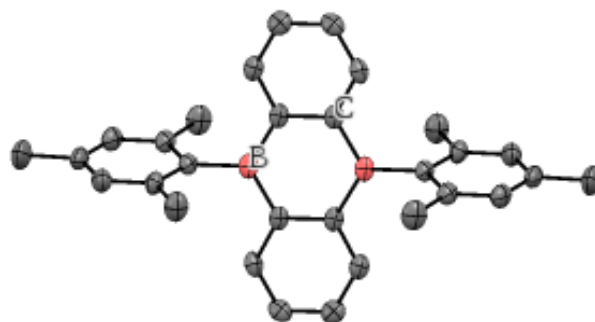
Figure 6-4: ORTEP view of molecular structure of DMesDBA. Anisotropic atomic displacement ellipsoids shown at 50% probability level. Hydrogen atoms have been omitted for clarity (R1 = 7.65%). Selected bond distances [Å] and angles [°]: C10-C11 1.411(3), C11-C12 1.393(4), C12-C13 1.389(4), C13-C14 1.394(3), C14-C15 1.401(4), C15-C10 1.444(4), B1-C15 1.573(4), B1-C10 1.567(5), B1-C6 1.588(4), C10-B1-C15 118.8(2), C10-B1-C6 120.3(2), C4-C6-B1 C10-C11-C12 122.4(2), B1-C15-C10 120.2(2).
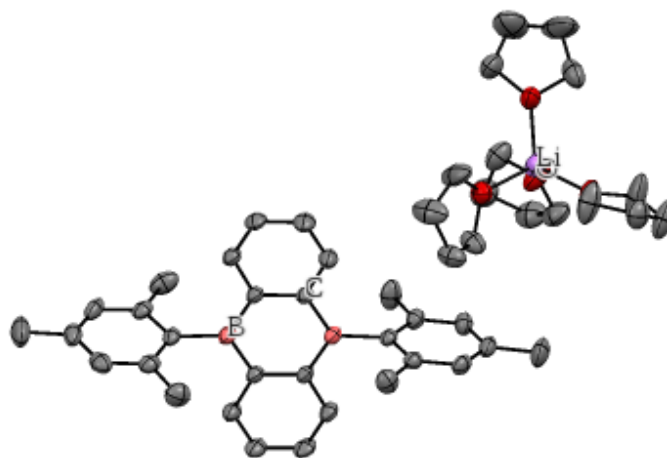
Figure 6-5: ORTEP view of molecular structure of Li(DMesDBA). Anisotropic atomic displacement ellipsoids shown at 50% probability level. Hydrogen atoms have been omitted for clarity (R1 = 9.32%). Selected bond distances [Å] and angles [°]: C10-C11 1.418(4), C11-C12 1.382(4), C12-C13 1.396(4), C13-C14 1.394(3), C14-C15 1.380(4), C15-C10 1.437(3), B1-C15 1.543(3), B1-C10 1.544(4), B1-C6 1.592(3), C10-B1-C15 118.8(2), C10-B1-C6 122.5(2), C4-C6-B1 C10-C11-C12 121.2(2), B1-C15-C10 120.6(2).
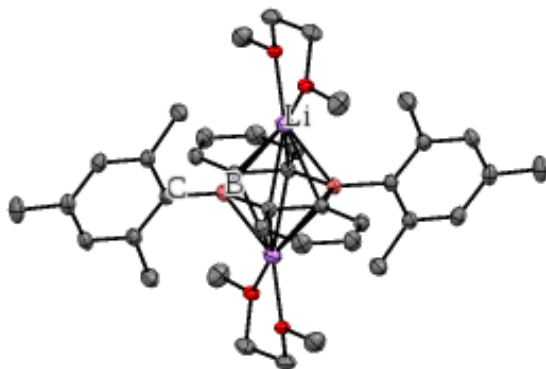
Figure 6-6: ORTEP view of molecular structure of Li₂(DMesDBA). Anisotropic atomic displacement ellipsoids shown at 50% probability level. Hydrogen atoms have been omitted for clarity (R1 = 6.02%). Selected bond distances [Å] and angles [°]: C10-C11 1.442(2), C11-C12 1.364(2), C12-C13 1.428(3), C13-C14 1.366(2), C14-C15 1.442(2), C15-C10 1.471(2), B1-C15 1.536(2), B1-C10 1.532(2), B1-C6 1.605(2), Li1-B1 2.440(4), Li1-C10 2.444(4), Li1-C15 2.442(3), C10-B1-C15 116.2(1), C10-B1-C6 122.8(1), C4-C6-B1 122.2(1) C10-C11-C12 123.0(1), B1-C15-C10 122.1(1).

For all three molecules **DMesDBA**, **LiDMesDBA** and **Li₂DMesDBA,** the anthracene rings are planar. The bond lengths of the mesityl rings and phenyl rings do not show any noticeable change and are within the normal range. However, it is interesting to observe that the B-C bond length of the central boron ring slightly decreases from 1.573(0) Å and 1.567(2) Å in **DMesDBA**, to 1.544(8) Å and 1.543(8) Å, in **LiDMesDBA** and 1.536(2) Å and 1.532(2) Å in **Li₂DMesDBA**, displaying the effect of aromatization on the bond length. The distance between the boron atom and the mesityl carbon atom increases with aromatization of the anthracene framework and varies form 1.588(0) Å for **DMesDBA**, 1.591(2) Å for **LiDMesDBA** to 1.605(2) Å for **Li₂DMesDBA**. Similarly, the mesityl groups for all the three molecules are almost perpendicular to the plane of anthracene molecule, but there is a slight difference in the dihedral angles, which are of 74.94° for **DMesDBA**, 86.22° for **LiDMesDBA** and 80.89° for **Li₂DMesDBA**.

In order to have a better understanding of the experimental results, we carried out DFT calculations for model **DMesDBA, LiDMesDBA** and **Li₂DMesDBA**. The geometry optimizations were performed with B3LYP functional. The 6-31G basis set were used for carbon, hydrogen and boron atoms. The HOMO and LUMO orbitals of the three species

106

are shown in Figure 6-7. The frontier orbital analysis reveals similar isosurfaces of SOMO of **LiDMesDBA,** the LUMO orbital of **DMesDBA** and HOMO of **Li₂DMesDBA.** These orbitals are in-phase combination of p orbitals of boron and carbon atoms. The π orbital is empty in **DMesDBA,** but is singly occupied in **LiDMesDBA** and doubly occupied in **Li₂DMesDBA.** Although the LUMO of **Li₂DMesDBA** is located on the mesityl carbon atoms, the LUMO of **LiDMesDBA** is distributed on the carbon atoms of the phenyl rings of anthracene molecule along with the boron atom (Figure 6-7), which further supports the SOMO nature of the boron heterocycle. The increase in the occupation of endocyclic π (C=B) orbitals leads to the shortening of the B-C bonds of the heterocyclic ring, which is clearly exhibited in their X-ray structures. This increase in the charge density on boron atom of the molecule is clearly exhibited in its ^{11}B NMR spectrum resulting in the shielding of boron atom from 66 ppm in **DMesDBA** to 26.4 ppm in **Li₂DMesDBA.** There is also an increase in the energy of LUMO orbitals of the three species. However, the energy of HOMO orbital of monoradical **LiDMesDBA** is lower than the other two derivatives. The energy differences between HOMO and LUMO are given in Table 6-1.

Table 6-1: Orbital energies and energy gaps for HOMO and LUMO.

Molecule	E(HOMO)/a.u.	E(LUMO)/a.u.	Egap/eV
DMesDBA	-0.220	-0.0948	3.407
LiDMesDBA	-0.049	0.0896	3.771
Li₂DMesDBA	0.1381	0.2118	2.005
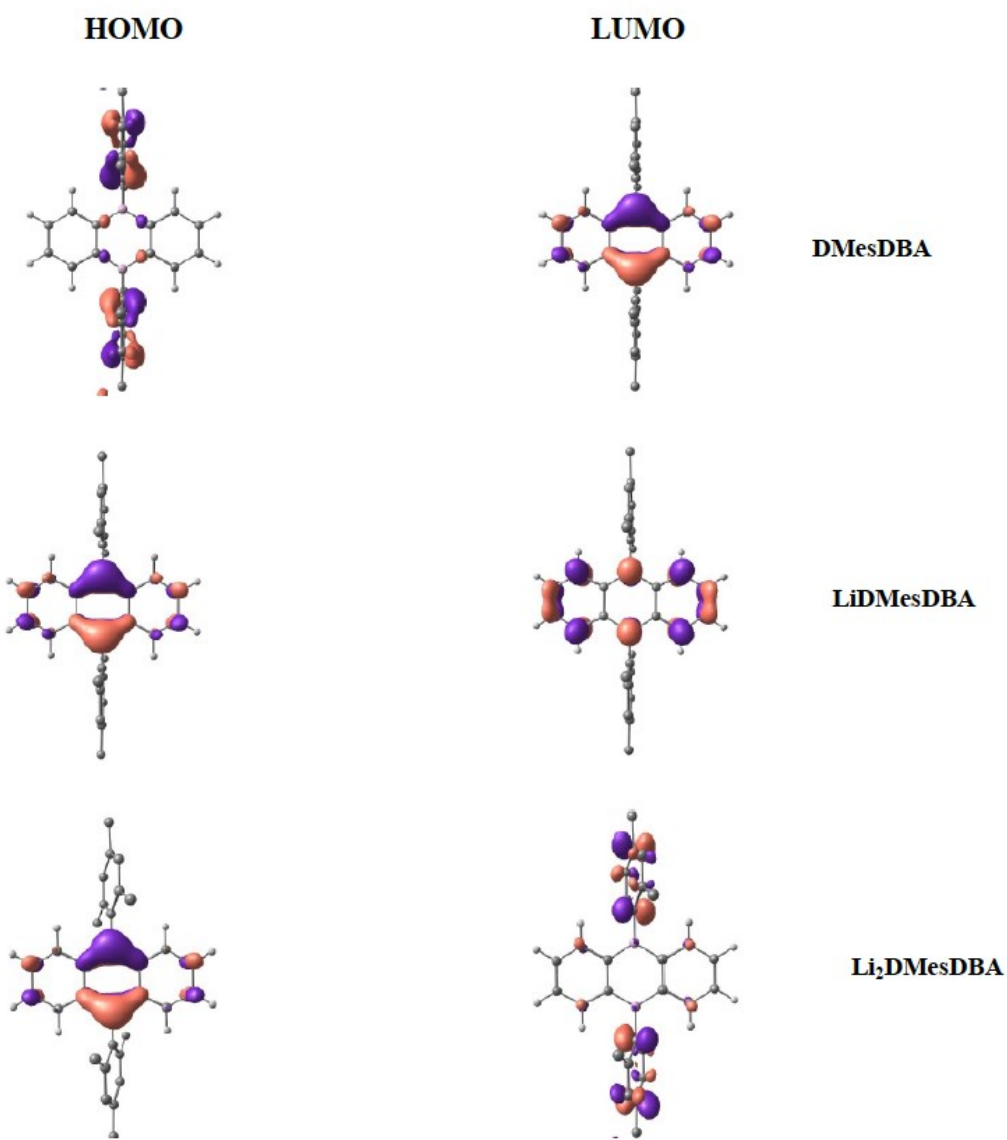
Figure 6-7: Distribution of HOMO and LUMO orbitals of DMesDBA derivatives.

6.1.3 Synthesis of 9,10-bis(dimethylamine)diboraanthracene derivatives.

In order to synthesize the dimethylamino derivative of diboraanthracene, the precursor **DBrDBA** was reacted with 2 equivalents of $LiNMe_2$ in toluene. After reacting for two hours at room temperature, the orange color of the solution disappeared and a white solid precipitated out. After filtration, the product 9,10-bis(dimethylamino)dihydrodiboraanthracene (**DADBA**) was obtained from the filtrate in

108

very limited amounts. Instead, the major product of the reaction was a lithium salt of boraanthracene that had two dimethylamino units bonded to each boron atom (Scheme 6-8).
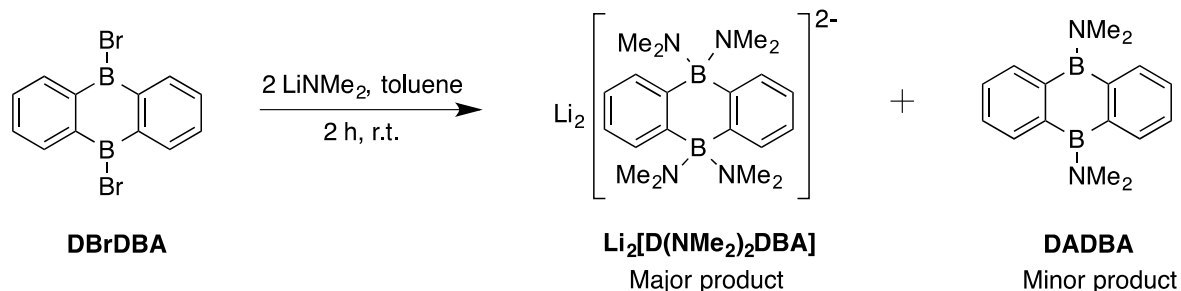
Scheme 6-8: Observed reactivity of LiNMe₂ with DBrDBA.

The small size of the NMe₂ group and the strong nucleophilicity of the LiNMe₂ base facilitate the second substitution on the boron atom giving the borate salts. In order to prevent the formation of tetracoordinate boron, we decided to use a milder nucleophile. N, N-dimethyltrimethylsilylamine was used as a source of dimethylamine and was refluxed with **DBrDBA** for 3 days to provide **DADBA** in 90% yield (Scheme 6-9). Removing the excess of silane under vacuum and extracting the residue with hexane gave the pure product.
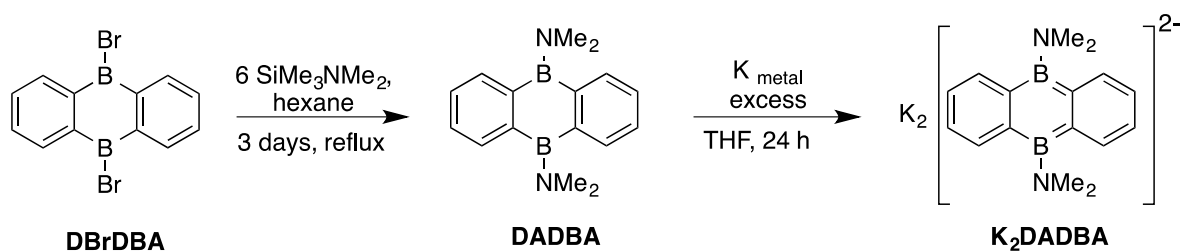
Scheme 6-9: Scheme for the synthesis of 9,10-dimethylaminodiboraanthracene derivatives.

The product **DADBA** was characterized by NMR spectroscopy. The proton signals of the aromatic rings were found to shift downfield to 7.60 and 7.24 ppm. Also the appearance of the boron signal at 41 ppm suggests the formation of a B-N bond. The aromatic analogue of **DADBA** was synthesized by reducing a THF solution of **DADBA** with excess of potassium metal. The reaction proceeds well at room temperature over 12 h. The dianionic salt, potassium 9,10-bis(dimethylamino)diborataanthracene (**K₂DADBA)**, was dark green both

in solution and in the solid state. The aromatization of the molecule was supported by the shift in the ^{1}H NMR signals to 8.71 and 6.95 ppm. The formation of an anionic boron center is also confirmed by the appearance of signal at 28.5 ppm in ^{11}B NMR spectrum. **K$_2$DADBA** is very unstable in solution at room temperature and starts decomposing in three days. However, it can be stored in the solid state for several months under inert conditions. At -30 °C both the solid and solution are stable for longer periods of time.

6.1.4 Synthesis of 9,10-dimethyldiboraanthracene derivatives

Initially, 9,10-dimethyldihydrodiboraanthracene (**DMDBA**) was synthesized by the reaction proposed by Müller and Siebert.[154] It involves the nucleophilic substitution of bromide of **DBrDBA** by methyl lithium at -80 °C. Although this reaction furnishes the desired product, the yields were very low at about 20%. As seen earlier with **DADBA,** the strong lithium salt carries out a second nucleophilic attack on the boron atom resulting in the formation of the borate salts. Attempts were made to remove the second methyl group from the boron center by using SiMe$_3$Cl to precipitate out lithium chloride and remove SiMe$_4$, but this method didn't work well. So the problem was addressed by using MeMgBr as a softer nucleophile. The reaction of MeMgBr with **DBrDBA** for two hours resulted in the complete conversion of **DBrDBA** into **DMDBA** (Scheme 6-10). The reaction was monitored by the change of the color of the solution from bright orange to light yellow. The magnesium salt precipitated out from the reaction and the liquid displayed blue-green luminescence. The pure **DMDBA** was obtained in the form of long white needles after sublimation of the reaction residue at 120 °C. The use of magnesium salts helps to improve the yield of the reaction to 70%. **DMDBA** shows resonances in the ^{1}H NMR spectrum for the aromatic protons at 8.00 and 7.32 ppm while the methyl groups appear at 1.84 ppm. The ^{11}B NMR signal shifts to 67.9 ppm, which is in accordance with the other dihydrodiboraanthracene derivatives.
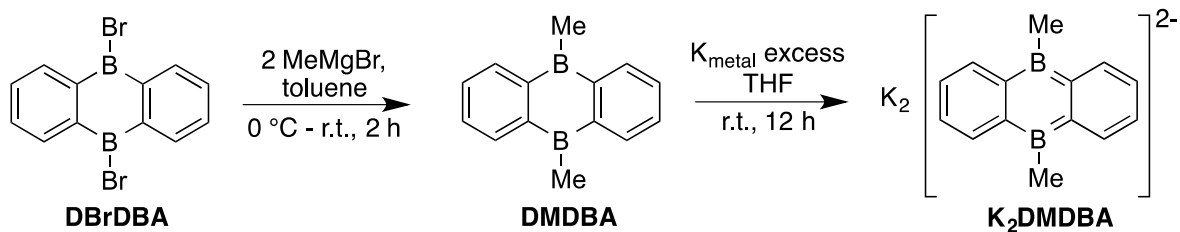
Scheme 6-10: Synthesis of derivatives of 9,10-dimethyldiboraanthracene.

The final product, the potassium salt of 9,10-dimethyldiboraanthracene (**K₂DMDBA**) was obtained by reducing **DMDBA** with excess of potassium metal at room temperature for 12 h. The product is dark green in solution and maroon in the solid state. Besides being very unstable to ambient conditions, it survived in the solid state for longer periods than in solution. The ^{1}H NMR signals of **K₂DMDBA** are shifted to 8.78 and 7.07 as compared to the anti-aromatic **DMDBA** (8.00 and 7.32 ppm). The ^{11}B NMR signal also shows a shift from 67.9 to 26.1 ppm, which is in the same range as observed for other aromatic anionic boron heterocycles. Unfortunately, the attempts to crystalize this highly sensitive product failed. However, Müller has reported the crystal structure of the dianion **K₂DMDBA**, in which each anthracene ring is coordinated η^6 to two potassium ions and η^2 to two more potassium ions. Each potassium ion is solvated by a molecule of tetraemethylethylenediamine (TMEDA).[154]

6.2 Coordination of 9,10-diboraanthracene ligands to lanthanides

After accomplishing the synthesis of the diboraanthracene ligands, we wanted to explore their coordination behavior to lanthanides. It was quite evident from the crystal structure of the lithium salts of 9,10-dimesitydiboraanthracene that the negative charge of the ligand is located in the central ring, which should prefer metal coordination. We set therefore to look at the coordination chemistry of this ligand to lanthanides.

6.2.1 Triple-decker $[(\eta^6$-DMesDBA$)$La$(\eta^6$-η^6,μ^2-DMesDBA$)$La$(\eta^6$-DMesDBA$)]$ complex

Initial attempts were made to coordinate **Li₂DMesDBA** to lanthanides to make the desired sandwich complexes. Since the lanthanide ions are tri-cationic and the ligands are dianionic, the final complexes are expected to be anionic salts. Therefore, the reactions and crystallizations were attempted in coordinating solvents like THF and DME to solubilize the corresponding salts. Two equivalents of **Li₂DMesDBA** was dissolved in THF to form a dark red solution and then added to a suspension of one equivalent of LaI₃ or LnCl₃ (Ln = Dy, Tb, Ho, Er) at room temperature. There was no change in the color of the reactions even after 48 hours. The reaction with LaI₃ was followed by NMR spectroscopy and there was no change in the proton and boron NMR spectrum of the ligand before and after reaction with the LaI₃. The reaction with other lanthanides could not be monitered by NMR spectroscopy since these species would give paramagnetic salts and broad NMR signals. The reaction mixtures were filtered after two days of reaction and kept for crystallization. The crystals that were obtained were those of the unreacted ligands. However, after the addition of HoCl₃, the red solution of **Li₂DMesDBA** became colorless within two hours. The colorless solution was crystalized and it was found to contain the oxidized **DMesDBA** ligand. From the reaction mixture of DyCl₃ and **Li₂DMesDBA** was isolated the crystals of monoradical LiDMesDBA, suggesting that the ligand gets oxidized and Dy(III) gets reduced to Dy(II). [216]

In order, to enhance the reactivity of **Li₂DMesDBA** with other lanthanides, their reaction mixtures were refluxed at 75 °C for three days. The reaction with LaI₃ was followed by ^{1}H and ^{11}B NMR spectroscopy and new signals appeared at 8.01, 7.75, 6.92 and 6.87 ppm for the anthracene protons and at 7.31, 7.08, 2.95, 2.45, 2.35 and 1.89 ppm for the mesityl groups. Also a new peak appeared in the ^{11}B NMR spectrum at -6.2 ppm along with a broad peak at 40.0 ppm. This suggests that two inequivalent boraanthracene rings are present in the reaction in addition to the starting material (Figure 6-8 and Figure 6-9). The integration values suggest that the two types of boraanthracene ligands are present in the ratio of 2:1. Two possibilities arise: either the formation of two new type of boraanthracene complexes or the formation of a triple-decker complex **[La₂(DMesDBA)₃]** where the two terminal

equivalent ligands coordinate each one lanthanide atom while as the bridging ligand coordinates two lanthanide ions (Scheme 6-11). Comparison of the ^{11}B NMR shifts of our complex with the values reported for the known transition metal complexes further supports the formation of triple-decker complex. For the triple-decker complexes Cp$_2$Fe$_2$(DMDBA) and (C$_3$H$_5$)$_2$Ni$_2$(DMDBA) the ^{11}B NMR shifts are at 1.0 and 7.0 ppm respectively, suggesting that the peak at -6.2 ppm corresponds to the bridging **DMesDBA** ligand.[157] Similarly, in sandwich complexes where the **DMDBA** is coordinated to only one metal center the ^{11}B NMR signal appears between 30 - 24 ppm which is close to the value of the non-coordinated ligand at 26 ppm.[157,217] It is possible for the peak of the terminal ligand of the triple-decker complex to overlap with the peak of the starting ligand at 26.7 ppm.
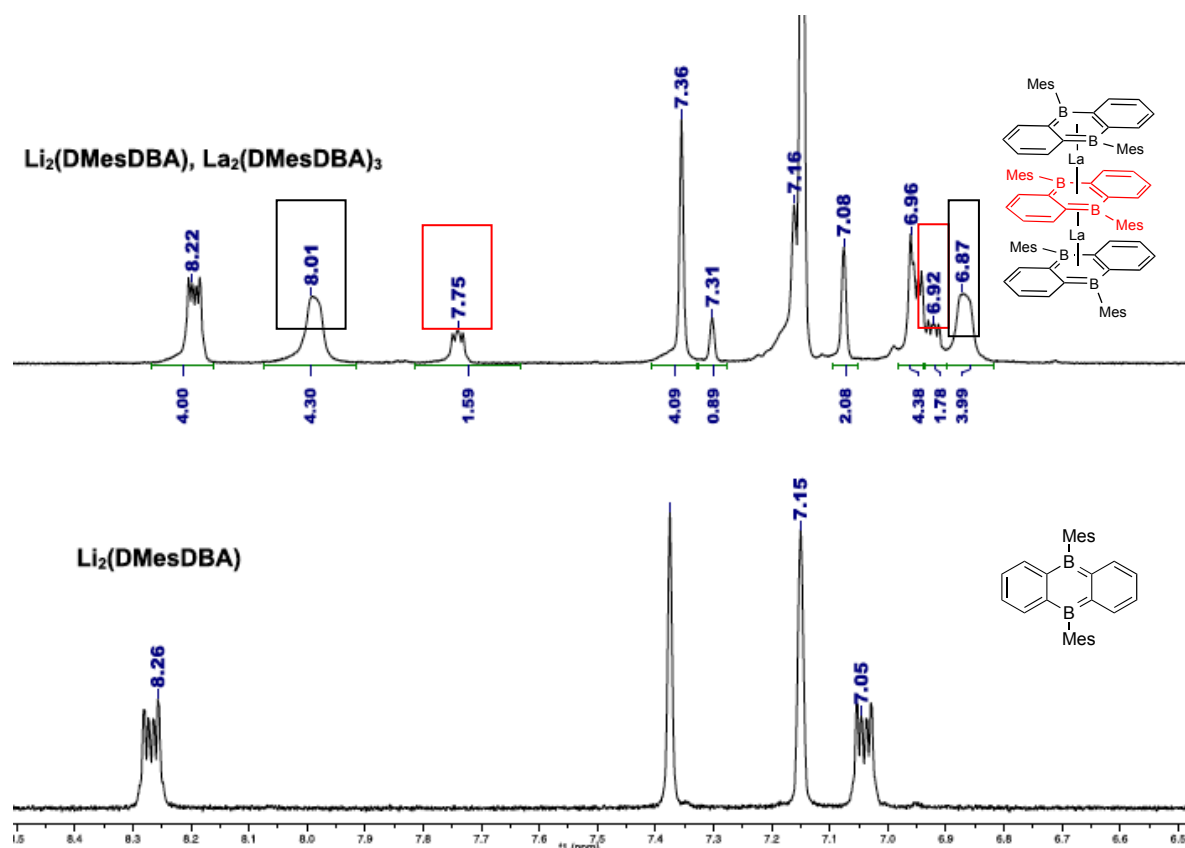
Figure 6-8: ^{1}H NMR spectrum of the Li$_2$(DMesDBA) with LaI$_3$.*
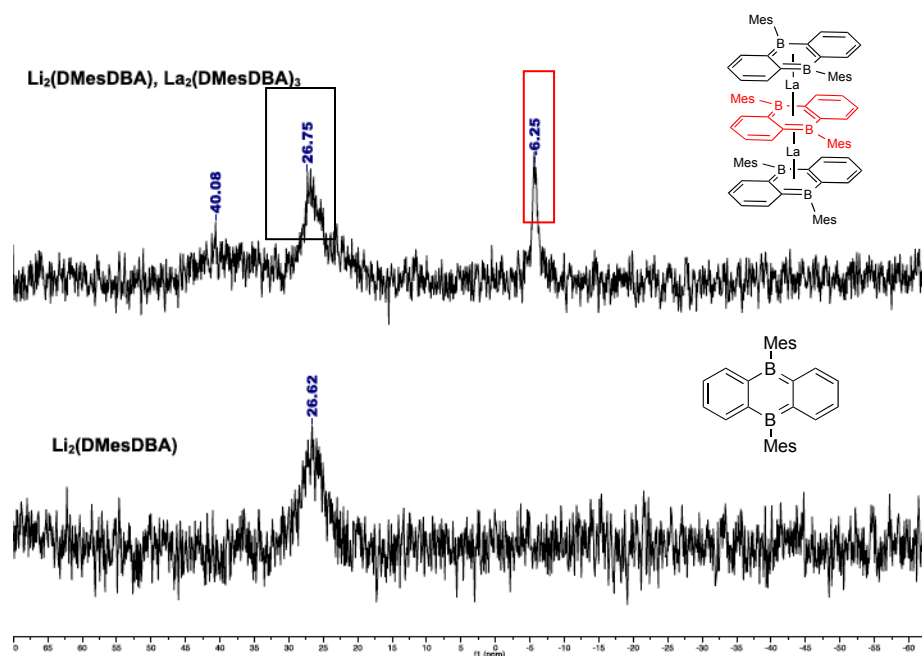
Figure 6-9: ^{11}B NMR spectrum of the Li$_2$(DMesDBA) with LaI$_3$.*

*These NMR spectra have been taken after heating for 3 days at 75°C. They display new sets of boraanthracene resonances that correspond to the formation of triple-decker complex.

However, there was still 50% of the unreacted ligand in the reaction mixture. The reaction was heated for two more days to increase the conversion, but new and broad signals in the aliphatic and aromatic regions were observed that suggested decomposition products. We tried to optimize this reaction with other lanthanide salts but it resulted in the formation of brown mixtures, which were difficult to characterize and did not furnish any crystals.
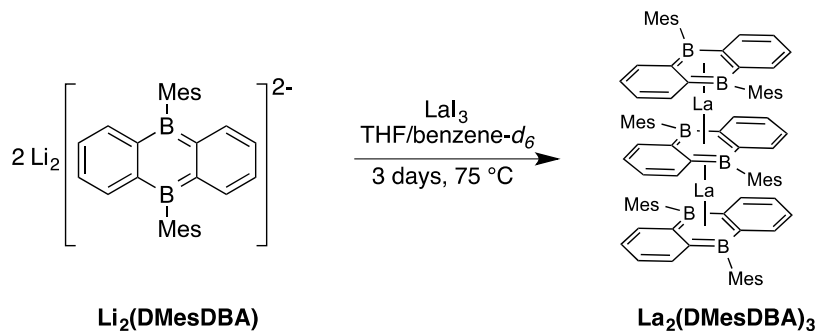
Scheme 6-11: Proposed scheme for the reaction of LaI$_3$ with Li$_2$(DMesDBA) at 75°C for 3-days.

114

These results suggested the boraanthracene ligand was too electron deficient to coordinate the metal atoms but since complexes of late transition metals with diboraanthracene ligand were reported in the literature, it was unlikely. The lithium ions are small in size and can easily coordinate the two faces of **Li$_2$(DMesDBA)** but since the mesityl groups are bulky, the coordination of larger lanthanide ions might be impeded, which would require heating the reaction mixtures but also leading to degradation. So we decided to use the smaller groups on the boron atoms in order to favor its coordination. Hence, we decided to study the coordination of the 9,10-dimethyldiboraanthracene derivatives with lanthanides.

6.2.2 Lanthanum inverse sandwich [LaI$_2$(THF)$_3$(η^6-η^6, μ^2 DMDBA)LaI$_2$(THF)$_3$]

An NMR scale reaction of LaI$_3$ was carried out with one equivalent of **K$_2$(DMDBA)** at room temperature. The green colored solution of **K$_2$(DMDBA)** in DME/ benzene-d_6 became dark red when reacted with a suspension of LaI$_3$ for 30 min. The reaction was left sonicating for 24 h to ensure the completion of the reaction. After 24 h, the reaction consisted of a clear light-red solution and a red solid. ^{1}H NMR of the clear solution showed peaks at 8.00, 7.33 and 1.31 ppm that are at similar shift as **DMDBA**, which at first suggested oxidation of the ligand. However, coordinated THF and DME were also observed in solution. Few drops of THF were added to the reaction mixture to dissolve the red solid, which generated a bright red solution and allowed the recording of the ^{1}H NMR spectrum. The aliphatic region had large solvent peaks which prevented the observation of signals for the methyl groups but there were two additional peaks in the aromatic region at 8.89 and 7.03 ppm which were very close to the shift of **K$_2$(DMDBA)** (8.86 and 7.11 ppm) (Figure 6-10). Due to the low concentration of the reaction mixture we could not record good ^{13}C{^{1}H} and ^{11}B{^{1}H} NMR spectra.
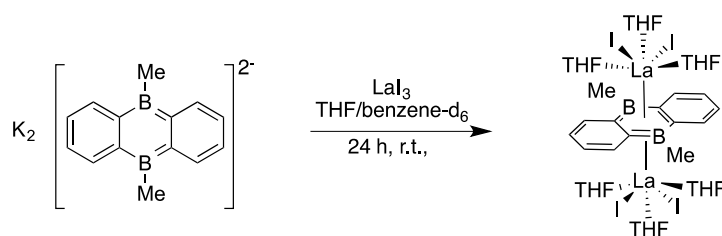
Scheme 6-12: Proposed scheme for the formation of La$_2$I$_4$(DMDBA) complex.
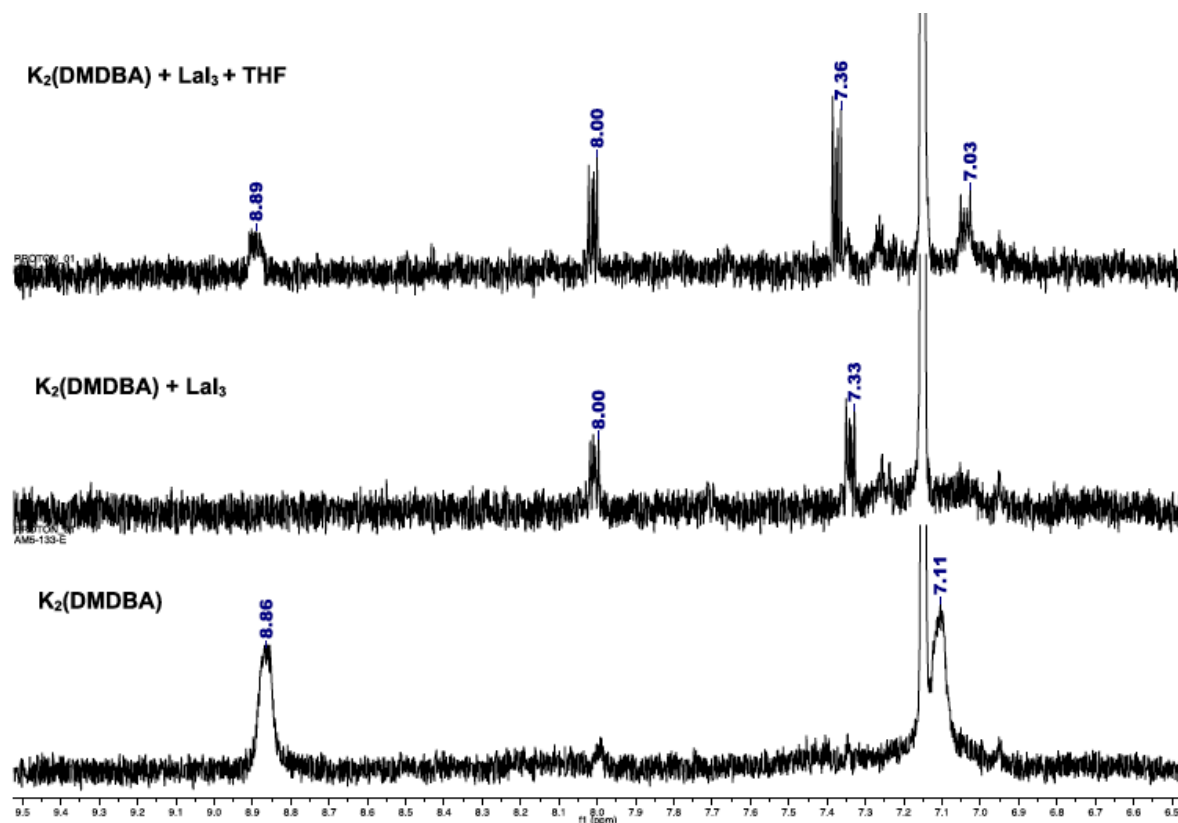
Figure 6-10: ^{1}H NMR spectrum of the K$_2$(DMDBA) with LaI$_3$.*

* The spectra represent the new set of boraanthracene resonances that are observed after reacting the reagents for 24 h at room temperature.

However, red block crystals grew in solution and X-ray analysis of these crystals suggested the formation of a lanthanide diboraanthracene complex. The ORTEP plot of the complex [LaI$_2$(THF)$_3$(η^6-η^6, μ^2 DMDBA)LaI$_2$(THF)$_3$] **La$_2$I$_4$(DMDBA)** is shown in Figure 6-12. It is very interesting to observe that the **K$_2$(DMDBA)** acts as a bridging ligand between two lanthanide atoms. The complex **La$_2$I$_4$(DMDBA)** is the first report of the coordination of a diboraanthracene ligand to an electron poor metal. All the complexes reported before were made with electron rich late transition metals. The proposed reaction for the synthesis of this product is given in Scheme 6-12. This type of complex where an aromatic ligand is bridging two lanthanide halides occurs very rarely in lanthanide chemistry. This type of geometry is termed as inverse sandwich structure.

116

With COT^{2-}, which is also a dianionic aromatic ligand, there is a preference for the formation of COTLnCl pianostool complexes which either exist as dimers or solvated species.[31] Only two examples of this type of inverse sandwich complexes have appeared in the literature. They include the Sm$_2${N(SiMe$_3$)$_2$}$_4$(COT) and Nd$_2$(Ph$_2$SiO$_2$)$_2$(COT).[218,219] However, these complexes have been obtained by reacting the COTSmCl complex with two equivalents of LiN(SiMe$_3$)$_2$ and COTNdCl with four equivalents of (LiOPhSi)$_2$O, respectively (Figure 6-11).
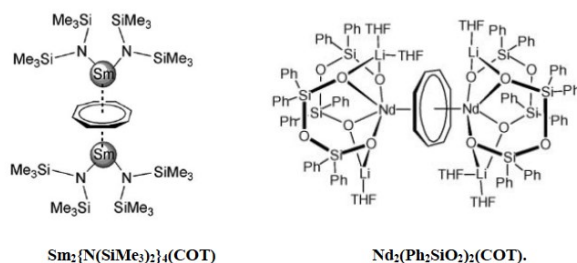
Figure 6-11: Representation of the inverse sandwich complexes of samarium and neodymium.
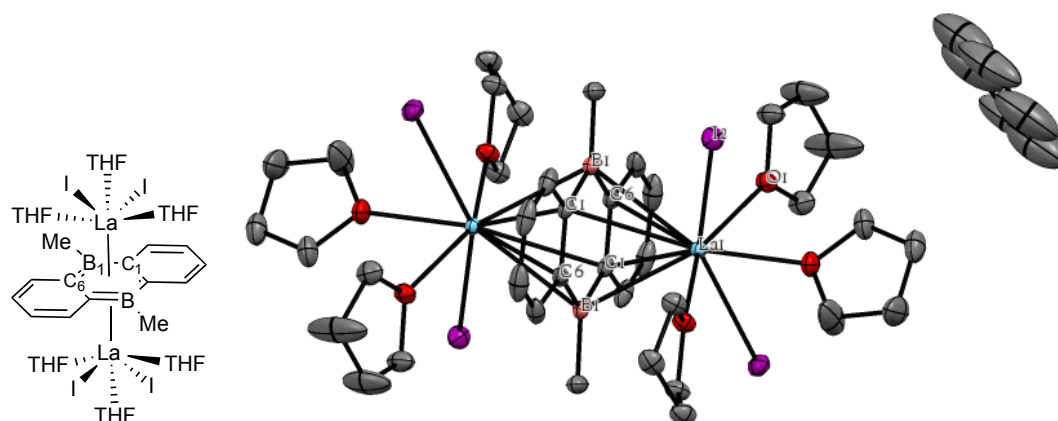
Figure 6-12: ORTEP view of molecular structure of [LaI$_2$(THF)$_3$(η^6-η^6, μ^2 DMDBA) LaI$_2$(THF)$_3$]. Anisotropic atomic displacement ellipsoids shown at 50% probability level. Hydrogen atoms have been omitted for clarity (R1 = 2.2%). Selected bond distances [Å] and angles [°]: C1-C2 1.442(2), C5-C6 1.445(3), C2-C3 1.355(4), C3-C4 1.418(4), C4-C5 1.363(5), C1-C6 1.460(3), B1-C6 1.534(4), B1-C1 1.545(2), B1-C7 1.604(4), La1-B1 3.011(2), La1-C1 2.995(2), La1-C6 2.977(2), La1-O3 2.494(2), La1-I1 3.218(5), La1-B1-La1 118.34(8), C1-B1-C6 115.8(2), C1-B1-C7 121.4(2), C1-C2-C3 122.8(2), B1-C6-C1 122.0(2).

The complexes **La$_2$I$_4$(DMDBA)** crystalizes in a P2$_1$/n space group. The two lanthanide atoms of the complex are coordinated on the opposite face of **DMDBA** in a η^6 manner. Each lanthanide atom is further coordinated to two iodide atoms and three THF molecules, which helps to satisfy the +3 charge and large coordination sphere of the lanthanide ions. In the lattice cell, each complex exists as a separate molecule and does not show any interaction with the neighboring molecules. However, a molecule of benzene-*d$_6$* is found to crystallize with each molecule of complex. The complex is highly symmetrical and possesses three mirror planes and three C$_2$ symmetry axes coincident with the planes (Figure 6-13). Because of the symmetry, both lanthanide atoms are equidistant from the diboraanthracene ring with a distance of 2.594 Å between the metal atom and ring centroid. It is noteworthy to mention that unlike other lanthanides, such inverse sandwich and triple-decker complexes where two lanthanum atoms are bridged by an aromatic ligand have not been reported before.
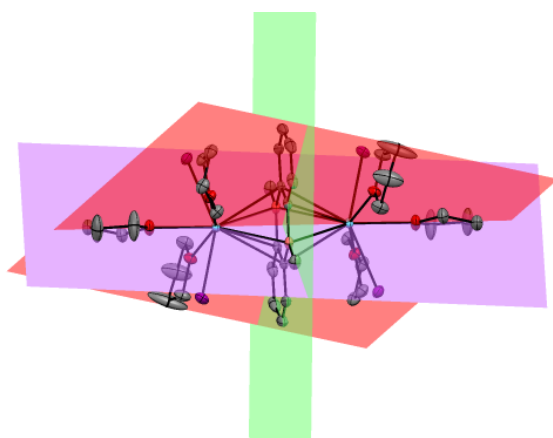
Figure 6-13: Representation of the symmetry planes of the complex La$_2$I$_4$(DMDBA).

The bond distances between the lanthanide ions and the carbon atoms of the central ring range between 2.977(2) Å – 2.995(3) Å, while the boron atoms are slightly farther from the metallic ions at 3.031(3) Å. These distances are in the same range as observed for the inverse sandwich complex Sm$_2${N(SiMe$_3$)$_2$}$_4$(COT) and Nd$_2$(Ph$_2$SiO$_2$)$_2$(COT) [2.970(3) – 3.106(3) Å]. However, in Cp$_2$Fe$_2$(DMDBA) and (C$_3$H$_5$)$_2$Ni$_2$(DMDBA) triple-decker complexes the bridging **DMDBA** ligand is 2.147(5) – 2.225(6) Å away from the metal centers. These smaller bond lengths with transition metals are in accordance with smaller size of transition metals as compare to lanthanides. The coordination of the lanthanide

118

atoms causes a slight increase in the bond lengths of the central boron ring while, as the other bonds do not show any noticeable change. The B1 – C1 and B1 – C6 bond lengths of the **La₂I₄(DMDBA)** complex increase to 1.545(3) Å and 1.534(4) Å as compared to 1.529(2) Å and 1.501(2) Å for **K₂DMDBA** respectively. The C1 - C6 bond does not show any significant increase (1.460(3) Å) as compared to 1.455(7) Å reported for $(C_3H_4)_2Ni(DMDBA)$ complex. The exocyclic B – C bond of the methyl group does not show any change and is 1.604(4) Å which is the same as the one observed for the B – C distance in case of **Li₂(DMesDBA).** The boraanthracene ring is completely planar. The THF molecules and the iodide ions are slightly bent away from the anthracene ring and have Centroid-La-O1 and Centroid-La-I angles of 102.6(2)° and 104.7(3)°, respectively. The value of bond angles C1-B1-C6 = 115.8(2)°, C6-C1-B1 = 122.2(2)° and C1-C6-B1 = 122.0(2)° are also consistent with the values observed for **K₂(DMDBA)**.

6.2.3 Lanthanum 9,10-dimethyldiboraanthracene sandwich and triple-decker complex

In order to synthesize a sandwich complex of lanthanum with **K₂(DMDBA)**, one equivalent of LaI₃ was reacted with two equivalents of **K₂(DMDBA)** in THF-d_8. As soon as the green solution of the ligand **K₂(DMDBA)** in THF-d_8 was added to the suspension of LaI₃, the color of the solution changed to dark red. After sonicating the reaction for 7 h, ¹H and ¹¹B NMR spectra were recorded and are shown in Figure 6-15. The ¹H NMR spectrum shows four different sets of peaks in the aromatic region, which are different from the starting ligand. The integration of the peaks suggests the formation of two different types of complexes, which can regarded as a sandwich complex $K(\eta^6-\eta^6,\mu^2-DMDBA)La(\eta^6-DMDBA)$ **K[La(DMDBA)₂]** and a triple-decker complex $(\eta^6-DMDBA)La(\eta^6-\eta^6,\mu^2-DMDBA)La(\eta^6-DMDBA)$ **[La₂(DMDBA)₃]** (Scheme 6-13). The tendency of lanthanides to form multidecker complexes with dianionic ligands has also been seen with different derivatives of the COT ligands. With 2 equivalents of COT^{2-} most of the lanthanides form multidecker complexes in addition to sandwich complexes (Figure 6-14).[24,56,220] The sandwich complexes with COT have been selectively obtained either by reacting LnCl₃ salts with 1.5 equivalents of COT^{2-} at room temperature or with 2 equivalents of COT^{2-} at -34 °C.[24,74,83]
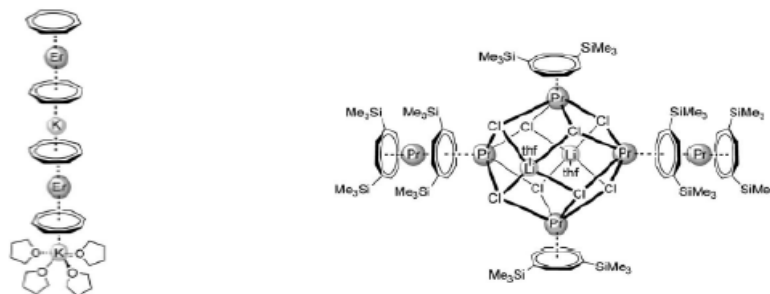
Figure 6-14: Representation of various multidecker complexes of lanthanides.

The two sets of signals in ^{1}H NMR at 8.21, 6.65 ppm and 7.74, 6.48 ppm (Figure 6-14) suggests the formation of the triple-decker complex **[La$_2$(DMDBA)$_3$]**. These peaks show the similar shifts and pattern as observed before for the **[La$_2$(DMesDBA)$_3$]** lanthanide complex (Figure 6-7). The integration of the ^{1}H NMR signals at 7.74, 6.48 ppm is twice as compared to the peaks at 8.21, 6.65 ppm, which is in agreement for a triple-decker complex where the two terminal **DMDBA** ligands are equivalent while as the bridging ligand is not equivalent to them. The two broad signals in the ^{11}B NMR spectrum at 34.4 and -8.4 ppm (Figure 6-13 bottom) can be attributed to the terminal and bridging **DMDBA** ligands of the triple-decker complex respectively. They are in accordance with the shifts observed for the **[La$_2$(DMesDBA)$_3$]** complex (Figure 6-8).

The second set of peaks at 7.83, 7.29, 6.77 and 6.60 ppm are in a 1:1:1:1 ratio (Figure 6-15), which suggests the formation of a sandwich complex **K[La(DMDBA)$_2$]** where the two boraanthracene rings are inequivalent because one of them is coordinated to lanthanum only while the other one will be coordinated to lanthanum and potassium (Scheme 6-12). This is also supported by the presence of four coordinated THF molecules. The ^{11}B NMR signals for the terminal **DMDBA** ligand would be expected in the same range as for the terminal ligands of triple-decker complex 34.4 ppm and is possible that the two signals overlap. This is in accordance with the ^{11}B NMR shifts observed for the transition metal complexes (24 – 30 ppm).[156,157] The ligand coordinating La and K probably appears at one of the three signals observed at -9.1, -11.5 and -14.5 ppm, which lies in the range, observed for the bridging ligands.

120
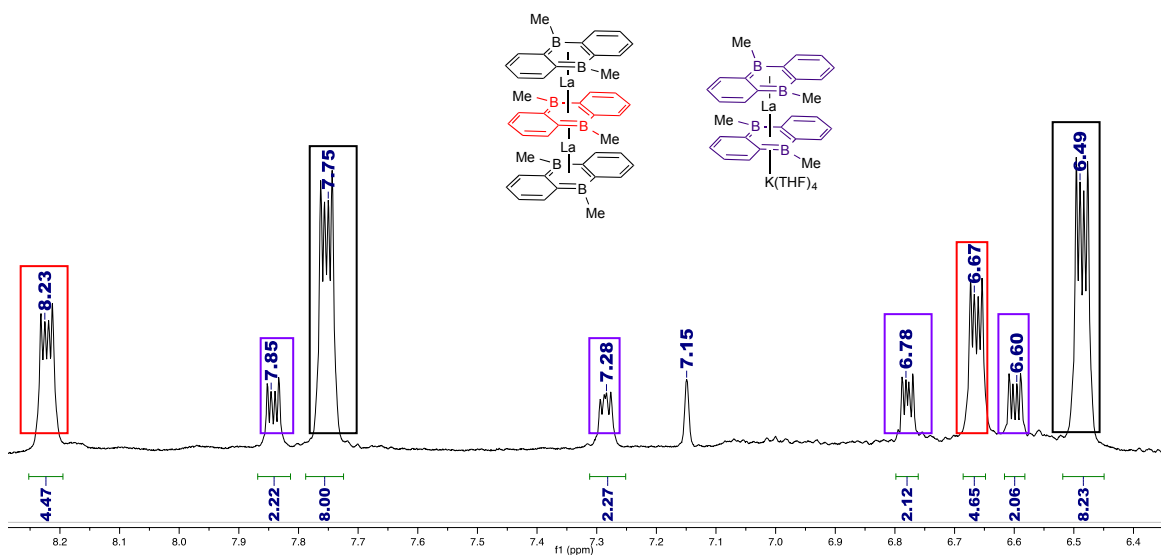
Figure 6-15: ^{1}H NMR spectrum of the reaction of LaI_3 with 2 equivalents of K_2DMDBA.
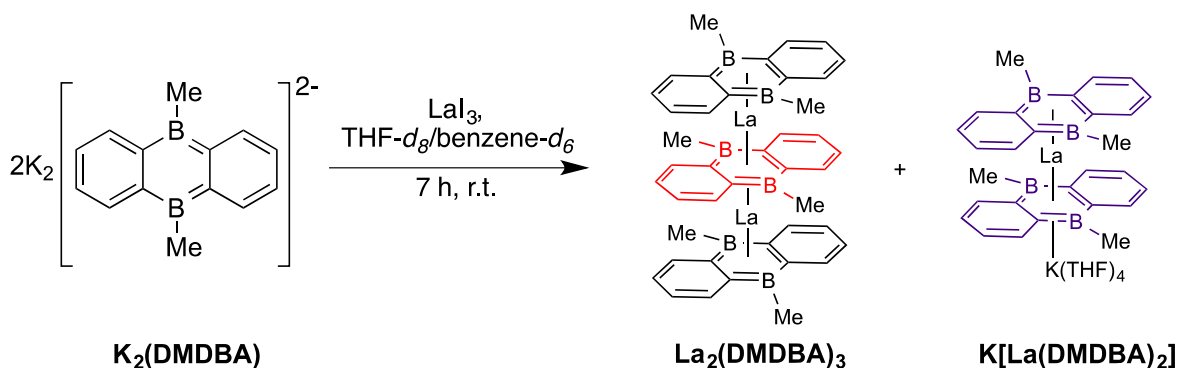
Scheme 6-13: Scheme proposed for the reaction of LaI_3 with two equivalents of K_2DMDBA.

From the above results, it was clear that with K_2DMDBA ligand, the formation of a triple-decker complex is favored. Thus, to selectively synthesize the triple-decker complex **La$_2$(DMDBA)$_3$**, we reacted a THF solution of 1.5 equivalent of **K$_2$(DMDBA)** with 1 equivalent of LaI_3. After reacting the two for 12 h, the solution was filtered to give a dark red filtrate and an orange solid. The filtrate was reduced to minimum and layered with hexane. It was kept at -30°C over several days but no crystals was formed. So the solution was evaporated and red solid obtained was dried. The ^{1}H and ^{11}B NMR of the solid shows signals which are consistent with the signals obtained for the triple-decker complex in Scheme 6-13. It also shows the formation of small amounts of sandwich complex. Crystallization was again attempted by making the solution of solid in THF and allowing

hexane to slowly diffuse into THF at room temperature. Red crystals that looked like square blocks were obtained but unfortunately decomposed at room temperature over 2 days before acquisition could be done for X-ray analysis. Recrystallization was attempted with no success.

So our next goal was to obtain the sandwich and triple-decker complexes of other lanthanides particularly Tb, Dy, Er, Ho and Yb, with **K₂DMDBA** ligand so as to explore their magnetic properties. In order to do so, we tried to scale up these reactions to selectively synthesize the sandwich and triple-decker complexes of lanthanum and establish a general procedure, which can be then used to access similar complexes of the other lanthanide ions. The most important step of these syntheses is the growth of crystals of these complexes. Although NMR spectroscopy can be used to study La^{3+} and Yb^{2+}, the other members of lanthanide series are paramagnetic ions and hence do not give good analyzable NMR spectra. To confirm the formation of aforementioned complexes with other lanthanides we will need to have their crystal structure data. So a lot of efforts were put in to get the crystals of these complexes.

Reactions were also carried out between 2 equivalents of K_2(DMDBA) and $DyCl_3$ and $ErCl_3$. Like lanthanum immediate color change of the solution from green to red was observed with both dysprosium and erbium. After stirring the reactions over 12 h, they were filtered and the filtrate was kept for crystallization after layering with hexane at -30°C. No crystals were formed. But we observed the formation of white crystals of KCl in the dysprosium reaction suggesting that the transmetallation of **DMDBA** ligand has successfully occurred from potassium to dysprosium. So in-order to remove these alkali metal salts from the reaction mixture, the THF solutions of the products were passed through celite and evaporated to give red solids. The low temperature crystallization, slow evaporation and vapor diffusion techniques with different combinations of polar and non-polar solvents was tried to get the crystals with these two samples. These complexes are very unstable in solution at room temperature and tend to decompose in 2-3 days in solution. This makes their crystallization challenging. However, preliminary magnetic measurements were conducted on the powdered samples. The dysprosium complex behaved as a single molecule magnet while as the erbium complex didn't not show

interesting magnetic properties. Since we were not able to get information about the structure and molecular weight of these complexes, therefore it was not possible to calculate the value of different magnetic parameters for these complexes.

The **K₂DADBA** molecule was also reacted with LaI₃. The reaction was followed by ^{1}HNMR spectroscopy. There was the appearance of new peaks in addition to the peaks of the starting material. The ligand seemed to react with lanthanides. However due to the results obtained with **K₂DMDBA**, more efforts were put in to obtain lanthanide complexes with **DMDBA** and the reactivity **K₂DADBA** was not further explored.

6.3 Experimental section

All manipulations were carried out under an atmosphere of nitrogen using standard Schlenk techniques or in nitrogen filled gloveboxes, unless specified otherwise. All solvents were distilled from sodium and benzophenone. Benzene-d_6 was distilled under reduce pressure from a Na/K alloy. Anhydrous lanthanum(III) iodide, dysprosium(III) chloride, terbium(III) chloride, erbium(III) chloride, and ytterbium(III) iodide were purchased from Alfa Aeser and used without further purification. 1-iodo-2-bromobenzene, 1,2-dibromobenzene and BBr$_3$ were purchased from Aldrich and used without further purification. NMR spectra were recorded on an Agilent Technologies NMR spectrometer at 500 MHz (^{1}H), 125.758 MHz (^{13}C), 160.46 MHz (^{11}B), and on a Varian Inova NMR AS400 spectrometer, at 400.0 MHz (^{1}H), 100.580 MHz (^{13}C). ^{1}H NMR and ^{13}C{^{1}H} NMR chemical shifts are referenced to residual solvent signals in deuterated solvent. Multiplicities are reported as singlet (s), doublet (d), triplet (t), quartet (q), multiplet (m) or broad (br). Chemical shifts are reported in ppm. Coupling constants are reported in Hz. HRMS characterization was possible using an Agilent Technologies 6210 LC Time of Flight Mass Spectrometer. Products in toluene and THF solutions were introduced to the nebulizer by direct injection. Neutral molecules were characterized using APPI ionization in positive mode.

6.3.1 Synthesis of compounds

Bis(2-bromophenyl)mesitylborane (PhBr)$_2$OMe. 4.08 ml (9.00 g, 31.8 mmol) of 1-iodo-2-bromobenzene in 100 ml of THF was cooled down to -80 °C. 16 ml of a 2.0 M solution of iPrMgCl (32.0 mmol) in THF was added to it. The reaction was stirred for 1 h at -80 °C then 1.72 ml (1.61 g, 15.5 mmol) of B(OMe)$_3$ was added and the reaction was allowed to warm to room temperature over 3 h. At room temperature, 24 ml (24 mmol) solution of a 1.0 M MesMgBr was added to the reaction mixture. The brown reaction mixture was refluxed at 67 °C overnight. The light yellow reaction mixture was quenched with a solution of HCl in ether. The reaction was evaporated and the residue was subjected to ether/water extractions. The ether fractions were evaporated to give a yellow solid that was

purified on silica column and eluted with 9 : 1 hexane : chloroform to give 7.07 g of the product as yellow solid (yield = 53%). The spectral properties are in accordance with the values reported in the literature.[155]

^{1}H NMR (500 MHz, chloroform-d): δ 7.59 (m, 2H, H^3), 7.30 (m, 4H, H^{4,5}), 7.25 (m, 2H, H^6), 6.84 (s, 2H, H^{mes}), 2.33 (s, 3H, CH$_3^{mes}$), 2.10 (s, 6H, CH$_3^{mes}$). ^{13}C{^{1}H} (126MHz, chloroform-d) δ 139.5, 139.1, 136.4, 132.7, 132.05, 128.7, 127.8, 127.7, 126.6, 23.0, 21.3. ^{11}B{^{1}H} NMR (161 MHz, benzene-d_6) δ 74.2 (br).

1,2-bis(trimethylsilyl)benzene [Ph(SiMe₃)₂]. A suspension of 4.00 g (164 mmol) of magnesium turnings in 120 ml of THF was cooled down to 5 °C. 58 ml (424 mmol) of trimethysilylchloride (TMSCl) was added to the solution, followed by the addition of 6.4 ml (12.5 g, 53 mmol) of 1,2-dibromobenzene. A solution of 1.2 ml (13.8 mmol) of 1,2-dibromoethane in 10 ml of THF was added slowly to the solution over 15 minutes. The solution was kept at about 5-10 °C for 1 h and then at room temperature for 1 h. The solvent was removed under vacuum and the residue was quenched with 50 ml hexane and 50 ml water at 0 °C. The aqueous fraction was extracted with 3 X 25 ml of hexane. The hexane extracts were dried over MgSO₄, filtered and evaporated. The yellow oil obtained was distilled under vacuum to give 6.50 g of 1,2-bis(trimethylsilyl)benzene as a clear oil (55% yield).

^{1}H NMR (500 MHz, chloroform-d): δ 7.68 (m, 2H), 7.34 (m, 2H), 0.36 (s, 18H). ^{13}C{^{1}H} (126MHz, chloroform-d) δ 146.2, 135.0, 1.9. DI-MSTOF (APPI, m/e): Calcd for $C_{12}H_{22}Si_2$ 222.1260; found 222.1265.

9,10-dibromodiboraanthracene (DBrDBA). 20 ml of toluene was added in a Schlenk bomb, then 3.91 g (17.6 mmol) of **Ph(SiMe₃)₂** and 8.03 g (3.08 ml, 32.1 mmol) of BBr₃ were added The reaction was refluxed at 120°C for 6 days during which it became orange in color. The hot reaction mixture was cannulated in a Schlenk tube and stored at -30 °C overnight. Bright orange needle like crystals were formed which were filtered and dried under vacuum for 4 h. (3.51 g, 60% yield).

^{1}H NMR (500 MHz, benzene-d_6): δ 8.27 (m, 4H), 7.13 (m, 4H). [13]C{[1]H} (126MHz, benzene-d_6) δ 138.7, 134.2. ^{11}B{^{1}H} NMR (161 MHz, benzene-d_6) δ 64.2 (br).

9,10-dimesityldihydrodiboraanthracene (DMesDBA). A suspension of mesityllithium (2.68 g, 21.30 mmol) in 10 ml of toluene was cooled down to 0 °C in an ice bath, then an orange solution of **DBrDBA** (2.37 g, 7.10 mmol) in 20 ml of toluene was added. The yellow-green fluorescent solution was left stirring at room temperature for 2 h. The sample was filtered and extracted with 2 X 15 ml of toluene. The filtrate was evaporated under vacuum to give 2.15 g of yellow solid (73.5% yield). X-ray quality crystals were obtained from a THF/Hexane solution by slow evaporation.

^{1}H NMR (500 MHz, benzene-d_6): δ 7.77 (m, 4H), 7.12 (m, 4H), 6.91 (s, 4H), 2.33 (s, 6H), 2.11 (s, 12H). [13]C{[1]H} (126MHz, benzene-d_6) δ 145.0, 140.8, 138.8, 137.9, 136.7, 133.4, 126.9, 22.6, 21.3. ^{11}B{^{1}H} NMR (161 MHz, benzene-d_6) δ 66.0 (br). DI-MSTOF (APPI, m/e): Calcd. for $C_{30}H_{30}B_2$ 412.2534; found 412.2552.

Mono lithium 9,10-dimesityldiboraanthracene [Li(DMesDBA)]. 200 mg (0.48 mmol) of **DMDBA** was dissolved in 8 ml of THF. To it was added 7 mg (1.00 mmol) of lithium metal. The reaction was stirred at room temperature for 3 h during which the solution turned red in color. The reaction mixture was filtered and reduced to half its volume by evaporation at kept at -30 °C overnight. Few crystals of **Li(DMesDBA)** were obtained from the solution that were enough for X-ray analysis.

Lithium 9,10-dimesityldiboraanthracene [Li$_2$(DMesDBA)]. 1.00 g of **DMesDBA** (2.42 mmol) was dissolved in 30 ml of THF affording a yellow solution. An excess of lithium (200 mg, 28.8 mmol) was then added. After 30 min, the reaction became dark red and was stirred for 24 h. The reaction was filtered and the residue left behind was extracted with 3 X 10 ml of THF. After removing the solvent under vacuum, 723 mg of a red solid was obtained (Yield 70%). X-ray quality crystals where obtained by cooling a concentrated solution of **Li$_2$(DMesDBA)** in DME layered with hexane at -30 °C.

^{1}H NMR (500 MHz, benzene-d_6): δ 8.25 (m, 4H), 7.37 (s, 4H), 7.03 (m, 4H), 2.60 (m, 12H^{THF}), 2.59 (s, 6H), 2.36 (s, 12H), 0.90 (m, 12H^{THF}). ^{13}C{^{1}H} (126MHz, benzene-d_6) δ 141.1, 136.8, 134.0, 119.8, 67.9, 25.7, 24.7, 21.6. ^{11}B (161 MHz, benzene-d_6) δ 26.4 (br).

9,10-bis(dimethylamino)dihydrodiboraanthracene (DADBA). 400 mg (1.20 mmol) of **DBrDBA** was dissolved in 20 ml of hexane to form an orange suspension. 1.15 ml (843 mg, 7.19 mmol) of N, N-dimethyltrimethylsilylamine (Me$_2$NSiMe$_3$) was added to the solution. The solution became light yellow in color and was refluxed for 3 days. The solvent was removed under vacuum and the residue was extracted with 3 X 10 ml of hexane. 238 mg of light yellow solid was obtained after evaporating the hexane filtrate (Yield = 87.3%).

^{1}H NMR (500 MHz, benzene-d_6): δ 7.60 (m, 4H), 7.24 (s, 4H), 2.85 (s, 12H). ^{13}C{^{1}H} (126MHz, benzene-d_6) δ 131.7, 126.6, 41.3. ^{11}B{^{1}H} NMR (161 MHz, benzene-d$_6$) δ 41.5. DI-MSTOF (APPI, m/e): Calcd for C$_{16}$H$_{20}$B$_2$N$_2$ 262.1813; found 262.1654.

Potassium 9,10-bis(dimethylamino)diboraanthracene (K$_2$DADBA). 150 mg (3.75 mmol) of potassium metal was added to a solution of 300 mg (1.15 mmol) of **DADBA** in 10 ml of THF. The reaction turned maroon and was left stirring overnight during which it became dark maroon. The reaction was filtered and evaporated to yield 234.7 mg of a dark green solid (Yield = 65.6%).

^{1}H NMR (500 MHz, benzene-d_6 with drops of THF)): δ 8.71 (m, 4H), 6.95 (s, 4H), 3.67 (s, 12H). ^{13}C{^{1}H} (126MHz, benzene-d_6 with drops of THF) δ 135.4, 114.0, 47.7. ^{11}B{^{1}H} NMR (161 MHz, benzene-d_6 with drops of THF) δ 28.5.

9,10-dimethyldihydrodiboraanthracene (DMDBA). An orange solution of 1.68 g (5.04 mmol) of **DBrDBA** was made in 20 ml of toluene. After cooling it down to 0 °C, 5 ml of a solution of methylmagnesiumbromide (15 mmol, 3 M solution in diethyl ether) was added dropwise while stirring continuously. The solution was stirred in an ice bath for 15 min during which its color changed to light orange and finally yellow-green. This fluorescent reaction mixture was stirred at room temperature for 90 min. Half of the solvent was removed under vacuum and then the reaction was filtered and extracted with 2 X 10 ml of

toluene. Evaporation of the toluene filtrate gave 800 mg of yellow solid. Long colorless needles of the product were obtained after sublimation of the solid at 120 °C (yield = 72%).

^{1}H NMR (500 MHz, benzene-d_6) δ 8.00 (m, 4H), 7.32 (s, 4H), 1.32 (s, 6H). ^{13}C {^{1}H} (126MHz, benzene-$d6$) δ 135.8, 132.6. CH$_3$ groups cannot be seen, as they are broad. ^{11}B{^{1}H} NMR (161 MHz, benzene) δ 67.9 (s, br). DI-MSTOF (APPI, m/e): Calcd for C$_{14}$H$_{14}$B$_2$ 204.1282; found 204.1284.

Potassium 9,10-dimethyldiboraanthracene (K$_2$DMDBA). 400 mg (1.96 mmol) of **DMDBA** was dissolved in 10 ml of THF. To this yellow-green solution was added 50 mg (1.22 mmol) of potassium metal. The reaction turned dark purple in 15 min and was left stirring overnight. A green solution was obtained which was filtered and evaporated to give 420 mg of a dark red solid (yield 72%). Crystalline solid was obtained by layering the THF with hexane and cooling it to -30 °C overnight.

^{1}H NMR (500 MHz, benzene-d_6 with drops of THF): δ 8.78 (m, 4H), 7.07 (s, 4H), 1.84 (s, 6H). ^{13}C{^{1}H} (126MHz, benzene-d_6 with drops of THF) δ 138.6 135.9, 114.3, 0.01. ^{11}B{^{1}H} NMR (161 MHz, benzene-d_6 with drops of THF) δ 26.1.

La$_2$(DMesDBA)$_3$ triple-decker complex. 4.40 mg (0.0057 mmol) of Li$_2$DMesDBA(THF)$_4$ was dissolved in benzene-d_6 with two drops of THF. 1.53 mg (0.0028 mmol) of LaI$_3$ was added to it. The reaction was sonicated for 3 h and then heated at 80 °C for two days during which a dark red solution was formed. As per the integrations of the ^{1}H NMR signals the ratio of product : reactant is 1 : 2.

For triple-decker complex ^{1}H NMR (500 MHz, benzene-d_6 with drops of THF): δ 8.01 (br, 8H), 7.75 (m, 4H), 7.31 (s, 2H), 7.16 (s), 6.92 (m, 4H), 6.87 (br, 8H), 1.04 (s, 12H, CH$_3$). ^{13}C {^{1}H} (126 MHz, benzene-d_6 with drops of THF) δ 146.9, 143.2, 142.8, 140.8, 136.8, 133.3, 129.2, 126.8, 126.3, 120.1, 28.7, 27.5, 25.8, 24.3, 21.4. ^{11}B{^{1}H} NMR (161 MHz, benzene-d_6 with drops of THF) δ 36.7, -6.2.

Lanthanum inverse sandwich [LaI$_2$(THF)$_3$(η^6-η^6,μ^2-DMDBA)LaI$_2$(THF)$_3$]. To 4.25 mg (0.0081 mmol) of LaI$_3$ in DME and benzene-d_6 was added a solution of **K$_2$DMDBA** (2.29 mg, 0.0081 mmol) in DME and benzene-d_6. The reaction mixture is sonicated for 24 h

128

during which a red solution is formed. X-ray quality crystals were obtained from the reaction mixture after 2 days.

^{1}H NMR (500 MHz, benzene-d_6 with THF/DME): δ 8.89 (m, 4H), 7.03 (s, 4H). The peak for the methyl groups could not be observed due to broad solvent peaks in aliphatic region.

Lanthanum dimethyldiboraanthracene complex. 6.5 mg (0.023 mmol) of **K₂DMDBA** was dissolved in THF-d_8 and was added to a suspension of 6.0 mg (0.012 mmol) of LaI₃. The solution changed color from green to red and was sonicated for 7 h at room temperature. The NMR showed 2:1 ratio of triple-decker and sandwich complex in the solution. The reaction was repeated one more time and similar ratio of the products was obtained.

For triple-decker complex **[La₂(DMeDBA)₃]**:^{1}H NMR (500 MHz, THF-d_8): δ 8.21 (m, 4H), 7.74 (m, 8H), 6.65 (m, 4H), 6.48 (m, 8H), 2.95 (s, 6H), 2.45 (s, 6H), 2.40 (s, 3H), 2.35 (s, 6H), 1.89 (s, 3H). [13]C{[1]H} (126MHz, THF-d_8) δ 140.9, 136.6, 135.8 118.6, 118.3, 0.62. ^{11}B{^{1}H} NMR (161 MHz, THF-d_8) δ 34.4, -8.4.

For sandwich complex **K[La(DMesDBA)₂]**: ^{1}H NMR (500 MHz, THF-d_8): δ 7.83 (m, 2H), 7.28 (m, 2H), 6.77 (m, 2H), 6.80 (m, 2H), 0.95 (s, 3H, CH₃). [13]C{[1]H} (126MHz, THF-d_8) δ 141.3, 135.6, 135.3 124.8, 118.9, 3.86 ^{11}B{^{1}H} NMR (161 MHz, THF-d_8) δ 34.4, -14.

Lanthanide dimethyldiboraanthracene complex. **K₂DMDBA** 2 equivalents were dissolved in 8 ml of THF and were added to a suspension of 1 equivalent of LnCl₃ in THF. The solution changed color from green to red and was sonicated for 12 h at room temperature. The reaction mixtures were filtered and evaporated to give red solids.

Dysprosium dimehyldiboraanthracene complex: DyCl₃ (98.8 mg, 0.367 mmol), K₂(DMDBA) (207 mg, 0.735 mmol). Yield: 110 mg.

Erbium dimehyldiboraanthracene complex: ErCl₃ (100.5 mg, 0.367 mmol), K₂(DMDBA) (207 mg, 0.735 mmol). Yield: 211 mg.

6.3.2 Crystallographic Studies:

Nice single crystals with suitable size of all compounds were mounted on CryoLoops with Paratone-N and optically aligned on a Bruker SMART APEX-II X-ray diffractometer with 1K CCD detector using a digital camera. Initial intensity measurements were performed using a fine-focused sealed tube, graphite-monochromated, X-ray source (Mo $K\alpha$, $\lambda = 0.71073$ Å) at 50 kV and 30 mA. Standard APEX-II software package was used for determining the unit cells, generating the data collection strategy, and controlling data collection. SAINT was used for data integration including Lorentz and polarization corrections. Semi-empirical absorption corrections were applied using SCALE (SADABS). The structures of all compounds were solved by direct methods and refined by full-matrix least-squares methods with SHELX-97 in the SHELXTL6.14 package. All of the H atoms were generated geometrically and refined in riding mode.

Chapter 7 - Chelating ether-amide ligands for selective recovery of rare earth elements

7.1 Introduction

The rare earth elements (REEs) and their alloys are used in many modern technologies including notably the production of consumer electronics, computers, cell phones, and network and communication devices.[78,170,221–224] Their unique electrochemical, luminescent and magnetic properties help to make these technologies perform with reduced weight and energy consumption, and give the devices greater efficiency, speed, performance, durability and thermal stability. As such, the global consumption rate and hence, the demand for pure REEs has dramatically increased over the past two decades. Since industrially useful ores contain several of the REEs among many other contaminants, including radioactive Uranium and Thorium, separation and purification of these mixtures are needed for further industrial processes. However, the chemical properties of all REEs are quite similar which complicate their separation. Industrial purification involves either liquid-liquid (LLE), supported liquid (SLE) or solid phase (SPE) extraction procedures, which rely on association constants between ligands and REEs based essentially on the lanthanide contraction effect. In LLE, cation- (carboxylic acids, phosphoric acids) and anion-exchangers (amines, diketones) have been used to recover the REEs.[6–8,225] However, this type of extraction utilizes large volume of solvents during the repeated cycles of extraction while generating a significant portion of undesired and radioactive waste. In comparison, SLE and SPE are greener approaches for REE extraction and purification as one of the liquid phase is reduced/eliminated. Chromatographic ion exchange resins have been used as early as 1947 but they lack selectivity between various lanthanide ions.[226–228] Recently, SLE resins containing impregnated ligands have been used for REE purification.[229–232] Among them, the diglycolamide (DGA) resin which consists of a DGA derivative (tetraoctyldiglycolamide - TODGA) immobilized on a solid support is nowadays one of the

131

most commonly used systems for separation of REEs from other elements.[233] Regrettably, as the ligand is only supported on the stationary phase, its leaching into the aqueous phase is frequently observed, limiting its reusability. The challenge in separating REEs from environmental and industrial samples resides in the fact that REEs, but more specifically the Ln, have very similar physical and chemical properties. Indeed, while other oxidation states are synthetically available for the REEs, they tend to exist in environmental conditions as trivalent ions.[234] In addition, all of the REEs have similar radii size ranging from 74.5 (Sc^{3+}) to 103.2 pm (La^{3+}).[4] They can adopt coordination numbers ranging from 6 to 9, and sometimes more because of the available f and d orbitals on these metal centers.[235,236] In order to satisfy their coordination sphere, they tend to coordinate different solvent molecules and have a predilection for chelating ligands.[237–239] This affects the solubility of REE complexes in various solvents and thus makes their purification by LLE less efficient. However, the Ln^{3+} cations are highly Lewis acidic and easily coordinate nucleophiles to form stable complexes and they show a clear tendency towards oxygen donors, both in acidic and basic conditions, which can be advantageous for their efficient extraction.[240,241] It is documented that the best ligands used for extraction of REEs are mostly oxygen donors (e.g., carboxylic acids, ketones, phosphoric acids).[10–13] In particular, the derivatives of DGA are used industrially for the selective extraction of REEs from aqueous solutions, as they are commonly recognized as effective and size selective binders of trivalent f-elements. They show high and rapid extraction even in strong acidic conditions (10^{-4} to 10^{0} M in HNO_3).[242–245] Notably, the DIAMEX industrial process uses DGA derivatives to selectively extract lanthanides during reprocessing of spent nuclear fuels.[246,247] Recently, the research group of Kleitz and Larivière have studied the effect of the chemical anchoring of chelating ligands on mesoporous silica supports for the selective extraction of actinides and trivalent f-element ions.[248,249] They observed that anchored phosphonate ligands were highly efficient in extracting uranium from acidic media. Anchoring a DGA ligand (diglycol-2,4-diamido-propyltriethoxysilane, Figure 7-1) on KIT-6 also demonstrated improved extractive properties for all REEs in comparison to SLE resin while exhibiting enhanced selectivity for some of them. In addition, the tethering of DGA on the silica surface was found to overcome the leaching of the ligand observed in SLE.

132

7.2 Design and synthesis of chelating ligands

The research group of Kleitz and Larivière published a novel hybrid system for selective extraction of lanthanides. They observed that after immobilization on the solid support (KIT-6) the DGA ligand shows greater affinity for the mid-size lanthanide ions (Eu^{3+}, Gd^{3+}, and Tb^{3+}). The structural analysis of the complexes bearing the DGA ligands shows that REEs bind traditionally in a tridentate fashion, where each metal ion is coordinated by the three oxygen atoms of DGA-type ligands (Figure 7-1). The lanthanide ions (La, Yb, Ce) are sterically saturated in their nine-coordinate geometry with three DGA ligands.[250–252]
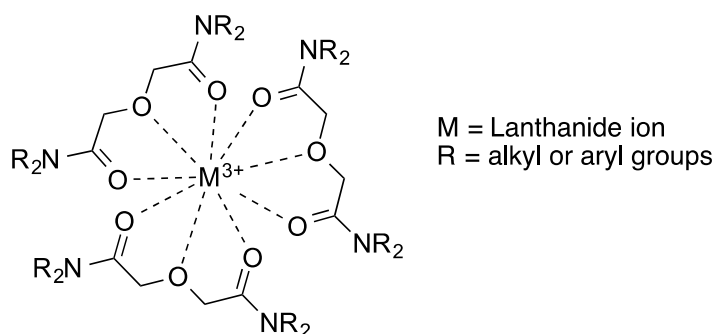
Figure 7-1: Tridentate binding mode of DGA ligand.

When such a chelate ligand binds a metal ion, an angle known as the *bite angle*, is formed between the two terminal coordinating atoms of the ligand and the metal ion. This bite angle greatly affect the binding properties of these ligands in the complexes (Figure 7-2).[253–256] If the terminal coordinating atoms of the ligand are far away from each other they will form a large *bite angle* while as a smaller *bite angle* will be formed if the coordinating atoms are closer to each other. The size of the *bite angle* dictates the binding affinity of the ligand. Ligands with large *bite angles* will have a higher affinity for larger metal ions whereas smaller *bite angles* will favor coordination to smaller ions. Careful tailoring of the ligand backbone can change the size of the *bite angle* and hence the binding affinities of the ligand. However, it is expected that if a chelating ligand is bound to a solid surface by more than one anchor point it will possess a rigid conformation and will exhibit less flexibility to adapt itself to the metal electronic requirements than in solution.

With this objective in mind our research group started this collaborative project with the research group of professor Kleitz and professor Larivière. We worked on the design of ligands having different bite angles, while the ligand immobilization and extraction studies (SPE and LLE) were carried out in the research groups of professor Kleitz and professor Larivière, respectively.

Since it was now clear that the DGA ligand after immobilization has larger affinity for mid-size ions, we decided to modify the backbone of DGA ligand so as to make it more selective for other lanthanide ions. The ligands that were synthesized with different *bite angles* are given in Figure 7-2.
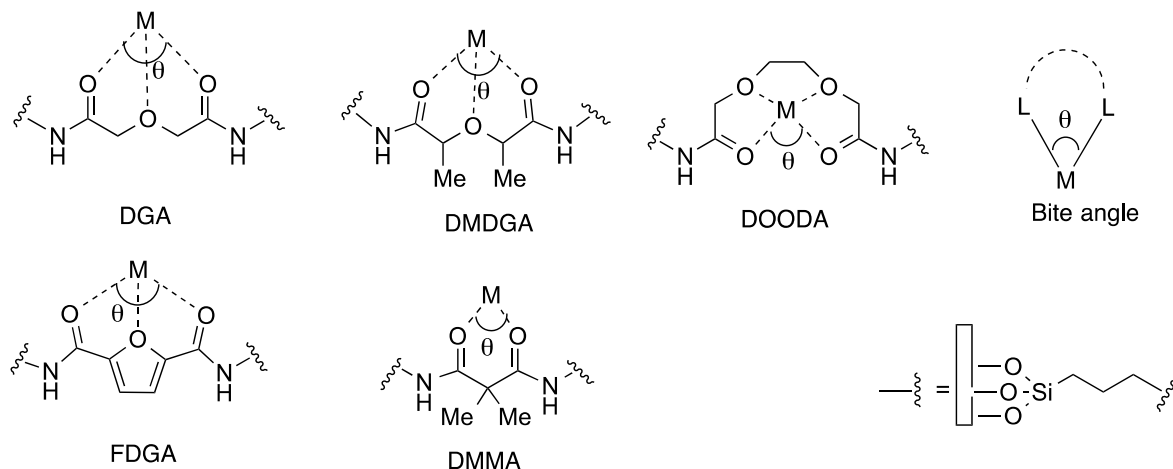
Figure 7-2: Ether-amide ligands with different bite angles.

7.2.1 Synthesis of 2,5-furandiglycolamide ligand (**FDGA**)

Our first objective was to increase the *bite angle* of **DGA** ligand to make it more selective for binding larger lanthanide ions. In order to achieve this, we decided to introduce some rigidity in the backbone of the **DGA** ligand that will decrease the flexibility of the coordinating arms of the ligand. This was done by introducing a furan ring into the **DGA** backbone (Figure 7-2 **FDGA**). The presence of this rigid furan backbone is expected to give a larger *bite angle* to the ligand. The most commonly used precursors for synthesizing amides are carboxylic acids and acid chlorides. In order to convert carboxylic acids directly into amides, they are reacted with an amine in presence of N,N'-dicyclohexylcarbodiimide (DCC) and 1-hydroxybenzotriazolate (HOBt). However, to remove DCC and HOBt to

134

isolate the pure amide product, column chromatography of the reaction residue is carried out. In order to graft our ligands on the solid support (**KIT-6**) the ligand is modified with (3-aminopropyl)triethoxysilane (**APTS**). The triethoxysilane groups get hydrolyzed in presence of water and hence will not survive the column chromatography. Therefore, we decide to synthesize our amides from acid chloride derivatives as the by products of this reaction can be removed by simple filtration and evaporation.

In order to synthesize the 2,5-furandioylchloride (**FDGA-Cl**), the 2,5-furandicarboxyllic acid was refluxed with excess of $SOCl_2$ for 6 hours in presence of catalytic amounts of dimethylformamide (DMF). Evacuation of the reaction mixture under vacuum gives a white solid, which was sublimed at 75 °C to give **FDGA-Cl** in 90% yield. The purity of the product was confirmed by NMR spectroscopy. In order to modify the ligand with **APTS**, one equivalent of **FDGA-Cl** was heated with 2 equivalents of **APTS** at 90 °C for 12 h. Excess of triethylamine (Et_3N) was used in the reaction in order to trap the HCl that was produced (Scheme 7.1). The Et_3NHCl was removed by filtration and the product was obtained after the evaporation of filtrate. The modification of **FDGA** with **APTS** on both sides was confirmed by the appearance of a broad peak at δ 7.26 in the ^1H NMR spectrum, integrating for two protons corresponding to the NH group. In $^{13}C\{^1H\}$ NMR, the disappearance of the carbonyl peaks at δ 155.4 (**FDGA-Cl**) and its appearance at δ 158.1 (**FDGA-APTS**) also confirmed the formation of amide bond. The product was obtained in 96% isolated yield.
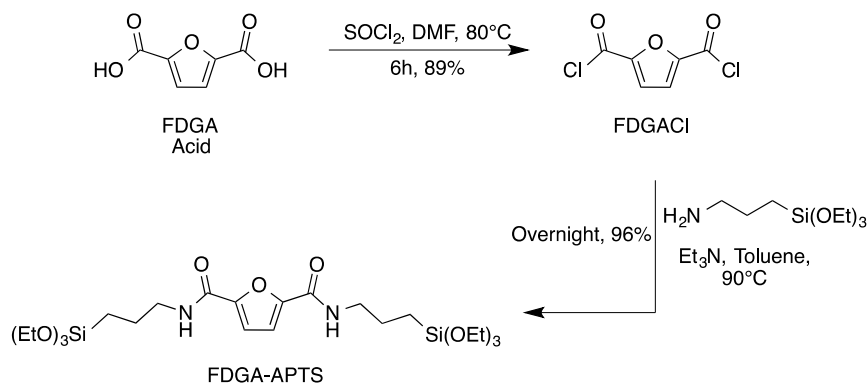
Scheme 7-1: Synthesis of FDGA-APTS from 2,5-furandicarboxyllic acid.

In order to study the extraction properties of **FDGA** ligand in LLE, a dioctylamide derivative of **FDGA** was synthesized. The presence of octyl chains increases the solubility of the ligand in the non-polar solvents, which are used for extracting lanthanide ions form aqueous acidic solutions. In order to synthesize N,N-dioctylfuran-2,4-diamide (**TOFDGA**), 2.5 equivalents of N,N'-dioctylamine was reacted with 1 equivalent of **FDGA-Cl** and excess of **Et₃N** in benzene (Scheme 7-2). The product was obtained after extracting the reaction residue with CH₂Cl₂ and 5% HCl in water. The product was characterized by ¹H and ¹³C NMR spectroscopy. The formation of amide bond was confirmed by the appearance of a peak at δ 159.6 in ¹³C{¹H} NMR spectrum.
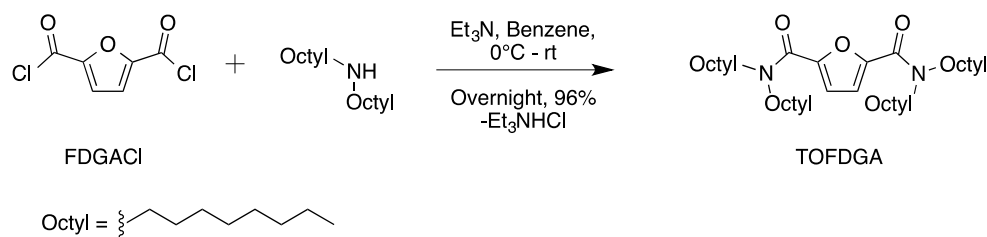
Scheme 7-2: Synthesis of TOFDGA.

7.2.2 Synthesis of **DMDGA** derivatives

In order to shift the selectivity of **DGA** to smaller lanthanides, its *bite angle* should be decreased. This can be achieved by introducing bulky substituents at the α-carbon atoms of the **DGA** framework. These bulky substituents will cause steric congestion in the **DGA** molecule, thus forcing the coordinating carbonyl groups to the move closer to each other. As a result the *bite angle* will decrease. We decided to start with a **DGA** molecule that has methyl groups at the α-carbon atoms. This 2,4-dimetyldiglycolamide (**DMDGA**) will be expected to have a smaller bite angle than **DGA** and will extract smaller lanthanides.

In order to introduce the methyl groups in **DGA** framework, 2-bromopropanoate and ethyl lactate were reacted together in THF to form 2,4-dimethyldiglycolic ester (**DMDGE**). The ethyl lactate was initially deprotonated by sodium hydride (NaH) to form the sodium salt, which reacts with 2-bromopropanoate to form 2,4-dimethyldiglycolic ester (**DMDGE**), with the release of NaBr (Scheme7-3). NMR spectroscopy was used to identify the product formed. The ethoxy groups appear at δ 1.28 and 4.18 while the methyl groups on the **DGA**

136

backbone appear as a doublet at δ 1.45 in ^{1}H NMR spectrum. The carbonyl groups are seen at δ 173.0, which is close to the value for **DGA**. The ester is then hydrolyzed to carboxylic acid with NaOH and H_2SO_4. The 2,4-dimethyldiglycolic acid (**DMDGA-acid**) was purified by extracting the aqueous solution of the reaction residue with ether. The 2,4-dimethyldiglycolic acid was characterized by ^{1}H NMR spectroscopy, which showed the disappearance of the ethoxy peaks δ 4.18 and 1.28 while as the peaks corresponding to the DMDGA backbone were observed at δ 1.20 and 3.49.
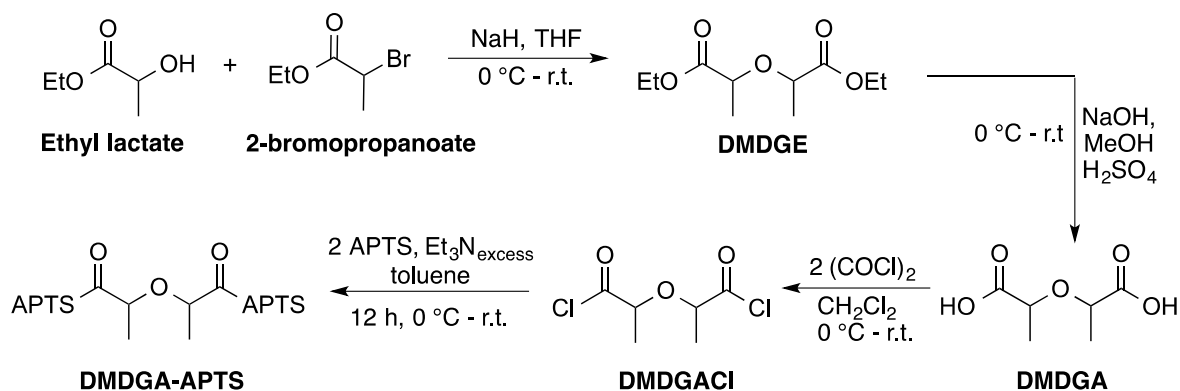
Scheme 7-3: Synthesis of DMDGA derivatives.

For synthesizing the corresponding acid chloride the **DMDGA-acid** was reacted with oxallyl chloride at room temperature with DMF as catalyst. The **DMDGA-Cl** was obtained as yellow oil in 64% yield after distillation of the reaction mixture. The product is sensitive to moisture and excessive heating. The next step, the modification with APTS was carried out by reacting 2 equivalents of **APTS** with 1 equivalent of **DMDGA-Cl** and excess of **NEt₃** (Scheme 7-3). The reaction was carried out at room temperature and the product was obtained as thick yellow oil after evaporating the filtrate of the reaction residue. Unlike FDGA, the purity of the product is highly dependent on the stoichiometry of the starting material. The product is difficult to purify if there is unreacted APTS in the system, as both the product and reactant have similar solubility. The modification of the ligand on both sides by APTS was confirmed by ^{1}H NMR spectroscopy, which showed a peak at δ 7.34 integrating for the two amide protons. The carbonyl peak in $^{13}C\{^1H\}$ NMR was also shifted form δ 166.1 for **DMDGA-Cl** to δ 174.0 for **DMDGA-APTS.**

The **DGA** ligand was also synthesized similarly from the commercially available diglycolic acid and oxallyl chloride. The **DGACl** obtained was modified with **APTS** by using the same protocol as for **DMDGA-APTS**. Both the **DGACl** and **DGA-APTS** were characterized by NMR spectroscopy and are given in the experimental section.

7.2.3 Synthesis of dioxaoctanediamide derivatives (**DOODA**)

Another type of ligand that we wanted to explore is the **DOODA** ligand. Like **DGA** it is also an ether-amide, but it has four coordinating atoms. The structural investigation of **DOODA** lanthanide complexes reveals that one or two molecules of **DOODA** bind to a lanthanide ion in a tetradentate-binding mode along with one or more solvent molecules. As compared to **DGA, DOODA** has a large bite angle since it has four coordinating atoms, and the terminal binding groups are separated by larger number of atoms in **DOODA** (8 atoms) than in **DGA** (5 atoms). However, **DOODA** has a tetradentate pocket, which brings the terminal carbonyl groups close to each other making a small complementary angle. As a result, of this small complementary angle and a tetradentate pocket, **DOODA** is expected to show more affinity for smaller lanthanides (Figure 7-3).
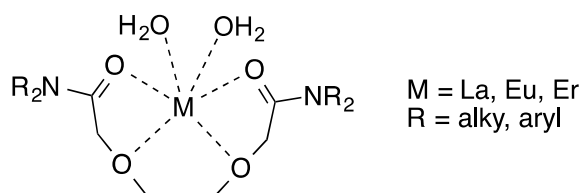
Figure 7-3: Tetradentate coordination mode of DOODA ligands.

DOODA has been initially used for extracting lanthanides in LLE, but it has not shown any appreciable selectivity. However, if **DOODA** is grafted on a solid support, its coordination pocket will become more rigid which can increase its selectivity towards smaller lanthanides.

The carboxylic acid and acid chloride of **DOODA** are not available commercially. So we started with the synthesis of 3,6-dioxaoctanedioic acid (**DOODA-acid**). It was synthesized by oxidizing triethylene glycol with concentrated nitric acid at 60 – 80 °C (Scheme 7-4). The progress of reaction was monitored by the evolution of orange fumes of NO_2 from the

reaction mixture. Once the evolution of orange fumes ceased, the reaction was heated for one hour at 80 °C to ensure complete conversion. The product was isolated from the reaction mixture as a light yellow oil, which solidified into a white solid in few days. The ^{1}H NMR shows peaks at δ 4.15, 3.73 for the CH$_2$ protons. ^{13}C{^{1}H} NMR consists of signals at δ 170.9 for the carbonyl carbon. The **DOODACl** was then synthesized by reacting **DOODA-acid** with SOCl$_2$ at room temperature. The reaction is exothermic and hence the addition of SOCl$_2$ was done at 0 °C and then the reaction was allowed to warm to room temperature. After reacting for 12 h the reaction mixture is evacuated to give a yellow oil. This oil was crystalized from a 1 : 1 solution of ether and pentane at -30 °C. The crystals were filtered at -30 °C and they melt at room temperature form oil. The **DOODACl** is very sensitive to moisture and heat. It decomposes into brown thick oil when heated above 50 °C.
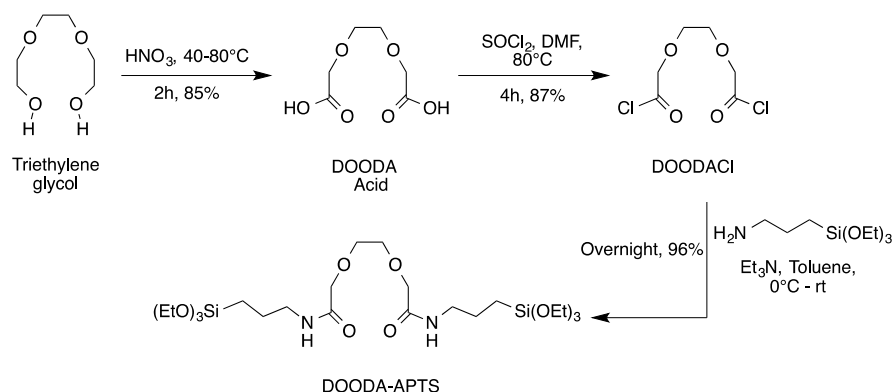
Scheme 7-4: Synthesis of DOODA-APTS from triethylene glycol.

The **DOODA-APTS** was then synthesized for **DOODACl** by following the same protocol as that of **DMDGA-APTS**. The product was isolated in 96% in the form of thick oil and was identified by NMR spectroscopy. The signal for the amide proton was observed at δ 6.61 in addition to other signals of **APTS** and **DOODA** backbone in ^{1}H NMR spectrum. The ^{13}C{^{1}H} NMR spectrum is also consistent with the other **APTS** derivatives.

For liquid-liquid extraction N,N-dioctyl-3,6-dioxaoctanediamide **(TODOODA)** was synthesized form **DOODACl** and N,N'-dioctylamine with excess of Et$_3$N in benzene. The reaction mixture was stirred overnight after which solvent and Et$_3$N was removed under vacuum and the residue was extracted with hexane to give pure **TODOODA** in 87% yield.
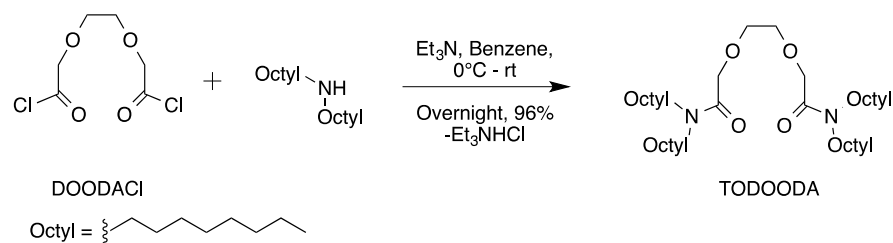
Scheme 7-5: Synthesis of TODOODA.

Another ligand that was designed for extracting smaller lanthanide was the dimethylmalonamide (**DMMA**). The malonyl chloride is commercially available and used to for **DMMA-APTS** by using the same protocol as mentioned for other **APTS** derivatives (Scheme 7-6). The malonylamide ligands have just one carbon atom between the amide carbonyls. This small *bite angle* of **DMMA** should make it selective for smaller lanthanide ions.
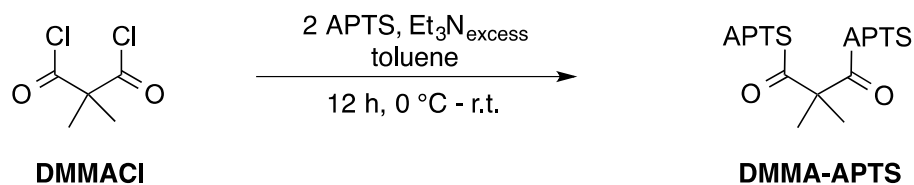
Scheme 7-6: Silanization of 2,2-dimethylmalonoylchloride.

The SPE and LLE of DOODA and FDGA ligand has been carried out and are discussed in the next section. However, DMDGA and DMMA have not been studied for their extraction properties yet.

7.3 Extraction results

The **DOODA-APTS** and **FDGA-APTS** were then grafted on KIT-6 support and were tested for SPE by the group of Kleitz while as **TODOODA** and **TOFDGA** were tested for LLE by group of Larivière. These extraction results have been taken from the paper that has been published in RSC Advances.

After grafting **DOODA-APTS** and **FDGA-APTS** on KIT-6, the resulting functionalized materials (**KIT-6-DOODA, KIT-6-FGDA**) were studied for the extraction of REEs from a mixture of lanthanides. The radioactive elements Uranium and Thorium and other metal

140

ions commonly found in industrial and mining wastes (i.e., Al^{3+}, Fe^{3+}) have also been looked at. The batch extraction results and the Kd values obtained for different metal ions are plotted in Figure 7-4. The results of SPE and LLE of the functionalized materials and free ligands are plotted against the DGA resin in-order to evaluate the efficiency of our system. The K_d values for **KIT-6-N-DGA** are also presented for comparing the results. The extraction results clearly showed that Kd values of all the functionalized materials are higher for lanthanides as compared to other ions commonly present in environmental and mining wastes. The radioactive uranium and thorium were found to have lower Kd values and are hence extracted less efficiently than rare earths. This selective extraction of REEs by these hybrid materials shows the benefits of chelating the ligands on the mesoporous materials.
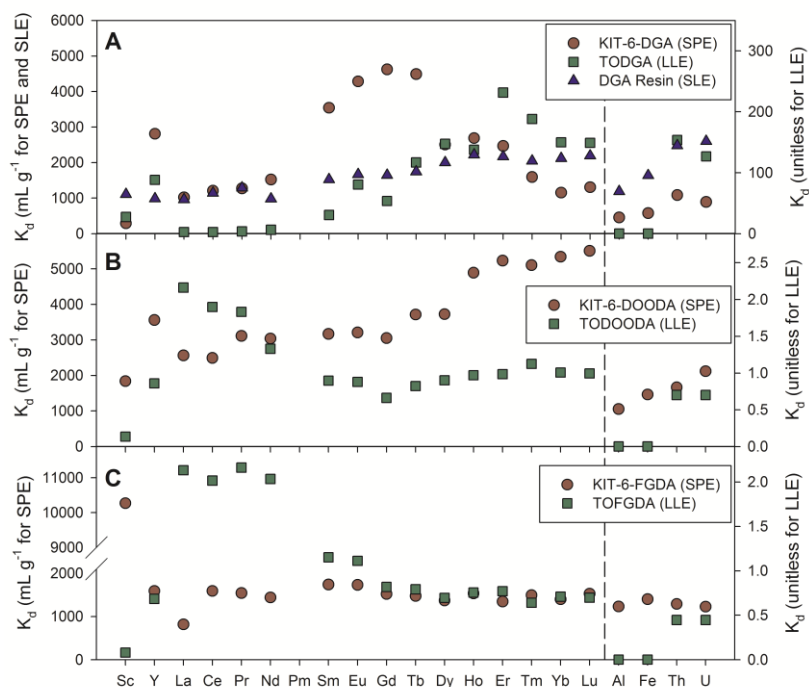
Figure 7-4: Plot of SLE and LLE of DGA, DOODA and FDGA. Distribution coefficient (Kd) values for functionalized hybrid materials (SPE; left scale) compared to LLE and SLE counterpart (right scale). The dashed line separates the REEs and other relevant elements.

The earlier results published by group Kleitz and Larivière showed that **KIT-6-DGA** was selective towards Eu^{3+}, Gd^{3+} and Tb^{3+}. The ionic radii of these mid-size lanthanide ions is 94.7, 93.8, and 92.3 pm, respectively. Interestingly, **KIT-6-DOODA** was found to selectively extract smaller lanthanides. The largest Kd values were highest for Ho, Er, Tm, Yb and Lu, having radii between 90.1 to 86.1 pm starting at 5100 mL.g^{-1}. This selectivity of **KIT-6-DOODA** for extracting smaller lanthanides is attributed to its smaller coordination pocket. Indeed, the tetradentate coordination mode of DOODA provides an appropriate *bite angle* for coordinating smaller lanthanides. It is interesting to note that these values differ greatly from liquid-liquid extractions, which is more selective for larger lanthanides, (Figure 7-4). It was also observed that the concentrations of HNO_3, water and of the ligand were found to affect this selectivity pattern. [14,243,257] Similar observation was found with the **TOFDGA** ligand (tetraoctyldiglycolamide) which shows higher selectivity for smaller lanthanides in LLE, but whereas the supported material was found to be more efficient for trapping middle lanthanides. The difference in the extracting properties of the ligands in SPE systems compared to liquid extraction can be attributed to the variable coordination sphere of the lanthanide ions in solution and of the ligand binding them. In LLE, the lanthanide ions can bind three to four ligand molecules to form complexes and in addition to interact with water and nitrate ions (NO_3^-). Since the smaller lanthanides have a smaller coordination sphere, they will prefer interacting with a smaller number of water molecules since they have a smaller hydration energy, which will consequently lead to being extracted more efficiently in non-polar solvents. The larger lanthanides, on the other hand, have a higher hydration energy and will have lower Kd values in non polar-solvents.[14–16] In the SPE systems, the ligands are immobilized on a solid surface and the metal ions have a lower number of chelating ligands to coordinate to. Thus, only the metal ions having an appropriate radius for the pocket created by the ligand chelation with be trapped by the materials, where the other metal ions will be easily washed off. This difference in the extraction properties of **DOODA** and **DGA** ligands in SPE and LLE is attributed to the decrease in the flexibility of the coordinating carbonyl groups due to the chemical anchoring of the ligand on the solid surface that adds to its rigidity.

It is seen that in LLE, the **TOFDGA** exhibits higher Kd values for larger lanthanides while smaller lanthanides have lower values. This is surprising since FDGA was designed to have a larger bite angle and exhibit selectivity towards larger lanthanides. Interestingly, the Kd values for Sc^{3+}were shown to be surprisingly high, of about 11 000 $mL.g^{-1}$ (Figure 7-4). This selectivity of **KIT-6-FDGA** is quite unexpected as scandium has an ionic radius of 74.5 pm, which is much less than the smallest lanthanide ion. This unexpected selectivity needs to be explored further.

7.4 Conclusions

In summary, by a careful tuning of the *bite angle* of chelating ligands and by imparting rigidity to the ligands on a surface, a more selective extraction of lanthanides can be achieved. The DOODA ligand grafted on mesoporous silica (KIT-6) has a smaller *complementary angle* than the *bite angle* of DGA ligand and shows preference for extracting smaller lanthanides (Ho-Lu). Interestingly, after immobilizing FDGA, exceedingly high K_d values were obtained for extracting Scandium from a mixture of REEs. The critical role of the support is discernible when comparing the extraction behavior of these ligands in LLE and the grafted systems.

7.5 Experimental

7.5.1 Ligands synthesis

General Procedures. All manipulations were carried out under an atmosphere of nitrogen using standard Schlenk techniques or in nitrogen filled gloveboxes, unless specified otherwise. The glassware was dried overnight prior to use. All solvents were dried prior to use. Benzene-d_6 was distilled under reduced pressure from a Na/K alloy. Chloroform-d and acetone were used as received. Triethylene glycol, 2,5-furandicarboxyllic acid, thionyl chloride (SOCl$_2$), oxallyl chloride (COCl)$_2$ and aminopropyltriethoxysilane (APTS), dimethyl malonoyl chloride were purchased from Sigma Aldrich and used without further purification. NMR spectra were recorded on an Agilent Technologies NMR spectrometer at 500 MHz (^{1}H), 125.758 MHz (^{13}C) and on a Varian Inova NMR AS400 spectrometer, at 400.0 MHz (^{1}H), 100.580 MHz (^{13}C). ^{1}H NMR and ^{13}C{^{1}H} NMR chemical shifts are referenced to residual solvent signals in deuterated solvent. Multiplicities are reported as singlet (s), doublet (d), triplet (t), quartet (q), multiplet (m) or broad (br). Chemical shifts are reported in ppm.

Synthesis of 2,5-furandioylchloride (FDGA-Cl). To 2.50 g (16.0 mmol) of 2,5-furandicarboxyllic acid was added 50 µl of DMF. 5 ml (8.19 g, 68.8 mmol) of SOCl$_2$ was added slowly to the acid mixture while stirring. The reaction was refluxed for 6 hr at 80 °C. The reaction was cooled down and put under vacuum for 1 h to remove excess of SOCl$_2$. A white crystalline solid was obtained. The solid was sublimated at 75 °C to give 2.74 g of product (yield = 89%). ^{1}H NMR *(benzene-d_6).* δ 6.22 (s, 2H, CH). ^{13}C{^{1}H} NMR *(benzene-d_6).* δ 155.4 (s, C=O), 148.7 (s, C-O), 122.7 (s, CH).

Synthesis of furan-2,4-diamido-propyltriethoxysilane (FDGA-APTS). 2.00 g (10.4 mmol) of **FDGACl** was dissolved in 25 ml of toluene and to the solution was slowly added a mixture of 5.07 ml (4.79 g, 21.8 mmol) of **APTS** and 14.37 ml (10.4 g, 103 mmol) of triethylamine in 20 ml of toluene. The reaction was put under reflux at 90 °C overnight. The reaction was cooled, filtered and the filtrate was evaporated and dried under vacuum to give 5.65 g of a white solid (yield = 96%). ^{1}H NMR *(benzene-d_6).* δ 7.26 (br, 2H, NH^{APTS}),

144

6.95 (s, 2H, CH), 3.74 (q, 12H, CH_2-O-$Si_{,}$APTS), 3.40 (q, 4H , CH_2-NHAPTS), 1.76 (m, 4H, CH_2-CH_2 APTS), 1.14 (t, 18H, CH_3APTS), 0.65 (t, 4H, CH_2-Si APTS). $^{13}C\{^1H\}$ NMR *(benzene-d_6)*. δ 158.1 (s, C=O), 149.4 (s, C-O), 114.9 (s, CH), 58.5 (s, CH_2-O-$Si_{,}$APTS), 42.0 (s, CH_2-NHAPTS), 23.8 (s, CH_2-CH_2 APTS), 18.5 (s, CH_3APTS), 8.3 (s, CH_2-Si APTS).

Synthesis of N,N-dioctylfuran-2,4-diamide (TOFDGA). 300 mg (1.55 mmol) of **FDGACl** in 10 ml of THF was added dropwise to a solution N,N-dioctylamine (1.17 ml, 0.937 g, 3.88 mmol) and triethylamine (2.15 ml, 1.56 g, 15.4 mmol) in 30 ml of THF at 0 °C. The reaction was allowed to warm to room temperature overnight. The reaction was evaporated and the residue was dissolved in 30 ml of dichloromethane and extracted with 3 X 20 ml of 5% HCl in water. The organic fraction was dried on $MgSO_4$, filtered and evaporated to give 845 mg of a yellow oil (yield = 90%). ^1H NMR *(chloroform-d)*. δ 6.93 (s, 2H, CH), 3.46 (br, 8H, CH_2-Noctyl), 1.60 (br, 8H, CH_2-CH_3octyl), 1.26 (s, 40H, CH_2octyl), 0.88 (t, 12H, CH_3octyl). $^{13}C\{^1H\}$ NMR *(chloroform-d)*. δ 159.6 (s, C=O), 148.6 (s, CH), 115.6 (s, CO), 46.7 (d, CH_2N), 31.7, 29.2, 27.5, 27.0, 26.7 (CH_2), 22.6 (s, CH_2- CH_3), 14.0 (s, CH_3).

Synthesis of 2,4-dimethyldiglycolic ester (DMDGE). 1.00 g (41.66 mmol) of NaH was suspended in 50 ml of THF and cooled to 0 °C. To it was added a solution of (±) ethyl lactate (4.10 g, 34.77 mmol) and 2-bromopropanoate (6.28 g, 34.77 mmol) in 25 ml of THF dropwise. The solution was reacted at 0 °C for 30 minutes and then refluxed for 2 h. The mixture was filtered, and the solvent was evaporated. The residue was dissolved in chloroform (50 ml) and the resulting solution was washed with 3 X 50 ml of 10% HCl solution in water, saturated $NaHCO_3$ solution (3 X 50 ml) and water (50 ml). The organic layer was dried over anhydrous MgSO4 and concentrated to give light yellow oil. Yield 5.28 g (69.58%).

^1H NMR *(chloroform-d)*. δ 4.18 (m, 4H, O-CH_2), 4.07 (m, 2H, O-CH), 1.45 (d, J = 6.9 Hz, 6H, CH_3), 1.27 (t, 6H, J = 7.8 Hz, CH_3CH_2). $^{13}C\{^1H\}$ NMR *(chloroform-d)*. δ 173.0 (s), 74.0(s), 60.9 (s), 18.7 (s), 14.2 (s)

Synthesis of 2,4-dimethyldiglycolic acid (DMDGA-acid). 0.70 g (35.82) of NaOH is dissolved in 100 ml of methanol and cooled to 0 °C. To it is added 4 g (18.32 mmol) of

DMDGE. The solution was warmed to room temperature and stirred overnight. The solvent was evaporated and the white powder obtained was dissolved in minimum amount of water. The solution was acidified with sulphuric acid and extracted with 3 x 50 ml of diethylether. The extract was concentrated to give the 2,2-dimethyldiglycolic acid, which was dried overnight under vacuum to give DMDGA-acid in 76% yield.

^{1}H NMR *(chloroform-d).* δ 4.20 (q, *J* = 6.9 Hz, 2H, O-CH), 1.52 (d, 6H, *J* = 7.0 Hz, CH$_3$CH$_2$). ^{13}C{^{1}H} NMR *(chloroform-d).* δ 178.5 (s), 73.72 (s), 18.5 (s).

Synthesis of 2,4-dimethyldiglycolyl chloride (DMDGA-Cl). DMDGA-acid (1.00 g, 6.16 mmol) is dissolved in 10 ml of CH$_2$Cl$_2$. 60 μL of DMF and excess of oxallyl chloride was added to it and the reaction was stirred overnight at room temperature. Solvant was removed under vacuum at 10 °C and excess of oxallyl chloride was removed by distillation at room temperature under vacuum to get the pure product. Yield = 64% mmol).

^{1}H NMR *(chloroform-d).* δ 4.61 (q, *J* = 7.1 Hz, 2H, O-CH), 1.60 (d, 6H, *J* = 6.8 Hz, CH$_3$CH$_2$). ^{13}C{^{1}H} NMR *(chloroform-d).* δ 166.1 (s), 67.4 (s), 15.78 (s).

Synthesis of APTS modified ligands. To a solution of 2 equivalent of **APTS** and 10 equivalent of Et$_3$N in 10 ml of toluene at 0 °C was added a solution of acid chloride in 5 ml of toluene. The reaction mixture was allowed to warm to room temperature and was stirred for 12 h. The precipitated Et$_3$NHCl was removed by filtration and the filtrate was evaporated under vacuum to give the product as yellow oil.

2,4-dimethyldiglycol-2,4-diamido-propyltriethoxysilane (DMDGA-APTS). DMDGACl (200 mg, 1.169 mmol), APTS (518.01 mg 2.339 mmol), Et$_3$N (3.2 ml, 23.39 mmol). Yield = 83.2%.

^{1}H NMR *(benzene-d$_6$).* δ 7.34 (br, 2H, NH^{APTS}), 4.17 (q, 2H, CH-O), 3.80 (q, 12H, CH$_2$-OSi^{APTS}), 3.39 (q, 4H , CH$_2$-NH^{APTS}), 1.65 (d, 6H, CH$_3$), 1.57 (m, 4H, CH$_2$-CH$_2$ ^{APTS}), 1.23 (t, 6H), 1.15 (t, 18H, CH$_3$^{APTS}), 0.75 (t, 4H, CH$_2$-Si ^{APTS}). ^{13}C{^{1}H} NMR *(benzene-d$_6$).* δ 174.0 (s, C=O), 75.8 (s, CH-O), 58.2 (s, CH$_2$-OSi^{APTS}), 41.8 (s, CH$_2$-NH^{APTS}), 22.7 (s, CH$_2$-CH$_2$ ^{APTS}), 20.6 (s, CH$_3$), 18.5 (s, CH$_3$^{APTS}), 8.3 (s, CH$_2$-Si ^{APTS}).

2,2-dimethylmalonyl-2,2-amido-propyltriethoxysilane (DMMA-APTS). 2,2-dimethylmalonylchloride (**DMMACl**) (1.00 g, 5.91 mmol), APTS (2.62 g 11.83 mmol), Et$_3$N (4.8 ml, 35.11 mmol). Yield = 86.4%.

^{1}H NMR *(benzene-d$_6$)*. δ 7.35 (br, 2H, NH^{APTS}), 3.69 (q, 12H, CH$_2$-OSi^{APTS}), 3.21 (q, 4H, CH$_2$-NH^{APTS}), 1.65 (m, 4H, CH$_2$-CH$_2$ ^{APTS}), 1.43 (s, 6H), 1.09 (t, 18H, CH$_3$^{APTS}), 0.57 (t, 4H, CH$_2$-Si ^{APTS}). ^{13}C{^{1}H} NMR *(benzene-d$_6$)*. δ 173.8 (s, C=O), 58.4 (s, CH$_2$-OSi^{APTS}), 49.7 (s), 42.6 (s, CH$_2$-NH^{APTS}), 24.2 (S), 23.4 (s, CH$_2$-CH$_2$ ^{APTS}), 18.5 (s, CH$_3$^{APTS}), 8.2 (s, CH$_2$-Si ^{APTS}).

Synthesis of diglycolyl chloride (DGACl). To 5.00 g (0.037 mol) of diglycolic acid was added 15 ml of CH$_2$Cl$_2$ and 40 μl of DMF. 17.4 ml (25.8 g, 0.200 mol) of C$_2$O$_2$Cl$_2$ was added slowly to the acid mixture while stirring in an ice bath. The reaction was allowed to warm up overnight. The reaction mixture was then distilled under nitrogen at 100 °C to distill off excess of C$_2$O$_2$Cl$_2$ and CH$_2$Cl$_2$. A yellow oil was recovered (5.5 g, yield = 88%). ^{1}H NMR *(benzene-d$_6$)*. δ 3.47 (s, 4H, CH$_2$-O). ^{13}C{^{1}H} NMR *(benzene-d$_6$)*. δ 170.5 (s, C=O), 74.7 (s, CH$_2$-O).

Synthesis of diglycol-2,4-diamido-propyltriethoxysilane (DGA-APTS). 600 mg (3.51 mmol) of **DGACl** was dissolved in 15 ml of toluene and was cooled down to 0 °C. To the solution was slowly added a mixture of 1.72 ml (1.63 g, 7.36 mmol) of **APTS** and 4.89 ml (3.55 g, 35.1 mmol) of triethylamine in 10 ml of toluene. The reaction was allowed to warm to room temperature overnight. The reaction was filtered and the filtrate was evaporated and dried under vacuum to give 1.37 g of a thick yellow oil (yield = 89%). ^{1}H NMR *(benzene-d$_6$)*. δ 7.52 (br, 2H, NH^{APTS}), 3.89 (4H, CH$_2$-O), 3.75 (q, 12H, CH$_2$-OSi^{APTS}), 3.31 (q, 4H, CH$_2$-NH^{APTS}), 1.75 (m, 4H, CH$_2$-CH$_2$ ^{APTS}), 1.15 (t, 18H, CH$_3$^{APTS}), 0.67 (t, 4H, CH$_2$-Si ^{APTS}). ^{13}C{^{1}H} NMR *(benzene-d$_6$)*. δ 169.0 (s, C=O), 71.6 (s, CH$_2$-O), 58.5 (s, CH$_2$-OSi^{APTS}), 41.8 (s, CH$_2$-NH^{APTS}), 23.6 (s, CH$_2$-CH$_2$ ^{APTS}), 18.5 (s, CH$_3$^{APTS}), 8.3 (s, CH$_2$-Si ^{APTS}).

Synthesis of 3, 6-dioxaoctanedioic acid (DOODA acid). 20 ml of HNO$_3$ was heated to 40 - 45 °C, under ambient atmosphere, and 7.00 g (0.046 mol) of triethylene glycol was added over 1 h. The temperature of the reaction was raised to 60 – 70 °C releasing orange fumes

in the process. After the addition is complete the reaction was cooled down to 40 - 45 °C then heated at 80 °C for 1 h. The acid formed was evacuated under vacuum for 1 h at 80 °C to get rid of all the nitrogen oxides. The light yellow oil formed solidified into a white sticky solid overnight (6.95 g, yield = 85%). ^{1}H NMR *(acetone-d₆)*. δ 4.15 (s, 4H, CH$_2$-C=O), 3.73 (s, 4H, CH$_2$-O). ^{13}C{^{1}H} NMR *(acetone-d₆)*. δ 170.9 (s, C=O), 70.4 (s, CH$_2$-C=O), 67.6 (s, CH$_2$-O).

Synthesis of 3, 6-dioxaoctanedioylchloride (DOODA-Cl). To 6.0 g (33.68 mmol) of 3, 6-dioxaoctanedioic acid was added 60 μl of DMF. 16 ml (26.2 g, 0.220 mol) of SOCl$_2$ was added slowly to the acid mixture while stirring. The reaction was refluxed for 4 h at 80 °C. The reaction was cooled down and put under vacuum for 1 h to remove the excess of SOCl$_2$. The yellow oil left behind was dissolved in 2 X 10 mL of benzene and filtered. The filtrate was evaporated to give a light yellow oil that was crystallized from a mixture of pentane and ether at -30 °C (6.30 g, yield = 87%). ^{1}H NMR *(benzene-d₆)*. δ 3.76 (s, 4H, CH$_2$-C=O), 3.09 (s, 4H, CH$_2$-O). ^{13}C{^{1}H} NMR *(benzene-d₆)*. δ 171.7 (s, C=O), 76.1 (s, CH$_2$-C=O), 70.9 (s, CH$_2$-O).

Synthesis of 3,6-dioxaoctanediamido-propyltriethoxysilane (DOODA-APTS). 2.00 g (9.30 mmol) of **DOODA-Cl** was dissolved in 25 ml of toluene and cooled down to 0 °C. To the solution was slowly added a mixture of 4.57 ml (4.32 g, 0.0195 mol) of APTS and 12.56 ml (9.10 g, 0.893 mol) of triethylamine in 20 ml of toluene. The reaction was allowed to warm to room temperature overnight. The reaction was filtered and the filtrate was evaporated and dried under vacuum to give 3.00 g of thick yellow oil (yield = 96%). ^{1}H NMR *(benzene-d₆)*. δ 6.61 (br, 2H, NH ^{APTS}), 3.77 (m, 16H, CH$_2$-O-Si^{APTS}, CH$_2$-C=O), 3.32 (q, 4H , CH$_2$-NH^{APTS}), 3.00 (s, 4H, CH$_2$-O), 1.72 (m, 4H, CH$_2$-CH$_2$ ^{APTS}), 1.16 (t, 18H, CH$_3$^{APTS}), 0.65 (t, 4H, CH$_2$-Si ^{APTS}). ^{13}C{^{1}H} NMR *(benzene-d₆)*. δ 168.6 (s, C=O), 71.1 (s, CH$_2$-C=O), 70.4 (s, CH$_2$-O), 58.5 (s, CH$_2$-O-Si,^{APTS}), 41.5 (s, CH$_2$-NH^{APTS}), 23.8 (s, CH$_2$-CH$_2$ ^{APTS}), 18.5 (s, CH$_3$^{APTS}), 8.2 (s, CH$_2$-Si ^{APTS}).

Synthesis of N,N-dioctyl-3,6-dioxaoctanediamide (TODOODA). 315 mg (1.46 mmoles) of **DOODACl** in 5 ml of benzene was added dropwise to a solution N,N-dioctylamine (840 mg, 1.05 ml, 3.48 mmol) and triethylamine (2.21 g, 3.04 ml, 21.8 mmol) in 30 ml of

benzene at 0 °C. The reaction was allowed to warm to room temperature overnight. The reaction was evaporated and then extracted with 3 X 10 ml of hexane. Evaporation of the hexane filtrate gave 802 mg of a yellow oil (yield = 87%). ^{1}H NMR *(chloroform-d)*. δ 4.20 (s, 4H, CH$_2$-C=O), 3.76 (s, 4H, CH$_2$-O), 3.23 (dt, 8H, CH$_2$-N ^{octyl}), 1.52 (br, 8H, CH$_2$-CH$_3^{octyl}$), 1.27 (S, 40H, CH$_2^{octyl}$), 0.87 (t, 12H, CH$_3^{octyl}$). ^{13}C{^{1}H} NMR *(chloroform-d)*. δ 168.5 (s, C=O), 77.1 (s, CH$_2$-C=O), 69.7 (s, CH$_2$-O), 45.7 (d, CH$_2$N), 31.7, 29.2, 28.8, 27.5, 26.9 (CH$_2$), 22.5 (s, CH$_2$- CH$_3$), 14.0 (s, CH$_3$).

7.6 Materials synthesis and modification

We are thankful to Dr. J. A. Florek, a postdoc working with professor F. Kleitz, professor D. Larivière, for performing the experiments of grafting of the APTS modified ligands on their solid supports, the characterization of the grafted materials and the extraction studies of the materials.

Chapter 8 - Conclusions and Perspectives

8.1 General conclusions

This dissertation describes the use of ligand design for exploring various magnetic properties and the extraction of lanthanides. The field of single molecule magnetism is very recent and still in its initial stage. A lot of research has been dedicated in finding the metal ions that have the best magnetic properties, but only recently have researchers beginning to understand the advantage of having the proper ligands and geometries to optimize the magnetic properties. We have tried to address this issue by designing mono-and dianionic boron heterocyclic ligands, which can be used to synthesize symmetric metal complexes that can provide new insights in various magnetic properties of these metal complexes. During our study we came across some unexpected reactivity that helped us to understand the various parameters that need to be optimized for achieving our goals.

In the beginning of the research program, we were more focused on studying the effect of boratabenzene ligands on the magnetic properties of transition metals. Our motivation towards this study was driven by the findings that for attaining higher blocking temperatures in molecular magnets, symmetric geometry and super-exchange between the metal centers of a complex are prerequisite. In order to attain both these parameters in our complexes, we decided to synthesize triple-decker complexes of lanthanides metals using boratabenzene as a bridging ligand. The choice of boratabenzene ligand was driven by two factors. The first is the aromatic nature of the ligand due to which it tends to form sandwich and triple-decker complex, which are very symmetric molecules. The second factor is the presence of low lying LUMO orbitals on boratabenzene which should give better accepting capabilities from metals than other carbocyclic ligands, and hence stronger overlap with metal orbitals and thus promote super-exchange when present at the bridging position.

Our initial study of the magnetic properties of the cobalt bisboratabenzene [Co(BBPh)$_2$] sandwich revealed that in sandwich geometries transition metals lose their orbital magnetic

moment and form low spin complexes, that do not behave as molecular magnets. This shifted our focus more towards lanthanides particularly to terbium and dysprosium, since these oblate ions have been reported to form high spin complexes in sandwich and triple-decker species with high unquenched orbital angular momentum. Attempts to obtain sandwich complexes of lanthanides with cyclooctatetraenyl (COT^{2-}) and boratabenzene ligands, analogous to (cyclooctatetraenyl)(cyclopentadienyl) lanthanide(III) (COTLnCp) complexes were not successful. The lower nucleophilicity of the boratabenzene ligand (LiBBPh) as compared to cyclopentadienyl (Cp^-) ion can account for its decreased reactivity towards (cyclooctatetraenyl) lanthanide chloride (COTLnCl) complexes, which exist as stable dimers. Thus, we tried to synthesize them by first coordinating one phenyl boratabenzene ligand to LnI_3 salts to form $(BBPh)LnI_2$ complexes and then substituting the other two halides with the more nucleophilic COT^{2-} ligands. We used the diamagnetic lanthanum ion for our initial study, since its reactivity can be monitored using NMR spectroscopy and then extended to other lanthanides. However, the tendency of lanthanides to undergo ligand redistribution resulted in the isolation of a tris(boratabenzene) lanthanum complex $[La(BBPh)_3(I)]Li$. These types of boratabenzene complexes with lanthanides are rare and are analogous to well known tris(cyclopentadienyl)lanthanide ($LnCp_3$) complexes.

In addition to the synthesis of sandwich complexes of lanthanides, we were also interested in synthesizing and characterizing the bis(boratabenzene) lanthanide halide complexes $(BBPh)_2LnCl$ that usually exist as bridged dimers. The replacement of the halide bridge by an aromatic radical bridge was one of our objectives to enhance super-exchange between the metal centers. However, with the small phenyl boratabenzene (LiBBPh) ligand we got complexes that were very insoluble and hence could not be characterized. The insolubility of these complexes was attributed to the formation of multimetallic or polymeric structures because of halide bridging. This type of bridging has also been seen in analogous dicyclopentadienyl lanthanide chloride (Cp_2LnCl) complexes. We then decided to synthesize a bulky boratabenzene ligand that provides steric hindrance in order to form the desired bridged structures. Work in this direction led to the synthesis of a new bulky mesitylboratabenzene ligand.

152

During the synthesis and characterization of bulky 1-mesityl-4-isopropylboratabenzene salt, we were able to observe and isolate two isomers of 1-mesityl-4-isopropylboracyclohexadiene, which are the intermediates formed during the aromatisation of boracycles. We also observed that 1-mesityl-4-isopropylboracyclohexa-2,5-diene could be isomerized to 1-mesityl-4-isopropylboracyclohexa-3,5-diene with the addition of a catalytic amounts of base. Another important property of these mesityl boracycles is their stability towards the hydrolysis of the boron center because of the steric protection by the bulky mesityl groups. Although these 1-mesityl-4-isopropylboratabenzene ligands coordinated well to transition metals, their coordination to lanthanides was very challenging. The bulky nature of the ligand made it difficult for the large lanthanide ions to coordinate to their π-electron cloud.

The tendency of the bulky mesityl groups to hinder coordination of lanthanide ions to the π-electron cloud was also observed with 9,10-dimesityldiboraanthracene ligand. However, the replacement of the mesityl group by a small methyl group allowed for the successful coordination of this dianionic boron heterocycle to lanthanum. However, it was observed that 9,10-dimethyldiboraanthracene (DMDBA) ligand has an increased tendency to act as a bridging ligand and stack the lanthanide atoms. This stacking behavior resulted in the formation of a rare inverse sandwich complex $[La_2I_4(DMDBA)]$. The formation of a triple-decker as well as sandwich complexes of lanthanum with 9,10-dimethyldiboraanthracene was also observed. Although NMR characterization of these complexes was achieved, it was challenging to grow the crystals of these complexes due to their sensitivity towards temperature and traces of moisture and oxygen. As a result the analogous complexes of dysprosium and erbium have not been fully characterized yet. This dianionic boron heterocycle was developed to study the effect of low lying LUMO of diboraanthracene ligands on the magnetic relaxation and exchange interaction of the lanthanide complexes in comparison to their COT_2Ln and COT_3Ln_2 analogues. It was observed that although being dianionic and aromatic like COT^{2-}, the reactivity of 9,10-dimethyldiboraanthracene is different from it. Indeed, 9,10-dimethyldiboraanthracene was found to have increased tendency to form triple-decker complexes.

Finally, the concept of this ligand design was further extended to the selective recovery of lanthanides from different mining and industrial wastes. The slight differences in the ionic radii of lanthanides were used as the basis for designing ligands with different *bite angles* that are selective towards the extraction of different lanthanide ions. Two new ligands 2,5-dioxaoctanediamide (DOODA) and furan-2,5-diglycolamide (FDGA) were synthesized and immobilized on the mesoporous KIT-6 support. The immobilization was found to provide rigidity to the ligand thus making the bite angle more pronounced and more selective than in liquid-liquid extraction. Thus, in solid-liquid extraction, DOODA, which has the smallest bite-angle was found to be more selective towards smaller lanthanides (Ho − Lu) while as FDGA with the largest bite angle was surprisingly found to extract the smallest rare earth element (Sc). The extraction coefficient and reusability of the system surpasses all available industrial techniques. It thus provides a greener approach for the selective extraction of lanthanides.

Although we have not yet been able to characterize the real impact of our ligands on the magnetic properties of lanthanides, our study in this direction has provided us a great deal of information about the reactivity of lanthanides and our boron heterocyclic ligands. Initially the boron heterocyclic ligands were considered to be electron deficient and hence their coordination to electron poor metals was considered to be difficult. That is why most of the boratabenzene ligands coordinated to lanthanides had amide or phosphide substituents on boron atom, which are electron-donating. However, during our study we have seen that the coordination of these boron heterocycles to lanthanides is thermodynamically favored and they can coordinate to lanthanides at room temperature. The lanthanide precursors used plays a very important role in coordination. The solvated trihalides show very good reactivity when compared to the non-solvated salts. Boron heterocycles with simple electron deficient phenyl and methyl groups have been coordinated successfully.

The slight differences in ionic radii and the oxophilic nature of lanthanide ions have also been used previously for selective extraction of lanthanides. This is evident from the family of carbonyl ligands that are being used commercially for rare earth extraction. But the chemical anchoring of these carbonyl ligands provides rigidity to the coordination sites and

makes them more selective as compared to their free and more flexible coordination in liquid-liquid systems. In other words, we can say that the silica support acts a giant ligand, which helps to conserve the specificity of the coordination site of the molecule.

8.2 Ongoing and Future Work

There are many aspects of the project that should be explored and will be discussed under the following headings.

8.2.1 Boratabenzene lanthanide complexes

The isolation of a trisboratabenzene lanthanum complex has provided another proof of the analogy of boratabenzene with the cyclopentadienyl ions. It would be interesting to study if like cyclopentadienyl, boratabenzene also generates a new family of trisboratabenzene complexes with all other lanthanides. Apart from being a new addition to the organometallic chemistry of lanthanides, these complexes could exhibit very interesting properties. Long and coworkers have carried out the reduction of $LnCp_3$ complexes to access the +2 oxidation state of lanthanide ions. The study of these complexes shows that during reduction of the complexes, the electron goes into the $5d$ orbital of the lanthanide ions, thus adding one more unpaired electron to the system along with an orbital angular momentum of 2 for the d-orbital. This helped in attaining highest magnetic moments of 11 BM for a single metal ion. It would be interesting to carry out similar reduction chemistry with the tris(boratabenzene) lanthanide complexes. Due to the low energy LUMO of boratabenzene and π-acidity of the boron atom, the reduction in these complexes is expected to be more favored than with the cyclopentadienyl analogues. Thus it would be very interesting to study the redox reactions of these complexes by cyclic voltammetry in order to know how many reductions and oxidations of the metal center can be achieved. Another property of boratabenzene that has been studied very well for transition metals is the UV absorption and fluorescence spectroscopy. The introduction of boratabenzene has been found to increase the electron accepting properties of metal complexes, thus making them important candidates for redox-switched NLO (non-linear optical) chromophores. It

would be very interesting to observe the effect of boratabenzene on the fine emission spectra of lanthanides and analyze their tendency to form redox-switched NLO molecules.

Another type of boratabenzene lanthanide complexes that needs to be studied are the (COT)Ln(BBPh) type of sandwich molecules. These complexes will provide very important information about the effect of Lewis acidic boron center on the magnetic properties of lanthanides by comparing them to analogous (COT)Ln(Cp) complexes. The shape of the hysteresis curves and the relaxation patterns will provide ample information in this case. In addition, the replacement of cyclopentadienyl ion by phenyl boratabenzene in these complexes will decrease their symmetry from C_5 to C_1. This reduction of symmetry will greatly affect the anisotropy of the molecule and the energy differences between various excited states. Thus, it will provide significant information that will be helpful in optimizing various ligand parameters for obtaining efficient molecular magnets.

8.2.2 Boraanthracene lanthanide complexes

During our study, we were able to observe the formation of triple-decker complexes of lanthanum, dysprosium and erbium with 9,10-dimethyldiboraanthracene ligand. Efforts are currently directed in obtaining the crystal structures of these molecules in order to confirm their identity, which is very important for studying their magnetic properties. We are also working on optimizing the reaction conditions for obtaining exclusively either the sandwich or the triple-decker complexes. It is very important to explore the magnetic properties of these sandwich complexes. A comparison of the magnetic behavior of these sandwich complexes with the triple-decker complexes will provide important information about the extent to which the diboraanthracene ligand promotes the super-exchange between the lanthanide atoms in a triple-decker complex.

Apart from synthesizing the sandwich and triple-decker complexes of oblate ions such as Tb, Dy, Ho and Nd, it would be interesting to form similar complexes with prolate ions like Er, Sm and Eu. There are two reasons that explain the importance of this study. The first reason is the shape of 9,10-dimethyldiboraanthracene molecule. It is not highly symmetrical like COT^{2-} ion. It has a C_2 axis of symmetry (Figure 8-1A) and the presence of

two boron atoms on opposite side of the framework introduces two lateral axes of anisotropy in the ligand.
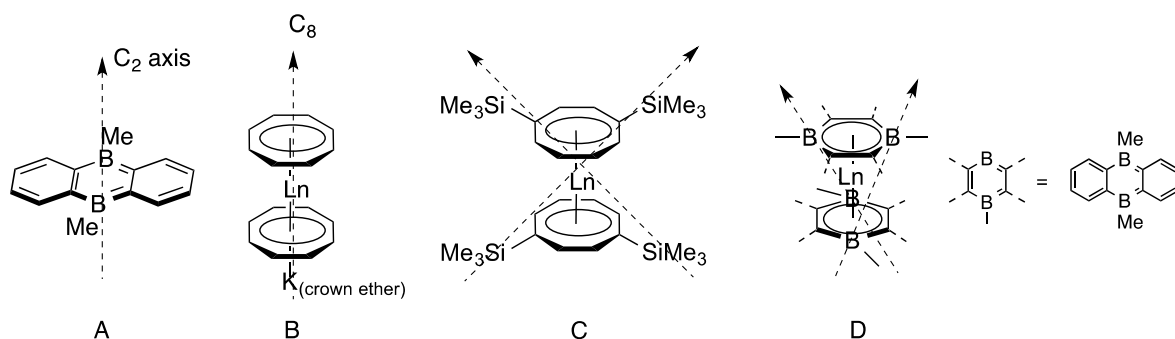
Figure 8-1: Representation of the symmetry axis of A) DMDBA B) COT$_2$Ln C) COT*$_2$Ln sandwich D) (DMDBA)$_2$Ln.

These lateral axes can have a positive effect on increasing the relaxation barrier of the prolate ions (Figure 8-1D). This type of effect has been observed in the case of COT* [1,4-bis(trimethylsilyl)cyclooctatetraenyl] complexes of erbium (Er(COT*)$_2$) (Figure 8-1C). The second reason of interest is the energy of the excited state that participates in the relaxation process through quantum tunneling, which in turn is governed by the contribution of axial and transverse components of anisotropy to this energy level. Although the oblate Dy^{3+} ion forms a symmetric sandwich in Dy(COT)$_2$ complex, which gives it a high spin orbit coupled ground state and hence high magnetic moment but the Er(COT)$_2$ which possess a prolate ion has a higher blocking temperature than dysprosium. The study of the two ions shows that for erbium the magnetic relaxation occurs by quantum tunneling through the second excited state (Orbrach process), which has a larger energy difference with the ground state. The ground state and the first excited state do not participate in quantum tunneling because they have negligible contribution from transverse anisotropies. But in the case of the dysprosium complex, the relaxation occurs by quantum tunneling through first excited state and the ground state that are lower in energy and have significant contributions from transverse anisotropies. These studies exhibit the complexity shown by these systems and prove that there are still a lot of parameters that needs to be investigated. Attaining a high value ground state is not the only thing we have to look for since identifying the energy levels that actively participates in the relaxation phenomenon are important parameters that need to be optimized. By maintaining the high symmetry of the

molecules and by being flexible in the different coordination geometries of these lanthanide ions, a lot of knowledge can be obtained about the important parameters for optimal materials.

8.2.3 Design of new ligands

In addition to the boratabenzene and diboraanthracene ligands, there are other boron heterocycles that can play a very important role in understanding and optimizing the magnetic properties of lanthanides. One such ligand is the seven membered tropylium analogues known as borepin. There are both monocyclic and polycyclic derivatives of borepins reported in the literature (Figure 8-2 A). It is a neutral aromatic ligand. However it will be interesting to carry out one electron reduction of borepin, which will result in the formation of an antiaromatic radical. This radical can be then used as a bridging ligand between two lanthanide ions for promoting super-exchange. One such structure that is in our interests is shown in Figure 8-2 A where we have two terminal boratabenzene ligands and a bridging borepin ligand.
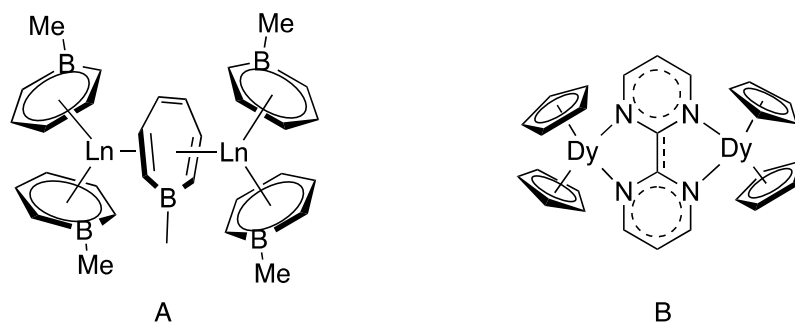
Figure 8-2: Representation of A) Borepin and B) Bipyrimidil bridged lanthanide complexes.

This type of geometry will be favorable for the prolate ions where equatorial distribution of ligand electron density will be favorable for maximizing anisotropy. In addition, the presence of a radical between two lanthanide ions will couple their magnetic moment and decrease quantum tunneling, which has been seen in $\{(Me_3Si)_2Ln(THF)_2\}_2(\mu-\eta^2:\eta^2-N_2)^-$ complex of Dy and Tb. Rinehart has tried to synthesize similar complexes with terminal cyclopentadienyl ligands and bridging radical ligands that are mostly bipyimidal and benzotriazolate derivatives and has achieved success to some extent (Figure 8-2 B).

158

However, with borepin as bridging ligand the radical ligand will lie parallel to the plane of boratabenzene ligands, which will be different from the bipyrimidal ligands that are perpendicular to the Cp planes. Moreover, borepin will have no atom directly lying on the symmetry axis of the metal and will hence enhance its axial symmetry. The boratabenzene ligands in these complexes can be replaced by other bulky mono anionic ligands so as to investigate the structural effects of the terminal ligands on the properties of these boron-bridged complexes.

In addition to the mono radical borepin, the diradical of diboraanthracene should also be used as bridging ligand in these complexes. This will help in investigating if the interaction between the metal centers through these mono and diradicals is ferromagnetic or antiferromagnetic and hence the effect of such interactions on the relaxation behaviors can be studied. A study of redox chemistry of these complexes will be a very important addition to this field of study. All these boron heterocycles are very good luminophores. Thus it would be always interesting to study the optical properties of these complexes.

8.2.4 Derivatization of DOODA and DGA

In our study of the development of ligands for selective extraction of lanthanides, we have seen that two types of ligands, DGA (Diglycolamide) and DOODA (2,5-dioxaoctanediamide), have very high extraction coefficients for specific lanthanide ions. Besides being selective, they do not bind these lanthanide ions too strongly and hence the extracted ions can easily be recovered from the system by washing the material with oxalate solutions. Thus it will be interesting to play with the bite angle of these two ligands so as to develop a series of ligands with selectivity towards different lanthanides.

The DGA ligand has been found to be selective for Eu, Gd and Tb. So in order to change its selectivity towards smaller lanthanides, the bite angle of the ligand should be decreased. This can be achieved by modifying the back bone of the ligand. One of the ways to do such modification is to add substituents on the α-carbon atom of the ether oxygen. By introducing alkyl and aryl groups like methyl, isopropyl and phenyl, the bite angle of the ligand can be gradually decreased with increasing size of the substituents (Figure 8-3). A study of the extraction using such ligands will help in predicting the effect of the bite angle

on the selectivity. This will give a clearer picture of the different combinations of alky and aryl groups that can be used to achieve a particular bite angle and hence increase selectivity. Similarly, in order to shift the selectivity of the DGA ligand towards larger lanthanides, the bite angle of the ligand will need to be increased in size. During our study we tried to increase the bite angle by introducing a five-membered ring into the DGA back bone. This new ligand with lager bite angle (FDGA – Furan-2,5-diglycolamide) was unexpectedly found to extract scandium. IR studies of the material suggested that scandium binds to the nitrogen and oxygen of the amide fragment. Thus suggesting that the bite angle of FDGA is too large to trap any of the lanthanide ions. Therefore, focus should be shifted to substituents that can provide a smaller bite angle than this. Instead of using unsaturated five and six-membered rings, that are more rigid, it will be interesting to use saturated five and six membered rings that are more flexible and hence will not give too large bite angle. Two such molecules are the tetrahydrofuran and tetrahydropyran (Figure 8-3). Another way to increase the bite angle of DGA molecule will be the increase in the size of the chain. By introducing one two or more carbon atoms in the DGA chain the bite-angle can be increased.

R = Me, *i*Pr, Ph, Cy...
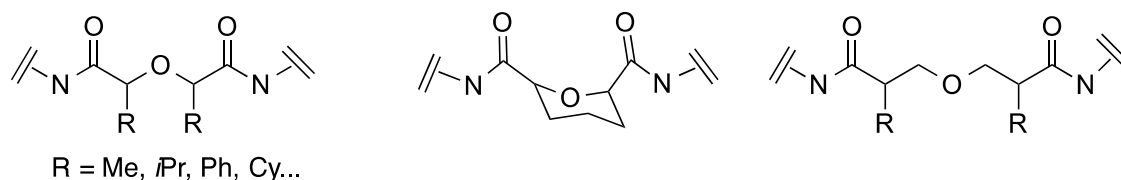
Figure 8-3: Representation of different derivatives of DGA.

DOODA with a tetradentate pocket has been found to be more selective towards smaller lanthanides such as Ho, Er, Tm, Yb and Lu. To modulate the selectivity of the 2,5-dioxaoctaneamide ligand to different lanthanide ions, various modifications can be brought out in the backbone of the ligand to increase or decrease the size of the pocket an hence the bite angle. In order to decrease the size of the pocket a phenyl or cyclopentadienyl backbone can be used. By being more rigid, a decrease inflexibility of coordination sites will be observed and that could fine tune their selectivity and make them more selective towards the smallest Yb and Lu ions and less selective to Ho and Er. Similarly, the

introduction of alkyl and aryl substituents in the backbone will modulate the size of the coordination pocket.

R = Alkyl or Aryl
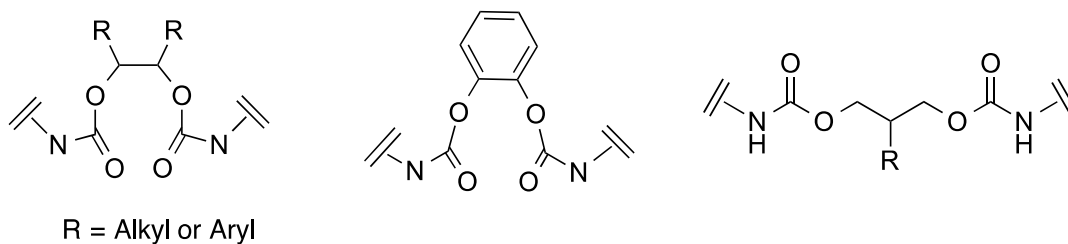
Figure 8-4: Representation of various derivatives of DOODA.

In order to increase the size of the pocket for extracting larger lanthanides, longer chains could be used.

Chapter 9 - Bibliography

(1)   Moeller, T. *The Chemistry of the Lanthanides*; Reinhold Publishing Corporation: New York, 1965.

(2)   Kaltsoyannis, N.; Scott, P. *The f-Elements*; Oxford University Press, New York, 1999.

(3)   Falconnet, P. *J. Alloy. Comp.* **1993**, *192*, 114–117.

(4)   Cotton, S. *Lanthanide and Actinide Chemistry*; John Wiley & Sons, Ltd: West Sussex, 2006.

(5)   O'Laughlin, J. W. *In Handbook on the Physics and Chemistry of Rare Earths.;* Karl A. Gschneidner, Jr., LeRoy, E., E. ., Ed.; Elsevier, 1979.

(6)   Reddy, M. L. P.; Rao, P.; Damodarm, A. D. *Miner. Process. Extr. Met. Rev.* **1995**, *12*, 91–113.

(7)   Zhu, T. *Hydrometallurgy* **1991**, *27*, 231–245.

(8)   Li, W.; Wang, X.; Zhang, H.; Meng, S.; Li, D. *J. Chem. Technol. Biotechnol.* **2007**, *82*, 376–381.

(9)   Huheey, J. E.; Keiter, E. A.; Keiter, R. L. *Inorganic Chemistry (principale of structure and reactivity)*, Fourth Edi.; Pearson Education (Singapore) Pte. Ltd., Indian Branch, 2002.

(10)   Singh, D. K.; Sing, H.; Mathur, J. N. *Hydrometallurgy* **2006**, *81*, 174–181.

(11)   Wang, Y. C.; Yue, S. T.; Li, D. Q.; Li, C. Z. *Solvent Extr. Ion Exch.* **2002**, *20*, 701–706.

(12)   Rabie, K. A. *Hydrometallurgy* **2007**, *85*, 81–86.

(13)   Xie, F.; Zhang, T. A.; Dreisinger, D.; Doyle, F. *J. Min. Eng.* **2014**, *56*, 10–28.

(14)   Narita, H.; Yaita, T.; Tachimori, S. *Solvent Extr. Ion Exch.* **2004**, *22*, 135–145.

(15)   Mohamed, E. A.; Mowafy, D. *Sep. Puri. Technol.* **2014**, *128*, 18–24.

(16)   Nave, S.; Modolo, G.; Madic, C.; Testard, F. *Solvent Extr. Ion Exch.* **2004**, *22*, 527–551.

(17)   Huang, C. *Rare Earth Coordination Chemistry Fundamentalsand Applications*; Chun-Hui Huang, Ed.; John Wiley & Sons, (Asia) Pte Ltd, 2009.

(18)   Evans, D. F. *J. Chem. S* **1959**, 2003–2005.

(19)   Ghimire, N.; Dagotto, E.; State, S.; Ii, P.; March, K. *Solid State Phys.* **2010**, 1–13.

(20) Rinehart, J. D.; Long, J. R. *Chem. Sci.* **2011**, *2*, 2078–2085.

(21) Ishikawa, N.; Sugita, M.; Ishikawa, T.; Koshihara, S. Y.; Kaizu, Y. *J. Am. Chem. Soc.* **2003**, *125*, 8694–8695.

(22) Layfield, R. A. *Organometallics* **2014**, *33*, 1084–1099.

(23) Meihaus, K. R.; Long, J. R. *J. Am. Chem. Soc.* **2013**, *135*, 17952–17957.

(24) Le Roy, J. J.; Ungur, L.; Korobkov, I.; Chibotaru, L. F.; Murugesu, M. *J. Am. Chem. Soc.* **2014**, *136*, 8003–8010.

(25) Rinehart, J. D.; Fang, M.; Evans, W. J.; Long, J. R. *Nat. Chem.* **2011**, *3*, 538–542.

(26) Rinehart, J. D.; Fang, M.; Evans, W. J.; Long, J. R. *J. Am. Chem. Soc.* **2011**, *133*, 14236–14239.

(27) Birmingham, J. M.; Wilkinson, G. *J. Am. Chem. Soc.* **1956**, *78*, 42–44.

(28) Edelmann, F. T. *Angew. Chem., Int. Ed.* **1995**, *34*, 2466–2488.

(29) Edelmann, F. T. *Coord. Chem. Rev.* **2014**, *261*, 73–155.

(30) Edelmann, F. T.; Freckmann, D. M. M.; Schumann, H. *Chem. Rev.* **2002**, *102*, 1851–1896.

(31) Schumann, H.; Meese-Marktscheffel, J. A.; Esser, L. *Chem. Rev.* **1995**, *95*, 865–986.

(32) Edelmann, F. T. *New J. Chem.* **2011**, *35*, 517–528.

(33) Kilimann, U.; Herbst-Irmer, R.; Stalke, D.; Edelmann, F. T. *Angew. Chem., Int. Ed.* **1994**, *33*, 1618–1621.

(34) Wetzel, T. G.; Dehnen, S.; Roesky, P. W. *Organometallics* **1999**, *18*, 3835–3842.

(35) Wilkinson, G.; Birmingham, J. M. *J. Am. Chem. Soc.* **1954**, *76*, 6210–6210.

(36) Maginn, R. E.; Manastyrskyj, S.; Dubeck, M. *J. Am. Chem. Soc.* **1963**, *85*, 672–676.

(37) Dornberger, E.; Klenze, R.; Kanellakopulos, B. *Inorg. Nucl. Chem. Lett.* **1978**, *14*, 319–324.

(38) Pappalardo, R. *J. Mol. Spectrosc.* **1969**, *29*, 13–36.

(39) Lamberts, W.; Lueken, H.; Hessner, B. *Inorganica Chim. Acta* **1987**, *134*, 155–157.

(40) Lueken, H.; Schmitz, J.; Lamberts, W.; Hannibal, P.; Handrick, K. *Inorganica Chim. Acta* **1989**, *156*, 119–124.

(41) B. Lobkovskii, E.; L. Soloveichik, G.; B. Erofeev, A.; M. Bulychev, B.; K. Bel'skii, V. *J. Organomet. Chem.* **1982**, *235*, 151–159.

(42) Lamberts, W.; Lueken, H.; Elsenhans, U. *Inorganica Chim. Acta* **1986**, *121*, 81–87.

(43) Deacon, G. B.; Wilkinson, D. L. *Inorganica Chim. Acta* **1988**, *142*, 155–159.

164

(44) Burns, C. J.; Anderson, R. A. *J. Chem. Soc. Chem. Commun.* **1989**, 136–137.

(45) Burns, C. J.; Berg, D. J.; Andersen, R. A. *J. Chem. Soc. Chem. Commun.* **1987**, 272–273.

(46) Paolucci, G.; D'Ippolito, R.; Ye, C.; Qian, C.; Gräper, J.; Fischer, D. R. *J. Organomet. Chem.* **1994**, *471*, 97–104.

(47) Sulway, S. A.; Layfield, R. A.; Tuna, F.; Wernsdorfer, W.; Winpenny, R. E. P. *Chem. Commun.* **2012**, *48*, 1508–1510.

(48) Layfield, R. A.; McDouall, J. W.; Sulway, S. A.; Tuna, F.; Collison, D.; Winpenny, R. E. P. *Chem.–Eur. J.* **2010**, *16*, 4442.

(49) Rinehart, J. D.; Fang, M.; Evans, W. J.; Long, J. *Nat. Chem.* **2011**, *3*, 538–542.

(50) Meihaus, K. R.; Fieser, M. E.; Corbey, J. F.; Evans, W. J.; Long, J. R. *J. Am. Chem. Soc.* **2015**, *137*, 9855–9860.

(51) Streitwieser, A.; Jr, N. *J. Am. Chem. Soc.* **1968**, *90*, 7364–7364.

(52) Hodgson, K. O.; Mares, F.; Starks, D.; Streitwieser, A. *J. Am. Chem. Soc.* **1973**, *95*, 8650–8658.

(53) Mares, F.; Hodgson, K. O.; Streitwieser, A. *J. Organomet. Chem.* **1970**, *24*, C68–C70.

(54) Hayes, R. G.; Thomas, J. L. *J. Am. Chem. Soc.* **1969**, *91*, 6876–6876.

(55) Kilimann, U.; Schäfer, M.; Herbst-Irmer, R.; Edelmann, F. T. *J. Organomet. Chem.* **1994**, *469*, C15–C18.

(56) Xia, J.; Jin, Z.; Chen, W. *J. Chem. Soc., Chem. Commun.* **1991**, 1214–1215.

(57) Hodgson, K. O.; Raymond, K. N. *Inorg. Chem.* **1972**, *11*, 3030–3035.

(58) Boussie, T. R.; Eisenberg, D. C.; Rigsbee, J.; Streitwieser, A.; Zalkin, A. *Organometallics* **1991**, *10*, 1922–1928.

(59) Jamerson, J. D.; Masino, A. P.; Takats, J. *J. Organomet. Chem.* **1974**, *65*, C33–C36.

(60) Sieler, J.; Simon, A.; Peters, K.; Taube, R.; Geitner, M. *J. Organomet. Chem.* **1989**, *362*, 297–303.

(61) Westerhof, A.; de Liefde Meijer, H. J. *J. Organomet. Chem.* **1978**, *144*, 61–64.

(62) Jiang, S.-D.; Wang, B.-W.; Sun, H.-L.; Wang, Z.-M.; Gao, S. *J. Am. Chem. Soc.* **2011**, *133*, 4730–4733.

(63) Schumann, H.; Winterfeld, J.; Köhn, R. D.; Esser, L.; Dietrich, A.; Sun, J. *Chem. Ber.* **1993**, *126*, 907–912.

(64) Schumann, H.; Janiak, C.; Köhn, R. D.; Loebel, J.; Dietrich, A. *J. Organomet. Chem.* **1989**, *365*, 137–150.

(65) Deacon, G. B.; MacKinnon, P.; Dickson, R. S.; Pain, G. N.; West, B. O. *Appl. Organomet. Chem.* **1990**, *4*, 439–449.

(66) Schumann, H.; Meesemarktscheffel, J. A.; Esser, L. *Chem. Rev.* **1995**, *95*, 865–986.

(67) Uwai, K.; Nakagome, H.; Takahei, K. *Appl. Phys. Lett.* **1987**, *50*, 977–979.

(68) Nakagome, H.; Uwai, K.; Takahei, K. *Appl. Phys. Lett.* **1988**, *53*, 1726–1728.

(69) Weber, J.; Molassioti, A.; Moser, M.; Stapor, A.; Scholz, F.; Hörcher, G.; Forchel, A.; Hammel, A.; Laube, G.; Weidlein, J. *Appl. Phys. Lett.* **1988**, *53*, 2525–2527.

(70) Visseaux, M.; Dormond, A.; Kubicki, M. M.; Moïse, C.; Baudry, D.; Ephritikhine, M. *J. Organomet. Chem.* **1992**, *433*, 95–106.

(71) Greco, A.; Cesca, S.; Bertolini, G. *J. Organomet. Chem.* **1976**, *113*, 321–330.

(72) Poremba, P.; Edelmann, F. T. *J. Organomet. Chem.* **1998**, *553*, 393–395.

(73) Lorenz, V.; Blaurock, S.; Hrib, C. G.; Edelmann, F. T. *Organometallics* **2010**, *29*, 4787–4789.

(74) Jeletic, M.; Lin, P. H.; Le Roy, J. J.; Korobkov, I.; Gorelsky, S. I.; Murugesu, M. *J. Am. Chem. Soc.* **2011**, *133*, 19286–19289.

(75) Bogani, L.; Wernsdorfer, W. *Nat. Mater.* **2008**, *7*, 179–286.

(76) Coronado, E.; Day, P. *Chem. Rev.* **2004**, *104*, 5419–5448.

(77) Magnani, N.; Apostolidis, C.; Morgenstern, A.; Colineau, E.; Griveau, J. C.; Bolvin, H.; Walter, O.; Caciuffo, R. *Angew. Chem., Int. Ed.* **2011**, *50*, 1696–1698.

(78) Maheswaran, S.; Chastanet, G.; Teat, S. J.; Mallah, T.; Sessoli, R.; Wernsdorfer, W.; Winpenny, R. E. P. *Angew. Chem., Int. Ed.* **2005**, *44*, 5044–5048.

(79) Ungur, L.; Le Roy, J. J.; Korobkov, I.; Murugesu, M.; Chibotaru, L. F. *Angew. Chem., Int. Ed.* **2014**, *53*, 4413–4417.

(80) Le Roy, J. J.; Jeletic, M.; Gorelsky, S. I.; Korobkov, I.; Ungur, L.; Chibotaru, L. F.; Murugesu, M. *J. Am. Chem. Soc.* **2013**, *135*, 3502–3510.

(81) Le Roy, J. J.; Korobkov, I.; Murugesu, M. *Chem. Commun.* **2014**, *50*, 1602–1604.

(82) Le Roy, J. J.; Korobkov, I.; Murugesu, M. *Dalton Trans.* **2014**, *43*, 2737–2740.

(83) Meihaus, K. R.; Long, J. R. *J. Am. Chem. Soc.* **2013**, *135*, 17952–17957.

(84) Hawthorne, M. F.; Young, D. C.; Wegner, P. A. *J. Am. Chem. Soc.* **1965**, *87*, 1818–1819.

(85) Grimes, R. N. *Comprehensive Organometallic Chemistry*; Elsevier, 1982.

(86) Callahan, K. P.; Hawthorne, M. F. *Adv. Organomet. Chem.* **1976**, *14*, 145–186.

(87) Hawthorne, M. F. *J. Organomet. Chem.* **1975**, *100*, 97–110.

(88)   Grimes, R. N. *Chem. Rev.* **1992**, *92*, 251–268.

(89)   Herberich, G. E.; Greiss, G.; Heil, H. F. *Angew. Chem., Int. Ed.* **1970**, *9*, 805–806.

(90)   Fu, G. C. *Adv. Organomet. Chem.* **2001**, *47*, 101–119.

(91)   Herberich, G. E.; Holger, O. *Adv. Organomet. Chem.* **1986**, *25*, 199–236.

(92)   Bazan, G. C.; Rodriguez, G.; Ashe, A. J.; Al-Ahmad, S.; Müller, C. *J. Am. Chem. Soc.* **1996**, *118*, 2291–2292.

(93)   Pammer, F.; Lalancette, R. A.; Jäkle, F. *Chem. Eur. J.* **2011**, *17*, 11280–11289.

(94)   Timms, P. L. *J. Am. Chem. Soc.* **1968**, *90*, 4585–4589.

(95)   Herberich, G. E. **1982**, *3127*, 3115–3127.

(96)   Herberich, G. E.; Hessner, B.; Hostalek, M. *Angew. Chem., Int. Ed.* **1986**, *25*, 642–643.

(97)   Wood, T. K.; Piers, W. E.; Keay, B. A.; Parvez, M. *Angew. Chem., Int. Ed.* **2009**, *48*, 4009–4012.

(98)   Wood, T. K.; Piers, W. E.; Keay, B. A.; Parvez, M. *Chem. Eur. J.* **2010**, *16*, 12199–12206.

(99)   Emslie, D. J. H.; Piers, W. E.; Parvez, M. *Angew. Chem., Int. Ed.* **2003**, *42*, 1252–1255.

(100)   Reus, C.; Weidlich, S.; Bolte, M.; Lerner, H. W.; Wagner, M. *J. Am. Chem. Soc.* **2013**, *135*, 12892–12907.

(101)   G. Raabe, W. Schleker, E. Heyne, and J. F. *J. Z. Naturforsch* **1987**, *42a*, 352–360.

(102)   Karadakov, P. B.; Ellis, M.; Gerratt, J.; Cooper, D. L.; Raimondi, M. *Int. J. Quantum Chem.* **1997**, *63*, 441–449.

(103)   Maier, G.; Reisenauer, H. P.; Henkelmann, J.; Kliche, C. *Angew. Chem., Int. Ed.* **1988**, *27*, 295–296.

(104)   Hoic, D. A.; Wolf, J. R.; Davis, W. M.; Fu, G. C. *Organometallics* **1996**, *15*, 1315–1318.

(105)   Légaré, M.-A.; Bélanger-Chabot, G.; De Robillard, G.; Languérand, A.; Maron, L.; Fontaine, F.-G. *Organometallics* **2014**, *33*, 3596–3606.

(106)   Lee, B. Y.; Wang, S.; Putzer, M.; Bartholomew, G. P.; Bu, X.; Bazan, G. C. *J. Am. Chem. Soc.* **2000**, *122*, 3969–3970.

(107)   Herberich, G. E.; Schmidt, B.; Englert, U.; Wagner, T. *Organometallics* **1993**, *12*, 2891–2893.

(108)   Hoic, D. A.; DiMare, M.; Fu, G. C. *J. Am. Chem. Soc.* **1997**, *119*, 7155–7156.

(109)   Herberich, G. E.; Gresis, G.; Heil, H. F. *Angew. Chem. Int. Ed.* **1970**, *9*, 805–806.

(110) Ashe, A. J.; Shu, P. *J. Am. Chem. Soc.* **1971**, *93*, 1804–1805.

(111) Zheng, X.; Wang, B.; Herberich, G. E. *Organometallics* **2002**, *21*, 1949–1954.

(112) Languérand, A.; Barnes, S. S.; Bélanger-Chabot, G.; Maron, L.; Berrouard, P.; Audet, P.; Fontaine, F. G. *Angew. Chem., Int. Ed.* **2009**, *48*, 6695–6698.

(113) Wang, B.; Zheng, X. L.; Herberich, G. E. *Eur. J. Inorg. Chem.* **2002**, 31–41.

(114) Macha, B. B.; Boudreau, J.; Maron, L.; Maris, T.; Fontaine, F.-G. *Organometallics* **2012**, *31*, 6428–6437.

(115) Cade, I. A.; Hill, A. F. *Dalton Trans.* **2011**, *40*, 10563–10567.

(116) Ashe, A. J.; Diephouse, T. R.; El-Sheikh, M. Y. *J. Am. Chem. Soc.* **1982**, *104*, 5693–5699.

(117) Herberich, G. E.; Englert, U.; Fischer, A.; Ni, J. H.; Schmitz, A. *Organometallics* **1999**, *18*, 5496–5501.

(118) Herberich, G. E.; Englert, U.; Schmidt, M. U.; Standt, R. *Organometallics* **1996**, *15*, 2707–2712.

(119) Herberich, G. E.; Klein, W.; Spaniol, T. P. *Organometallics* **1993**, *12*, 2660–2667.

(120) Herberich, G. E.; Ohst, H. *Adv. Organomet. Chem.* **1986**, *25*, 199–236.

(121) Fu, G. *Adv. Organomet. Chem.* **2001**, *47*, 101–119.

(122) Herberich, G. E.; Hessner, B.; Kho, T. T. *J. Organomet. Chem.* **1980**, *197*, 1–5.

(123) Putzer, M. a.; Rogers, J. S.; Bazan, G. C. *J. Am. Chem. Soc.* **1999**, *121*, 8112–8113.

(124) Tweddell, J.; Hoic, D. A.; Fu, G. C. *J. Org. Chem.* **1997**, *62*, 8286–8287.

(125) Amendola, M. C.; Stockman, K. E.; Hoic, D. A.; Davis, W. M.; Fu, G. C. *Angew. Chem., Int. Ed.* **1997**, *36*, 267–269.

(126) Qiao, S.; Hoic, D. A.; Fu, G. C. *J. Am. Chem. Soc.* **1996**, *118*, 6329–6330.

(127) Qiao, S.; Hoic, D. A.; Fu, G. C. *J. Am. Chem. Soc.* **1996**, *118*, 6329–6330.

(128) Languérand, A.; Barnes, S. S.; Bélanger-Chabot, G.; Maron, L.; Berrouard, P.; Audet, P.; Fontaine, F.-G. *Angew. Chem., Int. Ed.* **2009**, *48*, 6695–6698.

(129) Kostic, N. M.; Fenske, R. F. *Organometallics* **1983**, *2*, 1319–1325.

(130) Herberich, G. E.; Ohst, H. *Adv. Organomet. Chem.* **1986**, *25*, 199–236.

(131) Bazan, G. C.; Rodriguez, G.; Ashe, A. J.; Al-Ahmad, S.; Kampf, J. W. *Organometallics* **1997**, *16*, 2492–2494.

(132) Rogers, J. S.; Bu, X.; Bazan, G. C. *Organometallics* **2000**, *19*, 3948–3956.

(133) Ashe III, a; Al-Ahmad, S.; Fang, X.; Kampf, J. *Organometallics* **1998**, *17*, 3883–3888.

(134) Hagenau, U.; Heck, J.; Hendrickx, E.; Persoons, A.; Schuld, T.; Wong, H. *Inorg. Chem.* **1996**, *35*, 7863–7866.

(135) Pérez, V.; Barnes, S. S.; Fontaine, F.-G. *Eur. J. Inorg. Chem.* **2014**, *2014*, 5698–5702.

(136) Kudinov, A. R.; Loginov, D. A.; Starikova, Z. A.; Petrovskii, P. V. *J. Organomet. Chem.* **2002**, *649*, 136–140.

(137) Herberich, G. E.; Englert, U.; Ganter, B.; Lamertz, C. *Organometallics* **1996**, *15*, 5236–5241.

(138) Herberich, G. E.; Englert, U.; Fischer, A.; Ni, J.; Schmitz, A. *Organometallics* **1999**, *18*, 5496–5501.

(139) Cui, P.; Chen, Y.; Zeng, X.; Sun, J.; Li, G.; Xia, W. *Organometallics* **2007**, *26*, 6519–6521.

(140) Yuan, Y.; Chen, Y.; Li, G.; Xia, W. *Organometallics* **2010**, *29*, 3722–3728.

(141) Wang, X.; Peng, W.; Cui, P.; Leng, X.; Xia, W.; Chen, Y. *Organometallics* **2013**, *32*, 6166–6169.

(142) Cui, P.; Chen, Y.; Wang, G.; Li, G.; Xia, W. *Organometallics* **2008**, *27*, 4013–4016.

(143) Cui, P.; Chen, Y.; Li, G.; Xia, W. *Organometallics* **2011**, *30*, 2012–2017.

(144) Cui, P.; Chen, Y.; Li, G.; Xia, W. *Angew. Chem., Int. Ed.* **2008**, *47*, 9944–9947.

(145) Cui, P.; Chen, Y.; Zhang, Q.; Li, G.; Xia, W. *J. Organomet. Chem.* **2010**, *695*, 2713–2719.

(146) Wang, X.; Leng, X.; Chen, Y. *Dalton Trans.* **2015**, *44*, 5771–5776.

(147) Lu, E.; Yuan, Y.; Chen, Y.; Xia, W. *ACS Catal.* **2013**, *3*, 521–524.

(148) Yuan, Y.; Wang, X.; Li, Y.; Fan, L.; Xu, X.; Chen, Y.; Li, G.; Xia, W. *Organometallics* **2011**, *30*, 4330–4341.

(149) Bieller, S.; Zhang, F.; Bolte, M.; Bats, J. W.; Lerner, H.-W.; Wagner, M. *Organometallics* **2004**, *23*, 2107–2113.

(150) Hoffend, C.; Diefenbach, M.; Januszewski, E.; Bolte, M.; Lerner, H.-W.; Holthausen, M. C.; Wagner, M. *Dalton Trans.* **2013**, *42*, 13826–13837.

(151) Januszewski, E.; Lorbach, A.; Grewal, R.; Bolte, M.; Bats, J. W.; Lerner, H.-W.; Wagner, M. *Chemistry* **2011**, *17*, 12696–12705.

(152) Schacht, W.; Kaufmann, D. *J. Organomet. Chem.* **1987**, *331*, 139–152.

(153) Kaufmann, D. E.; Schacht, W. *Pure Appl. Chem.* **1991**, *63*, 383–386.

(154) Müller, P.; Huck, S.; Köppel, H.; Pritzkow, H.; Siebert, W. *Z. Naturforsch., B* **1995**, *50b*, 1476–1484.

(155) Agou, T.; Sekine, M.; Kawashima, T. *Tetrahedron Lett.* **2010**, *51*, 5013–5015.

(156) Müller, P.; Gangnus, B.; Pritzkow, H.; Schulz, H.; Stephan, M.; Siebert, W. *J. Organomet. Chem.* **1995**, *487*, 235–243.

(157) Muller, P.; Pritzkow, H.; Siebert, W. *J. Organomet. Chem.* **1996**, *524*, 41–47.

(158) Macha, B. B.; Boudreau, J.; Maron, L.; Maris, T.; Fontaine, F. *Organometallics* **2012**, *31*, 6428–6437.

(159) Hoic, D. A.; Davis, W. M.; Fu, G. C. *J. Am. Chem. Soc.* **1996**, *118*, 8176–8177.

(160) Cui, P.; Chen, Y.; Zeng, X.; Sun, J.; Li, G.; Xia, W. *Organometallics* **2007**, *26*, 6519–6521.

(161) Wang, C.; Leng, X.; Chen, Y. *Organometallics* **2015**, *34*, 3216–3221.

(162) Wang, C.; Leng, X.; Chen, Y. *Organometallics* **2015**, *34*, 3216–3221.

(163) Jiang, S. Da; Liu, S. S.; Zhou, L. N.; Wang, B. W.; Wang, Z. M.; Gao, S. *Inorg. Chem.* **2012**, *51*, 3079–3087.

(164) Herberich, G. E.; Koch, W. *Chem. Ber.* **1977**, *110*, 816–819.

(165) Fraenkel, G.; Subramanian, S.; Chow, A. *J. Am. Chem. Soc.* **1995**, *117*, 6300–6307.

(166) Rogers, J. S.; Bu, X.; Bazan, G. C. *Organometallics* **2000**, *19*, 3948–3956.

(167) Herberich, G. E.; Greißt, G. *Chem. Ber.* **1972**, *105*, 3413–3423.

(168) Jeletic, M.; Lin, P.-H.; Le Roy, J. J.; Korobkov, I.; Gorelsky, S. I.; Murugesu, M. *J. Am. Chem. Soc.* **2011**, *133*, 19286–19289.

(169) Zadrozny, J. M.; Xiao, D. J.; Atanasov, M.; Long, G. J.; Grandjean, F.; Neese, F.; Long, J. R. *Nat. Chem.* **2013**, *5*, 577–581.

(170) Ishikawa, N.; Sugita, M.; Ishikawa, T.; Koshihara, S.; Kaiz, Y. *J. Am. Chem. Soc.* **2003**, *125*, 8694–8695.

(171) Layfield, R. a.; McDouall, J. J. W.; Sulway, S. a.; Tuna, F.; Collison, D.; Winpenny, R. E. P. *Chem. - A Eur. J.* **2010**, *16*, 4442–4446.

(172) Kinsley, S. A.; Streitwieser, A.; Zalkin, A. *Organometallics* **1985**, *4*, 52–57.

(173) Bellama, J. M.; Davidson, J. B. *J. Organomet. Chem.* **1975**, *86*, 69–74.

(174) Schumann, H.; Meese-Marktscheffel, J. A.; Esser, L. *Chem. Rev.* **1995**, *95*, 865–986.

(175) Grimes, R. N. *Chem. Rev.* **1992**, *92*, 251–268.

(176) Braunschweig, H.; Kupfer, T. *Chem. Commun.* **2011**, *47*, 10903–10914.

(177) Ashe, A. J.; Al-Ahmad, S.; Fang, X. *J. Organomet. Chem.* **1999**, *581*, 92–97.

(178) Woodmansee, D. H.; Bu, X.; Bazan, G. C. *Chem. Commun.* **2001**, 619–620.

(179) Komon, Z. J. A.; Rogers, J. S.; Bazan, G. C. *Organometallics* **2002**, *21*, 3189–3195.

(180) Ashe III., A. J.; Kampf, J. W.; Müller, C.; Schneider, M. *Organometallics* **1996**, *15*, 387–393.

(181) Ashe, A. J.; Kampf, J. W.; Waas, J. R. *Organometallics* **1997**, *16*, 163–167.

(182) Cui, P.; Chen, Y.; Wang, G.; Li, G.; Xia, W. *Organometallics* **2008**, *27*, 4013–4016.

(183) Cui, P.; Chen, Y.; Zhang, Q.; Li, G.; Xia, W. *J. Organomet. Chem.* **2010**, *695*, 2713–2719.

(184) Yuan, Y.; Chen, Y.; Li, G.; Xia, W. *Organometallics* **2010**, *48*, 3722–3728.

(185) Bönnemann, H.; Brijoux, W.; Brinkmann, R.; Meurers, W. *Helv. Chem. Acta* **1984**, *67*, 1616–1624.

(186) Ashe, A. J.; Al-Ahmad, S.; Fang, X. G.; Kampf, J. W. *Organometallics* **1998**, *17*, 3883–3888.

(187) Rogers, J. S.; Bu, X. H.; Bazan, G. C. *J. Am. Chem. Soc.* **2000**, *122*, 730–731.

(188) Rogers, J. S.; Bazan, G. C.; Sperry, C. K. *J. Am. Chem. Soc.* **1997**, *119*, 9305–9306.

(189) Behrens, U.; Meyer-Friedrichsen, T.; Heck, J. *Z. Anorg. Allg. Chem.* **2003**, *629*, 1421–1430.

(190) Jaska, C. A.; Emslie, D. J. H.; Bosdet, M. J. D.; Piers, W. E.; Sorensen, T. S.; Parvez, M. *J. Am. Chem. Soc.* **2006**, *128*, 10885–10896.

(191) Hagenau, U.; Heck, J.; Hendrickx, E.; Persoons, A.; Schuld, T.; Wong, H. *Inorg. Chem.* **1996**, *35*, 7863–7866.

(192) Maier, G. *Pure Appl. Chem.* **1986**, *58*, 95–104.

(193) Barnes, S. S.; Légaré, M.-A.; Maron, L.; Fontaine, F.-G. *Dalton Trans.* **2011**, *40*, 12439–12442.

(194) Bélanger-Chabot, G.; Rioux, P.; Maron, L.; Fontaine, F.-G. *Chem. Commun.* **2010**, *46*, 6816–6818.

(195) Leusink, A. J.; Drenth, W.; Noltes, J. G.; van der Kerk, G. J. M. *Tetrahedron Lett.* **1967**, *8*, 1263–1266.

(196) van der Kerk, S. M.; Boersma, J.; van der Kerk, G. J. M. *J. Organomet. Chem.* **1981**, *215*, 303–313.

(197) Putzer, M. A.; Rogers, J. S.; Bazan, G. C. *J. Am. Chem. Soc.* **1999**, *121*, 8112–8113.

(198) Herberich, G. E.; Boveleth, W.; Hessner, B.; Koch, W.; Raabe, E.; Schmitz, D. *J. Organomet. Chem.* **1984**, *265*, 225–235.

(199) Herberich, G. E.; Baul, T. S. B.; Englert, U. *Eur. J. Inorg. Chem.* **2002**, 43–48.

(200) Huttner, G.; Gartzke, W. *Chem. Ber.* **1974**, *107*, 3786–3799.

(201) Herberich, G. E.; Raabe, E. *J. Organomet. Chem.* **1986**, *309*, 143–156.

(202) Ashe, A. J.; Butler, W.; Sandford, H. F. *J. Am. Chem. Soc.* **1979**, *101*, 7066–7067.

(203) Churchill, M. R.; See, R. F. *J. Organomet. Chem.* **1993**, *450*, 171–176.

(204) SADBS. *Bruker AXS Inc., Madison, WI* **2007**.

(205) Edelmann, A.; Lorenz, V.; Hrib, C. G.; Hilfert, L.; Edelmann, F. T. *Organometallics* **2013**, *32*, 1435–1444.

(206) Edelmann, F. T. *New J. Chem.* **2011**, *35*, 517–528.

(207) Herberich, G. E.; Ashe, A. J.; Butler, W.; Sandford, H. F.; Drone, F. J.; Kampf, J. W. *Organometallics* **1993**, *1*, 3786–3789.

(208) Ashe, A. J.; Kampf, J. W.; Klein, W.; Rousseau, R. *Angew. Chem., Int. Ed.* **1993**, *32*, 1065–1066.

(209) Fang, X.; Woodmansee, D.; Bu, X.; Bazan, G. C. *Angew. Chem., Int. Ed.* **2003**, *42*, 4510–4514.

(210) Poremba, P.; Reißmann, U.; Noltemeyer, M.; Schmidt, H.-G.; Brüser, W.; Edelmann, F. T. *J. Organomet. Chem.* **1997**, *544*, 1–6.

(211) Lorbach, A.; Reus, C.; Bolte, M.; Lerner, H.-W.; Wagner, M. *Adv. Synth. Catal.* **2010**, *352*, 3443–3449.

(212) Januszewski, E.; Lorbach, A.; Grewal, R.; Bolte, M.; Bats, J. W.; Lerner, H.-W.; Wagner, M. *Chem.-Eur. J.* **2011**, *17*, 12696–12705.

(213) Agou, T.; Sekine, M.; Kawashima, T. *Tetrahedron Lett.* **2010**, *51*, 5013–5015.

(214) Lee, R. A.; Lachicotte, R. J.; Bazan, G. C. *J. Am. Chem. Soc.* **1998**, *120*, 6037–6046.

(215) Mercier, L. G.; Piers, W. E.; Parvez, M. *Angew. Chem., Int. Ed.* **2009**, *48*, 6108–6111.

(216) Guillemot, G.; Castellano, B.; Prangé, T.; Solari, E.; Floriani, C. *Inorg. Chem.* **2007**, *46*, 5152–5154.

(217) Müller, P.; Gangnus, B.; Pritzkow, H.; Schulz, H.; Stephan, M.; Siebert, W. *J. Organomet. Chem.* **1995**, *487*, 235–243.

(218) Lorenz, V.; Blaurock, S.; Hrib, C. G.; Edelmann, F. T. *Dalton Trans.* **2010**, *39*, 6629–6631.

(219) Visseaux, M.; Dormond, A.; Barbier-Baudry, D. *Eur. J. Inorg. Chem.* **1999**, *1999*, 1827–1830.

(220) Edelmann, A.; Lorenz, V.; Hrib, C. G.; Hilfert, L.; Blaurock, S.; Edelmann, F. T. *Organometallics* **2013**, *32*, 1435–1444.

(221) Piguet, J. C. G. B. *Chem. Soc. Rev.* **2005**, *34*, 1048–1077.

172

(222) Carlos, L. D.; Ferreira, R. A. S.; Bermudez, V. Z.; Ribeiro, S. J. L. *Adv. Mater.* **2009**, *21*, 509–534.

(223) Binnemans, K. *Chem. Rev.* **2009**, *109*, 4283–4374.

(224) Rocha, A. R.; Suárez, V. M. G.-; Bailey, S. W.; Lambert, C. J.; Ferrer, J.; Sanvito, S. *Nat. Mater.* **2005**, *4*, 335–339.

(225) Benedetto, J. D. S.; Soares, M. L.; Greval, I.; Dresinger, D. *Sep. Sci. Technol.* **1995**, *30*, 3339–3349.

(226) Spedding, F. H. *J. Am. Chem. Soc.* **1947**, *69*, 2812–2818.

(227) Hamaguchi, H.; Ohuchi, A.; Inuma, N.; Kuroda, R. *J. Chromatogr. A.* **1964**, *16*, 396–402.

(228) Fernandez, R. G.; Alonso, J. I. G. *J. Chromatogr. A.* **2008**, *1180*, 59–65.

(229) Reddy, B. R.; Radhika, S.; Kumar, B. N. *Chem. Eng. J.* **2010**, *160*, 138–144.

(230) Menon, S. K.; Kaur, H.; Dave, S. R. *React. Funct. Polym.* **2010**, *70*, 692–698.

(231) Jia, Q.; Wang, Z. H.; D. Q. Li; Niu, C. J. *J. Alloy. Compd.* **2007**, *374*, 434–437.

(232) Kronholm, B.; Anderson, C.; Taylor, P. R. *J. Org. Chem.* **2013**, *65*, 1321–1326.

(233) Zhang, A.; Mei, C.; Wei, Y.; Kumagai, M. *Adsorpt. Sci. Technol.* **2007**, *25*, 257–272.

(234) Pesterfield, G. K.; Schweitzer, L. L. *The aqueous chemistry of the elements*; Oxford University Press, New York, 2009.

(235) T. Moeller. *Adv. Chem.* **2009**, *62*, 306–371.

(236) Cossy, C.; Helm, L.; Merbach, A. E. *Inorg. Chem.* **1988**, *27*, 1973–1979.

(237) Abbasi, A.; Lindqvist-Reis, P.; Eriksson, L.; Sandstrom, D.; Lidin, S.; Persson, I.; Sandstrom, M. *Chem. Eur. J.* **2005**, *11*, 4065–4077.

(238) Cossy, C.; Helm, L.; Merbach, A. E. *Inorg. Chem.* **1989**, *28*, 2699–2703.

(239) Meier, W.; Bopp, P.; Probst, M. M.; Spohr, E.; Lin, J. I. *J. Phys. Chem.* **1990**, *94*, 4672–4682.

(240) Hart, F. A. *Comprehensive Coordination Chemistry*, 3rd ed.; Pergamon Press, Oxford, 1987.

(241) Karraker, D. G. *J. Chem. Edu.* **1970**, *47*, 424–430.

(242) Narita, H.; Yaita, T.; Tamura, K.; Tachimori, S. *J. Radioanal. Nucl. Chem.* **1999**, *239*, 381–384.

(243) Sasaki, Y.; Sugo, Y.; Suzuki, S.; Tachimori, S. *Solvent Extr. Ion Exch.* **2001**, *19*, 91–103.

(244) Zhu, Z. X.; Sasaki, Y.; Suzuki, H.; Suzuki, S.; Kimura, T. *Anal. Chim. Acta* **2004**,

527, 163–168.

(245) Sasaki, Y.; Rapold, P.; Arisaka., M.; Hirata, M.; Kimura, T. *Solvent Extr. Ion Exch.* **2007**, *25*, 187–204.

(246) Sasaki, Y.; Zhu, Z.; Sugo, Y.; Kimura, T. *J. Nucl. Sci. Technol.* **2007**, *44*, 405–409.

(247) Kannan, S.; Moody, M. A.; Barnes, C. L.; Duval, P. B. *Inorg. Chem.* **2008**, *47*, 4691–4695.

(248) Lebed, P. J.; Savoie, J. D.; Florek, J.; Bilodeau, F.; Larivière, D.; Kleitz, F. *Chem. Mater.* **2012**, *24*, 4166–4176.

(249) Florek, J.; Chalifour, F.; Bilodeau, F.; Larivière, D.; Kleitz, F. *Adv. Funct. Mat.* **2014**, *24*, 2668–2676.

(250) Zhang, Y.; Wang, Y.; N. Tang, M. T.; Yu, K. *J. Coord. Chem.* **2002**, *55*, 1293–1299.

(251) Matloka, K.; Gelis, A.; Regalbuto, M.; Vandegrift, G.; Scott, M. J. *Dalton Trans.* **2005**, 3719–3721.

(252) Tian, G.; Xu, J.; Rao, L. *Angew. Chem., Int. Ed.* **2005**, *44*, 6200–6203.

(253) Jover, J.; Fey, N.; Harvey, J. N.; Lloyd-Jones, G. C.; Orpen, A. G.; Owen-Smith, G. J. J.; Murray, P.; Hose, D. R. J.; Osborne, R.; Purdie, M. *Organometallics* **2012**, *31*, 5302–5306.

(254) Birkholz, M. N.; Freixa, Z.; Leeuwan, P. W. N. *Chem. Soc. Rev.* **2009**, *38*, 1099–1118.

(255) Freixa, Z.; Leeuwan, P. W. N. *Dalton Trans.* **2003**, 1890–1901.

(256) Papp, T.; Kollar, L.; Kegl, T. *J. Quant. Chem.* **2014**, 1–5.

(257) Sasaki, Y.; Morita, Y.; Kitatsuji, Y.; Kimura, T. *Solvent Extr. Ion Exch* **2010**, *28*, 335–349.

174